Climate Dynamics:

Concepts, Scaling and Multiple Equilibria

by Gerrit Lohmann

Alfred Wegener Institute, Helmholtz Centre for Polar and Marine Research, Bremerhaven, Germany.

Department of Physics, University of Bremen, Bremen, Germany.

Lecture Notes 2020

version of April 16, 2020

Contents

II   Second part: Dynamics of the Climate System   92

3   Atmosphere and Ocean Dynamics   93

4   Atmospheric Models   132

5   Ocean Circulation   164

General framework: Climate dynamics

Over the last century, humans have altered the composition of the Earth's atmosphere and surface to the extent that these factors measurably affect current climate conditions. Paleoclimate reconstructions, in particular from ice cores have also shown that climate can change over relatively short periods such as a few years to decades. The objective of the book is to examine fundamental concepts used to understand climate dynamics. Here, we will approach climate dynamics from a fluid dynamics and complex systems point of view. The script has several parts, an application follows after every theoretical section. The content (part I-IV) is designed for 12 lessons for a master course at the University of Bremen (Dynamics II).

Part I deals with the general structure of fluid dynamical models. Like the ocean, the atmosphere is considered as a Newtonian Fluid. The concepts of scaling and vorticity are introduced. Ice dynamics is not explicitly considered here although it is an important part of the Earth system. One application deals with the Rayleigh-Bénard convection. In the script, a framework to analyze the stability of dynamical systems is presented. These systems provide the prototype of nonlinear dynamics, bifurcations, multiple equilibria. A bifurcation occurs when a parameter change causes the stability of an equilibrium. In his classic studies of chaotic systems, Lorenz has proposed a deterministic theory of climate change with his concept of the 'almost-intransitivity' of the highly non-linear climate systems. In the Lorenz equations exist the possibility of multiple stable solutions and internal variability, even in the absence of any variations in external forcing [Lorenz, 1976]. More complex models, e.g. Bryan [1986]; Dijkstra et al. [2004] also demonstrated this possibility.

In Part II, basic concepts of large-scale meteorology and oceanography are explored. The Coriolis effect is one of the dominating forces for the large-scale dynamics of the oceans and the atmosphere. In meteorology and ocean science, it is convenient to use a rotating frame of reference where the Earth is stationary. The resulting flow can be derived from scaling arguments. Several approximations can be done since the scales of the components in the dynamical equations differ in the orders of magnitude. One fundamental aspect of ocean dynamics are waves. A short theory

is given and numerical examples are provided. Furthermore, the deep ocean circulation is studied in a conceptual box model. Here, we introduce an interhemispheric box model of the deep ocean circulation to study the feedbacks in the climate system. Finally, some of the waves in the climate system are introduced.

Part III deals with the stochastic climate model. This part of the course touches also statistical mechanics and applications. Several additional sections are included for those who have some more time.

The numerical examples in part IV chapters are helpful for the students who are already familiar with programming (they can improve the code and follow the main ideas of the code etc.), for those who are not familiar they should take it as a starting point for more research. Several task do not require that the complete code is understood, but one can change initial conditions or parameters in the problems.

Part I

First part: Fluid Dynamics and Dynamical Systems

Chapter 1

Basics of Fluid Dynamics

Our starting point is a mathematical model for the system of interest. In physics a model typically describes the state variables, plus fundamental laws and equations of state. These variables evolve in space and time. For the ocean circulation, we proceed as follows:

- State variables: Velocity (in each of three directions), pressure, temperature, salinity, density
- Fundamental laws: Conservation of momentum, conservation of mass, conservation of temperature and salinity
- Equations of state: Relationship of density to temperature, salinity and pressure, and perhaps also a model for the formation of sea-ice

The state variables for the ocean model are expressed as a continuum in space and time, and the fundamental laws as partial differential equations[1]. Even at this stage, though, simplifications may be made. For example, it is common to treat seawater as incompressible. Furthermore, equations of state are often specified by empirical relationships or laboratory experiments.

In the following, the general structure of ocean circulation, atmospheric energy balance as well as ice sheet models are described. The dynamics of flow are based on the Navier-Stokes equations. The derivation of the Navier-Stokes equations begins with an application of Newton's second law: conservation of momentum (often alongside mass and energy conservation) being written for an

---

[1]If the atmosphere is becoming too thin in the upper levels, a more molecular, statistical description is appropiate (section 9)

arbitrary control volume. In an inertial frame of reference, the general form of the equations of fluid motion is:

$$\rho \left(\frac{\partial \mathbf{u}}{\partial t} + \mathbf{u} \cdot \nabla \mathbf{u} \right) = -\nabla p + \nabla \cdot \mathbb{T} + \mathbf{F}, \tag{1.1}$$

where $\mathbf{u}$ is the flow velocity (a vector), ρ is the fluid density, p is the pressure, $\mathbb{T}$ is the 3×3 (deviatoric) stress tensor, and $\mathbf{F}$ represents body forces (per unit volume) acting on the fluid and ∇ is the nabla operator. This is a statement of the conservation of momentum in a fluid and it is an application of Newton's second law to a continuum; in fact this equation is applicable to any non-relativistic continuum and is known as the Cauchy momentum equation (e.g., Landau and Lifshitz [1959]).

This equation is often written using the substantive derivative, making it more apparent that this is a statement of Newton's second law:

$$\rho \frac{D\mathbf{u}}{Dt} = -\nabla p + \nabla \cdot \mathbb{T} + \mathbf{F}. \tag{1.2}$$

The left side of the equation describes acceleration, and may be composed of time dependent or advective effects (also the effects of non-inertial coordinates if present). The right side of the equation is in effect a summation of body forces (such as gravity) and divergence of stress (pressure and stress). A very significant feature of the Navier-Stokes equations is the presence of advective acceleration: the effect of time independent acceleration of a fluid with respect to space, represented by the nonlinear quantity $\mathbf{u} \cdot \nabla \mathbf{u}$. A general framework can be generally formulated as a transport phenomenon, see section 1.8.

1.1 Material laws

The effect of stress in the fluid is represented by the ∇p and $\nabla \cdot \mathbb{T}$ terms, these are gradients of surface forces, analogous to stresses in a solid. ∇p is called the pressure gradient and arises from

the isotropic part of the stress tensor. This part is given by normal stresses that turn up in almost all situations, dynamic or not. The anisotropic part of the stress tensor gives rise to $\nabla \cdot \mathbb{T}$, which conventionally describes viscous forces. For incompressible flow, this is only a shear effect. Thus, $\mathbb{T}$ is the deviatoric stress tensor, and the stress tensor is equal to:

$$\boldsymbol{\sigma} = -p\,\mathbb{I} + \mathbb{T} \tag{1.3}$$

where $\mathbb{I}$ is the 3×3 identity matrix. Interestingly, only the gradient of pressure matters, not the pressure itself. The effect of the pressure gradient is that fluid flows from high pressure to low pressure.

The stress terms p and $\mathbb{T}$ are yet unknown, so the general form of the equations of motion is not usable to solve problems. Besides the equations of motion -Newton's second law- a force model is needed relating the stresses to the fluid motion. For this reason, assumptions on the specific behavior of a fluid are made (based on observations) and applied in order to specify the stresses in terms of the other flow variables, such as velocity and density.

The Cauchy stress tensor can be also written in matrix form:

$$\mathbb{T} = \begin{pmatrix} \mathbf{T}^{(\mathbf{e_1})} \\ \mathbf{T}^{(\mathbf{e_2})} \\ \mathbf{T}^{(\mathbf{e_3})} \end{pmatrix} = \begin{pmatrix} \sigma_{11} & \sigma_{12} & \sigma_{13} \\ \sigma_{21} & \sigma_{22} & \sigma_{23} \\ \sigma_{31} & \sigma_{32} & \sigma_{33} \end{pmatrix} \equiv \begin{pmatrix} \sigma_{xx} & \sigma_{xy} & \sigma_{xz} \\ \sigma_{yx} & \sigma_{yy} & \sigma_{yz} \\ \sigma_{zx} & \sigma_{zy} & \sigma_{zz} \end{pmatrix} \equiv \begin{pmatrix} \sigma_x & \tau_{xy} & \tau_{xz} \\ \tau_{yx} & \sigma_y & \tau_{yz} \\ \tau_{zx} & \tau_{zy} & \sigma_z \end{pmatrix} \tag{1.4}$$

where $\boldsymbol{\sigma}$ are the normal stresses and $\boldsymbol{\tau}$ are the shear stresses. From the Newton's third law (actio est reactio) the stress vectors $\mathbf{T}^{(\mathbf{e_i})} = \frac{d\mathbf{F}}{dA}$ with $\mathbf{e_i}$ as normalvector acting on opposite sides of the same surface are equal in amount and opposite in direction ($-\mathbf{T}^{(\mathbf{e_i})} = \mathbf{T}^{(-\mathbf{e_i})}$). According to conservation of angular momentum, summation of moments is zero. Thus the stress tensor is symmetrical: $\mathbb{T} = \mathbb{T}^T$. In Fig. 1.1 the stress vectors $\mathbf{T}^{(\mathbf{e_i})}$ can be decomposed in one normal stress and two shear stress components.
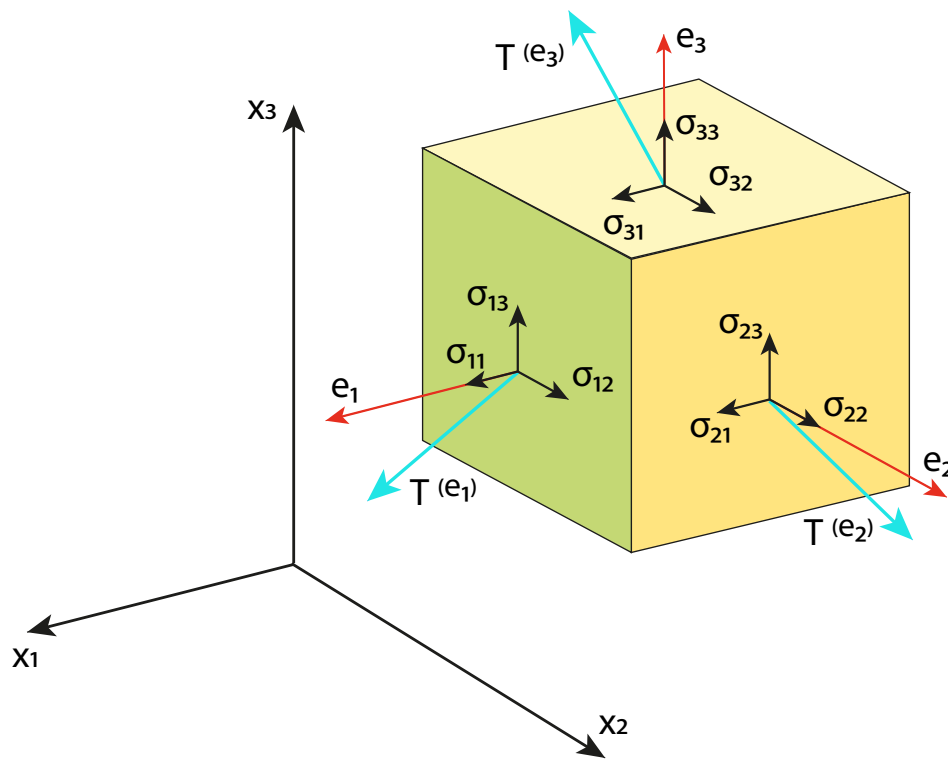
Figure 1.1: Components of stress in three dimensions.

1.2   Navier-Stokes equations

The so-called Navier-Stokes equations result from the following assumptions on the deviatoric stress tensor $\mathbb{T}$:

- the deviatoric stress vanishes for a fluid at rest, and by Galilean invariance also does not depend directly on the flow velocity itself, but only on spatial derivatives of the flow velocity

- in the Navier-Stokes equations, the deviatoric stress is expressed as the product of the tensor gradient $\boldsymbol{\nabla}\mathbf{v}$ of the flow velocity with a viscosity tensor $\mathbb{A}$, i.e. $\mathbb{T} = \mathbb{A}\left(\boldsymbol{\nabla}\mathbf{v}\right)$

- the fluid is assumed to be isotropic, as valid for gases and simple liquids, and consequently $\mathbb{A}$ is an isotropic tensor; furthermore, since the deviatoric stress tensor is symmetric, it turns out that it can be expressed in terms of two scalar dynamic viscosities μ and $\mu^{"}$: $\mathbb{T} = 2\mu\mathbb{E} + \mu''(\boldsymbol{\nabla}\cdot\mathbf{v})\mathbb{I}$, where $\mathbb{E} = \frac{1}{2}\left(\boldsymbol{\nabla}\mathbf{v}\right) + \frac{1}{2}\left(\boldsymbol{\nabla}\mathbf{v}\right)^{\mathrm{T}}$ is the rate-of-strain tensor and $\boldsymbol{\nabla}\cdot\mathbf{v}$ is the rate of expansion of the flow

- the deviatoric stress tensor has zero trace, so for a three-dimensional flow $2\mu + 3\mu^{"} = 0$

As a result, in the Navier-Stokes equations the deviatoric stress tensor has the following form:

$$\mathbb{T} = 2\mu\left(\mathbb{E} - \tfrac{1}{3}(\boldsymbol{\nabla}\cdot\mathbf{u})\mathbb{I}\right),\tag{1.5}$$

with the quantity between brackets the non-isotropic part of the rate-of-strain tensor $\mathbb{E}$. The dynamic viscosity μ does not need to be constant - in general it depends on conditions like temperature and pressure, and in turbulence modelling the concept of eddy viscosity is used to approximate the average deviatoric stress.

The Navier-Stokes equations are strictly a statement of the conservation of momentum. In order to fully describe fluid flow, more information is needed (how much depends on the assumptions made), this may include boundary data (no-slip, capillary surface, etc), the conservation of mass, the conservation of energy, and/or an equation of state. Regardless of the flow assumptions, a

statement of the conservation of mass is generally necessary. This is achieved through the mass continuity equation, given in its most general form as:

$$\frac{\partial \rho}{\partial t} + \nabla \cdot (\rho \mathbf{u}) = 0 \tag{1.6}$$

or, using the substantive derivative:

$$\frac{D\rho}{Dt} + \rho(\nabla \cdot \mathbf{u}) = 0. \tag{1.7}$$

A simplification of the resulting flow equations is obtained when considering an incompressible flow of a Newtonian fluid. The assumption of incompressibility rules out the possibility of sound or shock waves to occur; so this simplification is invalid if these phenomena are important. The incompressible flow assumption typically holds well even when dealing with a "compressible" fluid -such as air at room temperature- at low Mach numbers (even when flowing up to about Mach 0.3).[2] Taking this into account and assuming constant viscosity, the Navier-Stokes equations will read, in vector form:

$$\rho \left(\frac{\partial \mathbf{u}}{\partial t} + \mathbf{u} \cdot \nabla \mathbf{u} \right) = -\nabla p + \mu \nabla^2 \mathbf{u} + \mathbf{F}. \tag{1.8}$$

The vector field $\mathbf{F}$ represents "other" (body force) forces. Typically this is only gravity, but may include other fields (such as electromagnetic). In a non-inertial coordinate system, other "forces" such as that associated with rotating coordinates may be inserted[3]. Often, these forces may be represented as the gradient of some scalar quantity. Gravity in the z direction, for example, is the gradient of $-\rho g z$. Since pressure shows up only as a gradient, this implies that solving a problem

---

[2]The density and pressure fields can be expressed as a perturbation from a hydrostatically balanced state around a reference density $\rho_r(z)$ (e.g. a horizontal mean of density in the area of interest) and associated pressure $p_r(z)$ which are linked through $dp_r/dz = -g\rho_r$ and $p_r(z = 0) = 0$. Sound waves are filtered by realizing that the time rate of change of density due to diabatic effects and compressibility is much smaller than that due to change of volume.

[3]We will see later that the Coriolis force will be one of the main contributions in the rotating Earth system (section 3.1)

without any such body force can be mended to include the body force by modifying pressure. The shear stress term $\boldsymbol{\nabla}\mathbb{T}$ becomes the useful quantity $\mu\boldsymbol{\nabla}^2\mathbf{u}$ when the fluid is assumed incompressible and Newtonian, where μ is the dynamic viscosity.

It's well worth observing the meaning of each term (compare to the Cauchy momentum equation):

$$\rho\Big(\underbrace{\overbrace{\frac{\partial\mathbf{u}}{\partial t}}^{\text{Inertia (per volume)}} + \underbrace{\mathbf{u}\cdot\boldsymbol{\nabla}\mathbf{u}}_{\substack{\text{Advective}\\\text{acceleration}}}}_{\substack{\text{Unsteady}\\\text{acceleration}}}\Big) = \overbrace{\underbrace{-\boldsymbol{\nabla}p}_{\substack{\text{Pressure}\\\text{gradient}}}+\underbrace{\mu\boldsymbol{\nabla}^2\mathbf{u}}_{\text{Viscosity}}}^{\text{Divergence of stress}}+\underbrace{\mathbf{F}}_{\substack{\text{Other}\\\text{body}\\\text{forces}}}. \tag{1.9}$$

Note that only the advection terms are nonlinear for incompressible Newtonian flow. This acceleration is an acceleration caused by a (possibly steady) change in velocity over position, for example the speeding up of fluid entering a converging nozzle. Though individual fluid particles are being accelerated and thus are under unsteady motion, the flow field (a velocity distribution) will not necessarily be time dependent.

Another important observation is that the viscosity is represented by the vector Laplacian of the velocity field. This implies that Newtonian viscosity is diffusion of momentum, this works in much the same way as the diffusion of heat seen in the heat equation (which also involves the Laplacian).

If temperature effects are also neglected, the only "other" equation (apart from initial/boundary conditions) needed is the mass continuity equation. Under the incompressible assumption, density is a constant and it follows that the equation will simplify to:

$$\boldsymbol{\nabla}\cdot\mathbf{u} = \mathbf{0} \qquad . \tag{1.10}$$

This is more specifically a statement of the conservation of volume (see divergence). These equations are commonly used in 3 coordinates systems: Cartesian, cylindrical, and spherical. While the Cartesian equations seem to follow directly from the vector equation above, the vector form

of the Navier-Stokes equation involves some tensor calculus which means that writing it in other coordinate systems is not as simple as doing so for scalar equations (such as the heat equation).

Exercise 1   –   Questions about advection

1. A ship is steaming northward at a rate of 10 km/h. The surface pressure increases toward the northwest at a rate of 5 Pa/km. What is the pressure tendency recorded at a nearby island station if the pressure aboard the ship decreases at a rate of 100Pa/3h?

2. The temperature at a point 50 km north of a station is 3°C cooler than at the station. If the wind is blowing from the northeast at 20m/s and the air is being heated by radiation at a rate of 1°C/h, what is the local temperature change at the station?

3. The following data were received from 50 km to the east, north, west and south of a station, respectively: 90 degree, 10m/s; 120 degree,4m/s; 90degree,8m/s; 60 degree, 4m/s. Given are the angle and absolute value of the wind speed. Calculate the approximate horizontal divergence at the station.

4. Let the $x = (x_1, x_2, x_3)$ coordinates be inertial. What are the necessary and sufficient conditions that the coordinates $y_i = A_{ij}x_j + v_j(x, t)t$ be inertial for constant matrix $A = (A_{ij})$?

5. How can the movement of fluid particel be descibed in accordance with Newton's first law? Which forces can create accelerations or decelerations? Please use the definition of specific forces, that is, the force per unit mass: $f = F/m$.

6. The potential temperature in the atmosphere is defined as

$$\Theta = T(p_0/p)^{R/c_P} \tag{1.11}$$

With $p_0 = $ const. Calculate the vertical temperature gradient

$$\gamma = -\frac{dT}{dz} \tag{1.12}$$

What is the result when assuming the hydrostatic equillibrium

$$\frac{dp}{dz} = -g\rho$$

with $g = 9.81m/s^2$? What is the condition for which the the potential temperature is constant in the vertical?

Solution of 2. Temperature Advection

The total change of temperature is given by

$$\frac{\mathrm{d}T}{\mathrm{d}t} = \frac{\partial T}{\partial t} + \mathbf{u} \cdot \nabla T = \dot{q}$$
$$\Leftrightarrow \quad \frac{\partial T}{\partial t} = -\mathbf{u} \cdot \nabla T + \dot{q}$$

Here we use the velocity

$$\mathbf{u} = -20\frac{m}{s} \; \frac{1}{\sqrt{2}} \begin{pmatrix} 1 \\ 1 \\ 0 \end{pmatrix}, \qquad \nabla T = \frac{3°C}{50km} \begin{pmatrix} 0 \\ -1 \\ 0 \end{pmatrix}, \qquad \dot{q} = 1\frac{°C}{h}$$

Then we calculate

$$\frac{\partial T}{\partial t} = -\mathbf{u} \cdot \nabla T + \dot{q}$$
$$= 20\frac{m}{s} \frac{1}{\sqrt{2}} \begin{pmatrix} 1 \\ 1 \\ 0 \end{pmatrix} \cdot \begin{pmatrix} 0 \\ -1 \\ 0 \end{pmatrix} \frac{3°C}{50km} + 1\frac{°C}{h}$$
$$\approx -2.1\frac{°C}{h}$$

	Horizontal Length L	Velocity V	Time T
Microturbulence	1-10 cm	1-10 cm/s	seconds
Thunderstorms	1-10 km	10 m/s	hours
Weather patterns	100-1000 km	1-10 m/s	days to weeks
Climatic variations	global	1-10 m/s	decades and beyond

Table 1.1: Table shows the typical scales in the environmental, atmosphere, ocean and climate system. Using these orders of magnitude, one can derive estimates of the timescales.

Exercise 2 – Typical scales

Table 2 lists typical velocity, length and time scales of some fluid processes and systems. Not surprisingly, larger systems evolve on longer time scales. Depending on the size of the system under consideration, the spatial scale can be regional, continental or even global. Using the length and velocity scales (L and V), determine a typical time scale (T=L/V)! (Rough estimates are given in the last column in Table 2.)

Exercise 3 – Weather chart

From the weather chart (Figure 1.2), identify the horizontal extent of a major atmospheric sea level pressure and the associated wind speed. Determine a typical time scale T !
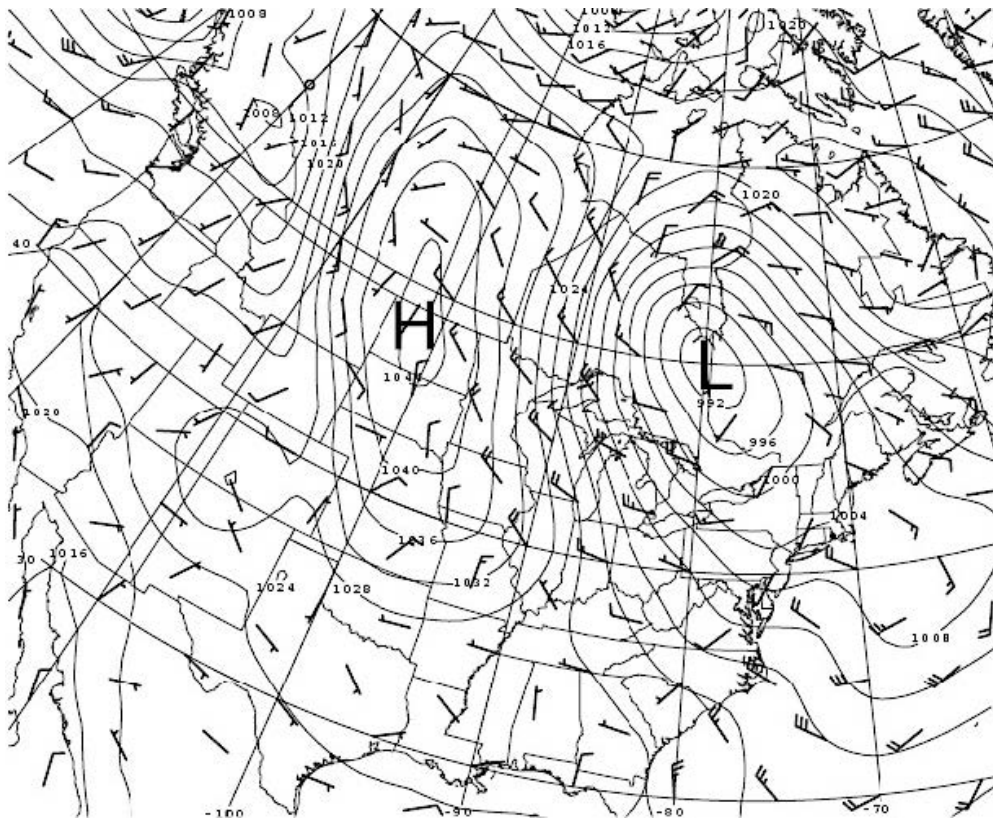
Figure 1.2: Surface pressure field and surface wind on 10th February 2008 at 12GMT. The contour interval is 4mbar. High and low pressure systems are marked as H and L. The dark segments represent wind arrows, whose arrowhead is not drawn in meteorological plots, by convention. The reader should imagine arrowhead at the end of segment that has no quivers. The quivers are drawn at only one side, at the tail end. The wind blows in the direction of the quiver base to the arrowhead. One full quiver represents a wind of 5m/s.

1.3   Elimination of the pressure term

Taking the curl of the Navier-Stokes equation results in the elimination of pressure. This is especially easy to see if 2D Cartesian flow is assumed ($w = 0$ and no dependence of anything on z), where the equations reduce to:

$$\rho \left(\frac{\partial u}{\partial t} + u\frac{\partial u}{\partial x} + v\frac{\partial u}{\partial y} \right) = -\frac{\partial p}{\partial x} + \mu \left(\frac{\partial^2 u}{\partial x^2} + \frac{\partial^2 u}{\partial y^2} \right) \tag{1.13}$$

$$\rho \left(\frac{\partial v}{\partial t} + u\frac{\partial v}{\partial x} + v\frac{\partial v}{\partial y} \right) = -\frac{\partial p}{\partial y} + \mu \left(\frac{\partial^2 v}{\partial x^2} + \frac{\partial^2 v}{\partial y^2} \right) \quad . \tag{1.14}$$

Differentiating the first with respect to y, the second with respect to x and subtracting the resulting equations will eliminate pressure and any potential force. Defining the stream function ψ through

$$u = \frac{\partial \psi}{\partial y} \quad ; \quad v = -\frac{\partial \psi}{\partial x} \tag{1.15}$$

results in mass continuity being unconditionally satisfied (given the stream function is continuous), and then incompressible Newtonian 2D momentum and mass conservation degrade into one equation:

$$\frac{\partial}{\partial t} \left(\nabla^2 \psi \right) + \frac{\partial \psi}{\partial y}\frac{\partial}{\partial x} \left(\nabla^2 \psi \right) - \frac{\partial \psi}{\partial x}\frac{\partial}{\partial y} \left(\nabla^2 \psi \right) = \nu \nabla^4 \psi \tag{1.16}$$

or using the total derivative

$$D_t \left(\nabla^2 \psi \right) = \nu \nabla^4 \psi \tag{1.17}$$

where ∇^4 is the (2D) biharmonic operator and ν is the kinematic viscosity $\nu = \frac{\mu}{\rho}$. This single equation together with appropriate boundary conditions describes 2D fluid flow, taking only kinematic viscosity as a parameter. Note that the equation for creeping flow results when the left

side is assumed zero. In axisymmetric flow another stream function formulation, called the Stokes stream function, can be used to describe the velocity components of an incompressible flow with one scalar function. The concept of taking the curl of the flow will become very important in ocean dynamics (section 3.7). The term $\zeta = \nabla^2 \psi$ is called relative vorticity, its dynamics can be described as

$$D_t \zeta = \nu \nabla^2 \zeta \quad . \tag{1.18}$$

1.4 Non-dimensional parameters: The Reynolds number

For the case of an incompressible flow in the Navier-Stokes equations, assuming the temperature effects are negligible and external forces are neglected, they consist of conservation of mass

$$\nabla \cdot \mathbf{u} = 0 \tag{1.19}$$

and conservation of momentum (1.8).

$$\partial_t \mathbf{u} + (\mathbf{u} \cdot \nabla)\mathbf{u} = -\frac{1}{\rho_0}\nabla p + \nu \nabla^2 \mathbf{u} \tag{1.20}$$

where $\mathbf{u}$ is the velocity vector and p is the pressure, ν denotes the kinematic viscosity. The equations can be made dimensionless by a length-scale L, determined by the geometry of the flow, and by a characteristic velocity U. For inter-comparison of analytical solutions, numerical results, and of experimental measurements, it is useful to report the results in a dimensionless system. This is justified by the important concept of dynamic similarity (Buckingham [1914]). The main goal for using this system is to replace physical or numerical parameters with some dimensionless numbers, which completely determine the dynamical behavior of the system[4]. The procedure for converting

---

[4]It is this fact that allows engineers to make solid predictions of how a large-scale system would perform based on a miniature model. The dimensionless quantities can often be kept constant when the size of the system is changed by using a fluid with a different viscosity during the tests. The miniature and the "real" flows are then equivalent. The Buckingham π theorem is a key theorem in dimensional analysis. It is a formalization of Rayleigh's method of

to this system first implies, first of all, the selection of some representative values for the physical quantities involved in the original equations (in the physical system). For our current problem, we need to provide representative values for velocity (U), time (T), distances (L). From these, we can derive scaling parameters for the time-derivatives and spatial-gradients also. Using these values, the values in the dimensionless-system (written with subscript d) can be defined:

$$u = U \cdot u_d \tag{1.21}$$

$$t = T \cdot t_d \tag{1.22}$$

$$x = L \cdot x_d \tag{1.23}$$

with $U = L/T$. From these scalings, we can also derive

$$\partial_t = \frac{\partial}{\partial t} = \frac{1}{T} \cdot \frac{\partial}{\partial t_d} \tag{1.24}$$

$$\partial_x = \frac{\partial}{\partial x} = \frac{1}{L} \cdot \frac{\partial}{\partial x_d} \tag{1.25}$$

Note furthermore the units of $[\rho_0] = kg/m^3$, $[p] = kg/(ms^2)$, and $[p]/[\rho_0] = m^2/s^2$. Therefore the pressure gradient term in (1.8) has the scaling U^2/L. Furthermore, devide the equation (1.8) by U^2/L and the scalings vanish completely in front of the terms except for the $\nabla_d^2 \mathbf{u_d}$-term! This procedure yields therefore for (1.19,1.20):

$$\nabla_d \cdot \mathbf{u_d} = 0 \tag{1.26}$$

---

dimensional analysis. Loosely, the theorem states that if there is a physically meaningful equation involving a certain number n of physical variables, then the original equation can be rewritten in terms of a set of $p = n - k$ dimensionless parameters constructed from the original variables where k is the number of physical dimensions involved. For the system (1.19,1.20), $n = 4$ for velocity, density, pressure, ν; $k = 3$ for mass, length and time; $p = 4 - 3 = 1$ one dimensionless parameter, the Reynolds number.

and conservation of momentum

$$\frac{\partial}{\partial t_d}\mathbf{u_d} + (\mathbf{u_d} \cdot \boldsymbol{\nabla}_d)\mathbf{u_d} = -\boldsymbol{\nabla}_d p_d + \frac{1}{Re}\boldsymbol{\nabla}_d^2\mathbf{u_d} \tag{1.27}$$

The dimensionless parameter $\boldsymbol{Re} = \boldsymbol{UL}/\boldsymbol{\nu}$ is the Reynolds number and the only parameter left! For large Reynolds numbers, the flow is turbulent. In most practical flows $\boldsymbol{Re}$ is rather large $(\mathbf{10^4} - \mathbf{10^8})$, large enough for the flow to be turbulent. A large Reynolds number allows the flow to develop steep gradients locally. The typical length-scale corresponding to these steep gradients can become so small that viscousity is not negligible. So the dissipation takes place at small scales. In this way different lengthscales are present in a turbulent flow, which range from L to the Kolmogorov length scale. This length scale is the typical length of the smallest eddy present in a turbulent flow. In the climate system, this dissipation by turbulence is modeled via eddy terms.

In the literature, the term "equations have been made dimensionless", means that this procedure is applied and the subscripts d are dropped.

Remark: For inter-comparison of analytical solutions, numerical results, and of experimental measurements, it is useful to report the results in a dimensionless system. The main goal for using this system is to replace physical or numerical parameters with some dimensionless numbers, which completely determine the dynamical behavior of the system.

Exercise 4   –   Repeat: Concept of dynamic similarity
1. Show: The equations (1.19,1.20) can be made dimensionless by a length-scale L, determined by the geometry of the flow, and by a characteristic velocity U.
2. What is the charateristic number? Discuss that it is $\frac{\text{Convective Inertial Force}}{\text{Shear Force}}$. When the number is large, it shows that the flow is dominated by convective inertial effects. When the number is small, it shows that the flow is dominated by shear effects.
3. Please start from the potential vorticity dynamics (1.18) instead of (1.19,1.20). Derive the non-dimensionalized potential vorticity dynamics.

Remark: Later we will include the Coriolis effect (exercise 26).

1.5 Characterising flows by dimensionless numbers

The advantage of dimensionless numbers is that they make model experiments possible: one has to make the dimensionless numbers which are important for the specific experiment equal for both model and the real situation. One can also deduce functional equalities without solving the differential equations. Some dimensionless numbers are given by:

$$\text{Strouhal:}\quad \mathbf{Sr} = \frac{\omega L}{v} \qquad \text{Froude:}\quad \mathbf{Fr} = \frac{v^2}{gL} \qquad \text{Mach:}\quad \mathbf{Ma} = \frac{v}{c}$$

$$\text{Fourier:}\quad \mathbf{Fo} = \frac{a}{\omega L^2} \qquad \text{Péclet:}\quad \mathbf{Pe} = \frac{vL}{a} \qquad \text{Reynolds:}\quad \mathbf{Re} = \frac{vL}{\nu}$$

$$\text{Prandtl:}\quad \mathbf{Pr} = \frac{\nu}{a} \qquad \text{Nusselt:}\quad \mathbf{Nu} = \frac{L\alpha}{\kappa} \qquad \text{Eckert:}\quad \mathbf{Ec} = \frac{v^2}{c\Delta T}$$

Here, $\nu = \eta/\varrho$ is the *kinematic viscosity*, c is the speed of sound and L is a characteristic length of the system. α follows from the equation for heat transport $\kappa\partial_y T = \alpha\Delta T$ and $a = \kappa/\varrho c$ is the thermal diffusion coefficient.

These numbers can be interpreted as follows:

- Re: (stationary inertial forces)/(viscous forces)

- Sr: (non-stationary inertial forces)/(stationary inertial forces)

- Fr: (stationary inertial forces)/(gravity)

- Fo: (heat conductance)/(non-stationary change in enthalpy)

- Pe: (convective heat transport)/(heat conductance)

- Ec: (viscous dissipation)/(convective heat transport)

- Ma: (velocity)/(speed of sound): objects moving faster than approximately Ma = 0,8 produce shockwaves which propagate with an angle θ with the velocity of the object. For this angle holds Ma$= 1/\arctan(\theta)$.

- Pr and Nu are related to specific materials.

Now, the dimensionless Navier-Stokes equation becomes, with $x_d = x/L$, $\vec{v}_d = \vec{v}/V$, $\nabla_d = L\nabla_d$, $\nabla_d^2 = L^2\nabla^2$ and $t_d = t\omega$:

$$\text{Sr}\frac{\partial \vec{v}_d}{\partial t_d} + (\vec{v}_d \cdot \nabla_d)\vec{v}_d = -\nabla_d p_d + \frac{\vec{g}}{\text{Fr}} + \frac{\nabla_d^2 \vec{v}_d}{\text{Re}} \qquad (1.28)$$

1.6   Dynamic similarity: Application in engineering*

Engineering models are used to study complex fluid dynamics problems where calculations and computer simulations are not reliable. Models are usually smaller than the final design, but not always. Scale models allow testing of a design prior to building, and in many cases are a critical step in the development process. Construction of a scale model, however, must be accompanied by an analysis to determine what conditions it is tested under. While the geometry may be simply scaled, other parameters, such as pressure, temperature or the velocity and type of fluid may need to be altered. Similitude is achieved when testing conditions are created such that the test results are applicable to the real design. The following criteria are required:

1. Geometric similarity: The model is the same shape as the application, usually scaled.
2. Kinematic similarity: Fluid flow of both the model and real application must undergo similar time rates of change motions. (fluid streamlines are similar)
3. Dynamic similarity: Ratios of all forces acting on corresponding fluid particles and boundary surfaces in the two systems are constant.

Dimensional analysis is used to express the system with as few independent variables and as many dimensionless parameters as possible. The values of the dimensionless parameters are held to be the same for both the scale model and application. The design of marine vessels remains more of an art than a science in large part because dynamic similitude is especially difficult to attain for a vessel that is partially submerged: a ship is affected by wind forces in the air above it, by hydrodynamic forces within the water under it, and especially by wave motions at the interface

Variable	Application	Scaled model	Units
L (diameter of submarine)	1	1/40	(m)
V (speed)	5	calculate	(m/s)
ρ (density)	1028	988	$(kg/m3)$
μ (dynamic viscosity)	$1.88 \cdot 10^{-3}$	$1.0 \cdot 10^{-3}$	$Pa \cdot s(Ns/m^2)$
F (force)	calculate	to be measured	N (kgm/s^2)

Table 1.2: Table shows the typical scales for the submarine model.

between the water and the air. The scaling requirements for each of these phenomena differ, so models cannot replicate what happens to a full sized vessel nearly so well as can be done for an aircraft or submarin–each of which operates entirely within one medium.

As an example, consider a submarine modeled at 1/40th scale. The application operates in sea water at $0.5°C$, moving at $5m/s$. The model will be tested in fresh water at $20°C$. Find the power required for the submarine to operate at the stated speed. A free body diagram is constructed and the relevant relationships of force and velocity are formulated. The variables which describe the system are listed in Table 1.2. This example has five independent variables and three fundamental units. The fundamental units are: metre, kilogram, second. Invoking the Buckingham π theorem shows that the system can be described with two dimensionless numbers and one independent variable. Dimensional analysis is used to re-arrange the units to form the Reynolds number (Re) and so-called pressure coefficient (pc). The pressure coefficient is a parameter for studying the flow of incompressible fluids such as water, and also the low-speed flow of compressible fluids such as air. The relationship between the dimensionless coefficient and the dimensional numbers is

$$pc = \frac{p - p_\infty}{\frac{1}{2}\rho_\infty V_\infty^2} = \frac{p - p_\infty}{p_0 - p_\infty} \tag{1.29}$$

where:

p is the static pressure at the point at which pressure coefficient is being evaluated

p_∞ is the static pressure in the freestream (i.e. remote from any disturbance)

p_0 is the stagnation pressure in the freestream (i.e. remote from any disturbance)

ρ_∞ is the freestream fluid density

V_∞ is the freestream velocity of the fluid, or the velocity of the body through the fluid.

Scaling laws:

$$Re = \left(\frac{\rho V L}{\mu}\right) \qquad\qquad \longrightarrow V_{\text{model}} = V_{\text{application}} \times \left(\frac{\rho_a}{\rho_m}\right) \times \left(\frac{L_a}{L_m}\right) \times \left(\frac{\mu_m}{\mu_a}\right)$$
$$(1.30)$$

$$pc = \left(\frac{2\Delta p}{\rho V^2}\right), F = \Delta p L^2 \quad \longrightarrow F_{\text{application}} = F_{\text{model}} \times \left(\frac{\rho_a}{\rho_m}\right) \times \left(\frac{V_a}{V_m}\right)^2 \times \left(\frac{L_a}{L_m}\right)^2 .$$
$$(1.31)$$

The pressure (p) is not one of the five variables, but the force (F) is. The pressure difference has thus been replaced with (F/L^2) in the pressure coefficient. This gives a required test velocity of:

$$V_{\text{model}} = V_{\text{application}} \times 21.9.$$

A model test is then conducted at that velocity and the force that is measured in the model (F_{model}) is then scaled to find the force that can be expected for the real application $(F_{application})$:

$$F_{\text{application}} = F_{\text{model}} \times 3.44$$

The power P in Watt required by the submarine is then:

$$P[\text{W}] = F_{\text{application}} \times V_{\text{application}} = F_{\text{model}}[\text{N}] \times 17.2 \text{ m/s}$$

Note that even though the model is scaled smaller, the water velocity needs to be increased for testing. This remarkable result shows how similitude in nature is often counterintuitive.

Similitude has been well documented for a large number of engineering problems and is the basis of many textbook formulas and dimensionless quantities. These formulas and quantities are easy to use without having to repeat the laborious task of dimensional analysis and formula

derivation. Similitude can be used to predict the performance of a new design based on data from an existing, similar design. In this case, the model is the existing design. Another use of similitude and models is in validation of computer simulations with the ultimate goal of eliminating the need for physical models altogether. Another application of similitude is to replace the operating fluid with a different test fluid. Wind tunnels, for example, have trouble with air liquefying in certain conditions so helium is sometimes used. Other applications may operate in dangerous or expensive fluids so the testing is carried out in a more convenient substitute.

1.7 Integral and differential formulation of fluid mechanics*

On a volume work two types of forces:

1. The force $\vec{F}$ on each volume element. For gravity holds: $\vec{F} = \varrho\vec{g}$.

2. Surface forces working only on the margins: $\vec{t}$. For these holds: $\vec{t} = \vec{n}\,\sigma$, where σ is the *stress tensor*.

σ can be split in a part $p\,\mathsf{I}$ representing the normal tensions and a part $\mathbb{T}$ representing the shear stresses: $\sigma = \mathbb{T} + p\,\mathsf{I}$, where I is the unit tensor or identity matrix. When viscous aspects can be ignored holds:

$$div\,\sigma = -\nabla p \quad . \tag{1.32}$$

When the flow velocity is $\vec{v}$ at position $\vec{r}$ holds on position $\vec{r} + d\vec{r}$:

$$\vec{v}(\vec{r} + d\vec{r}) = \underbrace{\vec{v}(\vec{r})}_{\text{translation}} + \underbrace{d\vec{r} \cdot (\nabla\vec{v})}_{\text{rotation, deformation, dilatation}}$$

The quantity $\mathsf{L} := \nabla\vec{v}$ can be split in a symmetric part D and an antisymmetric part W. $\mathsf{L} = \mathsf{D} + \mathsf{W}$

with

$$D_{ij} := \frac{1}{2}\left(\frac{\partial v_i}{\partial x_j} + \frac{\partial v_j}{\partial x_i}\right) \quad , \quad W_{ij} := \frac{1}{2}\left(\frac{\partial v_i}{\partial x_j} - \frac{\partial v_j}{\partial x_i}\right)$$

When the rotation or *vorticity* $\vec{\omega} = \mathrm{rot}\vec{v}$ is introduced holds: $W_{ij} = \frac{1}{2}\varepsilon_{ijk}\omega_k$. $\vec{\omega}$ represents the local rotation velocity: $\vec{dr} \cdot \mathsf{W} = \frac{1}{2}\omega \times \vec{dr}$.

For a *Newtonian liquid* holds: $\mathbb{T} = 2\eta\mathsf{D}$. Here, η is the dynamical viscosity. This is related to the shear stress τ by:

$$\tau_{ij} = \eta\frac{\partial v_i}{\partial x_j}$$

For compressible media can be stated: $\mathbb{T} = (\eta'\mathrm{div}\vec{v})\mathsf{I} + 2\eta\mathsf{D}$. From equating the thermodynamical and mechanical pressure it follows: $3\eta' + 2\eta = 0$. If the viscosity is constant holds: $\mathrm{div}(2\mathsf{D}) = \nabla^2\vec{v} + \mathrm{grad\ div}\vec{v}$.

The conservation laws for mass, momentum and energy for continuous media can be written in both integral and differential form. They are:

Integral notation:

1. Conservation of mass: $\dfrac{\partial}{\partial t}\iiint \varrho d^3V + \oiint \varrho(\vec{v} \cdot \vec{n})d^2A = 0$

2. Conservation of momentum: $\dfrac{\partial}{\partial t}\iiint \varrho\vec{v}d^3V + \oiint \varrho\vec{v}(\vec{v} \cdot \vec{n})d^2A = \iiint \vec{f_0}d^3V + \oiint \vec{n} \cdot T d^2A$

3. Conservation of energy: $\dfrac{\partial}{\partial t}\iiint (\frac{1}{2}v^2 + e)\varrho d^3V + \oiint (\frac{1}{2}v^2 + e)\varrho(\vec{v} \cdot \vec{n})d^2A =$

$$- \oiint (\vec{q} \cdot \vec{n})d^2A + \iiint (\vec{v} \cdot \vec{f_0})d^3V + \oiint (\vec{v} \cdot \vec{n}\,\mathsf{T})d^2A$$

Differential notation:

1. Conservation of mass: $\dfrac{\partial \varrho}{\partial t} + \mathrm{div} \cdot (\varrho\vec{v}) = 0$

2. Conservation of momentum: $\varrho\dfrac{\partial\vec{v}}{\partial t} + (\varrho\vec{v} \cdot \nabla)\vec{v} = \vec{f_0} + \mathrm{div}\mathsf{T} = \vec{f_0} - \mathrm{grad}p + \mathrm{div}\mathsf{T}'$

3. Conservation of energy: $\varrho T \dfrac{ds}{dt} = \varrho \dfrac{de}{dt} - \dfrac{p}{\varrho} \dfrac{d\varrho}{dt} = -\operatorname{div}\vec{q} + \mathbb{T} : \mathsf{D}$

Here, e is the internal energy per unit of mass E/m and s is the entropy per unit of mass S/m. $\vec{q} = -\kappa\vec{\nabla}T$ is the heat flow. Further holds:

$$p = -\frac{\partial E}{\partial V} = -\frac{\partial e}{\partial 1/\varrho} \quad, \quad T = \frac{\partial E}{\partial S} = \frac{\partial e}{\partial s}$$

so

$$C_V = \left(\frac{\partial e}{\partial T}\right)_V \quad \text{and} \quad C_p = \left(\frac{\partial h}{\partial T}\right)_p$$

with $h = H/m$ the enthalpy per unit of mass.

From this one can derive the *Navier-Stokes* equations for an incompressible, viscous and heat-conducting medium:

$$\operatorname{div}\vec{v} = 0$$
$$\varrho\frac{\partial \vec{v}}{\partial t} + \varrho(\vec{v}\cdot\nabla)\vec{v} = \varrho\vec{g} - \operatorname{grad}p + \eta\nabla^2\vec{v}$$
$$\varrho C\frac{\partial T}{\partial t} + \varrho C(\vec{v}\cdot\nabla)T = \kappa\nabla^2 T + 2\eta\mathsf{D} : \mathsf{D}$$

with C the thermal heat capacity. The force $\vec{F}$ on an object within a flow, when viscous effects are limited to the boundary layer, can be obtained using the momentum law. If a surface A surrounds the object outside the boundary layer holds:

$$\vec{F} = -\oiint [p\vec{n} + \varrho\vec{v}(\vec{v}\cdot\vec{n})]d^2A$$

1.8   Transport phenomena*

As preparation of the course, you may repeat several mathematical formulations. It is important

to notice that the fluid dynamical equations are generally formulated as a transport phenomenon.

An important relation is: if X is a quantity of a volume element which travels from position $\vec{r}$ to

$\vec{r} + d\vec{r}$ in a time dt, the total differential dX is then given by:

$$
\begin{aligned}
dX &= \frac{\partial X}{\partial x}dx + \frac{\partial X}{\partial y}dy + \frac{\partial X}{\partial z}dz + \frac{\partial X}{\partial t}dt \\
&\Rightarrow \\
\frac{dX}{dt} &= \frac{\partial X}{\partial x}v_x + \frac{\partial X}{\partial y}v_y + \frac{\partial X}{\partial z}v_z + \frac{\partial X}{\partial t}
\end{aligned}
\tag{1.33}
$$

This results in general to: $\dfrac{dX}{dt} = \dfrac{\partial X}{\partial t} + (\vec{v} \cdot \nabla)X$.

From this follows that also holds:

$$
\frac{d}{dt} \iiint X d^3V = \frac{\partial}{\partial t} \iiint X d^3V + \oiint X(\vec{v} \cdot \vec{n})d^2A
\tag{1.34}
$$

where the volume V is surrounded by surface A. Some properties of the ∇ operator are:

$$\text{div}(\phi\vec{v}) = \phi\text{div}\vec{v} + \nabla\phi \cdot \vec{v} \qquad \text{rot}(\phi\vec{v}) = \phi\text{rot}\vec{v} + (\nabla\phi) \times \vec{v} \qquad \text{rot}\nabla\phi = \vec{0}$$

$$\text{div}(\vec{u} \times \vec{v}) = \vec{v} \cdot (\text{rot}\vec{u}) - \vec{u} \cdot (\text{rot}\vec{v}) \qquad \text{rot rot}\vec{v} = \nabla\, \text{div}\vec{v} - \nabla^2\vec{v} \qquad \text{div rot}\tilde{v} = 0$$

$$\text{div}\, \nabla\phi = \nabla^2\phi \qquad\qquad\qquad \nabla^2\vec{v} \equiv (\nabla^2v_1, \nabla^2v_2, \nabla^2v_3)$$

Here, $\vec{v}$ is an arbitrary vector field and ϕ an arbitrary scalar field. Some important integral theorems are:

Gauss:
$$\oiint (\vec{v} \cdot \vec{n})d^2A = \iiint (\mathrm{div}\vec{v})d^3V$$

Stokes for a scalar field:
$$\oint (\phi \cdot \vec{e}_{\mathrm{t}})ds = \iint (\vec{n} \times \nabla\phi)d^2A$$

Stokes for a vector field:
$$\oint (\vec{v} \cdot \vec{e}_{\mathrm{t}})ds = \iint (\mathrm{rot}\vec{v} \cdot \vec{n})d^2A$$

This results in:
$$\oiint (\mathrm{rot}\vec{v} \cdot \vec{n})d^2A = 0$$

Ostrogradsky:
$$\oiint (\vec{n} \times \vec{v})d^2A = \iiint (\mathrm{rot}\vec{v})d^3A$$

$$\oiint (\phi\vec{n})d^2A = \iiint (\nabla\phi)d^3V$$

Here, the orientable surface $\iint d^2A$ is limited by the Jordan curve $\oint ds$.

Exercise 5   –   Self test

1. Given
$$f(x, y, z, t) = x^2 + y^2 + z^2 \sin(\omega t).$$

    What are the partial derivatives with respect to the variables x and t?

2. What is the definition of ∇, Laplace, divergence, total (substantial) derivative, total differential for a function $f(x, y, z, t)$?

3. Calculate the rotation of ∇f.

4. Given the function $g(x) = ax^2 - 3x^4 + 2x \sin(\alpha x)$, please provide the Taylor expansion of g around $x = 0$ up to the 3rd order in x !

5. In the atmosphere, ocean, ice system, we are dealing with forces. Please list some relevant real and apparent forces.

6. What is the differential equation describing radioactive decay? Please provide also the solution with initial condition $x(t = 0) = x_0$. How is the half-life time defined?

7. The potential temperature of a parcel of fluid at pressure p is the temperature that the parcel would acquire if adiabatically brought to a standard reference pressure p_0, usually 100 kPa. The potential temperature of air is often given by

$$\Theta = T \, (p_0/p)^{R/c_p}$$

where T is the current absolute temperature of the parcel, R is the gas constant of air, and c_p is the specific heat capacity at a constant pressure. $\kappa = R/c_p = 2/7$ for an ideal diatomic gas. For a constant lapse rate $\frac{dT}{dz} = \gamma = const.$, why does the potential temperature Θ increase with height? Hint: Atmospheric pressure decreases with height.

Exercise 6   –   Nabla

Calculate the following operations for the function

$$f(x, y, z) = x^3 + 3x - 4xz + z^4 \quad : \tag{1.35}$$

a)∇f,

b) calculate the divergence of the result!

c) Calculate the rotation of ∇f!

1.9 Rheology of ice*

Rheology is the study of the flow of matter, primarily in a liquid state, but also as 'soft solids' or solids under conditions in which they respond with plastic flow rather than deforming elastically in response to an applied force. It applies to substances which have a complex microstructure, such as muds, sludges, suspensions, polymers and other glass formers (e.g., silicates), as well as many foods and additives, bodily fluids (e.g., blood) and other biological materials or other materials which belong to the class of soft matter.

Newtonian fluids can be characterized by a single coefficient of viscosity for a specific temperature. Although this viscosity will change with temperature, it does not change with the strain rate. Only a small group of fluids exhibit such constant viscosity. The large class of fluids whose viscosity changes with the strain rate (the relative flow velocity) are called non-Newtonian fluids (http://en.wikipedia.org/wiki/Non-Newtonian_fluid).

Rheology generally accounts for the behavior of non-Newtonian fluids, by characterizing the minimum number of functions that are needed to relate stresses with rate of change of strain or strain rates. For example, ketchup can have its viscosity reduced by shaking (or other forms of mechanical agitation, where the relative movement of different layers in the material actually causes the reduction in viscosity) but water cannot. Ketchup is a shear thinning material, like yoghurt and emulsion paint, exhibiting thixotropy, where an increase in relative flow velocity will cause a reduction in viscosity, for example, by stirring. Some other non-Newtonian materials show the opposite behavior: viscosity going up with relative deformation, which are called shear thickening or dilatant materials. Since Sir Isaac Newton originated the concept of viscosity, the study of liquids with strain rate dependent viscosity is also often called Non-Newtonian fluid mechanics.

Other elements of the Earth system like the cryosphere are described by using concepts of continuum mechanics. As for the atmosphere and ocean, land ice or sea ice dynamics are based on the balance laws of mass, momentum, angular momentum, energy and some material properties. In order to get the field equations some constitutive relations are needed for land ice or sea ice. It is not intuitive that sea ice can be described as a continous fluid, but the ensemble of ice pieces

follows a continuum.

Land ice dynamics

Glacier flow is described by using concepts of continuum mechanics. As for the atmosphere and ocean, the model is based on the balance laws of mass, momentum, angular momentum, energy and some material properties. The density ρ does not change under conditions of interest to us, therefore:

$$\nabla \cdot \mathbf{v} = \mathbf{0}. \tag{1.36}$$

The Cauchy momentum equation is (1.2). Due to the fact that Froude number for ice flow is extremely small, the acceleration term $\rho \, D_t \mathbf{v}$ is neglected and we are left with the very simple statement that the gravitational driving force is balanced by forces resulting from the stresses:

$$\mathbf{0} = -\nabla p + \nabla \cdot \mathbf{T} + \rho g e_z \quad . \tag{1.37}$$

Let us denote ϵ as the internal energy per unit mass. q_{sl} is the sum of sensible and latent heat flux and r is the radiant power per unit mass.

$$\rho \dot{\epsilon} = -\operatorname{div} q_{sl} + \rho r + tr(\mathbf{TD}) \tag{1.38}$$

D = sym grad v and is called the material displacement gradient tensor. In general the energy balance is:

$$\rho \dot{\eta} = -\operatorname{div} \phi^\eta + \rho s + \rho \gamma \tag{1.39}$$

where η is entropy per unit mass, ϕ is the entropy-flux and γ the entropy production per unit mass. Note that entropy is not conserved but according to the second law of thermodynamics is always positive.

In order to get the field equations some constitutive relations are needed. There are three

constitutive relations: one for the stress-material displacement-relation, one for internal Energy and one for heat-flux q:

$$D = EA(T')f(\sigma)T^R \text{ with } \sigma := \sqrt{\frac{1}{2}tr(T^R)^2} \tag{1.40}$$

$$\dot{\epsilon} = c(T)\dot{T} \tag{1.41}$$

$$q = -\kappa(T)\,\mathrm{grad}\,T \tag{1.42}$$

with general temperature depended heat c and thermal conductivity κ. The first equation describes the fluidity of the ice as a fuction of $A(T')$ with the "rate- factor" of the homologous temperature T', the function $f(\sigma)$ "creep" of the normal stress σ. The homologous temperature T' is defined by $T' = T - T_M$, where T_M is the pressure-depended melting temperature of ice. The creep function after Glen's flow-law ?.

$$f(\sigma) = f_t(\sigma) = \sigma^{n-1} \text{ with } n = 3 \tag{1.43}$$

rate-factor for cold ice: Arrhenius-law ?:

$$A(T') = A_0 e^{-Q/R(T0+T')} \tag{1.44}$$

The second equation (1.41) conects changes of internal energy with temperature and the last equation is Fourier's law of heat conduction. Neglecting r, the radiant power, leads to the energy balance:

$$\rho\dot{\epsilon} = -\,\mathrm{div}\,q + tr(T^R D) \tag{1.45}$$

where T^R is the frictional part in $T = -p1 + T^R$

With the three constitutive relation eqn. 1.45 leads to

$$\rho c\dot{T} = \mathrm{div}(\kappa\,\mathrm{grad}\,T) + 2EA(T')f(\sigma)\sigma^2 \tag{1.46}$$

This is the local temperature-balance with advection, heat transfer and dissipative heat production.
The equations of the ice sheet are to complex to be solved numerically. Furthermore, some scaling
is needed. Most of todays three-dimensional ice sheet model are using the so-called "shallow ice
approximation" (SIA) **?**, which is valid for ice-masses where $H << L$, i.e. ice thickness is small
compared to the horizontal dimension. The model equations are scaled with respect to the aspect
ration ϵ (ratio of typical thickness to typical length) and only lowest-order terms are kept. Flow
is dominated by internal shear deformation, ice flow is driven by gravity and vertical shearing is
concentrated close to bedrock **?**.

links: http://pism-docs.org/wiki/lib/exe/fetch.php?media=manual.pdf

Ice thickness

$$\frac{\partial H}{\partial t} = \frac{\partial (h - b)}{\partial t} = -\frac{\partial q_x}{\partial x} - \frac{\partial q_y}{\partial y} + a_s^\perp - \frac{\mathcal{P}_b^w}{\rho} \tag{1.47}$$

where t is the time; h the z-coordinate of the ice surface; b the z-coordinate of the ice base; H is
the ice thickness, q are the horizontal components of mass flux; $a_s^\perp$ the surface mass balance; $\mathcal{P}_b^w$
is the basal melting rate.

Lithosphere response to ice load

$$\frac{\partial b}{\partial t} = -\frac{1}{\tau_v} \left[b - \left(b_0 - \frac{\rho}{\rho_a} H \right) \right] \tag{1.48}$$

wher τ_v is the time lag for the lithosphere response; b_0 the postion b for relaxed lithosphere
surface without ice load; and ρ_a the density of the asthenosphere.

Age of the ice (cold and temperate ice regions)

$$\frac{\partial \mathcal{A}}{\partial t} + v_x \frac{\partial \mathcal{A}}{\partial x} + v_y \frac{\partial \mathcal{A}}{\partial y} + v_z \frac{\partial \mathcal{A}}{\partial z} = 1 \; \left(+D_A \frac{\partial^2 \mathcal{A}}{\partial z^2} \right) \tag{1.49}$$

where $\mathcal{A}$ is the age of the ice and D_A is the artificial numerical diffusity that is needed for reasons
of numerical stability.

Temperature (cold ice regions)

$$\frac{\partial T}{\partial t} + v_x\frac{\partial T}{\partial x} + v_y\frac{\partial T}{\partial y} + v_z\frac{\partial T}{\partial z} = \frac{1}{\rho c}\frac{\partial}{\partial z}\left(\kappa\frac{\partial T}{\partial z}\right) + \frac{2}{\rho c}EA(T')f(\sigma)\sigma^2 \qquad (1.50)$$

where T is the temperature; v_x, v_y, v_z are the components of ice velocity; c is the specific heat of ice.

Sea ice Dynamics

Land-fast ice, or simply fast ice, is sea ice that has frozen along coasts ("fastened" to them) or to the sea floor over shallow parts of the continental shelf, and extends out from land into sea. Unlike drift ice, it does not move with currents and wind. Drift ice consists of ice that floats on the surface of the water, as distinguished from the fast ice, attached to coasts. When packed together in large masses, drift ice is called pack ice. Pack ice may be either freely floating or blocked by fast ice while drifting past. The most important areas of pack ice are the polar ice packs formed from seawater in the Earth's polar regions: the Arctic ice pack of the Arctic Ocean and the Antarctic ice pack of the Southern Ocean. Polar packs significantly change their size during seasonal changes of the year. Because of vast amounts of water added to or removed from the oceans and atmosphere, the behavior of polar ice packs have a significant impact of the global changes in climate.

Sea ice is largely formed from ocean water that freezes. Because the oceans consist of salt-water, this occurs at about -1.8°C. Sea ice ice is one of the worlds's more complex materials. It is a conglomerate of fresh water crystals interlaced with inclusions of brine, air and salt which have formed between the crystals and crystal plates (Weeks and Ackley, 1986). In general, it is nonhomogeneous and anistotropic. Since component parts of sea ice are never in equilibrium the physical properties of sea ice are not constant. However, the manifistations of nonhomogeneity and anisotropy depend on the scale of the region of interest. On small scale (dimensions of of individual floes) the ice cover is homogeneous and highly anisotropic. On large scale (several hundred kilometers) the ice cover is nonhomogeneous and behaves practically as isotropic medium.

Figure 1.3: Arctic sea ice cover in summer: a view on RV Polarstern

Sea ice near shore is in one sense an extension of land as it remains quasi-immobile during the winter. Offshore ice is in perpetual motion, slowly twisting, turning, breaking into smaller pieces, compacting and rarefying. This motion is an extremely complex resultant of a combination of factors. These include wind stress, water stress, Coriolis force, tidal force, atmospheric pressure gradients, internal ice stress and resistance, boundary layer conditions and sea surface tilt. It has, however, been long recognized that ice drift is dependent primarily upon wind stress and secondly upon water stress (Thorndike and Colony, 1982).

The nature of sea ice deformation depends on its characteristic scale. Large-scale deformations with characteristic linear dimentions of the order of 100 km and more are determined mainly by external forces (internal forces are mostly balanced). Medium-scale deformations (10-20 km) are associated with the block structure of ice fields and determined by external as well as internal forces. Small-scale deformations (average diameter of single ice floe) are caused by interaction of individual ice floes (internal forces) and can be described in terms of a few basic deformation processes. During the passage of anomalous atmospheric-pressure fields, the internal forces in the sea ice field present one of the most hazardous conditions for constructions and ships in the sea-ice field.

Large scale deformation processes play the fundamental role in determining the distribution of ice thickness, which in itself controls heat and moisture fluxes between the ocean and atmosphere (Maykut, 1982). On a large scale, despite of discontinuities (cracks and fractures), the ice cover can be treated as continuous medium. That allows to apply well-developed rheological models to relate large scale deformations and internal forces. A realistic sea ice rheology must include the following general properties of sea ice cover (Häkkinen, 1987):

a) on large scale ice cannot support tension - openning occurs with nearly no stress;

b) with high compactness ice will resist more compression and shearing than with low compactness;

c) thick ice resists deformation more than thin ice;

c) the higher the compression is, the more ice will resist it (strain hardening).

Two different approaches were used to derive large-scale rheological properties (strength, viscositiy coefficients) of sea ice cover based on mechanics of basic deformation processes. The first one is based on linking the amount of energy consumed in basic compressive processes (rafting and ridging) to the large scale strength of the pack ice (Rothrock, 1975). Another approach appeals to self-similarity theory to determine scale-invariant parameters of deformation field (Erlingsson, 1988).

Viscous-plastic rheology is based on quasi-linear dependence between stress and strain rate (ice pack behaves as viscous fluid for small strain rates, whereas for large strain rates it flows in a plastic manner (Hibler, 1979). It has been demonstrated that if time and/or length scales are chosen large enough, then the averaging of nonlinear (plastic) stochastic fluctuations in sea ice deformation rates yields viscouslike law (Hibler, 1977).

Chapter 2

Fluid-dynamical Examples and Stability Theory

2.1 Potential flow

In fluid dynamics, potential flow describes the velocity field as the gradient of a scalar function: the velocity potential. As a result, a potential flow is characterized by an irrotational velocity field, which is a valid approximation for several applications. The irrotationality of a potential flow is due to the curl of a gradient always being equal to zero. In the case of an incompressible flow the velocity potential satisfies Laplace's equation. However, potential flows also have been used to describe compressible flows. The potential flow approach occurs in the modeling of both stationary as well as nonstationary flows.

A potential flow is described by means of a velocity potential, being a function of space and time. The flow velocity v is a vector field equal to the gradient of the velocity potential ϕ

$$\mathbf{v} = \boldsymbol{\nabla}\phi. \tag{2.1}$$

From vector calculus it is known, that the curl of a gradient is equal to zero:

$$\nabla \times \nabla \phi = 0, \tag{2.2}$$

and consequently the vorticity, the curl of the velocity field v, is zero:

$$\nabla \times \mathbf{v} = 0. \tag{2.3}$$

This implies that a potential flow is an irrotational flow. This has direct consequences for the applicability of potential flow. In flow regions where vorticity is known to be important, such as wakes and boundary layers, potential flow theory is not able to provide reasonable predictions of the flow. Fortunately, there are often large regions of a flow where the assumption of irrotationality is valid, which is why potential flow is used for various applications.[1]

In case of an incompressible flow[2] the velocity v has zero divergence:

$$\nabla \cdot \mathbf{v} = 0, \tag{2.4}$$

with the dot denoting the inner product. As a result, the velocity potential satisfies Laplace's equation

$$\nabla^2 \phi = 0 \quad . \tag{2.5}$$

In this case the flow can be determined completely from its kinematics: the assumptions of irrotationality and zero divergence of the flow. Dynamics only have to be applied afterwards, if one is interested in computing pressures: for instance for flow around airfoils through the use of Bernoulli's principle. In two dimensions, potential flow reduces to a very simple system that is analyzed using complex analysis (section 2.3).

---

[1] For instance in: flow around aircraft, groundwater flow, acoustics and water waves.
[2] for instance of a liquid, or a gas at low Mach numbers; but not for sound waves

2.1.1   Kelvin's circulation theorem

In fluid mechanics, Kelvin's circulation theorem states In a barotropic ideal fluid with conservative body forces, the circulation around a closed curve (which encloses the same fluid elements) moving with the fluid remains constant with time.

$$\frac{\mathrm{D}\Gamma}{\mathrm{D}t} = 0 \tag{2.6}$$

where the circulation Γ is the circulation around a material contour

$$\Gamma = \oint (\vec{v} \cdot \vec{e}_t) ds \tag{2.7}$$

The circulation is the line integral of the tangential component of velocity taken about a closed curve in the flow field. The integral is taken in a counterclockwise direction about the contour C and ds is a differential length along the contour. No singularities can lie directly on the contour. The origin (center) of the potential vortex is considered as a singularity point in the flow since the velocity goes to infinity at this point. If the contour encircles the potential vortex origin, the circulation will be non-zero. If the contour does not encircle any singularities, however, the circulation will be zero. Stated more simply this theorem says that if one observes a closed contour at one instant, and follows the contour over time (by following the motion of all of its fluid elements), the circulation over the two locations of this contour are equal. This theorem does not hold in cases with viscous stresses, nonconservative body forces (for example Coriolis force) or non-barotropic pressure-density relations.

In the case of a potential flow, the vorticity is zero (2.3), Kelvin's theorem can be derived using

$$\Gamma = \iint (\nabla \times \vec{v}) \cdot \vec{n} \, d^2 A = 0 \tag{2.8}$$

Exercise 7   –   **Circulation theorem**

Show (2.6) using that the governing equation for an inviscid fluid with a conservative body force is

$$\frac{\mathrm{D}\boldsymbol{u}}{\mathrm{D}t} = -\frac{1}{\rho}\boldsymbol{\nabla} p + \boldsymbol{\nabla}\Phi$$

where Φ is the potential for the body force.

Hint: Potential flow, Kelvin's theorem

2.1.2   Streamlines

For a 2-dimensional flow a flow function $\psi(x, y)$ can be defined: $u = \partial\psi/\partial y, v = -\partial\psi/\partial x$. With Ψ_{AB} the amount of liquid flowing through a curve s between the points A and B:

$$\Psi_{AB} = \int_A^B (\vec{v}\cdot\vec{n})ds = \int_A^B (u dy - v dx) \tag{2.9}$$

$$= \int_A^B d\psi = \psi(B) - \psi(A) \quad . \tag{2.10}$$

The lines of constant $\phi = 0$ are called potential lines of the flow.

$$d\phi = \frac{\partial\phi}{\partial x}dx + \frac{\partial\phi}{\partial y}dy = u dx + v dy \tag{2.11}$$

Since $d\phi = 0$ along a potential line, we have

$$\frac{dy}{dx} = -\frac{u}{v} \tag{2.12}$$

Recall that streamlines are lines everywhere tangent to the velocity,

$$\frac{dy}{dx} = \frac{u}{v} \tag{2.13}$$

so potential lines are perpendicular to the streamlines. For inviscid and irrotational flow is indeed quite pleasant to use potential function to represent the velocity field. As a point to note here, many texts use stream function instead of potential function as it is slightly more intuitive to consider a line that is everywhere tangent to the velocity.

2.2   Convection in the Rayleigh-Bénard system

Here, we shall introduce a system of three ordinary differential equations whose solutions afford the simplest example of deterministic flow that we are aware of. The system is a simplification of the one derived by Saltzman [1962], to study finite-amplitude convection. Although our present interest is in the non-periodic nature of its solutions rather than in its contributions to the convection problem, we shall describe its physical background briefly.
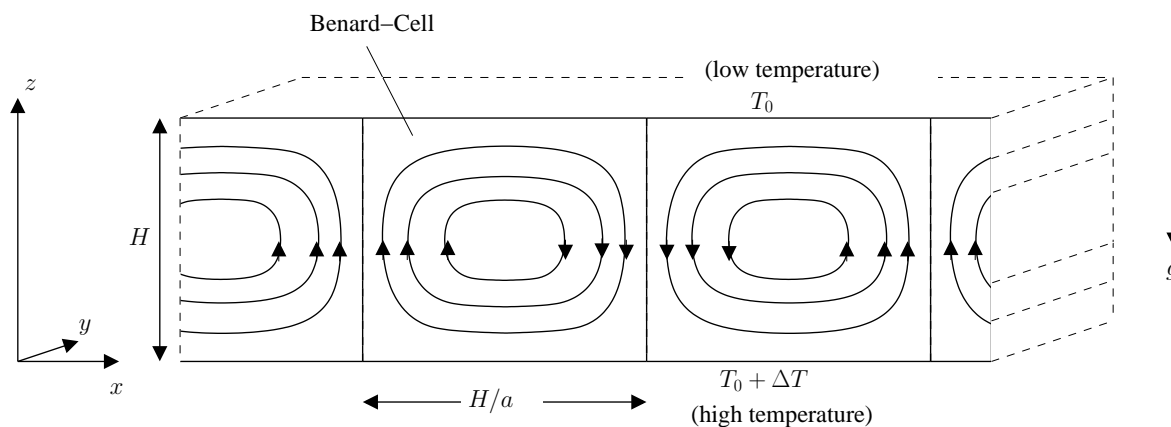
Figure 2.1: Geometry of the Rayleigh-Bénard system (see text for details).

Rayleigh [1916] studied the flow occurring in a layer of fluid of uniform depth $\boldsymbol{H}$, when the temperature difference between the upper- and lower-surfaces is maintained at a constant value

ΔT.

$$T(x, y, z = H) = T_0$$
$$T(x, y, z = 0) = T_0 + \Delta T \tag{2.14}$$

The Boussinesq approximation is used, which results in a buoyancy force term which couples the thermal and fluid velocity fields. Therefore

$$\rho \approx \rho_0 = const. \tag{2.15}$$

except in the buoyancy term, where:

$$\varrho = \varrho_0(1 - \alpha(T - T_0)) \text{ with } \alpha > 0 \quad . \tag{2.16}$$

ρ_0 is the fluid density in the reference state. This assumption reflects a common feature of geophysical flows, where the density fluctuations caused by temperature variations are small, yet they are the ones driving the overall flow. We have the following relations. Furthermore, we assume that the density depends linearly on temperature T.

For some experiments go to the trailer 1, trailer 2, trailer in German, KIT trailer: Rayleigh Benard Thermal Convection 3D Simulation.

This system possesses a steady-state solution in which there is no motion, and the temperature varies linearly with depth:

$$u = w = 0$$
$$T_{eq} = T_0 + \left(1 - \frac{z}{H}\right) \Delta T \tag{2.17}$$

When this solution becomes unstable, convection should develop.

2.2.1 Elimination of pressure and vorticity dynamics

In the case where all motions are parallel to the $x - z$-plane, and no variations in the direction of the y-axis occur, the governing equations may be written (see Saltzman [1962]) as:

$$D_t u = -\frac{1}{\rho_0}\partial_x p + \nu \nabla^2 u \tag{2.18}$$

$$D_t w = -\frac{1}{\rho_0}\partial_z p + \nu \nabla^2 w + g(1 - \alpha(T - T_0)) \tag{2.19}$$

$$D_t T = \kappa \nabla^2 T \tag{2.20}$$

$$\partial_x u + \partial_z w = 0 \tag{2.21}$$

where w and u are the vertical and horizontal components of the velocity[3], respectively. Furthermore, $\nu = \eta/\rho_0$, $\kappa = \lambda/(\rho_0 C_v)$ the momentum diffusivity (kinematic viscosity) and thermal diffusivity, respectively.

Now, compare the procedure with the elimination of the pressure term in section 1.3 where we derive the vorticity equation $D_t\left(\nabla^2\psi\right) = \nu\nabla^4\psi$. Here, it is useful to define the stream function Ψ for the two-dimensional motion, i.e.

$$\frac{\partial \Psi}{\partial x} = w \tag{2.22}$$

$$\frac{\partial \Psi}{\partial z} = -u \quad . \tag{2.23}$$

We take the

$$\frac{\partial}{\partial x}(2.19) - \frac{\partial}{\partial z}(2.18) = \frac{\partial}{\partial x}D_t w - \frac{\partial}{\partial z}D_t u = D_t\frac{\partial w}{\partial x} - D_t\frac{\partial u}{\partial z} \tag{2.24}$$

$$= = D_t\frac{\partial^2 \Psi}{\partial x^2} - D_t\frac{\partial^2 \Psi}{\partial z^2} = D_t\nabla^2\Psi \quad . \tag{2.25}$$

---

[3]Note that $D_t u = \partial_t u + u\partial_x u + w\partial_z u$, $D_t w = \partial_t w + u\partial_x w + w\partial_z w$, and $D_t T = .\partial_t T + u\partial_x T + w\partial_z T$

Note that $D_t \nabla^2 \Psi$ does not contain u, w anymore:

$$D_t \left(\nabla^2 \Psi \right) = \partial_t \nabla^2 \Psi - \frac{\partial \Psi}{\partial z} \frac{\partial \nabla^2 \Psi}{\partial x} + \frac{\partial \Psi}{\partial x} \frac{\partial \nabla^2 \Psi}{\partial z} \quad .$$

Furthermore, we introduce the function Θ as the departure of temperature from that occurring in the state of no convection (2.17):

$$T = T_{eq} + \Theta \tag{2.26}$$

In the temperature term in $\frac{\partial}{\partial x}$ (**2.19**) on the right hand side:

$$\frac{\partial}{\partial x} g(1 - \alpha(T_{eq} + \Theta - T_0)) = -g\alpha \frac{\partial}{\partial x} \Theta$$

The left hand side of (2.20) reads

$$D_t T = D_t T_{eq} + D_t \Theta = w \cdot \frac{-\Delta T}{H} + D_t \Theta = -\frac{\Delta T}{H} \frac{\partial \Psi}{\partial x} + D_t \Theta$$

Then, the dynamics can be formulated as

$$D_t \left(\nabla^2 \Psi \right) = \nu \nabla^4 \Psi - g\alpha \frac{\partial \Theta}{\partial x} \tag{2.27}$$

$$D_t \Theta = \frac{\Delta T}{H} \frac{\partial \Psi}{\partial x} + \kappa \nabla^2 \Theta \quad . \tag{2.28}$$

Non-dimensionalization of the problem yields equations including the dimensionless Prandtl number[4] σ and the Rayleigh number R_a which are the control parameters of the problem. One can

---

[4]The Prandtl number is a dimensionless number; the ratio of momentum diffusivity (kinematic viscosity) to thermal diffusivity. It is named after the German physicist Ludwig Prandtl. Note that whereas the Reynolds number and Grashof number are subscripted with a length scale variable, the Prandtl number contains no such length scale in its definition and is dependent only on the fluid and the fluid state. As such, the Prandtl number is often found in property tables alongside other properties such as viscosity and thermal conductivity. Typical values for are:
1) Low - thermal diffusivity dominant: 13.4 and 7.2 for seawater at $0°$ and $20°$ Celsius respectively.
2) High - momentum diffusivity dominant: For mercury, heat conduction is very effective compared to convection: thermal diffusivity is dominant. For engine oil, convection is very effective in transferring energy from an area,

take the layer thickness H as the length of unit, the time $T = H^2/\kappa$ of vertical diffusion of heat as the unit of time, and the temperature difference ΔT as the unit of temperature. See exercise 8 for the non-dimensionalization procedure.

Exercise 8 – **Non-dimensional Rayleigh-Bénard system**

Write down the non-dimensional version of the Rayleigh-Bénard. Non-dimensionalization yields equations including the dimensionless Prandtl number σ and the Rayleigh number R_a which is also the control parameter. One can take the layer thickness H as the length of unit, the time $T = H^2/\kappa$ of vertical diffusion of heat as the unit of time, $U = H/T = \kappa/H$ the unit of velocity, and the temperature difference ΔT as the unit of temperature. Rayleigh and Prandtl numbers are

$$R_a = \frac{g\alpha H^3 \Delta T}{\nu\kappa} \quad , \tag{2.29}$$

$$\sigma = \frac{\nu}{\kappa} \quad . \tag{2.30}$$

The Prandtl number is a dimensionless number describing the ratio of momentum diffusivity (kinematic viscosity) to thermal diffusivity.

Solution of exercise 8

---

compared to pure conduction: momentum diffusivity is dominant.
In heat transfer problems, the Prandtl number controls the relative thickness of the momentum and thermal boundary layers. When σ is small, it means that the heat diffuses very quickly compared to the velocity (momentum). This means that for liquid metals the thickness of the thermal boundary layer is much bigger than the velocity boundary layer. The Rayleigh number is named after Lord Rayleigh and is defined as the product of the Grashof number, which describes the relationship between buoyancy and viscosity within a fluid, and the Prandtl number, which describes the relationship between momentum diffusivity and thermal diffusivity. Hence the Rayleigh number itself may also be viewed as the ratio of buoyancy and viscosity forces times the ratio of momentum and thermal diffusivities.

For an elegant solution we use the (2.27, 2.28) system.

$$\frac{1}{T}\frac{1}{L^2}\frac{L^2}{T}D_{\text{t,d}}\left(\nabla_d^2\Psi_d\right) = \nu\frac{1}{L^4}\frac{L^2}{T}\nabla_d^4\Psi_d - g\alpha\frac{\Delta T}{L}\frac{\partial\Theta_d}{\partial x_d} \tag{2.31}$$

$$\frac{\Delta T}{T}D_{\text{t,d}}\Theta_d = \frac{\Delta T}{H}\frac{L^2}{TL}\frac{\partial\Psi_d}{\partial x_d} + \kappa\frac{\Delta T}{L^2}\nabla_d^2\Theta_d \quad . \tag{2.32}$$

This yields (remember $L = H$)

$$D_{\text{t,d}}\left(\nabla_d^2\Psi_d\right) = \nu\frac{T}{H^2}\nabla_d^4\Psi_d - g\alpha\frac{T^2\Delta T}{H}\frac{\partial\Theta_d}{\partial x_d} \tag{2.33}$$

$$D_{\text{t,d}}\Theta_d = \frac{\partial\Psi_d}{\partial x_d} + \kappa\frac{T}{H^2}\nabla_d^2\Theta_d \quad . \tag{2.34}$$

Inserting $T = H^2/\kappa$, gives

$$D_{\text{t,d}}\left(\nabla_d^2\Psi_d\right) = \frac{\nu}{\kappa}\nabla_d^4\Psi_d - g\alpha\frac{H^3\Delta T}{\kappa^2}\frac{\partial\Theta_d}{\partial x_d} \tag{2.35}$$

$$D_{\text{t,d}}\Theta_d = \frac{\partial\Psi_d}{\partial x_d} + \nabla_d^2\Theta_d \quad . \tag{2.36}$$

Finally, inserting the Rayleigh $R_a = \frac{g\alpha H^3\Delta T}{\nu\kappa}$ and Prandtl $\sigma = \frac{\nu}{\kappa}$ numbers:

$$\boxed{D_{\text{t,d}}\left(\nabla_d^2\Psi_d\right) = \sigma\nabla_d^4\Psi_d - R_a\sigma\frac{\partial\Theta_d}{\partial x_d}}$$

2.2.2   Boundary conditions

We shall now discuss the boundary conditions: $\Theta = 0$ at $z = 0, H$. As further boundary condition, the normal component could be set to zero straightaway and we have $\mathbf{v}_{normal} = w = 0$ at $z = 0, H$.

In many applications, one may assume **no-slip boundary condition** as the appropriate conditions for velocity components at the wall. In general, while the tangential component is set to the

velocity of the wall:

$$\mathbf{v}_{tangential} = \mathbf{v}_{wall} \quad . \tag{2.37}$$

The fluid velocity at all fluid-solid boundaries is equal to that of the solid boundary. Conceptually, one can think of the outermost molecules of fluid as stuck to the surfaces past which it flows. Because the solution is prescribed at given locations, this is an example of a Dirichlet boundary condition. Particles close to a surface do not move along with a flow when adhesion is stronger than cohesion. At the fluid-solid interface, the force of attraction between the fluid particles and solid particles (adhesive forces) is greater than that between the fluid particles (cohesive forces). This force imbalance brings down the fluid velocity to zero. In our case: since the wall is not moving $u = 0$ at $z = 0, H$.

Another boundary condition is called **free boundary condition.** All the normal velocities normal to the wall should be zero, and furthermore the gradient of velocity parallel to wall should be zero:

$$\frac{\partial}{\partial z}\mathbf{v}_{tangential} = \mathbf{0} \tag{2.38}$$

Here, we assume a free surface both the upper- and the lower-boundaries because then the problem is most analytically tractable.[5] In our case this means no tangential stress is for $\frac{\partial u}{\partial z} = \frac{\partial^2 \psi}{\partial z^2} = 0$ One can show that in which case $\mathbf{\Psi}$ and $\mathbf{\nabla^2 \Psi}$ vanish at both boundaries. The basis functions can be chosen as sinus and cosinus as orthogonal set of base functions. In chapter 9.4, the dynamics is solved numerically using the Lattice Boltzmann approach. Other techniques and experimental approaches are summarized in Tritton [1988].

2.2.3 Galerkin approximation: Obtaining a low-order model

Saltzman [1962] derived a set of ordinary differential equations by expanding $\mathbf{\Psi}$ and $\mathbf{\Theta}$ in double

---

[5]In practical applications, the boundaries are not free and there is friction.

Fourier series in x and z, with functions of t alone for coefficients, and substituting these series into (2.27) and (2.28) A complete Galerkin approximation

$$\Psi(x, z, t) = \sum_{k=1}^{\infty}\sum_{l=1}^{\infty} \Psi_{k,l}(t) \, \sin\left(\frac{k\pi a}{H}x\right) \times \sin\left(\frac{l\pi}{H}z\right) \tag{2.39}$$

$$\Theta(x, z, t) = \sum_{k=1}^{\infty}\sum_{l=1}^{\infty} \Theta_{k,l}(t) \cos\left(\frac{k\pi a}{H}x\right) \times \sin\left(\frac{l\pi}{H}z\right) \tag{2.40}$$

yields an infinite set of ordinary differential equations for the time coefficients. He arranged the right-hand sides of the resulting equations in double Fourier-series form, by replacing products of trigonometric functions of x (or z) by sums of trigonometric functions, and then equated coefficients of similar functions of x and z. He then reduced the resulting infinite system to a finite system by omitting reference to all but a specified finite set of functions of t. He then obtained time-dependent solutions by numerical integration. In certain cases all, except three of the dependent variables, eventually tended to zero, and these three variables underwent irregular, apparently non-periodic fluctuations. These same solutions would have been obtained if the series had been at the start truncated to include a total of three terms. Accordingly, in this study we shall let

$$\frac{a}{1+a^2}\kappa \quad \Psi = X\sqrt{2}\sin\left(\frac{\pi a}{H}x\right)\sin\left(\frac{\pi}{H}z\right) \tag{2.41}$$

$$\pi\frac{R_a}{R_c}\frac{1}{\Delta T} \quad \Theta = Y\sqrt{2}\cos\left(\frac{\pi a}{H}x\right)\sin\left(\frac{\pi}{H}z\right) - Z\sin\left(2\frac{\pi}{H}z\right) \tag{2.42}$$

where $X(t)$, $Y(t)$, and $Z(t)$ are functions of time alone.

It is found that fields of motion of this form would develop if the Rayleigh number

$$R_a = \frac{g\alpha H^3 \Delta T}{\nu\kappa} \quad , \tag{2.43}$$

exceeds a critical value

$$R_c = \pi^4 a^{-2}(1+a^2)^3 \quad . \tag{2.44}$$

The minimum value of R_c, namely $27\pi^4/4 = 657.51$, occurs when $a^2 = 1/2$. In fluid mechanics, the Rayleigh number for a fluid is a dimensionless number associated with the relation of buoyancy and viscosity in a flow. When the Rayleigh number is below the critical value for that fluid, heat transfer is primarily in the form of conduction; when it exceeds the critical value, heat transfer is primarily in the form of convection.

When the above truncation (2.41,2.42) is substituted into the dynamics, we obtain the equations

$$\dot{X} = -\sigma X + \sigma Y \tag{2.45}$$

$$\dot{Y} = rX - Y - XZ \tag{2.46}$$

$$\dot{Z} = -bZ + XY \tag{2.47}$$

Here a dot denotes a derivative with respect to the dimensionless time $t_d = \pi^2 H^{-2}(1 + a^2)\kappa t$, while $\sigma = \nu\kappa^{-1}$ is the Prandtl number, $r = R_a/R_c$, and $b = 4(1 + a^2)^{-1}$.

Except for multiplicative constants, our variables X, Y, Z are the same as Saltzman's variables A, D, and G. These equations are the convection equations whose solutions we shall study. In these equations X is proportional to the intensity of the convective motion, while Y is proportional to the temperature difference between the ascending and descending currents, identical signs of X and Y denoting that warm fluid is rising and cold fluid is descending. The variable Z is proportional to the distortion of the vertical temperature-profile from linearity, a positive value indicating that the strongest gradients occur near the boundaries.

2.3 Bernoulli flow*

Starting with the momentum equation one can find for a non-viscous medium for stationary flows, with

$$(\vec{v} \cdot \nabla)\vec{v} = \tfrac{1}{2}\nabla(v^2) + (\mathrm{rot}\,\vec{v}) \times \vec{v}$$
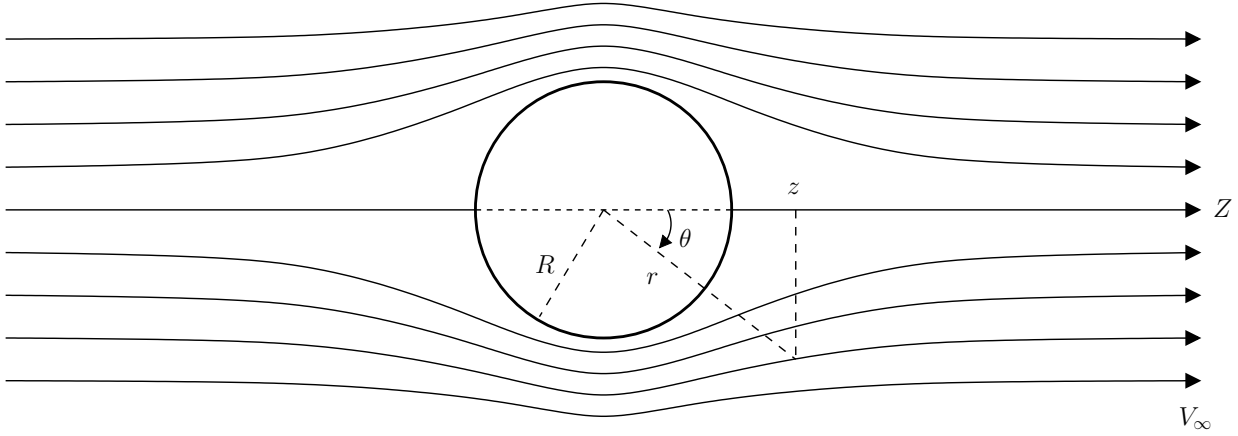
Figure 2.2: Streamlines for the incompressible potential flow around a circular cylinder in a uniform onflow.

and the potential equation $\vec{g} = -\nabla(gh)$ that:

$$\tfrac{1}{2}v^2 + gh + \int \frac{dp}{\varrho} = \text{constant along a streamline}$$

For compressible flows holds: $\tfrac{1}{2}v^2 + gh + p/\varrho =$ constant along a line of flow. If also holds $\text{rot}\vec{v} = 0$ and the entropy is equal on each streamline holds $\tfrac{1}{2}v^2 + gh + \int dp/\varrho =$ constant everywhere. For incompressible flows this becomes:

$$\tfrac{1}{2}v^2 + gh + p/\varrho = \text{constant everywhere.} \tag{2.48}$$

For ideal gases with constant C_p and C_V holds, with $\gamma = C_p/C_V$:

$$\tfrac{1}{2}v^2 + \frac{\gamma}{\gamma - 1}\frac{p}{\varrho} = \tfrac{1}{2}v^2 + \frac{c^2}{\gamma - 1} = \text{constant}$$

With a velocity potential defined by $\vec{v} = \mathbf{grad}\phi$ holds for instationary flows:

$$\frac{\partial \phi}{\partial t} + \tfrac{1}{2}v^2 + gh + \int \frac{dp}{\varrho} = \text{constant everywhere}$$

The solution for ϕ is obtained in polar coordinates r and θ, related to conventional Cartesian coordinates by $x = r \cos \theta$ and $y = r \sin \theta$. In polar coordinates, Laplace's equation is:

$$\frac{1}{r}\frac{\partial}{\partial r}\left(r\frac{\partial \phi}{\partial r}\right) + \frac{1}{r^2}\frac{\partial^2 \phi}{\partial \theta^2} = 0 \tag{2.49}$$

The solution that satisfies the boundary conditions is

$$\phi(r, \theta) = U\left(r + \frac{R^2}{r}\right)\cos \theta. \tag{2.50}$$

The velocity components in polar coordinates are obtained from the components of $\nabla\phi$ in polar coordinates:

$$V_r = \frac{\partial \phi}{\partial r} = U\left(1 - \frac{R^2}{r^2}\right)\cos \theta \tag{2.51}$$

and

$$V_\theta = \frac{1}{r}\frac{\partial \phi}{\partial \theta} = -U\left(1 + \frac{R^2}{r^2}\right)\sin \theta. \tag{2.52}$$

Being invisicid and irrotational, Bernoulli's equation (2.48) allows the solution for pressure field to be obtained directly from the velocity field:

$$p = \frac{1}{2}\rho\left(U^2 - V^2\right) + p_\infty, \tag{2.53}$$

where the constants U and p_∞ appear so that $p \to p_\infty$ far from the cylinder, where $V = U$. Using

$$V^2 = V_r^2 + V_\theta^2, \tag{2.54}$$

$$p = \frac{1}{2}\rho U^2 \left(2\frac{R^2}{r^2}\cos(2\theta) - \frac{R^4}{r^4} \right) + p_\infty. \tag{2.55}$$

In Fig. 2.3, the colorized field referred to as "pressure" is a plot of

$$2\frac{p - p_\infty}{\rho U^2} = 2\frac{R^2}{r^2}\cos(2\theta) - \frac{R^4}{r^4}. \tag{2.56}$$

On the surface of the cylinder, or $r = R$, pressure varies from a maximum of 1 (red color) at the stagnation points at $\theta = 0$ and $\theta = \pi$ to a minimum of -3 (purple) on the sides of the cylinder, at $\theta = \frac{1}{2}\pi$ and $\theta = \frac{3}{2}\pi$. Likewise, V varies from $V = 0$ at the stagnation points to $V = 2U$ on the sides, in the low pressure.

The flow being incompressible, a stream function can be found such that $\vec{V} = \nabla\psi \times \widehat{k}$. It follows from this definition, using vector identities, $\vec{V} \cdot \nabla\psi = 0$. Therefore a contour of a constant value of ψ will also be a stream line, a line tangent to $\vec{V}$. For the flow past a cylinder, we find:

$$\psi = U\left(r - \frac{R^2}{r} \right)\sin\theta. \tag{2.57}$$

Physical interpretation

Laplace's equation is linear, and is one of the most elementary partial differential equations. The dynamic pressure at the upstream stagnation point has value of $\rho U^2/2$, a value needed to decelerate the free stream flow of speed U. This same value appears at the downstream stagnation point, this high pressure is again need to decelerate the flow to zero speed. This symmetry arises only because the flow is completely frictionless. The low pressure on sides on the cylinder is needed to provide the centripetal acceleration of the flow:

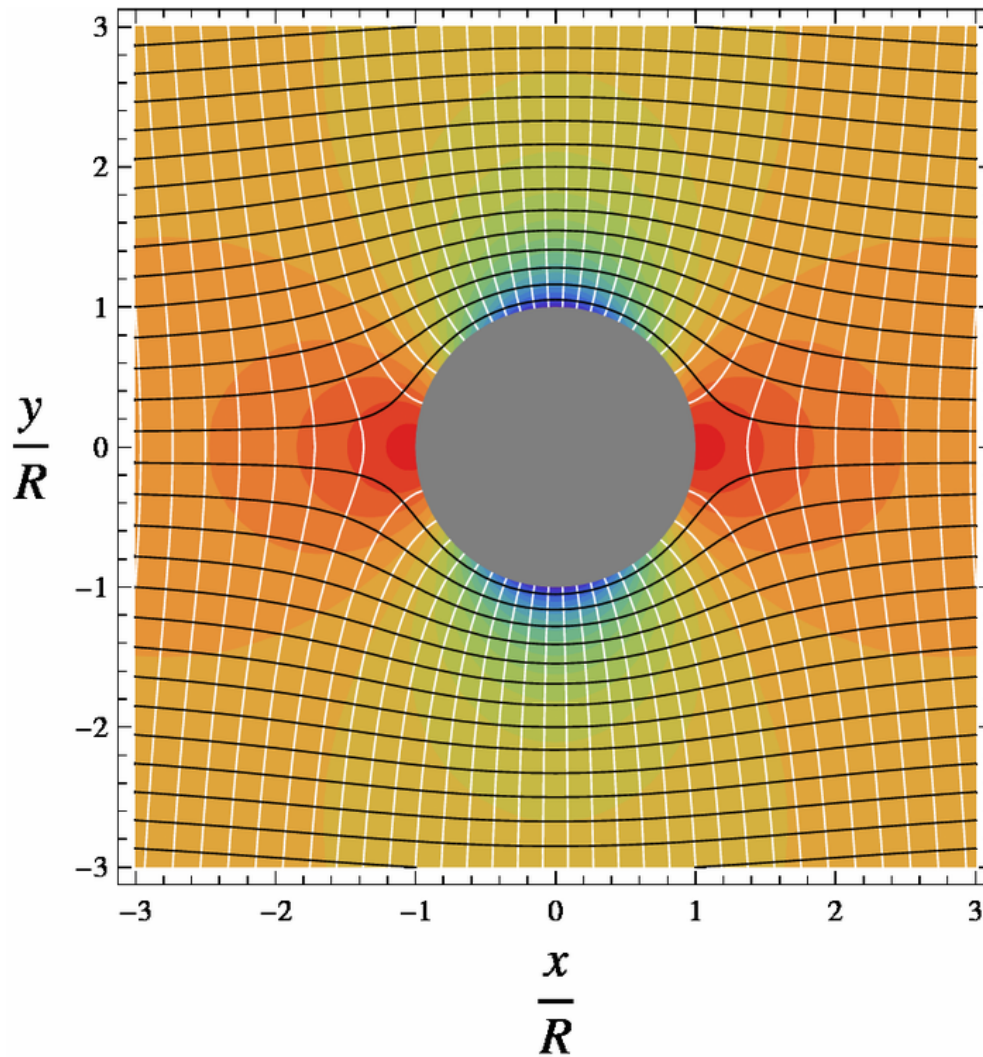$$\frac{\partial p}{\partial r} = \frac{\rho V^2}{L}, \tag{2.58}$$

Figure 2.3: Pressure field (colors), stream function (black) with contour interval of $0.2Ur$ from bottom to top, velocity potential (white) with contour interval $0.2Ur$ from left to right.

where L is the radius of curvature of the flow. But $L \approx R$, and $V \approx U$. The integral of the equation for centripetal acceleration, which will over a distance $\Delta r \approx R$ will thus yield

$$p - p_\infty \approx -\rho U^2. \tag{2.59}$$

The exact solution has, for the lowest pressure,

$$p - p_\infty = -\frac{3}{2}\rho U^2. \tag{2.60}$$

The low pressure, which must be present to provide the centripetal acceleration, will also increase the flow speed as the fluid travels from higher to lower values of pressure. Thus we find the maximum speed in the flow, $V = 2U$, in the low pressure on the sides of the cylinder. A value of $V > U$ is consistent with conservation of the volume of fluid. With the cylinder blocking some of the flow, V must be greater than U somewhere in the plane through the center of the cylinder and transverse to the flow.

Comparison with flow of a real fluid past a cylinder*

This symmetry of this ideal solution has the peculiar property of having zero net drag on the cylinder, a property known as d'Alembert's paradox. Unlike an ideal inviscid fluid, a viscous flow past a cylinder, no matter how small the viscosity, will acquire vorticity in a thin boundary layer adjacent to the cylinder. Boundary layer separation can occur, and a trailing wake will occur behind the cylinder. The pressure will be lower on the wake side of the cylinder, than on the upstream side, resulting in a drag force in the downstream direction. A particular aspect are the Von Karman Vortices.

Fig. 2.4 features a ubiquitous occurrence in the motion of fluids–a vortex street, which is a linear chain of spiral eddies called von Karman vortices. Von Karman vortices are named after Theodore von Karman, who first described the phenomenon in the atmosphere. von Karman vortices form nearly everywhere that fluid flow is disturbed by an object and form at all scales of
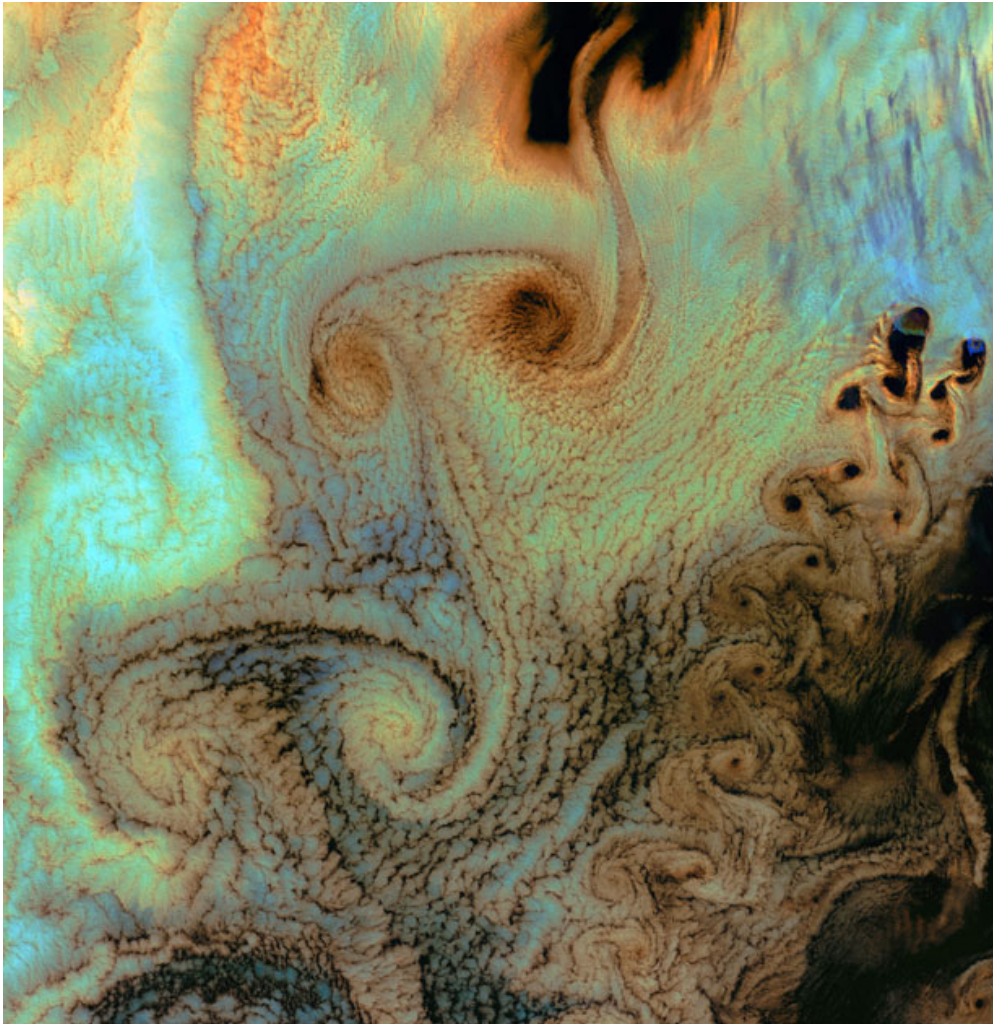
Figure 2.4:   Von Karman Vortices - As air flows over and around objects in its path, spiraling eddies, known as Von Karman vortices, may form. The vortices in this image were created when prevailing winds sweeping east across the northern Pacific Ocean encountered Alaska's Aleutian Islands. The image is from the Landsat 7 satellite.

fluid motion. The "object" that is disturbing the fluid flow is an island or group of islands. As a prevailing wind encounters the island, the disturbance in the flow propagates downstream of the island in the form of a double row of vortices which alternate their direction of rotation.

As a fluid particle flows toward the leading edge of a cylinder, the pressure on the particle rises from the free stream pressure to the stagnation pressure. The high fluid pressure near the leading edge impels flow about the cylinder as boundary layers develop about both sides. The high pressure is not sufficient to force the flow about the back of the cylinder at high Reynolds numbers. Near the widest section of the cylinder, the boundary layers separate from each side of the cylinder surface and form two shear layers that trail aft in the flow and bound the wake. Since the innermost portion of the shear layers, which is in contact with the cylinder, moves much more slowly than the outermost portion of the shear layers, which is in contact with the free flow, the shear layers roll into the near wake, where they fold on each other and coalesce into discrete swirling vortices. A regular pattern of vortices, called a vortex street, trails aft in the wake.

Analysis for two-dimensional flow using conformal mapping*

Potential flow does not include all the characteristics of flows that are encountered in the real world. Potential flow theory cannot be applied for viscous internal flows. Richard Feynman considered potential flow to be so unphysical that the only fluid to obey the assumptions was "dry water" (quoting John von Neumann). More precisely, potential flow cannot account for the behaviour of flows that include a boundary layer. Nevertheless, understanding potential flow is important in many branches of fluid mechanics. In particular, simple potential flows (called elementary flows) such as the free vortex and the point source possess ready analytical solutions. These solutions can be superposed to create more complex flows satisfying a variety of boundary conditions. These flows correspond closely to real-life flows over the whole of fluid mechanics; in addition, many valuable insights arise when considering the deviation (often slight) between an observed flow and the corresponding potential flow. Potential flow finds many applications in fields such as aircraft design. For instance, in computational fluid dynamics, one technique is to couple a potential

flow solution outside the boundary layer to a solution of the boundary layer equations inside the boundary layer.

Potential flow in two dimensions is simple to analyze using conformal mapping, by the use of transformations of the complex plane. The basic idea is to use a holomorphic (also called analytic) or meromorphic function f, which maps the physical domain (x,y) to the transformed domain (ϕ, ψ). While x, y, ϕ, ψ are all real valued, it is convenient to define the complex quantities $z = x + iy$ and $w = \phi + i\psi$. Now, if we write the mapping f as $f(x + iy) = \phi + i\psi$ or $f(z) = w$. Then, because f is a holomorphic function, it has to satisfy the Cauchy-Riemann equations

$$\frac{\partial \varphi}{\partial x} = \frac{\partial \psi}{\partial y}, \qquad \frac{\partial \varphi}{\partial y} = -\frac{\partial \psi}{\partial x}. \tag{2.61}$$

The velocity components (u,v), in the (x,y) directions respectively, can be obtained directly from f by differentiating with respect to z. That is

$$\frac{df}{dz} = u - iv \tag{2.62}$$

So the velocity field (u,v) is specified by

$$u = \frac{\partial \varphi}{\partial x} = \frac{\partial \psi}{\partial y}, \qquad v = \frac{\partial \varphi}{\partial y} = -\frac{\partial \psi}{\partial x}. \tag{2.63}$$

Both φ and ψ then satisfy Laplace's equation:

$$\Delta\varphi = \frac{\partial^2 \varphi}{\partial x^2} + \frac{\partial^2 \varphi}{\partial y^2} = 0 \qquad \text{and} \qquad \Delta\psi = \frac{\partial^2 \psi}{\partial x^2} + \frac{\partial^2 \psi}{\partial y^2} = 0. \tag{2.64}$$

So φ can be identified as the velocity potential and ψ is called the stream function. Lines of constant ψ are known as streamlines and lines of constant φ are known as equipotential lines.

Streamlines and equipotential lines are orthogonal to each other, since

$$\nabla\phi \cdot \nabla\psi = \frac{\partial\phi}{\partial x}\frac{\partial\psi}{\partial x} + \frac{\partial\phi}{\partial y}\frac{\partial\psi}{\partial y} = \frac{\partial\psi}{\partial y}\frac{\partial\psi}{\partial x} - \frac{\partial\psi}{\partial x}\frac{\partial\psi}{\partial y} = 0. \tag{2.65}$$

Thus the flow occurs along the lines of constant ψ and at right angles to the lines of constant φ. It is interesting to note that $\Delta\psi = 0$ is also satisfied, this relation being equivalent to $\nabla \times v = 0$.

Exercise 9   –   Conformal mapping

We note that the complex velocity potential must be an analytic function respecting the boundary conditions, and once we have it, we can easily obtain the flow field. Let us see how we can use this fact to solve some basic fluid mechanics problems. In case the following power-law conformal map is applied, from $z = x + iy$ to $w = \phi + i\psi$:

$$w = Az^n, \tag{2.66}$$

then, writing z in polar coordinates as $z = x + iy = re^{i\Theta}$, we have

$$\varphi = Ar^n \cos(n\theta) \text{ and } \psi = Ar^n \sin(n\theta). \tag{2.67}$$

Study the cases $n = 1/2, 2/3, 3/2, 2, 3$ and draw the streamlines and equipotential!

Hint: web site for conformal mapping

Solution $n = 1$: uniform flow

Uniform flow: $v = V$ If w = Az, that is, a power law with n = 1, the streamlines (i.e. lines of constant ψ) are a system of straight lines parallel to the x-axis. This is easiest to see by writing in terms of real and imaginary components: $f(x + iy) = Uz = Ux + iUy$ thus giving $\phi = Ux$ and $\psi = Uy.$ This flow may be interpreted as uniform flow parallel to the x-axis.

Think on the problem of flow around a corner. What is a consistent flow pattern past a corner

according to the ideal fluid conditions? $f(z) = Uz^2$ Why ? One uses analytic functions to map a fluids problem (or more generally a Laplace equation problem) from a given domain to a domain on which the problem is solved.

Another problem where we know the solution from the last section: Flow around a cylinder with $f(z) = U(z + 1/z)$.

One of the more important potential flow results obtained using conformal mapping begins with the known solution for the flow past a circular cylinder (with circulation) and maps the circle into an airfoil shape using waht is called the Joukowski mapping.

2.4 Couette flow*

Couette flow refers to the laminar flow of a viscous fluid in the space between two parallel plates, one of which is moving relative to the other. The flow is driven by virtue of viscous drag force acting on the fluid and the applied pressure gradient parallel to the plates. This type of flow is named in honor of Maurice Marie Alfred Couette, a Professor of Physics at the French university of Angers in the late 19th century. Couette flow is frequently used in undergraduate physics and engineering courses to illustrate shear-driven fluid motion. The simplest conceptual configuration finds two infinite, parallel plates separated by a distance h. One plate, say the top one, translates with a constant velocity u0 in its own plane. Neglecting pressure gradients, the Navier-Stokes equations simplify to

$$\frac{d^2 u}{dy^2} = 0, \tag{2.68}$$

where y is a spatial coordinate normal to the plates and u (y) is the velocity distribution. This equation reflects the assumption that the flow is uni-directional. That is, only one of the three velocity
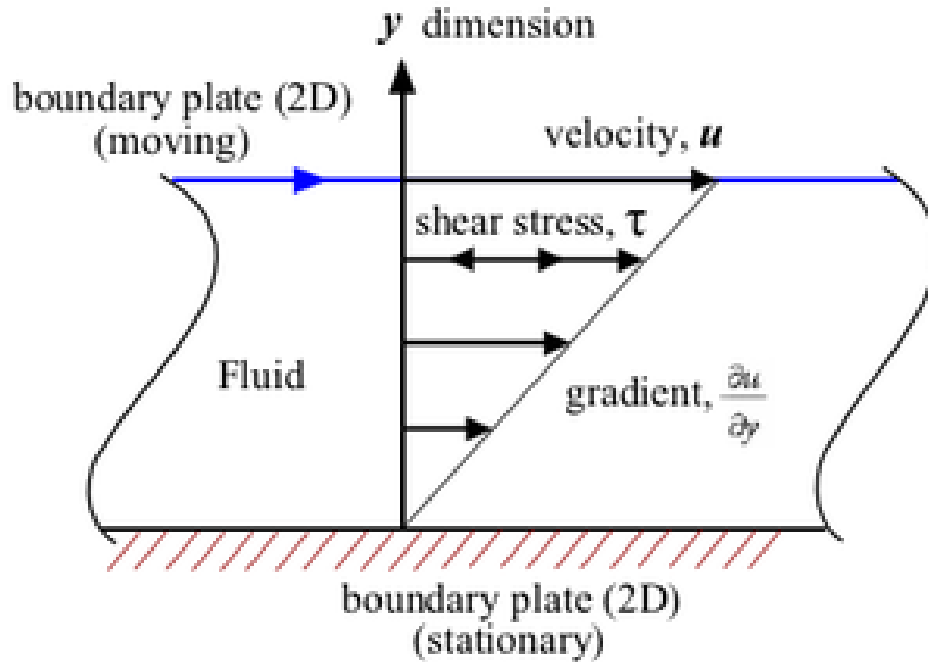
Figure 2.5: Simple Couette configuration using two infinite flat plates.

components (u,v,w) is non-trivial. If y originates at the lower plate, the boundary conditions are $u(0) = 0$ and $u(h) = u_0$. The exact solution

$$u(y) = u_0 \frac{y}{h} \qquad (2.69)$$

can be found by integrating twice and solving for the constants using the boundary conditions.

A notable aspect of this model is that shear stress is constant throughout the flow domain. In particular, the first derivative of the velocity, u_0/h, is constant. (This is implied by the straight-line profile in the figure.) According to Newton's Law of Viscosity (Newtonian fluid), the shear stress is the product of this expression and the (constant) fluid viscosity.

A more general Couette flow situation arises when a pressure gradient is imposed in a direction

parallel to the plates. The Navier-Stokes equations, in this case, simplify to

$$\frac{d^2u}{dy^2} = \frac{1}{\mu}\frac{dp}{dx}, \tag{2.70}$$

where dp/dx is the pressure gradient parallel to the plates and μ is fluid viscosity. Integrating the above equation twice and applying the boundary conditions (same as in the case of Couette flow without pressure gradient) to yield the following exact solution

$$u(y) = u_0\frac{y}{h} + \frac{1}{2\mu}\left(\frac{dp}{dx}\right)(y^2 - hy). \tag{2.71}$$

The shape of the above velocity profile depends on the dimensionless parameter

$$P = -\frac{h^2}{2\mu u_0}\left(\frac{dp}{dx}\right). \tag{2.72}$$

The pressure gradient can be positive (adverse pressure gradient) or negative (favorable pressure gradient). It may be noted that in the limiting case of stationary plates, the flow is referred to as plane Poiseuille flow with a symmetric (with reference to the horizontal mid-plane) parabolic velocity profile.

In fluid dynamics, the Taylor-Couette flow consists of a viscous fluid confined in the gap between two rotating cylinders. For low angular velocities, measured by the Reynolds number Re, the flow is steady and purely azimuthal. This basic state is known as circular Couette flow, after Maurice Marie Alfred Couette who used this experimental device as a means to measure viscosity. Sir Geoffrey Ingram Taylor investigated the stability of the Couette flow in a ground-breaking paper which has been a cornerstone in the development of hydrodynamic stability theory.

2.5   Bifurcations

Before we start with some applications of fluid stability, I provide a framework to analyze the stability of dynamical systems. A bifurcation occurs when a parameter change causes the stability of an equilibrium (or fixed point) to change [Strogatz, 2000]. In continuous systems, this corresponds to the real part of an eigenvalue of an equilibrium passing through zero. In discrete systems (those described by maps rather than ordinary differential equations (ODEs)), this corresponds to a fixed point having a Floquet multiplier with modulus equal to one. In both cases, the equilibrium is "non-hyperbolic" at the bifurcation point (for a sketch: Fig. 2.6). The topological changes in the phase portrait of the system can be confined to arbitrarily small neighbourhoods of the bifurcating fixed points by moving the bifurcation parameter close to the bifurcation point. We will discuss as one particular example the Lorenz system (Rayleigh [1916], Saltzman [1962], Lorenz [1976]).

Figure 2.6: Bifurcation sketch. The boys Max and Moritz torment Schneider Böck, a well-liked tailor who has a fast stream flowing in front of his house. They saw through the planks of his wooden bridge, making a precarious gap, then taunt him by making goat noises, until he runs outside. The bridge breaks; the tailor is swept away and nearly drowns (but for two geese, which he grabs a hold of and which fly high to safety). Source: Busch [1865].

Linear stability analysis

Consider the continuous dynamical system described by the ODE

$$\dot{x} = f(x, \lambda) \quad f \colon \mathbb{R}^n \times \mathbb{R} \to \mathbb{R}^n. \tag{2.73}$$

A bifurcation occurs at (x_0, λ_0) if the Jacobian matrix $\mathrm{d}f_{x_0, \lambda_0}$ has an Eigenvalue with zero real part. If the eigenvalue is equal to zero, the bifurcation is a steady state bifurcation, but if the eigenvalue is non-zero but purely imaginary, this is a Hopf bifurcation.

For discrete dynamical systems, consider the system

$$x_{n+1} = f(x_n, \lambda). \tag{2.74}$$

Then a local bifurcation occurs at (x_0, λ_0) if the matrix $\mathrm{d}f_{x_0, \lambda_0}$ has an eigenvalue with modulus equal to one. If the eigenvalue is equal to one, the bifurcation is either a saddle-node (often called fold bifurcation in maps), transcritical or pitchfork bifurcation. If the eigenvalue is equal to -1, it is a period-doubling (or flip) bifurcation, and otherwise, it is a Hopf bifurcation.

Examples of bifurcations include [Strogatz, 2000]:

- A transcritical bifurcation is one in which a fixed point exists for all values of a parameter and is never destroyed. However, such a fixed point interchanges its stability with another fixed point as the parameter is varied. The normal form of a transcritical bifurcation is

$$\frac{dx}{dt} = rx - x^2. \tag{2.75}$$

  This equation is similar to logistic equation but in this case we allow r and x to be positive or negative. The two fixed points are at $x = 0$ and $x = r$. When the parameter r is negative, the fixed point at $x = 0$ is stable and the fixed point $x = r$ is unstable. But for $r > 0$, the point at $x = 0$ is unstable and the point at $x = r$ is stable. So the bifurcation occurs at $r = 0$.

- A '"saddle-node bifurcation'" is a bifurcation in which two fixed points collide and annihilate each other. If the phase space is one-dimensional, one of the equilibrium points is unstable (the saddle), while the other is stable (the node). The normal form of a saddle-node bifurcation is:

$$\frac{dx}{dt} = r + x^2 \tag{2.76}$$

Here x is the state variable and r is the bifurcation parameter. If $r < 0$ there are two equilibrium points, a stable equilibrium point at $-\sqrt{-r}$ and an unstable one at $+\sqrt{-r}$. At $r = 0$ (the bifurcation point) there is exactly one equilibrium point. At this point the fixed point is no longer hyperbolic. In this case the fixed point is called a saddle-node fixed point. If $r > 0$ there are no equilibrium points. Saddle-node bifurcations may be associated with hysteresis loops. The term 'saddle-node bifurcation' is most often used in reference to continuous dynamical systems. In discrete dynamical systems, the same bifurcation is often instead called a '"fold bifurcation'".

- A Hopf is a bifurcation in which a fixed point of a dynamical system loses stability as a pair of complex conjugate eigenvalues of the linearization around the fixed point cross the imaginary axis of the complex plane. In a bifurcation, a small-amplitude limit cycle branching from the fixed point. The normal form of a Hopf bifurcation is:

$$\frac{dz}{dt} = z((\lambda + i) + b|z|^2), \tag{2.77}$$

where z, b are both complex and λ is a parameter. Write $b = \alpha + i\beta$. The number 'α is called the first Lyapunov coefficient. If α is negative then there is a stable limit cycle for $\lambda > 0$:

$$z(t) = re^{i\omega t} \tag{2.78}$$

where

$$r = \sqrt{-\lambda/\alpha} \quad \text{and} \quad \omega = 1 + \beta r^2. \tag{2.79}$$

The bifurcation is then called "'supercritical.'" If α is positive then there is an unstable limit cycle for $\lambda < 0$. The bifurcation is called "'subcritical.'"

- Pitchfork bifurcations occur generically in systems with symmetry. Pitchfork bifurcations, like Hopf bifurcations have two types - supercritical or subcritical. The normal form of the supercritical pitchfork bifurcation is

$$\frac{dx}{dt} = rx - x^3. \tag{2.80}$$

For negative values of r, there is one stable equilibrium at $x = 0$. For $r > 0$ there is an unstable equilibrium at $x = 0$, and two stable equilibria at $x = \pm\sqrt{r}$. The normal form for the subcritical case is

$$\frac{dx}{dt} = rx + x^3. \tag{2.81}$$

In this case, for $r < 0$ the equilibrium at $x = 0$ is stable, and there are two unstable equilbria at $x = \pm\sqrt{-r}$. For $r > 0$ the equilibrium at $x = 0$ is unstable.

For computational methods to obtain bifurcations: [Doedel et al., 1997; Kuznetsov, 1998].

Exercise 10 – Graphical method for bifurcations

We introduce a graphical method to obtain stability or instability. Consider the "'saddle-node bifurcation'", one of the equilibrium points is unstable (the saddle), while the other is stable (the node). In Fig. 2.7, we can plot $\frac{dx}{dt} = f(x)$ dependent on x (left panel) for

$$\frac{dx}{dt} = b + x^2 \tag{2.82}$$

with $b < 0$ in this particular case (For $b > 0$ we would have no equilibrium, and we have no

point x_e with $f(x_e) = 0$.). We just consister the slope $f'(x_e)$ and see that the filled circles with positive slope are unstable, the open circles with negative slopes are stable (right panel in Fig. 2.7).

1. Draw the bifurcations as in Fig. 2.7 for the pitchfork bifurcation.
2. Draw the bifurcations as in Fig. 2.7 for the transcritical bifurcation.
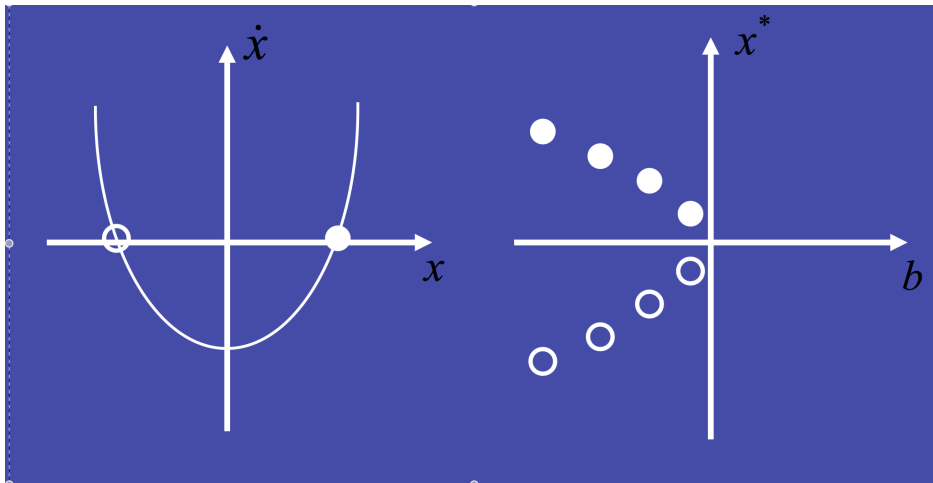
Figure 2.7: Saddle-node bifurcation diagram using the graphical method.

Exercise 11   –   Bifurcation of one dimensional differential equations

1. Consider the system

$$\frac{d}{dt}x = r_0(1 - x)x \tag{2.83}$$

Calculate the bifurcation with respect to parameter r! Draw the bifurcation diagram!

2. as in 1., but for

$$\frac{d}{dt}x = r_0 + x^2 \tag{2.84}$$

3. as in 1., but for

$$\frac{d}{dt}x = x\sqrt{(r_0 + x)^2} \tag{2.85}$$

Solution of Bifurcation of one dimensional differential equations 11

1. Given the logistic equation

$$f(x) \equiv \frac{dx}{dt} = r_0 x(1 - x)$$
$$\implies \quad f'(x) = r_0 - 2r_0 x$$

we calculate the corresponding equilibrium points x_i:

$$f(x) = r_0 x(1 - x) = 0$$
$$\implies \quad x_1 = 0, \quad x_2 = 1$$

Hence, both equilibrium points do not depend on the parameter r_0. To check whether we are dealing with stable or unstable equilibrium points, we need to calculate the second derivative at the equilibrium points.

$$f'(x_1) = r_0$$
$$f'(x_2) = r_0 - 2r_0 = -r_0$$

That is, the equilibrium points x_1 and x_2 are independent of r_0. x_1 is stable for $r_0 < 0$ and unstable for $r_0 > 0$, x_2 is stable for $r_0 > 0$ and unstable for $r_0 < 0$.

2. Given the equation

$$f(x) \equiv \frac{\mathrm{d}x}{\mathrm{d}t} = r_0 + x^2$$

$$\implies \quad f'(x) = 2x$$

we calculate the corresponding equilibrium points x_i:

$$f(x) = r_0 + x^2 = 0$$

$$\implies \quad x_{1,2} = \begin{cases} \pm\sqrt{-r_0} & , r_0 \leq 0 \\ \pm i\sqrt{r_0} & , r_0 > 0 \end{cases}$$

We just consider real solutions and neglect the imaginary ones. Then the stability conditions for the equilibrium points are given by

$$f'(x_1) = 2\sqrt{-r_0} \quad \begin{cases} < 0 & \text{stable} \\ \geq 0 & \text{unstable} \end{cases}$$

$$f'(x_2) = -2\sqrt{-r_0} \quad \begin{cases} < 0 & \text{stable} \\ \geq 0 & \text{unstable} \end{cases}$$

From the condition $r_0 \leq 0$ follows that x_1 is always unstable and x_2 is always stable. For the special case $r_0 = 0$ there is just one equilibrium point $x_1 = 0$ which is unstable as well.

3. Given the equation

$$f(x) \equiv \frac{\mathrm{d}x}{\mathrm{d}t} = x\sqrt{(r_0 + x)^2} = \begin{cases} x(r_0 + x) & , x \geq -r_0 \\ -x(r_0 + x) & , x < -r_0 \end{cases}$$

$$\implies \quad f'(x) = \begin{cases} r_0 + 2x & , x > -r_0 \\ -r_0 - 2x & , x < -r_0 \\ \text{not defined} & , x = -r_0 \end{cases}$$

we calculate the corresponding equilibrium points x_i:

$$f(x) = x\sqrt{(r_0 + x)^2} = 0$$

$$\implies \quad x_1 = 0, \quad x_2 = -r_0$$

Since for $x_2 = -r_0$ the derivative $f'(x)$ does not exist, we need to treat both cases of a small deviation $\delta > 0$ from the equilibrium point x_2 to each side separately. The stability conditions then yield:

$$f'(x_1) = \begin{cases} r_0 & , x_1 = 0 > -r_0 \quad \Rightarrow \quad r_0 > 0 \quad \Rightarrow \quad \text{unstable} \\ -r_0 & , x_1 = 0 < -r_0 \quad \Rightarrow \quad r_0 < 0 \quad \Rightarrow \quad \text{unstable} \end{cases}$$

$$f'(x_2 + \delta) = -r_0 + \delta \quad \Rightarrow \quad \begin{cases} \text{stable} & , r_0 > 0 \\ \text{unstable} & , r_0 < 0 \end{cases}$$

$$f'(x_2 - \delta) = r_0 - \delta \quad \Rightarrow \quad \begin{cases} \text{unstable} & , r_0 > 0 \\ \text{stable} & , r_0 < 0 \end{cases}$$

Exercise 12   –   **Bifurcation example** $rx\,(1-x)^2$

Consider the differential equation

$$\frac{d}{dt}x \;=\; rx\,(1-x)^2 \tag{2.86}$$

a) Calculate the bifurcation with respect to parameter r, consister the slope $f'(x_e)$. Draw the bifurcation diagram!

b) Discuss the stability in terms of the potential V(x) ! Remember that the potential can be calculated from the right hand side of equation (2.86): rhs of (2.86)) $= -\frac{dV(x)}{dx}$

Solution of Bifurcation example Exercise 12

a) Equilibria solutions are $x_e = 0, 1$. $f'(x) = r\,(1-x)^2 - 2rx\,(1-x)$

Check $f'(x_e)$:

$f'(0) = r$ (stability or instability depending on r)

$f'(1) = 0$ (indifferent stability)

b) $V(x) = -r/2x^2 + 2/3rx^3 - 1/4rx^4$

Plotting of the potential using R:

```
y=-100:100
x=y/10
x=y/50
r=1
z=-r * x^2/2 +2/3 * x^3 -r/4 * x^4
plot(x,z,type='lines')
```

2.6 Dynamics of Logistic Equation

It is worth to analyze a one dimensional logistic equation (also known as Malthus-Verhulst model), which was originally proposed to describe the evolution of a biological population. Let x denote the number (or density) of individuals of a certain population. This number will change due to growth, death, and competition. The standard logistic function is the solution of the simple first-order non-linear ordinary differential equation

$$\frac{d}{dx}f(x) = f(x)(1 - f(x)) \tag{2.87}$$

with boundary condition $f(0) = 1/2$. The qualitative behavior is easily understood in terms of the phase line: the derivative is 0 when the function is 1; and the derivative is positive for f between 0 and 1, and negative for f above 1 or less than 0 (though negative populations do not generally accord with a physical model). This yields an unstable equilibrium at 0, and a stable equilibrium at 1, and thus for any function value greater than 0 and less than 1, it grows to 1. The logistic equation is a special case of the Bernoulli differential equation and has the following solution:

$$f(x) = \frac{e^x}{e^x + C}f(x) \tag{2.88}$$

Choosing the constant of integration $C = 1$ gives the other well-known form of the definition of the logistic curve

$$f(x) = \frac{e^x}{e^x + 1} = \frac{1}{1 + e^{-x}} \tag{2.89}$$

More quantitatively, as can be seen from the analytical solution, the logistic curve shows early exponential growth for negative argument, which slows to linear growth of slope $1/4$ for an argument near 0, then approaches 1 with an exponentially decaying gap.

A typical application of the logistic equation is a common model of population growth, where the rate of reproduction is proportional to both the existing population and the amount of available

resources, all else being equal. Verhulst derived his logistic equation to describe the self-limiting growth of a biological population. Letting N represent population size and t represent time, this model is formalized by the differential equation:

$$\frac{dN}{dt} = rN \cdot \left(1 - \frac{N}{K}\right) \tag{2.90}$$

where the constant r defines the growth rate and K is the carrying capacity.

In the equation, the early, unimpeded growth rate is modeled by the first term rN. The value of the rate r represents the proportional increase of the population N in one unit of time. Later, as the population grows, the modulus of the second term (which multiplied out is $-rN^2/K$) becomes almost as large as the first, as some members of the population N interfere with each other by competing for some critical resource, such as food or living space. This antagonistic effect is called the bottleneck, and is modeled by the value of the parameter K. The competition diminishes the combined growth rate, until the value of N ceases to grow (this is called maturity of the population). The solution to the equation (with N_0 being the initial population) is

$$N(t) = \frac{KN_0 e^{rt}}{K + N_0 \left(e^{rt} - 1\right)} = \frac{K}{K/N_0 e^{-rt} + 1 - e^{-rt}} \tag{2.91}$$

where $\lim_{t \to \infty} N(t) = K$. Which is to say that K is the limiting value of N: the highest value that the population can reach given infinite time (or come close to reaching in finite time). It is important to stress that the carrying capacity is asymptotically reached independently of the initial value $N(0) > 0$, and also in the case that $N(0) > K$. In ecology, species are sometimes referred to as r-strategist or K-strategist depending upon the selective processes that have shaped their life history strategies. Choosing the variable dimensions so that n measures the population in units of carrying capacity, and τ measures time in units of 1/r, gives the dimensionless differential equation

$$\frac{d}{dt} n(t) = r(1 - n)\, n \tag{2.92}$$

In climate, the logistic equation is also important for Lorenz's error growth model [Lorenz, 1982] where $n(t)$ is then the algebraic forecast error at time t and a is the linear growth rate.

The Corona Dynamics

The logistic growth model (2.90) can also be used for the recent coronavirus epidemic. The underlying assumption of the model is that the rate of change in the number of new cases per capita linearly decreases with the number of cases. So, if N is the number of cases, and t is the time, then the model is (2.90) where r is infection rate, and K the final epidemic size. We obtain that the growth rate dN/dt peak occurs when $d^2N/dt^2 = 0$ and in time $t_{pmax} = \ln(K/N_0 - 1)/r$. At this time the number of cases and the growth rate are $N_{pmax} = K/2$ and $\frac{dN(t_{pmax})}{dt} = rK/4$, respectively.

Exercise 13   –   Population Dynamics

Consider population dynamics with population $x > 0$ and reproduction (birth-death) r:

$$\frac{d}{dt}x = r(x)\ x \tag{2.93}$$

1. Solve the differential equation for constant $r = r_0$! What happens for $t \to \infty$ when $r_0 > 0$ or $r_0 < 0$?

2. Solve the differential equation for $r = r_0(1 - x)$! (limited growth)! What happens for $t \to \infty$?

3. Consider the case $r = r_0(1 - x/K)$ with $K > 0$! Give a physical interpretation for K!

Solution of Population Dynamics 13

1. Solve for $r(x) = r_0$ using separation of variables:

$$\frac{\mathrm{d}x}{\mathrm{d}t} = r_0 x$$

$$\int \frac{\mathrm{d}x}{x} = \int r_0 \mathrm{d}t$$

$$\ln(x) = r_0 t + A'$$

$$\implies x = A e^{r_0 t} \quad \text{with} \quad A = e^{A'}$$

$$\text{with} \quad \lim_{t \to \infty} x = \begin{cases} \infty & , r_0 > 0 \\ 0 & , r_0 < 0 \end{cases}$$

2. Solve for $r(x) = r_0(1 - x)$ using separation of variables:

$$\frac{\mathrm{d}x}{\mathrm{d}t} = r_0(1 - x)x$$

$$\frac{\mathrm{d}x}{x(1 - x)} = r_0 \mathrm{d}t$$

$$\int \left(\frac{1}{x} + \frac{1}{1 - x} \right) \mathrm{d}x = \int r_0 \mathrm{d}t$$

$$\ln(x) - \ln(1 - x) = r_0 t + A'$$

$$\implies x = \frac{A e^{r_0 t}}{1 + A e^{r_0 t}} \quad \text{with} \quad A = e^{A'}$$

$$\text{and the limiting cases} \quad \lim_{t \to \infty} x = \begin{cases} 1 & , r_0 > 0 \\ 0 & , r_0 < 0 \end{cases}$$

3. Consider $r(x) = r_0\left(1 - \frac{x}{K}\right)$ with $K > 0$. Analogous procedure results then in a similar

solution with an additional scaling factor K which provides an upper limit for any population.

$$\frac{\mathrm{d}x}{\mathrm{d}t} = r_0(1 - \frac{x}{K})x$$

$$\vdots$$

$$\implies x = \frac{KAe^{r_0t}}{1 + Ae^{r_0t}}$$

$$\text{with} \quad \lim_{t\to\infty} x = \begin{cases} K & , r_0 > 0 \\ 0 & , r_0 < 0 \end{cases}$$

Exercise 14   –   Logistic map and Mandelbrot set

We analyze a discrete version of the logistic equation.

1. Write a function which solves the logistic difference-equation $x_{n+1} = rx_n(1 - x_n)$ and returns the vector x_n. Use an initial value $x_0 \in [0, 1]$, and a parameter-value $r \in [1, 4]$.

2. Investigate the sensitivity of the solution on the parameter r (especially using $r \in [3, 4]$).

3. Now, investigate the solution dependence on r systematically: write a function which saves the local extrema of a vector (fixed points) and returns them in a vector.

4. For each value of r, iterate the logistic difference equation 500 times, discard the first 200 times, and plot the fix-points / local extrema against r. What do you observe? *Hint: use the zoom-in function of your plotting software of choice!*

5. Think of a climate analogy with x being the temperature. Describe the ice albedo feedback!

6. Calculate the map

$$z_{n+1} = z_n^2 + c \tag{2.94}$$

in the complex plane with c being a complex number. This set is called Mandelbrot set [Mandelbrot, 1967]. This set is a mathematical set of points whose boundary is a distinctive and easily recognizable two-dimensional fractal shape, and is named after Mandelbrot [1967]. Images of the Mandelbrot set display an elaborate boundary that reveals progressively ever-finer recursive detail at increasing magnifications.

Solution logistic map, Solution Mandelbrot
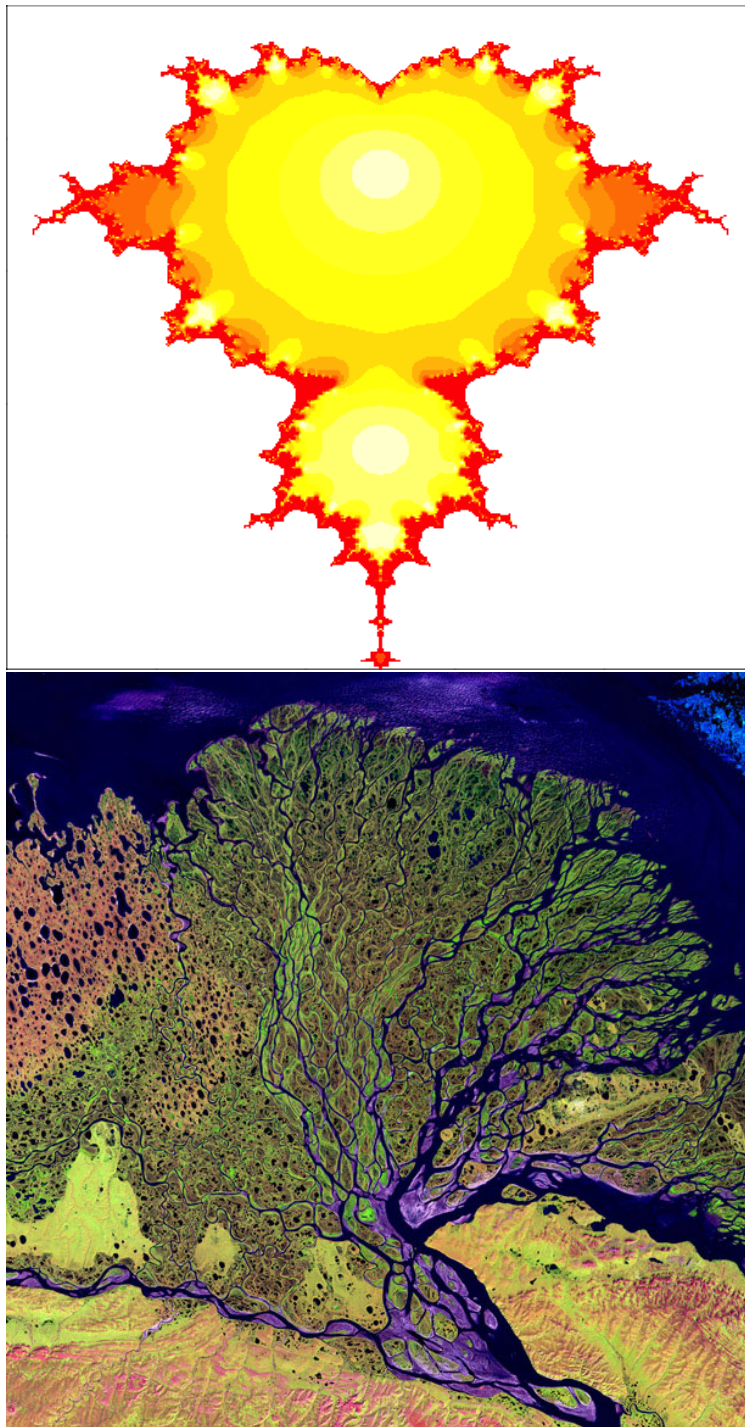
Figure 2.8: Upper panel: Mandelbrot set. The set's boundary also incorporates smaller versions of the main shape, so the fractal property of self-similarity applies to the entire set, and not just to its parts [Peitgen and Richter, 1986; Mandelbrot, 1983]. Lower panel: Lena Delta. The image is from the Landsat 7 satellite. Landsat satellites have taken specialized digital photographs of Earth's continents and surrounding coastal regions. The coastlines and morphometric subtypes may be characterized by a statistical self-similarity Mandelbrot [1967].

logistic map
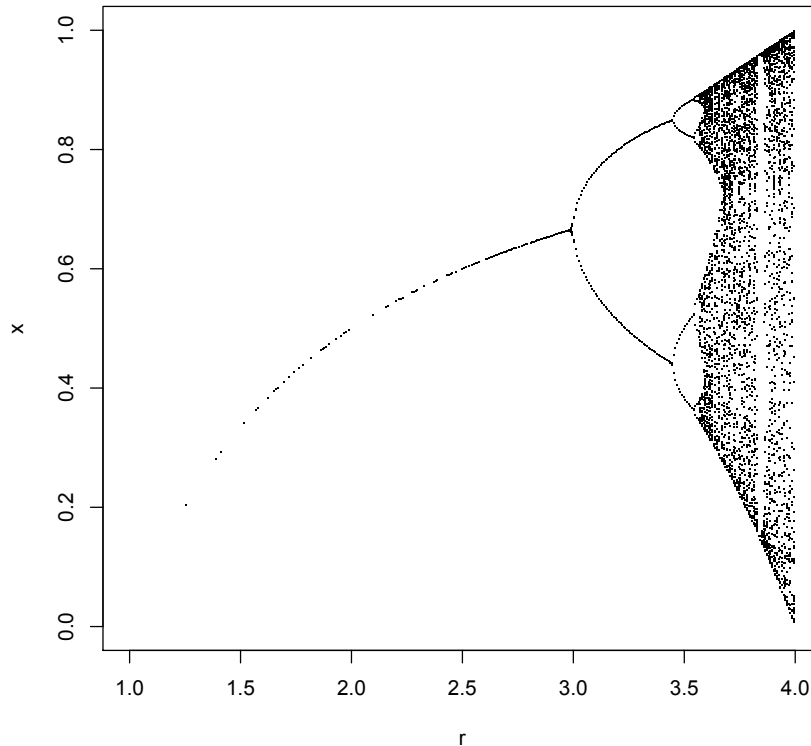
Figure 2.9: Bifurcation diagram for the Logistic map by using r as the order parameter. The logistic map is an iterative function able to give chaotic dynamics in some of its parameter space. The parameter r is the responsible to cause the bifurcation scenario characterized by one of the most well-known route to chaos: the period doubling. The chaotic domain leaves a cloud of points in parameter space with a fractional dimensionality (Cantor set).

Exercise 15   –   Bifurcation of the logistic map

1. Write a function which solves the logistic difference equation $x_{n+1} = ax_n(1 - x_n)$ and returns the vector $x(n)$. Use an initial value $x_0 \in [0, 1]$, and a parameter value $a \in [1, 4]$

2. Investigate the sensitivity of solution on the parameter a (especially using $a \in [3, 4]$)

3. Now investigate the solutions dependent on r systematically: write a function which saves the local extrema of a vector (fixed points) and returns them in a vector.

4. For each value of a, iterate the logistic difference equation 500 times, discard the first 200 times, and plot the fix-points/local extrema against a. What do you see? Zoom into the plot!

Solution: Bifurcation of the logistic map, The Feigenbaum Constant (4.669)

2.7   Lorenz system

This system is an idealization of the Rayleigh-Bénard problem (section 2.2) and provides an example for chaotic behavior in a dissipative system.

$$\dot{X} = -\sigma X + \sigma Y \tag{2.95}$$

$$\dot{Y} = rX - Y - XZ \tag{2.96}$$

$$\dot{Z} = -bZ + XY \tag{2.97}$$

Equations (2.95, 2.96, 2.97) are called *Lorenz model* in the literature [Lorenz, 1960, 1963, 1984; Maas, 1994; Olbers, 2001]. As we will see later in section 2.2, the system may give realistic results when the Rayleigh number is slightly supercritical, but their solutions cannot be expected to resemble those of the complete dynamics when strong convection occurs, in view of the extreme truncation. Figure 2.10 shows the numerical solution in the phase-space with the parameters $r = 28$, $\sigma = 10$, and $b = 8/3$.

As see in Fig. 2.11, the Lorenz system can exhibit chaotic behavior after a series of bifurcations. This concept is known as the Feigenbaum cascade Feigenbaum [1980]. In this scenario the solution undergoes a series of period-doublings, until the bifurcation parameter reaches a critical value where the system has an accumulation point of period-doublings. Feigenbaum also found the convergence behavior of the bifurcation points to the critical value. When the bifurcation parameter passes this point, chaos appears.

For some experiments go to the Lorenz model, Lorenz model 2

The same equations as (2.95, 2.96, 2.97) appear in studies of lasers, batteries, and in a simple chaotic waterwheel that can be easily built. Lorenz found that the trajectories of this system, for certain settings, never settle down to a fixed point, never approach a stable limit cycle, yet never diverge to infinity. What Lorenz discovered was at the time unheard of in the mathematical community, and was largely ignored for many years. Now this beautiful attractor is the most well-known strange attractor that chaos has to offer.
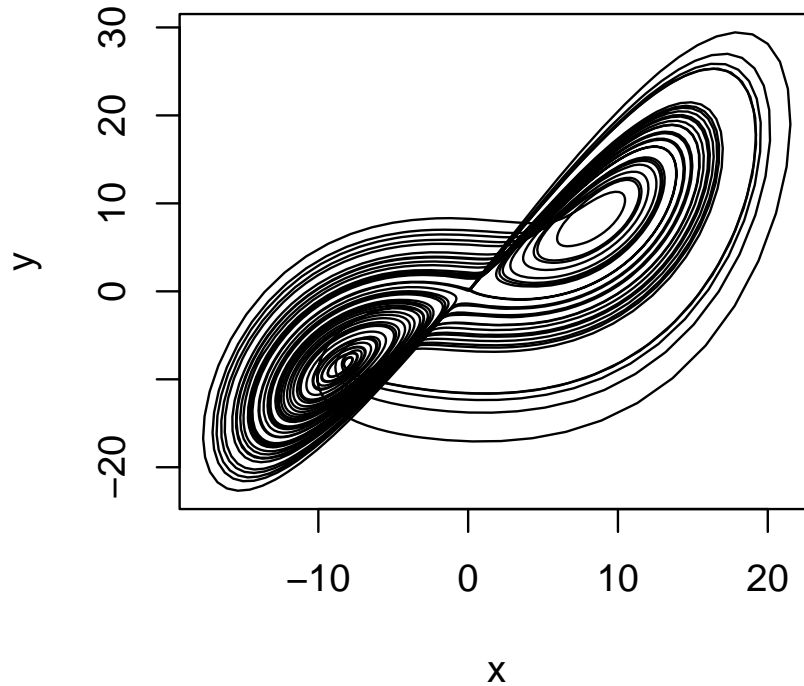
Figure 2.10: Numerical solution of the Lorenz model, in the $X - Y$ phase-space with the parameters $r = 28$, $\sigma = 10$, and $b = 8/3$. For the numerics, see Exercise 18.

Properties of the Lorenz equations

- Symmetry: The Lorenz equations have the following symmetry of ordinary differential equations: $(X, Y, Z) \rightarrow (-X, -Y, Z)$. This symmetry is present for all parameter-values of the Lorenz system.

- Invariance: The Z-axis is invariant, meaning that a solution that starts on the Z-axis (i.e. $X = Y = 0$) will remain on the z-axis. In addition, the solution will tend toward the origin if the initial conditions are on the z-axis.

- Equilibrium points: To solve for the equilibrium points we let $|f\rangle (X, Y, Z) = 0$, where we used the ket-notation to denote the vector $|f\rangle = (\dot{X}, \dot{Y}, \dot{Z})^T$. It is easy to notice that $(X, Y, Z) = (0, 0, 0)$ is a trivial equilibrium-point. The other equilibrium-points, when $X \neq 0$, are also easy to determine analytically. We leave this task as an exercise to the

reader.

- Solutions stay close to the origin: If $\sigma, b, a > 0$, then all solutions of the Lorenz system will enter an ellipsoid in finite time. In addition, the solution will remain inside the ellipsoid once it has entered. It follows that the ellipsoid is an attracting set. To quantify this, we define an ellipsoid centered at $(0, 0, 2r)$ in finite time, and the solution will remain inside the ellipsoid once it has entered. To observe this, we define a Lyapunov function

$$V(X, Y, Z) = \tau X^2 + \sigma Y^2 + \sigma (Z - 2r)^2 \quad .$$

It then follows that

$$\dot{V} = 2rX\dot{X} + 2\sigma Y\dot{Y} + 2\sigma (Z - 2r)\dot{Z}$$
$$= 2rX\sigma(Y - X) + 2\sigma Y(X(r - Z) - Y) + 2\sigma (Z - 2r)(XY - bZ)$$
$$= -2\sigma(rX^2 + Y^2 + b(Z - r)^2 - br^2).$$

We then choose an ellipsoid which all solutions will enter and remain inside. This is done by choosing a constant $C > 0$ such that the ellipsoid

$$rX^2 + Y^2 + b(Z - r)^2 = br^2$$

is strictly contained in the ellipsoid

$$rX^2 + \sigma Y^2 + \sigma (Z - 2r)^2 = C \quad .$$

Therefore all solutions will eventually enter and remain inside the above ellipsoid since $\dot{V} < 0$ when a solution is located at the exterior of the ellipsoid.

- The Lorenz system exhibit bifurcations. If $r < 1$ then there is only one equilibrium point, which is at the origin. This point corresponds to no convection. A saddle-node bifurcation

occurs at $r = 1$, and for $r > 1$ two additional critical points appear at

$$\left(\pm\sqrt{b(r-1)}, \pm\sqrt{b(r-1)}, r-1 \right) . \tag{2.98}$$

These correspond to steady convection. This pair of equilibrium points is stable only if

$$r < r_c = \sigma\frac{\sigma + b + 3}{\sigma - b - 1} \quad (\approx 24.74) \quad , \tag{2.99}$$

which can hold only for positive r if $\sigma > b+1$. At the critical value, both equilibrium points lose stability through a (inverse) Hopf bifurcation. One normally assumes that the parameters σ, r, and b are positive. Lorenz used the values $\sigma = 10, b = 8/3$ and $r = 28$. At such large r the three mode approximation for the Rayleigh-Bénard system describing thermal convection has of course ceased to be physically realistic, but mathematically the model now starts to show its most fascinating properties, because the aperiodic strange attractor behavior becomes dominant for $r > r_c$. The system exhibits chaotic behavior[6] for these values (Fig. 2.10) and the state variables that can be represented in phase space[7]. Repeating, X is proportional to the circulatory fluid velocity, Y characterizes the temperature difference between ascending and descending fluid elements, and Z is proportional to the distortion of the vertical temperature profile from its equilibrium (which is linear with height). The Lorenz system has either stable or unstable fixed points, a globally attracting periodic or nonperiodic solutions, bistability and hysteresis, and a variety of cascading bifurcations (see Fig. 2.11).

---

[6]Lorenz's conclusions about weather forecasting stated: "When our results concerning the instability of non-periodic flow are applied to the atmosphere, which is ostensibly nonperiodic, they indicate that prediction of the sufficiently distant future is impossible by any method, unless the present conditions are known exactly. In view of the inevitable inaccuracy and incompleteness of weather observations, precise very-long-range forecasting would seem to be non-existent".

[7]The set of chaotic solutions make up the Lorenz attractor with a Hausdorff dimension which is estimated to be 2.06 ± 0.01 and the correlation dimension estimated to be 2.05 ± 0.01. For other values of r, the system displays knotted periodic orbits. For example, with $r = 99.96$ it becomes a "T"(3,2) torus knot (Grassberger and Procaccia [1983]).
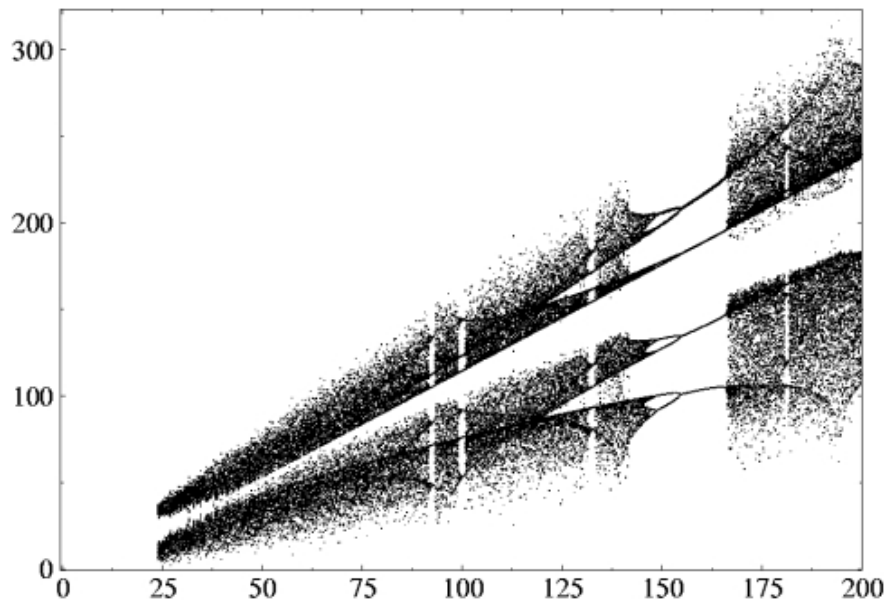
Figure 2.11: Bifurcation diagram for the Lorenz system by using r as the order parameter.

Exercise 16   –   Bifurcation Lorenz and map

1. Following Fig. 2.11, show the bifurcation diagram for the intervals $45 < \sigma < 55$ and $8.0 < \sigma < 9.5.$ Notice, that except for their different scales the pictures are much like mirror images of each other.

2. Show that in both cases the scenarios coincide in many aspects (though not completely) with the bifurcation scheme of the antisymmetric cubic map

$$x_{n+1} = (1 - c)x_n + cx_n^3 \quad , -1 \le x \le 1, \tag{2.100}$$

in the ranges $3.2 \le c \le 3.4$ and $0.25 \le x \le 0.8.$

3. Show that the reason for the good correspondence seems to be that (2.100) is the simplest polynomial 1-dim map that shares with the Lorenz model a reflection symmetry.

Exercise 17   –   Lorenz equations

Consider the Lorenz equations (which were derived from the Rayleigh-Bernard system)

$$\dot{x} = \sigma(y - x) \tag{2.101}$$

$$\dot{y} = rx - xz - y \tag{2.102}$$

$$\dot{z} = xy - bz \tag{2.103}$$

with $\sigma, r, b > 0$. σ is the Prandtl number. Furthermore, Rayleigh number $R_a \sim \Delta T$, critical Rayleigh number R_c, and $r = R_a/R_c$.

1. Evaluate the equilibrium points.

2. Determine the stability of the $(0, 0, 0)-$equilibrium through linearization! Control parameter is r.

3. Show the symmetry: The Lorenz equation has the following symmetry $(x, y, z) \rightarrow (-x, -y, z)$ independent on the parameters σ, r, b.

4. Show the invariance: The z-axis is invariant, meaning that a solution that starts on the z-axis (i.e. $x = y = 0$) will remain on the z-axis. In addition the solution will tend toward the origin if the initial condition are on the z-axis.

5. Lorenz system has bounded solutions: Show that all solutions of the Lorenz equation will enter an ellipsoid centered at $(0, 0, 2r)$ in finite time, and the solution will remain inside the ellipsoid once it has entered. To observe this, define a Lyapunov function

$$V(x, y, z) = rx^2 + \sigma y^2 + \sigma(z - 2r)^2 \tag{2.104}$$

Exercise 18   –   Numerical solution of the Lorenz system

1. Write the numerical solution for the Lorenz system.

2. Use an initial value $x_0 \in [0, 1]$, and a parameter value $r \in [0, 1]$

3. Investigate the sensitivity of the solution on the parameter r (especially using $r = 13, 14$ and $r \in [20, 30]$)

4. Display the function in the phase-space and time-dependence.

5. Now investigate the solution dependence on r systematically: write a function which saves the local extrema of a vector (fixed points) and returns them in a vector. This vector shall be displayed (use the experience you gained from exercise 14).

6. Nonlinear systems are often sensitive to initial conditions, and an error in the restart-file would lead the model to evolve on a completely different phase-space trajectory on the long term. Such a (seemingly trivial) technical problem was encountered by Lorenz himself (see e.g. Kambe [2007]), which led him to the notion of deterministic chaos in the first place. Please document the sensitivity with respect to the initial conditions.

Here is the most simple way to get the Lorenz system (using R): Solution 1 of the Lorenz Problem. The more sophisticated implementation Solution 2 of the Lorenz Problem can be also used for Fig. 2.10.

Here is the method how to obtain the bifurcation diagram. Try to understand the method and modify the code. For entertainment: An Introduction to Chaos Theory with the Lorenz Attractor.

Part II

Second part: Dynamics of the Climate System

Chapter 3

Atmosphere and Ocean Dynamics

3.1 Pseudo forces and the Coriolis effect

A pseudo force on an object arises when the frame of reference used to describe the object's motion is accelerating compared to a non-accelerating frame. It acts on all masses whose motion is described using a non-inertial frame of reference, such as a rotating reference frame. The inertial frame is the Sun and not the Earth.[1] Assuming Newton's second law in the form F = ma, pseudo forces are always proportional to the mass m. The surface of the Earth is a rotating reference frame. To solve classical mechanics problems exactly in an Earth-bound reference frame, three pseudo forces must be introduced, the Coriolis force, the centrifugal force (described below) and the Euler force. The Euler force is typically ignored because the variations in the angular velocity

---

[1]Galilean invariance or Galilean relativity states that the laws of motion are the same in all inertial frames. Galileo Galilei first described this principle in 1632 in his Dialogue Concerning the Two Chief World Systems using the example of a ship travelling at constant velocity, without rocking, on a smooth sea; any observer doing experiments below the deck would not be able to tell whether the ship was moving or stationary. Galilean relativity can be shown as follows. Consider two inertial frames S and S' . A physical event in S will have position coordinates $r = (x, y, z)$ and time t; similarly for S' . By the second axiom above, one can synchronize the clock in the two frames and assume $t = t'$. Suppose S' is in relative uniform motion to S with velocity v. Consider a point object whose position is given by $r'(t) = r(t)$ in S. We see that $r'(t) = r(t) - vt$. and acceleration is identical in the two frames $a'(t) = \frac{d^2}{dt^2} r'(t) = \frac{d^2}{dt^2} r(t) = a(t)$. A side remark: All approximations of the dynamical equations shall be Galilean invariant. In numerical examples, the lack of invariance for unresolved solutions is because the truncation error is not Galilean invariant. While advanced methods reduce the truncation error, none of them eliminate it entirely, and therefore formally solutions will still violate Galilean invariance at the level of the truncation error.

of the rotating Earth surface are usually insignificant. Both of the other pseudo forces are weak compared to most typical forces in everyday life, but they can be detected under careful conditions. For example, Foucault was able to show the Coriolis force that results from the Earth's rotation using the Foucault pendulum (see Exercise 20). If the Earth were to rotate a thousand times faster (making each day only $\approx$ 86 seconds long), people could easily get the impression that such fictitious forces are pulling on them, as on a spinning carousel.

In the rotating framework, we have the Coriolis and centrifugal forces which stem from the rotating framework. We derive from the simple relation for the time derivative in the inertial system (i) to the Earth system (e)

$$(d_t A)_i = (d_t A)_e + \Omega \times A \tag{3.1}$$

where the $\times$ symbol represents the cross product operator. For the case $A = r$, it follows for the velocity

$$v_i = v_e + \Omega \times r \tag{3.2}$$

and the relation for the acceleration (case $A = v_i$)

$$
\begin{aligned}
a_i &= (d_t v_i)_e + \Omega \times v_i \\
&= d_t v_e + \Omega \times v_e + \Omega \times (v_e + \Omega \times r) = a_e + 2\Omega \times v_e + \Omega \times \Omega \times r
\end{aligned}
\tag{3.3}
$$

At a given rate of rotation of the observer, the magnitude of the Coriolis acceleration of the object is proportional to the velocity of the object and also to the sine of the angle between the direction of movement of the object and the axis of rotation. In the following the subscript $_e$ is dropped, since we are only interested in the dynamics in the rotating Earth system. The forces in the rotating system are thus the forces in the inertial system plus the Coriolis and centrifugal

forces:

$$F = F_i + F_C + F_{cf} \tag{3.4}$$

where
$$F_C = -2\,m\,\Omega \times v. \tag{3.5}$$

Ω is the angular velocity vector which has magnitude equal to the rotation rate ω and is directed along the axis of rotation of the rotating reference frame. The formula implies that the Coriolis acceleration is perpendicular both to the direction of the velocity of the moving mass and to the frame's rotation axis.

The centrifugal term is equal to

$$F_{cf} = -\Omega \times (\Omega \times r) = -\omega^2 R, \tag{3.6}$$

where r is the space vector and R the component of r perpenticular to the axis of rotation. This term can be absorbed into the gravitation is then called gravity. One can introduce the gravitational potential

$$\phi = gz - \frac{\omega^2 R^2}{2} = gz - \frac{\omega^2 (a+z)^2 \cos^2(\varphi)}{2} \simeq gz - \frac{\omega^2 a^2 \cos^2(\varphi)}{2} \quad . \tag{3.7}$$

where a is the Earth radius and φ the latitude. The combined vector $\nabla \phi$ shows only minor modification with respect to the vertical coordinate defined by the gravitation. In practice, the gravity is used for the vertical coordinate.

Exercise 19   –   Earth's curvature

1. The highest building on the campus of the University of Bremen is the so-called drop tower with a hight of h=110 metres (Fig. **??** upper panel). How far one can look onto the horizon under good weather conditions?

Hint: Denote this distance by d. Remember the Earth's radius $a = 6378km$ and apply Pythogoras!

2. Why is the rule-of-thumb

$$d = \sqrt{2ha}$$

a good approximation? (For h=10m this means d=11 km.) When h is in m, d in km, the formula can be written as

$$d = 3.5\sqrt{\frac{h}{m}} \text{ km.}$$

3. The town Bremerhaven where the Alfred Wegener Institute is located lies about 60 km north of Bremen. How big must a tower in Bremen be in order to see the coast in Bremerhaven? (Fig. 3.1 lower panel).

Figure 3.1: Upper panel: Drop tower in Bremen. Lower panel: Harbor in Bremerhaven, ca. 60 km north of Bremen.

3.2 Pendulum and Earth rotation

The simple pendulum is another mechanical system that exhibits periodic motion. It consists of a particle-like bob of mass m suspended by a light string of length L that is fixed at the upper end, as shown in Fig. 3.2. The motion occurs in the vertical plane and is driven by the force of gravity. We shall show that, provided the angle Θ is small (less than about $10°$), the motion is that of a simple harmonic oscillator. The forces acting on the bob are the force T exerted by the string and the
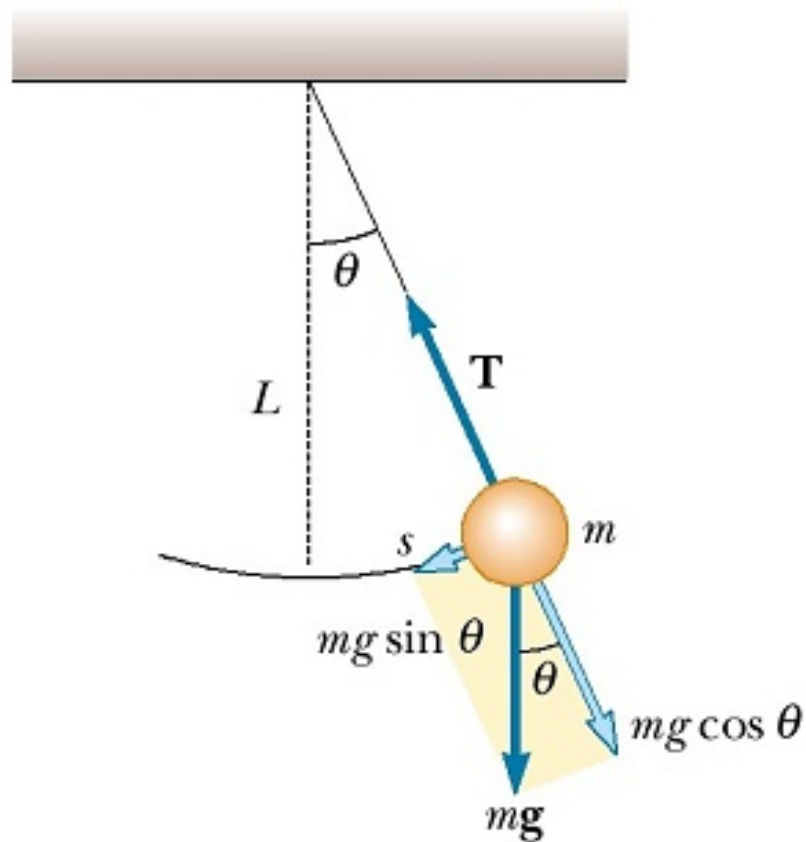
Figure 3.2: When Θ is small, a simple pendulum oscillates in simple harmonic motion about the equilibrium position $\Theta = 0$. The restoring force is $mg \sin \Theta$, the component of the gravitational force tangent to the arc.

gravitational force mg. The tangential component of the gravitational force, $mg \sin \Theta$, always acts toward $\Theta = 0$, opposite the displacement. Therefore, the tangential force is a restoring force,

and we can apply Newton's second law for motion in the tangential direction:

$$F = -mg \sin \Theta = m \frac{d^2 s}{dt^2} \tag{3.8}$$

where s is the bob's displacement measured along the arc and the minus sign indicates that the tangential force acts toward the equilibrium (vertical) position. Because $s = L\Theta$ and L is constant, this equation reduces to the equation of motion for the simple pendulum.

$$\frac{d^2 \Theta}{dt^2} = -\frac{g}{L} \sin \Theta \tag{3.9}$$

If we assume that Θ is small, we can use the approximation $\sin \Theta = \Theta$, thus the equation of motion for the simple pendulum becomes equation of motion for the simple pendulum

$$\frac{d^2 \Theta}{dt^2} = -\frac{g}{L} \Theta \tag{3.10}$$

with solution

$$\Theta = \Theta_0 \cos(\omega t) \tag{3.11}$$

where $\omega = \sqrt{\frac{g}{L}}$ is the angular frequency.

The period and frequency of a simple pendulum depend only on the length of the string and the acceleration due to gravity. Because the period is independent of the mass, we conclude that all simple pendulums that are of equal length and are at the same location (so that g is constant) oscillate with the same period. The simple pendulum can be used as a timekeeper because its period depends only on its length and the local value of g. It is also a convenient device for making precise measurements of the free-fall acceleration. Such measurements are important because variations in local values of g can provide information on the location of oil and of other valuable underground resources.

Rule of thumb for pendulum length

It is useful to have a Rule of thumb for the period of the motion, the time for a complete oscillation (outward and return) is

$$T = 2\pi\sqrt{\frac{L}{g}} \quad \text{can be expressed as} \quad L = \frac{g}{\pi^2}\frac{T^2}{4}. \tag{3.12}$$

If SI units are used (i.e. measure in metres and seconds), and assuming the measurement is taking place on the Earth's surface, then $g \approx 9.81 m/s^2$, and $g/\pi^2 \approx 1$ (0.994 is the approximation to 3 decimal places). Therefore, a relatively reasonable approximation for the length and period are,

$$L \approx \frac{T^2}{4},$$
$$T \approx 2\sqrt{L} \tag{3.13}$$

where T is the number of seconds between two beats (one beat for each side of the swing), and L is measured in metres.

Full problem without the approximation

If we consider the full problem without the approximation, the period is modified according to

$$T = 4\sqrt{\frac{L}{g}}K(k), \quad k = \sin\frac{\theta_0}{2} \tag{3.14}$$

where K is the complete elliptic integral of the first kind defined by

$$K(k) = \int_0^{\frac{\pi}{2}} \frac{1}{\sqrt{1 - k^2\sin^2 u}}\, du\,. \tag{3.15}$$

For comparison of the approximation to the full solution, consider the period of a pendulum of length 1 m on Earth at initial angle 10 degrees is

$$4\sqrt{\frac{1\ \text{m}}{g}}\ K\left(\sin\frac{10°}{2}\right) \approx 2.0102\ \text{s.} \tag{3.16}$$

The linear approximation gives

$$2\pi\sqrt{\frac{1\ \text{m}}{g}} \approx 2.0064\ \text{s.} \tag{3.17}$$

The difference between the two values, less than 0.2%, is much less than that caused by the variation of g with geographical location.

Foucault pendulum

Exercise 20   –   Foucault pendulum

The Foucault pendulum was the brainchild of the French physicist Leon Foucault. It was intended to prove that Earth rotates around its axis. Let us denote x, y the pendulum bob coordinates as seen by an observer on Earth. L is the length of the pendulum string and Θ is the pendulum angle. The pendulum moves, according to the restoring force from gravity. The string tension components can be expressed using small angle approximations, which also considerably simplify the problem, making it two-dimensional. The string tension due to the gravity force is

$$F_g = mg \begin{pmatrix} \sin\Theta \\ \sin\Theta \\ \cos\Theta \end{pmatrix} \approx mg \begin{pmatrix} x/L \\ y/L \\ 1 - z/L \end{pmatrix}.$$

Figure 3.3: Foucault's famous pendulum in the Pantheon, Paris. What keeps it moving? Air resistance would normally stop the pendulum after a few hours – so an iron collar is installed on the wire surrounded by an electromagnet that attracts the collar as the bob swings out, then shuts off automatically as it swings back, thus, keeping pendulum going. The magnet is turned on and off by a switch which is activated when the support wire interrupts a beam of light shining across its path. Similar idea is followed by the Bremen Foucault's pendulum in our department.

Then, the horizontal dynamics can be described as

$$\ddot{x} = f\dot{y} - \frac{g}{L}x \tag{3.18}$$

$$\ddot{y} = -f\dot{x} - \frac{g}{L}y \tag{3.19}$$

where $f = 2\Omega \sin\varphi$.

1. Show the analytic solution to the Foucault pendulum problem introducing the complex number $\xi = x + i \cdot y$. Furthermore, call $\omega = \sqrt{\frac{g}{L}}$ is the angular frequency. Then,

$$\ddot{\xi} + if\dot{\xi} + \omega^2\xi = 0 \tag{3.20}$$

With the ansatz

$$\xi = H(t) \cdot \exp\left(-\frac{if}{2}t\right) \tag{3.21}$$

we obtain an equation for H

$$\ddot{H} + \left(\omega^2 + \frac{f^2}{4}\right)H = 0 \tag{3.22}$$

$$H(t) = C \exp\left[\pm it\sqrt{\omega^2 + \frac{f^2}{4}}\right] \tag{3.23}$$

and therefore

$$\xi = C \exp\left[it\left(-\frac{f}{2} \pm \sqrt{\omega^2 + \frac{f^2}{4}}\right)\right] \approx C \exp\left[it\left(-\frac{f}{2} \pm \omega\right)\right] \tag{3.24}$$

where C is a complex integration constant. The pendulum swing has a natural frequency

(also called pulsation) $\omega = \sqrt{g/L}$, which depends on the length of the pendulum string.[2]
Looking at the last term in (3.29): At either the North Pole or South Pole, the plane of oscil-
lation of a pendulum remains fixed relative to the distant masses of the universe while Earth
rotates underneath it, taking one day to complete a rotation (frequency $\Omega = 2\pi/24h$). So,
relative to Earth, the plane of oscillation of a pendulum at the North Pole undergoes a full
clockwise rotation during one day, a pendulum at the South Pole rotates counterclockwise.[3]

When a Foucault pendulum is suspended at the equator, the plane of oscillation remains fixed
relative to Earth. At other latitudes, the plane of oscillation precesses relative to Earth with
a frequency $f/2 = \Omega \sin\varphi$ proportional to the sine of the latitude, where latitudes north
and south of the equator are defined as positive and negative, respectively. For example, a
Foucault pendulum at $30°$ S, viewed from above by an earthbound observer, rotates coun-
terclockwise $360°$ in two days.

2. For Foucault's famous pendulum in Paris: The plane of the pendulum's swing rotated clock-
   wise $11°$ per hour, making a full circle in 32.7 hours. What is the time period in Bremen,
   Germany?

3. Display the solution and compare it with the numerical solution with the following initial
   condition:

```
g = 9.81            # acceleration of gravity (m/s^2)
L = 67              # pendulum length (m) for the experiment in Paris
initial_x = L/100   # initial x coordinate (m)
initial_y = 0       # initial y coordinate (m)
initial_u = 0       # initial x velocity (m/s)
initial_v = 0       # initial y velocity (m/s)
Omega=2*pi/86400    # Earth's angular velocity of rotation (rad/s)
phi=49/180*pi       # 49 deg latitude in (rad)  for Paris 1851
```

---

[2]For Foucault's famous pendulum: he suspended a 28 kg brass-coated lead bob with a 67 meter long wire from the
dome of the Pantheon in Paris (about $49°$N). The natural frequency is $\sqrt{g/L} = 0.381/s$ related to a time period of
16 s.

[3]for the South Pole, there was indeed an experiment [Baker and Blackburn, 2005].

FOUCAULT'S PENDULUM EXPERIMENT TO SHOW
THE EARTH'S AXIAL ROTATION.
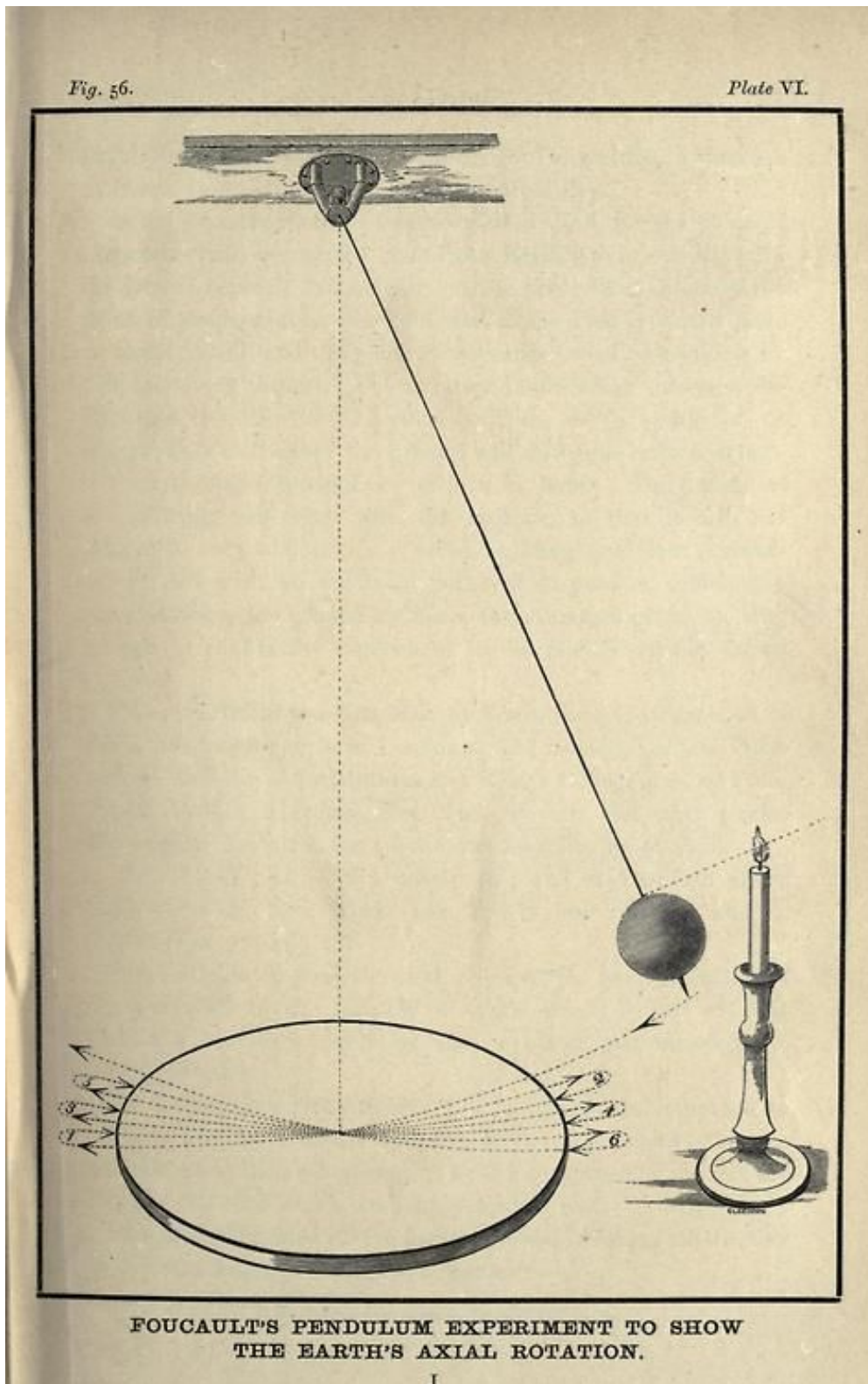
Figure 3.4: Foucault's pendulum experiment.

Exercise 21   –   Foucault pendulum 2

The horizontal dynamics of the Foucault pendulum with length L is given by

$$\ddot{x} = f\dot{y} - \frac{g}{L}x \tag{3.25}$$

$$\ddot{y} = -f\dot{x} - \frac{g}{L}y \tag{3.26}$$

with $f = 2\Omega \sin\varphi$. The length is typically on the order of 1-10 m.

a) Show that the solution is given by

$$x = x_0 \cos\omega^* t \tag{3.27}$$

$$y = x_0 \sin\omega^* t \tag{3.28}$$

$$\text{with}\quad \omega^* = \left(-\frac{f}{2} + \sqrt{\omega^2 + \frac{f^2}{4}}\right) \tag{3.29}$$

where x_0 is the initial condition, and $\omega = \sqrt{g/L}$.

b) Show that $\omega^2 \gg \frac{f^2}{4}$ and that

$$\omega^* \approx -\frac{f}{2} + \omega \quad . \tag{3.30}$$

c) Explain that the natural frequency (also called pulsation) ω can be used to measure gravity.

d) Show that the precession cycle can be used to determine the latitude! Discuss the special cases equator and South Pole!

3.3   Scaling of the dynamical equations

As we will see now, the Coriolis effect is one of the dominating forces for the large-scale dynamics of the oceans and the atmosphere. It is convenient to work in the rotating frame of reference of the Earth. The equation can be scaled by a length-scale L, determined by the geometry of the flow, and by a characteristic velocity U. Starting from (1.9), we can estimate the relative contributions in units of m/s^2 in the horizontal momentum equations:

$$\underbrace{\frac{\partial \mathbf{v}}{\partial t}}_{U/T \sim 10^{-8}} + \underbrace{\mathbf{v} \cdot \nabla \mathbf{v}}_{U^2/L \sim 10^{-8}} = \underbrace{-\frac{1}{\rho} \nabla p}_{\delta P/(\rho L) \sim 10^{-5}} + \underbrace{2\Omega \times \mathbf{v}}_{f_0 U \sim 10^{-5}} + \underbrace{fric}_{\nu U/H^2 \sim 10^{-13}} \tag{3.31}$$

where fric denotes the contributions of friction due to eddy stress divergence (usually $\sim \nu \nabla^2 \mathbf{v}$). Typical values are given in Table 3.3. The values have been taken for the **ocean.** You may repeat the estimate for the atmosphere using Table 3.3.

It is useful to think about the orders of magnitude: Because of the continuity equation $U/L \sim W/H$ and since the horizonatal scales are orders of magnitude larger than the vertical ones, the vertical velocity is very small relative to the horizontal. For small scale motion (like small-scale ocean convection or cumuls clouds) the horizontal length scale is of the same order as the vertical one and therefore the vertical motion is in the same order of magnitude as the horizontal motion. The timescales are related to $T \sim L/U \sim H/W$.

It is already useful to think about the relative importance of the different terms in the momentum balance (3.31). The Rossby number Ro is the ratio of inertial (the left hand side) to Coriolis (second term on the right hand side) terms

$$Ro = \frac{(U^2/L)}{(fU)} = \frac{U}{fL} \quad . \tag{3.32}$$

It is used in the oceans and atmosphere, where it characterizes the importance of Coriolis accelerations arising from planetary rotation. It is also known as the Kibel number. Ro is small when the flow is in a so-called geostrophic balance. This will be the subject in the next paragraphs.

	Quantity	Atmosphere	Ocean
horizontal velocity	U	$10 \ ms^{-1}$	$10^{-1} \, ms^{-1}$
vertical velocity	W	$10^{-1} \, ms^{-1}$	$10^{-4} \, ms^{-1}$
horizontal length	L	$10^6 \, m$	$10^6 \, m$
vertical length	H	$10^4 \, m$	$10^3 \, m$
horizonal Pressure changes	δP (horizontal)	$10^3 \, Pa$	$10^4 \, Pa$
mean pressure	P_0	$10^5 \, Pa$	$10^7 \, Pa$
time scale	T	$10^5 \, s$	$10^7 \, s$
gravity (gravitation+centrifugal)	g	$10 \, ms^{-2}$	$10 \, ms^{-2}$
Earth radius	a	$10^7 \, m$	$10^7 \, m$
Coriolis parameter at 45°N	$f_0 = 2\Omega \sin \varphi_0$	$10^{-4} \, s^{-1}$	$10^{-4} \, s^{-1}$
2nd Coriolis parameter at 45°N	$f_1 = 2\Omega \cos \varphi_0$	$10^{-4} \, s^{-1}$	$10^{-4} \, s^{-1}$
density	ρ	$1 \ kgm^{-3}$	$10^3 \, kgm^{-3}$
viscosity (turbulent)	ν	$10^{-5} \, kgm^{-3}$	$10^{-6} \, kgm^{-3}$

Table 3.1: Table shows the typical scales in the atmosphere and ocean system. Using these orders of magnitude, one can derive estimates of the different terms in (3.31).

Exercise 22   –   Non-dimensional system

a) Write down the non-dimensional version of (3.31) ! What are the characteristic numbers?

b) Use Table 3.3 to estimate the order of magnitude of the characteristic numbers !

c) Compare the procedure to exercise 8.

3.4 The coordinate system

The equations have to be solved on a proper coordinate system. Consider a location with latitude φ on a sphere that is rotating around the north-south axis. A local coordinate system is set up with the x axis horizontally due east, the y axis horizontally due north and the z axis vertically upwards. The axis of rotation is then expressed by a y-component $\sim \cos\varphi$ and a z-component $\sim \sin\varphi$. The rotation vector expressed in this local coordinate system is

$$\Omega = \Omega \begin{pmatrix} 0 \\ \cos\varphi \\ \sin\varphi \end{pmatrix}. \tag{3.33}$$

Likewise, the components of the velocity vector are listed in the order East (u), North (v) and Upward (w):

$$v = \begin{pmatrix} u \\ v \\ w \end{pmatrix}, \tag{3.34}$$

and Coriolis acceleration is therefore in this coordinate system

$$a_C = -2\Omega \times v = 2\,\Omega \begin{pmatrix} v\sin\varphi - w\cos\varphi \\ -u\sin\varphi \\ u\cos\varphi \end{pmatrix}. \tag{3.35}$$

In the following, $f = 2\Omega\sin\varphi$ is called the Coriolis parameter, $f^{(2)} = 2\Omega\cos\varphi$ is called the second Coriolis parameter.

When considering atmospheric or oceanic dynamics, the vertical velocity is small and therefore the vertical component of the Coriolis acceleration is small compared to gravity (see table 3.3 and the following paragraph). For such cases, only the horizontal (East and North) components matter.
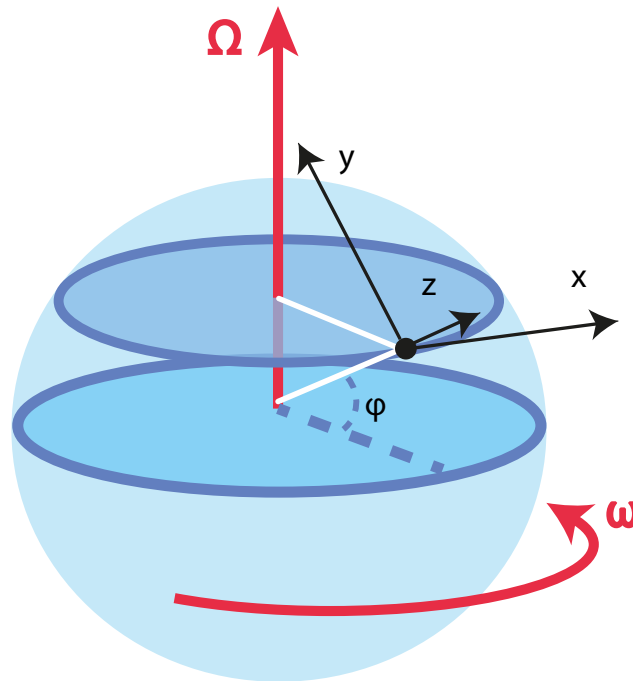
Figure 3.5:   Coordinate system at a local latitude φ with x-axis east, y-axis north and z-axis upward (that is, radially outward from center of sphere). $(x, y, z) = (a\lambda \cos \varphi, a\varphi, z)$ where (λ, φ, z) denote longitude, latitude, hight. a is the Earth radius. Ω is the the Earth rotation and equal to $2\pi/(24h)$. Note that the axis of rotation has a y- and z-component in this coordinate system (see text for details).

If we further assume $v = 0$, it can be seen immediately that (for positive φ) a movement to the east results in an acceleration to south. Similarly, for $u = 0$, it is seen that a movement due north results in an acceleration due east. In general, observed horizontally, looking along the direction of the movement causing the acceleration, the acceleration always is turned $90°$ to the right on the Northern Hemisphere (left on the Southern Hemisphere) and of the same size regardless of the horizontal orientation.

Exercise 23 – **Calculate the Double Vector Product**

Examine the double vector product $\Omega \times (\Omega \times r)$ with vectors $\Omega = (0, 0, \omega)$, $r = (x, y, z)$.

Solution

$$
\Omega \times (\Omega \times r) = \begin{pmatrix} 0 \\ 0 \\ \omega \end{pmatrix} \times \left(\begin{pmatrix} 0 \\ 0 \\ \omega \end{pmatrix} \times \begin{pmatrix} x \\ y \\ z \end{pmatrix} \right)
$$

$$
= \begin{pmatrix} 0 \\ 0 \\ \omega \end{pmatrix} \times \begin{pmatrix} -\omega y \\ \omega x \\ 0 \end{pmatrix}
$$

$$
= \begin{pmatrix} -\omega^2 y \\ -\omega^2 x \\ 0 \end{pmatrix} = -\|\Omega\|^2 \mathbf{R}
$$

with $\mathbf{R} = (x, y, 0)^T$ and $\|\Omega\|^2 = \omega^2$.

Exercise 24 – **Some questions about the stmosphere**

1. Consider the heat diffusion-advection equation

$$
\frac{\partial T}{\partial t} = k \frac{\partial^2 T}{\partial x^2} + u \frac{\partial T}{\partial x}
$$

and determine the time evolution with initial conditions

a) $T(x, 0) = \exp(-x^2/a)$ with a = constant.

b) $T(x, 0) = T_0$ for $x \geq 0$ and $T(x, 0) = 0$ elsewhere.

Discuss the special cases $k = 0$ (no diffusion) and $u = 0$ (no advection).

2. A tornado rotates with constant angular velocity ω. Show that the surface pressure at the center of the tornado is given by:

$$p = p_0 \exp\left(-\omega^2 r_0^2/(2RT)\right)$$

where p_0 is the surface pressure at the distance r_0 from the center and T is the temperature (assumed constant). [Hint: What are the dominant forces? Pressure gradient and centrifugal force.]

If temperature is 288K, pressure at 100m from the center is 10^2 kPa, and wind speed at 100m from the center is 100m/s, what is the central pressure?

3. Suppose a 1kg parcel of dry air is rising at a constant vertical velocity. If the parcel is being heated by radiation at a rate of $10^{-1} W/kg$, what must the speed of rise be in order to maintain the parcel at a constant temperature. [Hint: Energy equation.]

4. Show that for an atmosphere with an adiabatic lapse rate (i.e. constant potential temperature), the geopotential $Z(z) := \Phi(z)/g_0$ is given by

$$Z = H_\Theta[1 - (p/p_0)^a]$$

where p_0 is the pressure at $Z = 0$ and $H_\Theta = c_p\Theta/g_0$ is the total geopotential in the atmosphere. $a = R/c_p$.

Exercise 25   –   Some simple repetition questions

1. Please write down the equation of state for the ocean and atmosphere!

2. What is the hydrostatic approximation in the momentum equations?

3. Please clarify: On the Northern Hemisphere, particles tend to go to the right or left relative to the direction of motion due to the Coriolis force?

3.5 Geostrophy

The momentum equations (3.31) can be also written in the coordinate system (Fig. 3.5) above as

$$\frac{\partial u}{\partial t} + \mathbf{v} \cdot \nabla u - \frac{uv \tan \varphi}{a} - \frac{uw}{a} = -\frac{1}{\rho}\frac{\partial p}{\partial x} + fv - f^{(2)}w + \nu \nabla^2 u \qquad (3.36)$$

$$\frac{\partial v}{\partial t} + \mathbf{v} \cdot \nabla v - \frac{u^2 \tan \varphi}{a} - \frac{vw}{a} = -\frac{1}{\rho}\frac{\partial p}{\partial y} - fu \qquad\qquad + \nu \nabla^2 v \qquad (3.37)$$

complemented by the dynamics for the vertical component w :

$$\underbrace{\frac{\partial w}{\partial t}}_{W/T \sim 10^{-11}} + \underbrace{\mathbf{v} \cdot \nabla w}_{UW/L \sim 10^{-11}} - \underbrace{\frac{u^2 + v^2}{a}}_{U^2/a \sim 10^{-9}} = \underbrace{-\frac{1}{\rho}\frac{\partial p}{\partial z}}_{P_0/(\rho H) \sim 10} + \underbrace{g}_{\sim 10} + \underbrace{f^{(2)}u}_{\sim 10^{-5}} + \underbrace{\nu \partial_z^2 w}_{\nu W/H^2 \sim 10^{-16}} \quad (3.38)$$

As boundary conditions, equations (3.36, 3.37) are complemented by the horizontal wind stresses $\partial_z \tau_{xz}$ and $\partial_z \tau_{yz}$ at the ocean surface, respectively.

$$\frac{\partial u}{\partial t} + \mathbf{v} \cdot \nabla u + \ldots = -\frac{1}{\rho}\frac{\partial p}{\partial x} + fv - f^{(2)}w + \nu \nabla^2 u + \frac{1}{\rho}\partial_z \tau_{xz} \qquad (3.39)$$

$$\frac{\partial v}{\partial t} + \mathbf{v} \cdot \nabla v + \ldots = -\frac{1}{\rho}\frac{\partial p}{\partial y} - fu \qquad\qquad + \nu \nabla^2 v + \frac{1}{\rho}\partial_z \tau_{yz} \qquad (3.40)$$

It should be noted that due to sperical coordinates (see Fig. 3.5), one has metric terms, e.g. on the left hand sides of (3.36,3.37,3.38): $-\frac{uv \tan \varphi}{a} - \frac{uw}{a}$, $\frac{u^2 \tan \varphi}{a} - \frac{vw}{a}$, and $\frac{u^2+v^2}{a}$, respectively. In the geostropic approximation, one can drop these terms.[4]

A small Rossby number signifies a system which is strongly affected by Coriolis forces, and a large Rossby number signifies a system in which inertial forces dominate. For example, in tornadoes, the Rossby number is large ($\approx 10^3$), in atmospheric low-pressure systems it is low ($\approx 0.1 - 1$), but depending on the phenomena can range over several orders of magnitude ($\approx 10^{-2} - 10^2$).[5] Using the values in table 3.3, Ro in oceanic systems is of the order of 10^{-3}.

---

[4]Task: Calculate the order of magnitude of the metric terms in (3.36,3.37) by using table 3.3.

[5]As a result, in tornadoes the Coriolis force is negligible, and balance is between pressure and centrifugal forces (called cyclostrophic balance). This balance also occurs at the outer eyewall of a tropical cyclone.

When the Rossby number is large (either because f is small, such as in the tropics and at lower latitudes; or because L is small, that is, for small-scale motions such as flow in a bathtub; or for large speeds), the effects of planetary rotation are unimportant and can be neglected. Repeating: When the Rossby number is small, then the effects of planetary rotation are large and the net acceleration is comparably small allowing the use of the so-called geostrophic approximation: The force balance is largely between the pressure gradient force acting towards the low-pressure area and the Coriolis force acting away from the center of the low pressure in equation (3.31). By scaling arguments, one can derive the geostrophic horizontal flow components (u_g, v_g) as:

$$u_g \;=\; -\; \frac{1}{f\rho}\frac{\partial p}{\partial y} \tag{3.41}$$

$$v_g \;=\; \frac{1}{f\rho}\frac{\partial p}{\partial x} \tag{3.42}$$

The validity of this approximation depends on the local Rossby number. It is invalid at the equator, because $f = 2\Omega \sin\varphi$ is equal to zero there, and therefore generally not used in the tropics.

Equations (3.41,3.42) show that large-scale motions in the atmosphere and ocean tend to occur perpendicular to the pressure gradient, instead of flowing down the gradient. This circulation is called geostrophic flow. On a non-rotating planet, fluid would flow along the straightest possible line, quickly eliminating pressure gradients.[6]

---

[6]Task: Think how the geostrophy can be derived in the inertial system with a fixed reference frame, e.g. the Sun. The final result shall be independent on the reference system used!
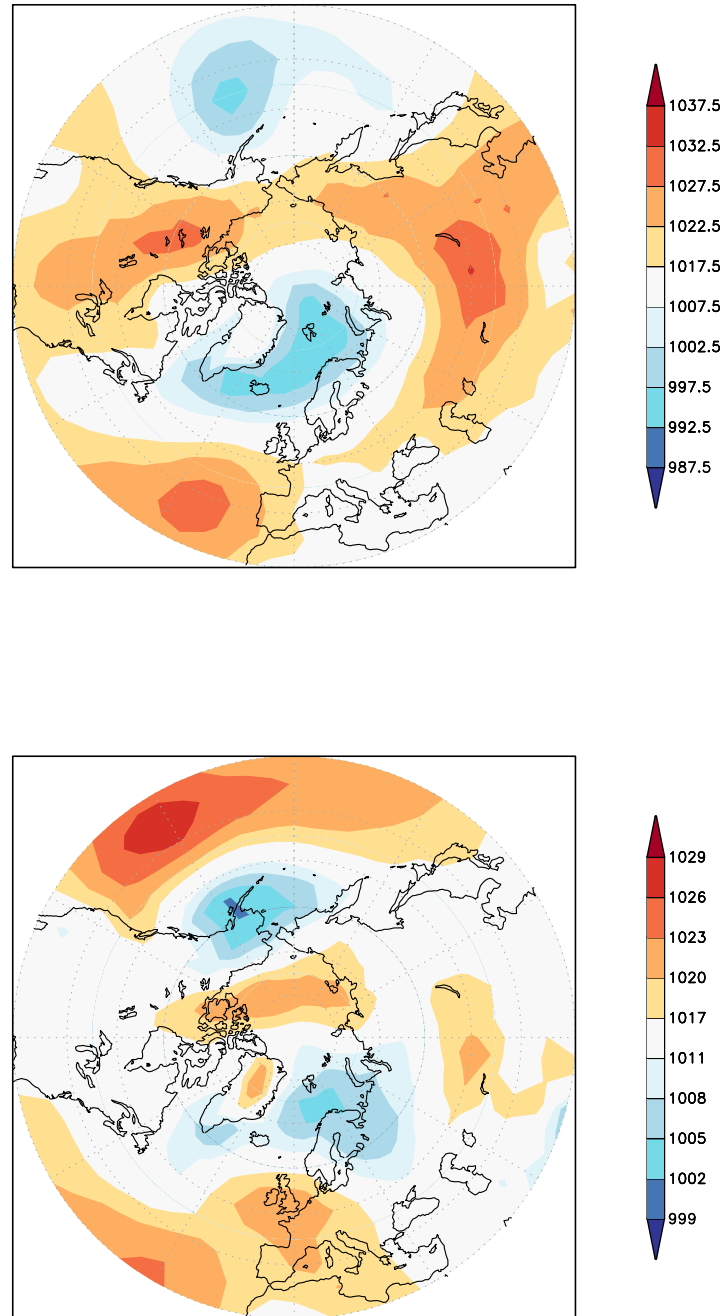
Figure 3.6: Sea level pressure (hPa) field for February (upper) and April (lower) 2015. In February, the circulation is characterized by a low pressure over the Greenland-Iceland-Norwegian Sea, and a surrounded high pressure. In April, the circulation was dominated by a high pressure over northern France and the subtropical Atlantic and Pacific Oceans, a low pressure over Scandianavia and the Aleutian Islands. Task: Draw the direction of large-scale motions in the atmosphere using the geostrophic balance (3.41,3.42). Data are from Trenberth and Paolino (1980).

3.6   Geostrophic Stream Lines and Stream Function

At each instant in time, we can represent a flow field by a vector velocity at each point in space. The instantaneous curves that are everywhere tangent to the direction of the vectors are called the *stream lines* of the flow. If the flow is unsteady, the pattern of stream lines change with time. The trajectory of a fluid particle, the path followed by a Lagrangian drifter, is called the path line in fluid mechanics. The path line is the same as the stream line for steady flow, and they are different for an unsteady flow. We can simplify the description of two-dimensional, incompressible flows by using the *stream function ψ* defined by:

$$u \equiv \frac{\partial \psi}{\partial y}, \qquad v \equiv -\frac{\partial \psi}{\partial x}, \tag{3.43}$$

The stream function is often used because it is a scalar from which the vector velocity field can be calculated. This leads to simpler equations for some flows.

The volume rate of flow between any two stream lines of a steady flow is $d\psi$, and the volume rate of flow between two stream lines $\psi 1$ and ψ_2 is equal to $\psi_1 - \psi_2$. To see this, consider an arbitrary line $d\boldsymbol{x} = (dx, dy)$ between two stream lines (Fig. 3.7). The volume rate of flow between the stream lines is:

$$v \ dx + (-u) \ dy = -\frac{\partial \psi}{\partial x} \ dx - \frac{\partial \psi}{\partial y} \ dy = -d\psi \tag{3.44}$$

and the volume rate of flow between the two stream lines is numerically equal to the difference in their values of ψ.

Now, lets apply the concepts to satellite-altimeter maps of the oceanic topography. One can show that

$$u_s = -\frac{g}{f}\frac{\partial \eta}{\partial y}, \qquad v_s = -\frac{g}{f}\frac{\partial \eta}{\partial x}, \tag{3.45}$$

where g is gravity, f is the Coriolis parameter, and η is the height of the sea surface above a level
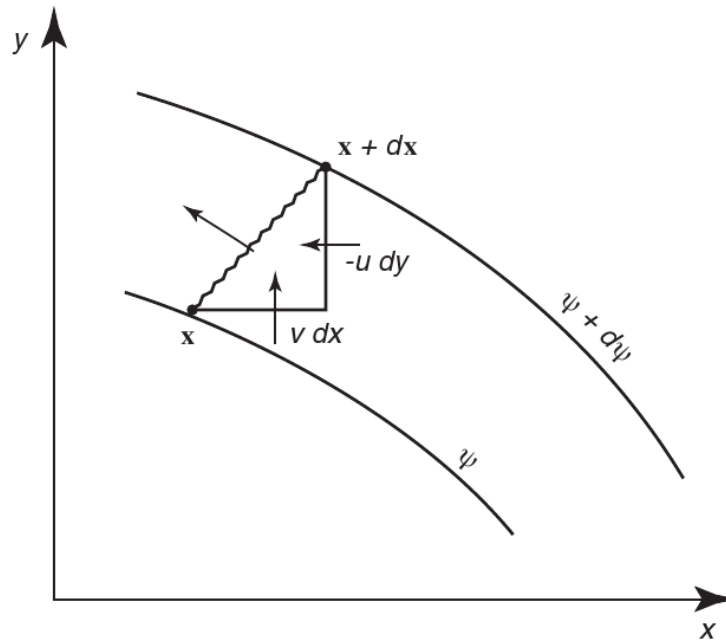
Figure 3.7: Volume transport between stream lines in a two-dimensional, steady flow. After Kundu (1990: 68).

surface. Comparing 3.45 with 3.43 it is clear that

$$\psi = -\frac{g}{f}\,\eta \tag{3.46}$$

and the sea surface is a stream function scaled by g/f. The lines of constant height are stream lines, and flow is along the lines. The surface geostrophic transport is proportional to the difference in height, independent of the distance between the stream lines. The transport is relative to transport at the **1000** decibars surface, which is roughly one kilometer deep.

In addition to the stream function, oceanographers use the mass-transport stream function Ψ defined by:

$$M_x \equiv \frac{\partial \Psi}{\partial y}, \qquad M_y \equiv -\frac{\partial \Psi}{\partial x} \tag{3.47}$$

3.7   Conservation of vorticity

In simple words, vorticity is the rotation of the fluid. The rate of rotation can be defined in various ways. Consider a bowl of water sitting on a table in a laboratory. The water may be spinning in the bowl. In addition to the spinning of the water, the bowl and the laboratory are rotating because they are on a rotating earth. The two processes are separate and lead to two types of vorticity.

Everything on earth, including the ocean, the atmosphere, and bowls of water, rotates with the earth. This rotation is the *planetary vorticity* f. It is twice the local rate of rotation of earth:

$$f \equiv 2\,\Omega \sin\varphi \quad \left(\frac{1}{s}\right) = 2\,\sin\varphi \quad \left(\frac{cycles}{day}\right) \tag{3.48}$$

Planetary vorticity is also called the Coriolis parameter. It is greatest at the poles where it is twice the rotation rate of earth. Note that the vorticity vanishes at the equator and that the vorticity in the Southern Hemisphere is negative because φ is negative.

The ocean and atmosphere do not rotate at exactly the same rate as the Earth. They have some rotation relative to Earth due to currents and winds. *Relative vorticity* ζ is the vorticity due to currents in the ocean.[7] Mathematically it is:

$$\zeta \equiv \frac{\partial v}{\partial x} - \frac{\partial u}{\partial y} \tag{3.49}$$

where we have assumed that the flow is two-dimensional.

For a rigid body rotating at rate Ω, $\zeta = 2\,\Omega$. Of course, the flow does not need to rotate as a rigid body to have relative vorticity. Vorticity can also result from shear. For example, at a north/south western boundary in the ocean, $u = 0$, $v = v\,(x)$ and $\zeta = \partial v\,(x)\,/\partial x$.

ζ is usually much smaller than f. To make an estimate for ζ : It is greatest at the edge of fast currents such as the Gulf Stream. To obtain some understanding of the size of ζ, consider the edge

---

[7]ζ is the vertical component of the threedimensional vorticity vector ω, and it is sometimes written ω_z. ζ is positive for counter-clockwise rotation viewed from above. This is the same sense as Earth's rotation in the Northern Hemisphere. One could use ω_z for relative vorticity, but ω is also commonly used to mean frequency in radians per second.

of the Gulf Stream off Cape Hatteras where the velocity decreases by $1\,ms^{-1}$ in 100km at the boundary. The curl of the current is approximately

$$\zeta = \frac{\partial v}{\partial x} = \frac{1\,ms^{-1}}{100\,km} = \quad 0.14 \quad \frac{cycles}{day} = \quad 1 \quad \frac{cycle}{week} \quad = 1.62 \cdot 10^{-6}\,\frac{1}{s}. \quad (3.50)$$

Hence even this large relative vorticity is still almost seven times smaller than f (compare 3.48). A more typical value of relative vorticity, such as the vorticity of eddies, is a cycle per month. The sum of the planetary and relative vorticity is called absolute vorticity:

$$\text{Absolute Vorticity} \equiv (\zeta + f) \quad (3.51)$$

We can obtain an equation for absolute vorticity in the ocean by manipulating the equations of motion for frictionless flow. We begin with:

$$\frac{Du}{Dt} - f\,v = -\frac{1}{\rho}\frac{\partial p}{\partial x} \quad (3.52)$$

$$\frac{Dv}{Dt} + f\,u = -\frac{1}{\rho}\frac{\partial p}{\partial y} \quad (3.53)$$

If we expand the substantial derivative, and if we subtract $\partial/\partial y$ of (3.52) from $\partial/\partial x$ of (3.53) to eliminate the pressure terms, we obtain

$$\frac{D}{Dt}\left(\partial_x v - \partial_y u\right) \;+\; \left(\partial_x u \partial_x v + \partial_x v \partial_y v\right) - \left(\partial_y u \partial_x u + \partial_y v \partial_y u\right)$$
$$+\; f\left(\partial_x u + \partial_y v\right) + v\,\partial_y f \;= 0 \quad (3.54)$$

Using $\frac{D}{Dt} f = v\,\partial_y f$:

$$\frac{D}{Dt}\zeta \;+\; \partial_x v\left(\partial_x u + \partial_y v\right) - \partial_y u\left(\partial_x u + \partial_y v\right)$$
$$+\; f\left(\partial_x u + \partial_y v\right) + \frac{D}{Dt} f \;= 0 \quad (3.55)$$

this yields

$$\frac{D}{Dt}\left(\zeta + f\right) + \left(\zeta + f\right)\left(\frac{\partial u}{\partial x} + \frac{\partial v}{\partial y}\right) = 0 \quad . \tag{3.56}$$

Exercise 26   –   **Non-dimensional system of the vorticity dynamics**

a) For cnstant depth, derive the the non-dimensional version of the vorticity equation

$$\frac{D}{Dt}\left(\zeta + f\right) = \nu\nabla^2\zeta \quad .$$

Hint: Repeat exercise 4. b) What are the characteristic numbers?

c) Estimate the order of magnitude of the characteristic numbers for the atmosphere and ocean !
You can use Table 3.3 and other references.

3.7.1   Potential vorticity equation $(\zeta + f)/h$

3.7.2   Examples for conservation of Vorticity

The rotation rate of a column of fluid changes as the column is expanded or contracted. This changes the vorticity through changes in ζ. To see how this happens, consider barotropic, geostrophic flow in an ocean with depth $h\left(x, y, t\right)$, where h is the distance from the sea surface to the bottom. That is, we allow the surface to have topography (Fig. 3.8). Integrating the continuity equation from the bottom to the top of the ocean gives:

$$\left(\frac{\partial u}{\partial x} + \frac{\partial v}{\partial y}\right)\int_b^{b+h} dz + w|_b^{b+h} = 0 \tag{3.57}$$

where b is the topography of the bottom, and h is the depth of the water. Notice that $\partial u/\partial x$ and $\partial v/\partial y$ are independent of z because they are barotropic, and the terms can be taken outside the integral. The boundary conditions require that flow at the surface and the bottom be along the
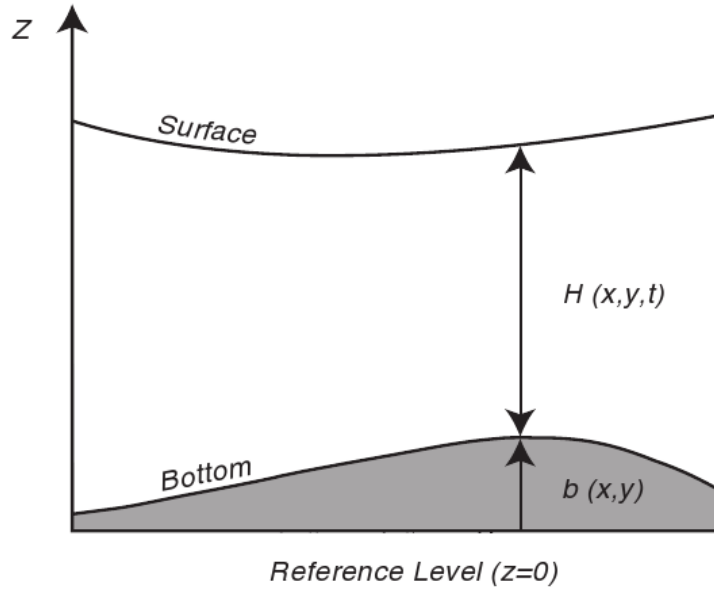
Figure 3.8: Sketch of fluid flow used for deriving conservation of potential vorticity. Here $H = h$. After Cushman-Roisin (1994: 55).

surface and the bottom. Thus the vertical velocities at the top and the bottom are:

$$w|_{b+h} = D_t(b+h) = \frac{\partial (b+h)}{\partial t} + u \frac{\partial (b+h)}{\partial x} + v \frac{\partial (b+h)}{\partial y} \tag{3.58}$$

$$w|_b = D_b = u \frac{\partial b}{\partial x} + v \frac{\partial b}{\partial y} \tag{3.59}$$

where we used $\partial b/\partial t = 0$ because the bottom does not move, and $\partial h/\partial z = 0$. Substituting (3.58) and (3.59) into (3.57) we obtain

$$\left(\frac{\partial u}{\partial x} + \frac{\partial v}{\partial y} \right) + \frac{1}{h} \frac{Dh}{Dt} = 0 \tag{3.60}$$

Substituting this into (3.56) gives:

$$\frac{D}{Dt} (\zeta + f) - \frac{(\zeta + f)}{h} \frac{Dh}{Dt} = 0 \tag{3.61}$$
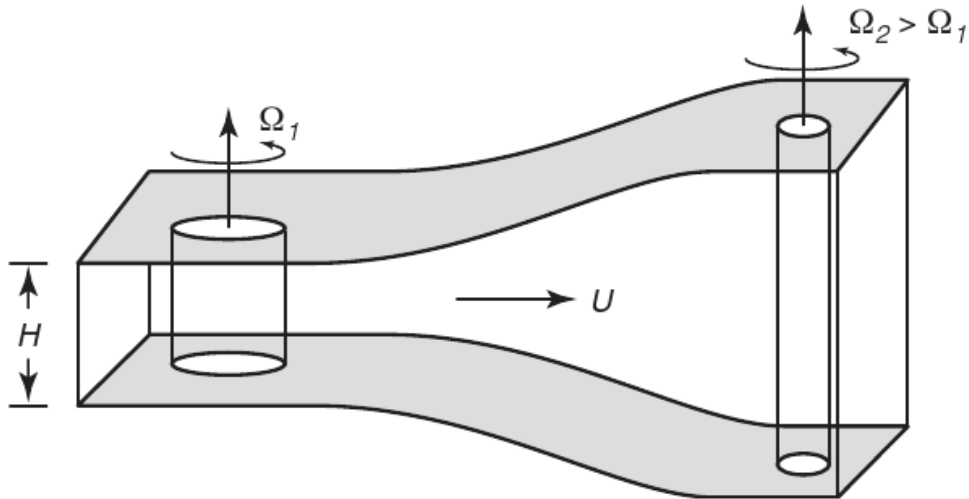
Figure 3.9: Sketch of the production of relative vorticity by change in the height of a fluid column. As the vertical fluid column moves from left to right, vertical stretching reduces the moment of inertia of the column, causing it to spin faster.

which can be rewritten as

$$\frac{1}{h}\frac{D}{Dt}(\zeta + f) - (\zeta + f)\frac{D_t h}{h^2} = 0 \qquad (3.62)$$

$$\frac{D}{Dt}\left(\frac{\zeta + f}{h}\right) = 0 \quad . \qquad (3.63)$$

The quantity within the parentheses must be constant. It is called *potential vorticity* Π. Potential vorticity is conserved along a fluid trajectory:

$$\text{Potential Vorticity} = \Pi \equiv \frac{\zeta + f}{h} \qquad (3.64)$$

The angular momentum of any isolated spinning body is conserved. The spinning body can be an eddy in the ocean or the earth in space. If the spinning body is not isolated, that is, if it is linked to another body, then angular momentum can be transferred between the bodies. The conservation of potential vorticity couples changes in depth, relative vorticity, and changes in latitude. All three interact:
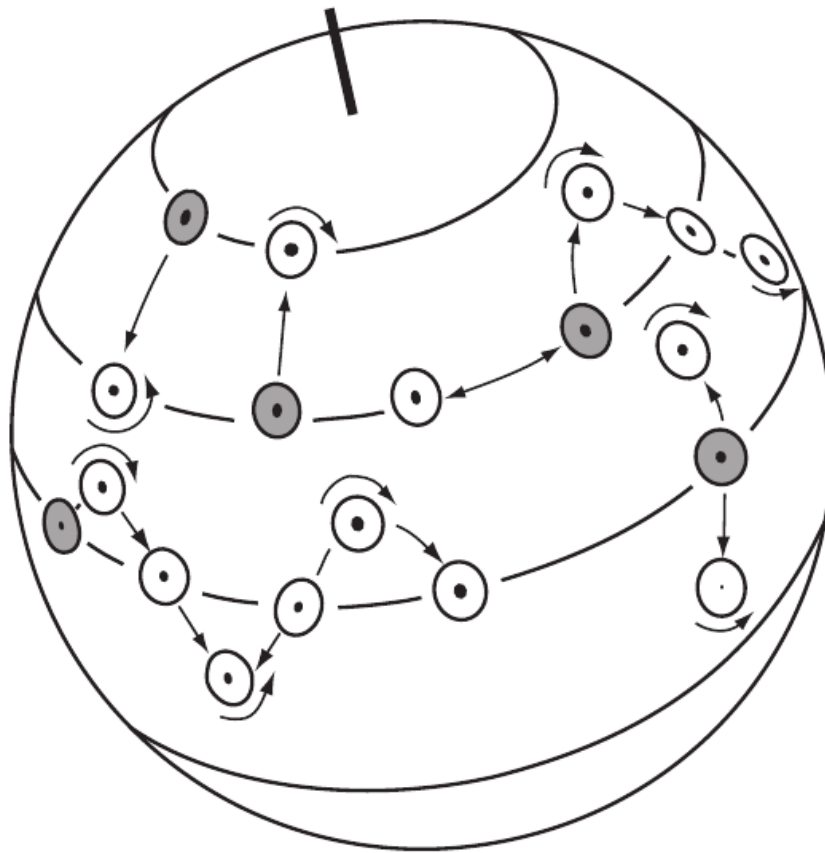
Figure 3.10: Angular momentum tends to be conserved as columns of water change latitude. This changes the relative vorticity of the columns. After von Arx (1962).

- Changes in the depth h of the flow results in change of the relative vorticity. The concept is analogous with the way figure skaters decrease their spin by extending their arms and legs. The action increases their moment of inertia and decreases their rate of spin (Fig. 3.9).

- Changes in latitude require a corresponding change in ζ. As a column of water moves equatorward, f decreases, and ζ must increase (Fig. 3.10). If this seems somewhat mysterious, von Arx (1962) suggests we consider a barrel of water at rest at the north pole. If the barrel is moved southward, the water in it retains the rotation it had at the pole, and it will appear to rotate counterclockwise at the new latitude where f is smaller.

3.7.3 Potential vorticity conservation $(\zeta + f)/h$: Implications

The concept of conservation of potential vorticity has far reaching consequences, and its application to fluid flow in the ocean gives a deeper understanding of ocean currents.

Flow Tends to be Zonal

In the ocean f tends to be much larger than ζ and thus $f/h = $ constant. This requires that the flow in an ocean of constant depth be zonal. Of course, depth is not constant, but in general, **currents tend to be east-west rather than north-south**. Wind makes small changes in ζ, leading to a small meridional component of the flow (see Fig. 3.10).

Topographic Steering

Barotropic flows are diverted by sea floor features. Consider what happens when a flow that extends from the surface to the bottom encounters a sub-sea ridge (Fig. 3.11). As the depth decreases, $\zeta + f$ must also decrease, which requires that f decrease, and the flow is turned toward the equator. This is called topographic steering. If the change in depth is sufficiently large, no change in latitude will be sufficient to conserve potential vorticity, and the flow will be unable to cross the ridge. This is called topographic blocking.

Streamfunction f/h

In the ocean, f tends to be much larger than ζ and

$$\frac{D}{Dt}\left(\frac{f}{h}\right) = 0 \tag{3.65}$$
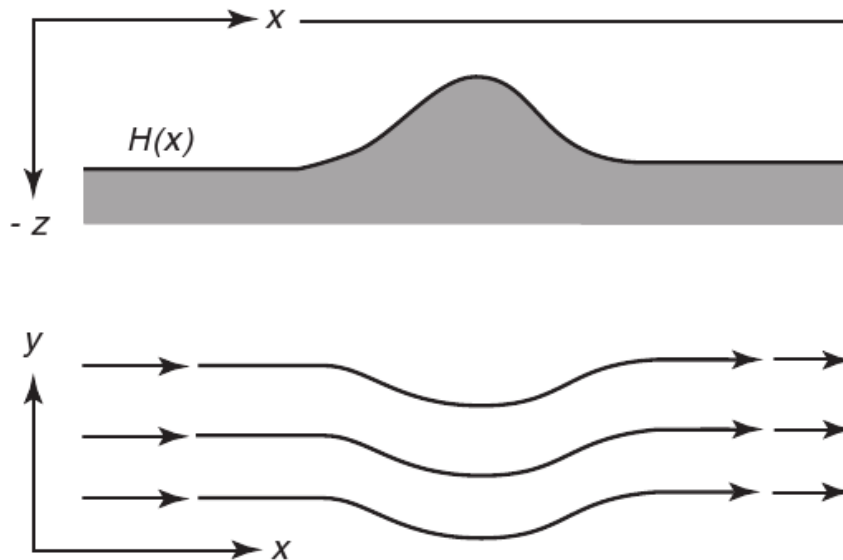
Figure 3.11: Barotropic flow over a sub-sea ridge is turned equatorward to conserve potential vorticity. After Dietrich et al. (1980: 333).

implies $f/h =$ constant along the flow. In this case, we have a streamfunction Ψ and pressure p that are functions of f/h:

$$\Psi = \Psi(f/h) \quad ; \qquad p = p(f/h). \tag{3.66}$$

This requires that the flow in an ocean of constant depth be zonal. Of course, depth is not constant, but in general, currents tend to be east-west rather than north-south. Wind makes small changes in ζ, leading to a small meridional component of the flow (see figure 3.10). The geostrophic contours f/h turn out to be an interesting combination of latitude circles and bottom topographic contours. Over small horizontal distances[8] and at high latitude topography, h tends to dominate (as in the example in Fig.3.13), but over longer distances or in the tropics, the latitude-variation of f dominates.

---

[8] Then $\frac{D}{Dt}\left(\frac{f}{h}\right) = 0$ can be transformed into $\frac{D}{Dt}h = 0$.

Exercise 27   –   Differential operators for the potential vorticity equation

Deriving the vorticity equation

$$\frac{D}{Dt}\left(\frac{\zeta + f}{h}\right) = 0 \quad,$$

we need to evaluate the terms $\partial_y \frac{D}{Dt} u$ and $\partial_x \frac{D}{Dt} v$. Write down the explicit terms!

Exercise 28   –   Calculation of potential vorticity in the atmosphere

An air column at $53°$N with $\zeta = 0$ initially streches from the surface to a fixed tropopause at 10 km height. If the air column moves until it is over a mountain barrier 2.5 km hight at $30°$N, what is its absolute vorticity and relative vorticity as it passes the mountain top?

Assume: $\sin 53° = 0.8; \sin 30° = 0.5$. The angular velocity of the Earth $\Omega = 2\pi/(1day)$.

Exercise 29   –   f/h contours

Geostrophic contours using available topography data. Barotropic flows are diverted by sea floor features. Consider what happens when a flow that extends from the surface to the bottom encounters a sub-sea ridge.

1. Show the f/h contours for the North Atlantic Ocean! See Fig. 3.12.

2. Show it for low latitudes regions: region around $20°S$ to $20°N$ in the Atlantic and Pacific Ocean. One problem is that the geostrophic contours bump into continents, so that ocean currents running along them have a serious difficulty there. Actually all such f/h contours head toward the Equator as they run up into shallow water (as $h \rightarrow 0 \quad f \rightarrow 0$ also, hence $\varphi \rightarrow 0$). This shows that we need more terms in the vorticity dynamics to describe the ocean circulation.

3. The examination of tidal rhythmites and theories about the Earth-Moon dynamics suggest that the length of day 900 million years ago was 18 h instead of 24h. How are the results of the vorticity dynamics are affected?
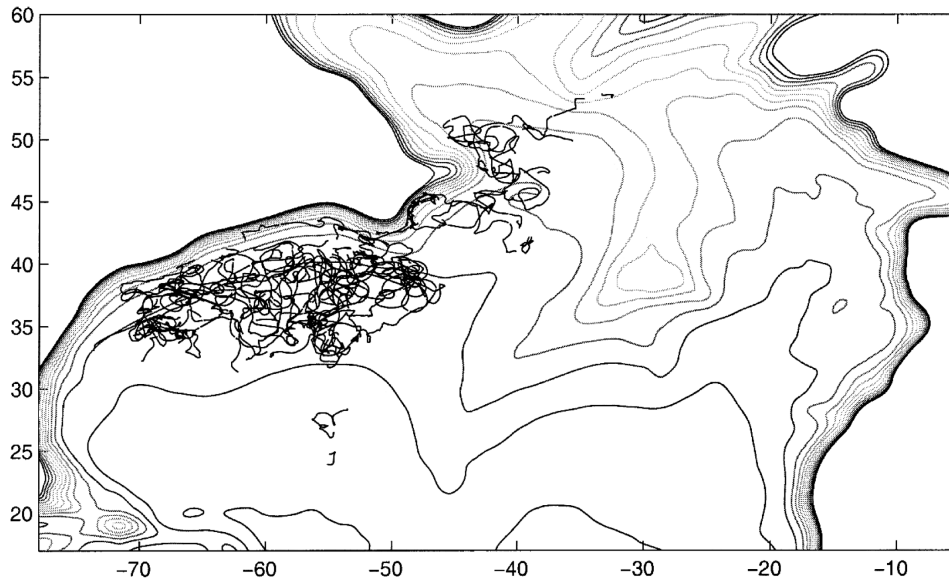
Figure 3.12: Floats in the northwestern NorthAtlantic below 1000m. The trajectories, superimposed on the smoothed f/h contours (LaCasce, 2000).
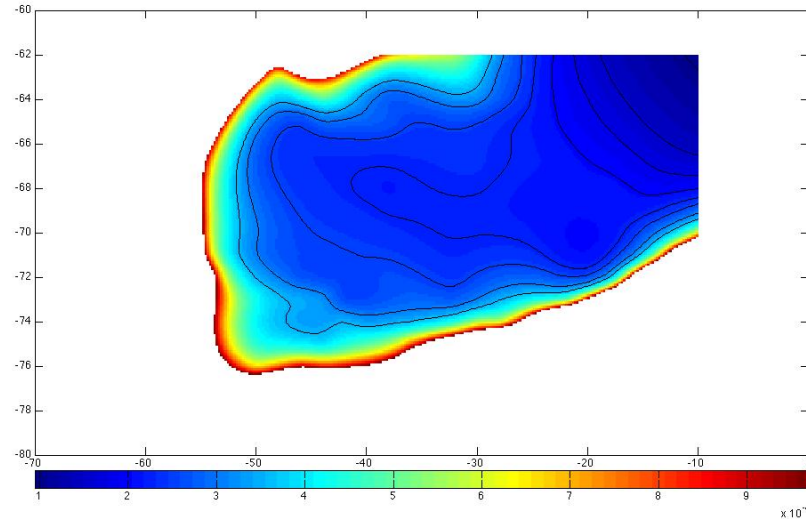
Figure 3.13: f/h countour in the Weddell Sea for 34 Ma ($34 \cdot 10^6$ years before present).

4. For the Miocene (about 34 Million years ago), the topography data were provided in the course. Calculate the f/h-contours! The length of the day was nearly as today. See Fig. **??**.

Baroclinic flow in a continuously stratified fluid

For baroclinic flow in a continuously stratified fluid, the potential vorticity can be written (Pedlosky, 1987)

$$\Pi = \frac{\zeta + f}{\rho} \cdot \nabla \lambda \tag{3.67}$$

where λ is any conserved quantity for each fluid element. In particular, if $\lambda = \rho$ then:

$$\Pi = \frac{\zeta + f}{\rho} \frac{\partial \rho}{\partial z} \tag{3.68}$$

assuming the horizontal gradients of density are small compared with the vertical gradients, a good assumption in the thermocline. In most of the interior of the ocean, $f \gg \zeta$ and (3.68) is written (Pedlosky, 1996)

$$\Pi = \frac{f}{\rho} \frac{\partial \rho}{\partial z} \tag{3.69}$$

This allows the potential vorticity of various layers of the ocean to be determined directly from hydrographic data without knowledge of the velocity field.

3.7.4 Taylor-Proudman Theorem

The influence of vorticity due to Earth's rotation is most striking for geostrophic flow of a fluid with constant density ρ_0 on a plane with constant rotation $f = f_0$. The components of the geostrophic and hydrostatic pressure equations are:

$$-f\,v = -\frac{1}{\rho_0}\frac{\partial p}{\partial x} \tag{3.70}$$

$$f\,u = -\frac{1}{\rho_0}\frac{\partial p}{\partial y} \tag{3.71}$$

$$g = -\frac{1}{\rho_0}\frac{\partial p}{\partial z} \tag{3.72}$$

and the continuity equation is:

$$0 = \frac{\partial u}{\partial x} + \frac{\partial v}{\partial y} + \frac{\partial w}{\partial z} \tag{3.73}$$

Taking the z derivative of (3.70) and using (3.72) gives:

$$-f_0\frac{\partial v}{\partial z} = -\frac{1}{\rho_0}\frac{\partial}{\partial z}\left(\frac{\partial p}{\partial x}\right) = \frac{\partial}{\partial x}\left(-\frac{1}{\rho_0}\frac{\partial p}{\partial z}\right) = \frac{\partial g}{\partial x} = 0 \tag{3.74}$$

Therefore for $f_0 \neq 0$

$$\frac{\partial v}{\partial z} = 0$$

Similarly, for the u-component of velocity (3.71). Thus, the vertical derivative of the horizontal velocity field must be zero.

$$\frac{\partial u}{\partial z} = \frac{\partial v}{\partial z} = 0 \tag{3.75}$$

The flow is two-dimensional and does not vary in the vertical direction. This is the *Taylor-Proudman Theorem*, which applies to slowly varying flows in a homogeneous, rotating, inviscid fluid. The theorem places strong constraints on the flow[9]. The physical origin of this strangely

---

[9]Taylor (1921): If therefore any small motion be communicated to a rotating fluid the resulting motion of the fluid must be one in which any two particles originally in a line parallel to the axis of rotation must remain so, except for

constrained flow is in the stiffness endowed to the fluid by rapid rotation of the Earth, which has a peculiarly strong sense along the axis of rotation. Taylor's laboratory experiments showed how homogeneous fluid tends to move in vertical columns. Dye in the water forms curtains, and viewing the dye from above shows fine twists and whirls that are vertically coherent.

Hence, rotation greatly stiffens the flow! Geostrophic flow cannot go over a seamount, it must go around it. Taylor [1917] explicitly derived (3.75) and (3.77) below. Proudman [1916] independently derived the same theorem but not as explicitly.

Laboratory experiments showing the formation of a Taylor column, go to 2:50, other material: vorticity and circulation, boundary layers, good introduction, Taylor column

Vertical velocity in the the Taylor-Proudman theorem

Further consequences of the theorem can be obtained by eliminating the pressure terms from (3.70, 3.71) to obtain:

$$
\begin{aligned}
\frac{\partial u}{\partial x} + \frac{\partial v}{\partial y} &= -\frac{\partial}{\partial x}\left(\frac{1}{f_0\rho_0}\frac{\partial p}{\partial y}\right) + \frac{\partial}{\partial y}\left(\frac{1}{f_0\rho_0}\frac{\partial p}{\partial x}\right) \\
&= \frac{1}{f_0\rho_0}\left(-\frac{\partial^2 p}{\partial x \partial y} + \frac{\partial^2 p}{\partial x \partial y}\right) = 0
\end{aligned}
\tag{3.76}
$$

Because the fluid is incompressible, the continuity equation (3.73) requires

$$
\frac{\partial w}{\partial z} = 0
\tag{3.77}
$$

Furthermore, because $w = 0$ at the sea surface and at the sea floor, if the bottom is level, there can be no vertical velocity on an f-plane.

---

possible small oscillations about that position.

Geostrophic flow: Vertical velocity leads to north-south currents

If the Taylor-Proudman theorem in (3.77) is true, the flow cannot expand or contract in the vertical direction, and it is indeed as rigid as a steel bar. Since we observe gradients of vertical movements, one of the constraints used in deriving (3.77) must be violated, i.e. our assumption that $f = f_0$ can not be a good approximation.

Going back to (3.56):

$$\frac{D}{Dt}(\zeta + f) + (\zeta + f)\left(\frac{\partial u}{\partial x} + \frac{\partial v}{\partial y}\right) = 0 \quad . \tag{3.78}$$

we obtain

$$\beta v \quad + \quad f\left(\frac{\partial u}{\partial x} + \frac{\partial v}{\partial y}\right) = 0 \quad . \tag{3.79}$$

Using the continuity equation, we obtain

$$f\frac{\partial w_g}{\partial z} = \beta v \tag{3.80}$$

where we have used the subscript $_g$ to emphasize that (3.80) applies to the ocean's interior, geostrophic flow. Thus the variation of Coriolis force with latitude allows vertical velocity gradients in the geostrophic interior of the ocean, and the vertical velocity leads to north-south currents.

Chapter 4

Atmospheric Models

4.1 Angular momentum and Hadley Cell

Exercise 30 – Angular momentum and Hadley Cell

Consider a zonally symmetric circulation (i.e., one with no longitudinal variations) in the atmosphere. In the inviscid upper troposphere one expects such a flow to conserve absolute angular momentum, i.e.,

$$\frac{DA}{Dt} = 0,$$

where A is the absolute angular momentum per unit mass (parallel to the Earth's rotation axis)

$$A = r\left(u + \Omega r\right) = \Omega a^2 \cos^2 \varphi + ua \cos \varphi \quad .$$

Ω is the Earth rotation rate, u the eastward wind component, $r = a \cos \varphi$ is the distance from the rotation axis, a the Earth's radius, and φ latitude.

1. Show, for inviscid zonally symmetric flow, that the relation $\frac{DA}{Dt} = 0$ is consistent with the zonal component of the equation of motion (using our standard notation, with F_x the
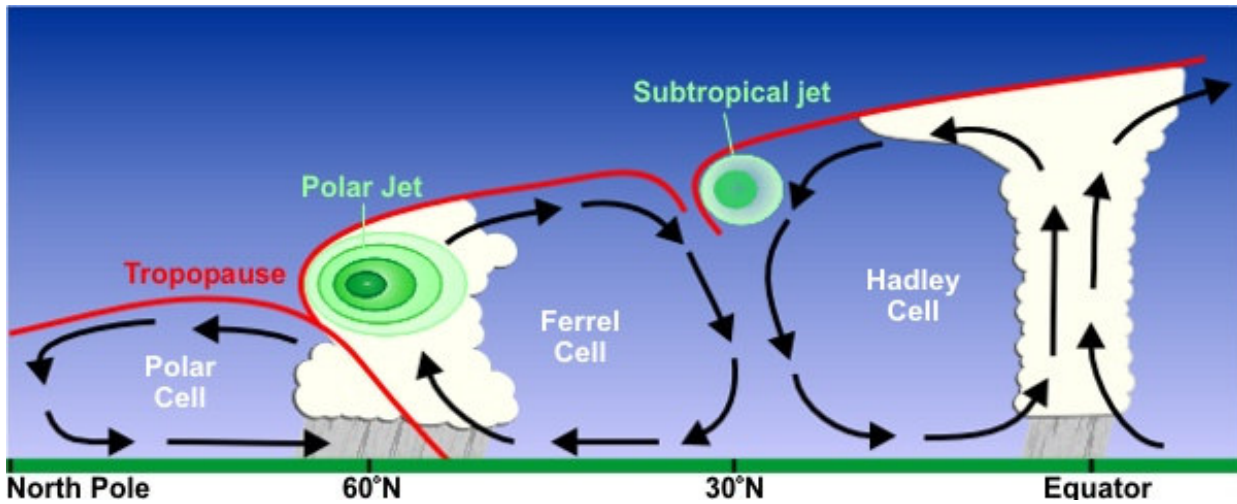
Figure 4.1: Cross section of the subtropical and polar jet streams by latitude.

x-component of the friction force per unit mass)

$$\frac{Du}{Dt} - fv = -\frac{1}{\rho}\frac{\partial p}{\partial x} + F_x$$

in (x, y, z) coordinates, where $y = a\varphi$.

2. Use angular momentum conservation to describe how the existence of the Hadley circulation explains the existence of both the subtropical jet in the upper troposphere.

   Hint: In the upper troposphere, the flow leaves the rising branch of the Hadley cell at the equator (cf. Fig. 4.2) with angular momentum density $A_0 = \Omega a^2$, if we assume that the flow rises from the ground there with no relative motion. The zonal flow can then be described as $u = \Omega a \sin^2 \varphi / \cos \varphi$. Show that the zonal flow will be greatest at the edge of the cell, where φ is greatest, thus producing the subtropical jet.

   Note that $\Omega a^2 = \frac{2\pi}{86400\,s} \cdot (6.371 \cdot 10^6 m)^2 = 3 \cdot 10^9 m^2 s^{-1}$.

3. Describe the near-surface trade winds by recognizing that this low-level flow is under the influence of surface friction and A will therefore be progressively reduced. Show that

$$u_{low} < \Omega a \frac{\sin^2 \varphi}{\cos \varphi}.$$
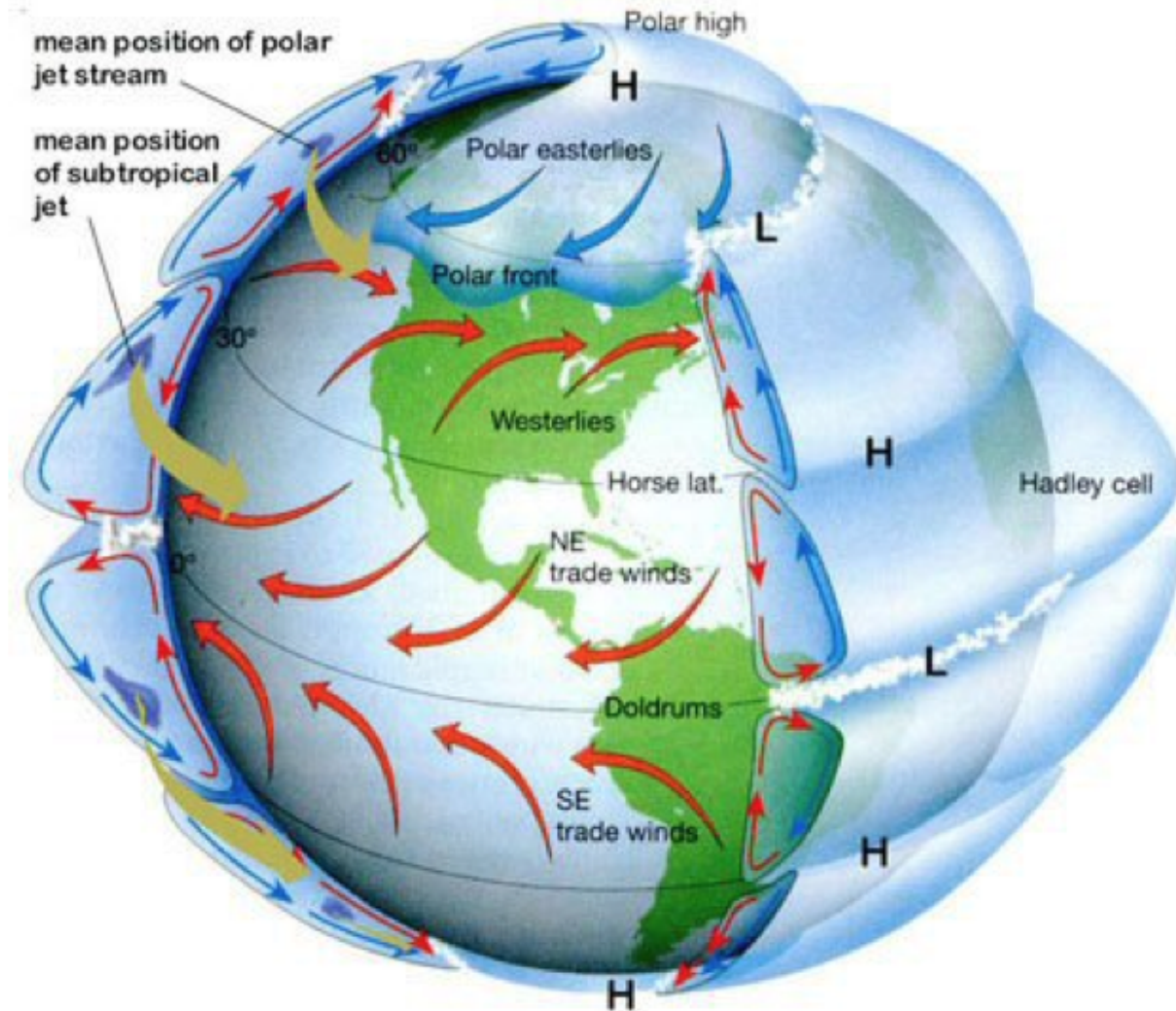
Figure 4.2: Schematic picture of the Hadley Cell and the jet streams. Subtropical jet forms at the poleward limit of the tropical Hadley cell and to first order this circulation is symmetric with respect to longitude. Tropical air rises to the tropopause, and moves poleward before sinking; this is the Hadley cell circulation. As it does so it tends to conserve angular momentum, since friction with the ground is slight. Air masses that begin moving poleward are deflected eastward by the Coriolis force (true for either hemisphere), which for poleward moving air implies an increased westward component of the winds (note that leftward deflection in the southern hemisphere).

and some φ that u_{low} becomes negative (eastward winds).

4. If the Hadley circulation is symmetric about the equator, and its edge is at $\mathbf{20°}$ latitude, determine the strength of the subtropical jet.

   (The observed zonal winds are weaker than the value. In reality, non-axisymmetric atmospheric eddies act to reduce angular momentum in the outflow, and hence reduce the strength of the jets.)

5. Consider the tropical Hadley circulation in northern winter. The circulation rises at $\mathbf{10°S}$, moves northward across the equator in the upper troposphere, and sinks at $\mathbf{20°N}$. Assuming that the circulation, outside the near-surface boundary layer, is zonally symmetric (independent of x) and inviscid (and thus conserves absolute angular momentum about the Earth's rotation axis), and that it leaves the boundary layer at $\mathbf{10°S}$ with zonal velocity u = 0, calculate the zonal wind in the upper troposphere and provide the numbers for the equator, $\mathbf{10°N}$, and $\mathbf{20°N}$.

Solution of Exercise 30

1. For inviscid axisymmetric flow, conservation of angular momentum implies

$$D_t(\Omega a^2 \cos^2 \varphi + ua \cos \varphi) = 0$$

Remember that $y = a\varphi,\ dx = a \cos \varphi\, d\lambda$. Here, we reformulate the planetary term:

$$D_t(\Omega a^2 \cos^2 \varphi) = v\partial_y(\Omega a^2 \cos^2 \varphi) \tag{4.1}$$
$$= \Omega av\partial_\varphi(\cos^2 \varphi) \tag{4.2}$$
$$= -2\Omega av \sin \varphi \cos \varphi \tag{4.3}$$
$$= -fv \cdot a \cos \varphi \tag{4.4}$$

Similar
$$D_t(ua \cos \varphi) = a \cos \varphi D_t u + u \cdot v\, \partial_\varphi \cos \varphi \tag{4.5}$$

where in the coordinate system

$$D_t u = (\partial_t + u\partial_x + v\partial_y)u + \frac{uv}{a}\tan\varphi \qquad (4.6)$$

(the last term is a metric term). Therefore and under the assumption $\partial_x p = 0$:

$$D_t u - fv = 0 \qquad (4.7)$$

2. Use angular momentum conservation to describe how the existence of the Hadley circulation explains the existence of both the subtropical jet in the upper troposphere. In the upper troposphere, the flow leaves the rising branch of the Hadley cell at the equator (cf. Fig. 4.2) with angular momentum density $A_0 = \Omega a^2$, if we assume that the flow rises from the ground there with no relative motion. We have

$$A = \Omega a^2 \cos^2\varphi + ua\cos\varphi = A_0 = \Omega a^2$$

and therefore the zonal flow can then be described as

$$u = \Omega a \sin^2\varphi/\cos\varphi .$$

The zonal flow will be greatest at the edge of the cell, where φ is greatest, thus producing the subtropical jet.

3. If the return flow, in the lower troposphere, were inviscid and thus also conserved angular momentum with $A_{low} = A_0$, then at a given latitude the low level flow would be the same as that aloft, since in u is a function of φ only. However, in reality this low-level flow is under the influence of surface friction and A will therefore be progressively reduced. Thus,

$$A_{low} = \Omega a^2 \cos^2\varphi + u_{low}a\cos\varphi < A_0 = \Omega a^2$$

$$\text{Thus} \quad u_{low} < \Omega a \frac{\sin^2 \varphi}{\cos \varphi}$$

and some φ_0 north of the equator that u_{low} becomes negative (eastward winds), and so the low level flow will be equatorward and eastward there. (Note that $\Omega a^2 = \frac{2\pi}{86400\ s} \cdot (6.371 \cdot 10^6 m)^2 = 3 \cdot 10^9 m^2 s^{-1}$.)

4. Assume the Hadley circulation is symmetric about the equator, and its edge is at $20°$ latitude, determine the strength of the subtropical jet by

$$u(20°) = \Omega a \sin^2(20°)/\cos(20°) = 57.6\ m\ s^{-1}$$

The observed zonal winds are weaker than the value. In reality, non-axisymmetric atmospheric eddies act to reduce angular momentum in the outflow, and hence reduce the strength of the jets.

5. Consider the angular momentum $A = \Omega a^2 \cos^2 \varphi + ua \cos \varphi = A_0 = \Omega a^2$ with $A_0 = \Omega a^2 \cos^2(10°S) = 2.952 \cdot 10^9 m^2 s^{-1}$.

$$\text{Therefore} \quad u = \frac{A_0 - \Omega a^2 \cos^2 \varphi}{a \cos \varphi}$$

At $\varphi = 0°, u = -13.9\ ms^{-1}$, at $\varphi = 10°, u = 0\ ms^{-1}$, at $\varphi = 20°, u = 42.8\ ms^{-1}$.

4.2 Engery balance model

Energy balance models (EBM) are highly simplified systems of the climate system. A zero-dimensional model of the radiative equilibrium of the Earth is

$$(1 - \alpha)S\pi R^2 = 4\pi R^2 \epsilon \sigma T^4 \tag{4.8}$$

where the left hand side represents the incoming energy from the Sun (the disk) the right hand side represents the outgoing energy from the Earth (the globe), calculated from the Stefan-Boltzmann law assuming a constant radiative temperature, T, that is to be found, and S is the solar constant - the incoming solar radiation per unit area– about $1367 W m^{-2}$, α is the Earth's average albedo, measured to be 0.3. R is Earth's radius = 6.371×10^6 m, σ is the Stefan-Boltzmann constant = $5.67 \times 10^{-8} J K^{-4} m^{-2} s^{-1}$, and ϵ is the effective emissivity of earth (about 0.612). The geometrical constant πR^2 can be factored out, giving

$$(1 - \alpha)S = 4\epsilon\sigma T^4 \tag{4.9}$$

Solving for the temperature,

$$T = \sqrt[4]{\frac{(1 - \alpha)S}{4\epsilon\sigma}} \tag{4.10}$$

This yields an average earth temperature of **288** K. This is because the above equation represents the effective radiative temperature of the Earth (including the clouds and atmosphere). The use of effective emissivity and albedo account for the greenhouse effect.

Note that S itself stems from effective temperature of the sun is the temperature of a black body with the same luminosity per surface area (FBol) as the star and is defined according to the Stefan-Boltzmann law σT_{eff}^4. Notice that the total (bolometric) luminosity of a star is then $L = 4\pi R2\sigma T_{eff}^4$, where R is the stellar radius. The effective temperature of our Sun is around 5780 K.

Stars have a decreasing temperature gradient, going from their central core up to the atmosphere. The "core temperature" of the Sun-the temperature at the centre of the Sun where nuclear reactions take place-is estimated to be 15,000,000 K The effective (blackbody) temperature of a planet can be calculated by equating the power received by the planet with the power emitted by a blackbody of temperature T.

Take the case of a planet at a distance D from the star, of luminosity L.

Assuming the star radiates isotropically and that the planet is a long way from the star, the power absorbed by the planet is given by treating the planet as a disc of radius r, which intercepts some of the power which is spread over the surface of a sphere of radius D (the distance of the planet from the star).

The average emissivity of the earth is estimated from available data. The emissivities of terrestrial surfaces are all in the range of 0.96 to 0.99 (except for some small desert areas which may be as low as 0.7). Clouds, however, which cover about half of the earth's surface, have an average emissivity of about 0.5 (which must be reduced by the fourth power of the ratio of cloud absolute temperature to average earth absolute temperature) and an average cloud temperature of about 258 K. Taking all this properly into account results in an effective earth emissivity of about 0.64 (earth average temperature 285 K). This simple model determines the effect of changes in solar output or change of earth albedo or effective earth emissivity on average earth temperature. It says nothing, however about what might cause these things to change. Zero-dimensional models do not address the temperature distribution on the earth or the factors that move energy about the earth.

Exercise 31 – **Energy balance**

The EMB (4.8) determines the effect on average earth temperature of changes in solar constant or change of albedo or effective earth emissivity. Show: The percent change of the average amount of each parameter, considered independently, to cause a one degree Kelvin change in steady-state average earth temperature is Solar constant 1.4%, Albedo 3.3%, Effective emissivity 1.4% using (4.10).

```
## here is the simple calculation:
alpha=0.3
S=1367
sigma=5.67e-8
epsilon=0.612
T= sqrt(sqrt( (1-alpha ) * S/(4 *epsilon* sigma) ))
T
```

Let us have a closer look onto (4.8). The local radiative equilibrium of the Earth is

$$\epsilon\sigma T^4 = (1-\alpha)S\cos\varphi\cos\Theta \quad \times 1_{[-\pi/2<\Theta<\pi/2]}(\Theta) \tag{4.11}$$

Integration over the Earth surface is

$$\int_{-\pi/2}^{\pi/2} Rd\varphi \int_0^{2\pi} R\cos\varphi d\Theta\,\epsilon\sigma T^4 = \int_{-\pi/2}^{\pi/2} R\cos^2\varphi d\varphi \int_{-\pi/2}^{\pi/2} R\cos\Theta d\Theta\,(1-\alpha)S$$

$$\epsilon\sigma R^2 \int_{-\pi/2}^{\pi/2} d\varphi \int_0^{2\pi}\cos\varphi d\Theta\,T^4 = (1-\alpha)SR^2 \underbrace{\int_{-\pi/2}^{\pi/2} d\varphi\cos^2\varphi}_{\frac{\pi}{2}} \underbrace{\int_{-\pi/2}^{\pi/2}\cos\Theta d\Theta}_{2}$$

$$\epsilon\sigma 4\pi\overline{T^4} = (1-\alpha)S\,\pi \tag{4.12}$$

giving a similar formula as (4.10) with the definition for the average

$$\overline{T^4} = \frac{1}{4\pi}\int_{-\pi/2}^{\pi/2} d\varphi \int_0^{2\pi}\cos\varphi d\Theta \quad T^4 \quad .$$

What we really want is the mean of the temperature $\overline{T}$. Therefore, we take the fourth root of (4.11):

$$T = \sqrt[4]{\frac{(1-\alpha)S\cos\varphi\cos\Theta}{\epsilon\sigma}} \quad \times 1_{[-\pi/2<\Theta<\pi/2]}(\Theta) \tag{4.13}$$

and integrate this over the sphere:

$$\overline{T} = \sqrt[4]{\frac{(1-\alpha)S}{\epsilon\sigma}}\frac{1}{4\pi}\int_{-\pi/2}^{\pi/2} d\varphi \int_{-\pi/2}^{\pi/2}\cos\varphi d\Theta\sqrt[4]{\cos\varphi\cos\Theta}$$

$$\overline{T} = \sqrt[4]{\frac{(1-\alpha)S}{4\epsilon\sigma}}\frac{\sqrt{2}}{4\pi}\underbrace{\int_{-\pi/2}^{\pi/2}(\cos\varphi)^{5/4}d\varphi}_{1.86}\underbrace{\int_{-\pi/2}^{\pi/2}(\cos\Theta)^{1/4}d\Theta}_{2.70} \tag{4.14}$$

$$= 0.4\sqrt{2}\sqrt[4]{\frac{(1-\alpha)S}{4\epsilon\sigma}} = 0.57\sqrt[4]{\frac{(1-\alpha)S}{4\epsilon\sigma}} \tag{4.15}$$

Therefore, $\overline{T} \approx 163\text{K}$ is a factor **0.57** lower than **288 K** as stated at (4.8). This zero-dimensional

models do not address the heat capacity and the proper temperature distribution on the earth.

```
## here is the simple calculation:
integrand1 <- function(x) {(cos(x))^(5/4)}
integrand2 <- function(x) {(cos(x))^(1/4)}
a1=integrate(integrand1, lower = -pi/2, upper = pi/2)
a2=integrate(integrand2, lower = -pi/2, upper = pi/2)
a=a1$value*a2$value/(4 * pi) *sqrt(2)
```

Which effective ϵ we would expect then? Basically an $\epsilon = \mathbf{0.065}$ is a factor 10 lower than above

which is unrealistic (see below).

If we calculate the zonal mean of (4.13) by integration at the latitudinal cycles

$$\frac{1}{2\pi} \int_0^{2\pi} d\Theta$$

we have

$$T(\varphi) = 0.61 \cdot \sqrt[4]{\frac{(1-\alpha)S}{4\epsilon\sigma}} \quad (\cos\varphi)^{1/4} \tag{4.16}$$

as a function on latitude. Here is the calculation:

```
## here is the simple calculation:
alpha=0.3
S=1367
sigma=5.67e-8
epsilon0=0.612
lat=pi/2/90
phi=c(-89:89)

integrand2 <- function(x) {(cos(x))^(1/4)}
a2=integrate(integrand2, lower = -pi/2, upper = pi/2)
b=a2$value/(2 * pi) *sqrt(2)
T= b*sqrt(sqrt( (1-alpha ) * S/(4*epsilon0* sigma) * (cos(lat*phi))^(1/4) ))
Tc=T -273
plot(phi,Tc,type="l",col="red")

dev.copy(png,'ebm_model.png')
dev.off()
```

What happens here is that the heat capacity of the Earth is neglected. During night, the temperature is zero and there is a a strong non-linearity of the outgoing radiation. Furthermore, the
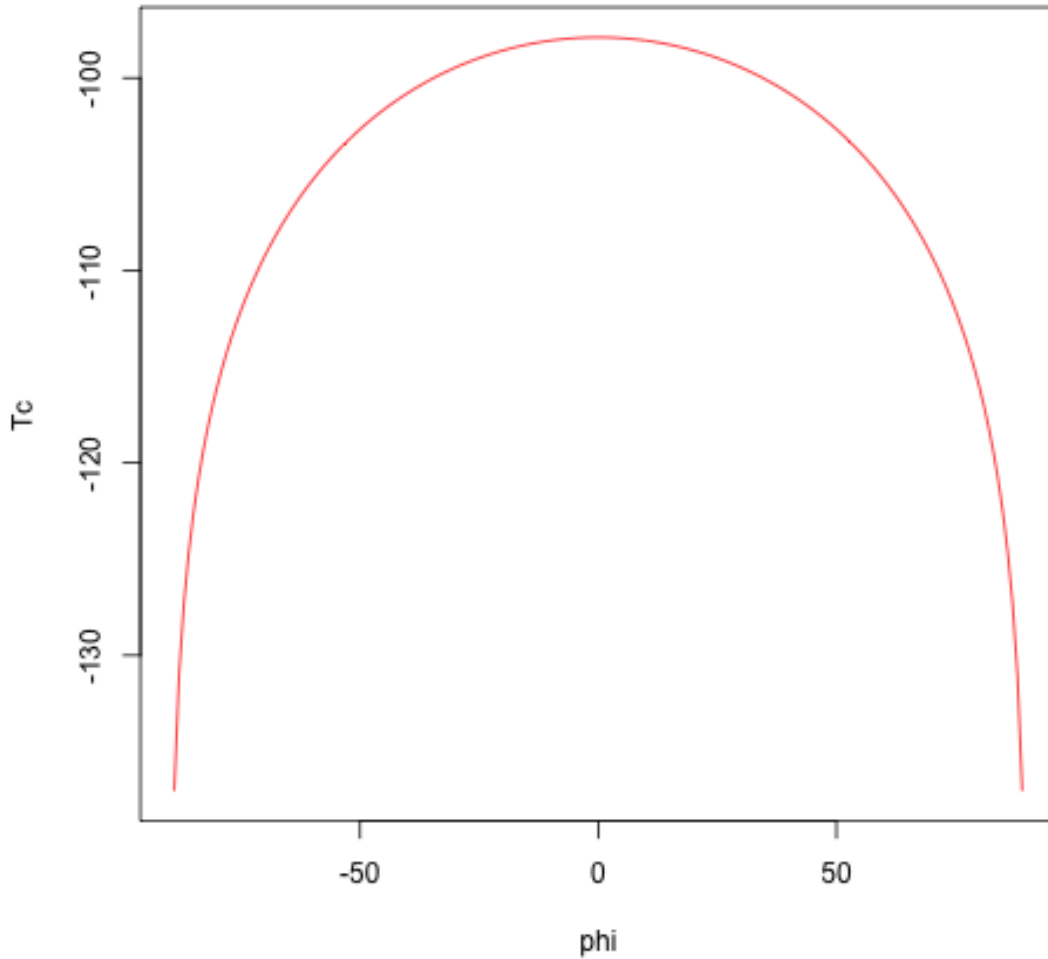
Figure 4.3: Latitudinal temperatures of the EBM with zero heat capacity (4.16).

Earth is a rapidly rotating object. (4.13) can be better used for an object like the moon without an atmosphere, without a significnt heat capacity, and a slowly rotating body. The correct energy balance shall be

$$C_p\,\partial_t T \;=\; (1-\alpha)S\cos\varphi\cos\Theta \quad \times \mathbf{1}_{[-\pi/2<\Theta<\pi/2]}(\Theta) \;-\; \epsilon\sigma T^4 \quad . \qquad (4.17)$$

with C_p representing the heat capacity multiplied with the depth of the atmosphere-ocean layer. If we consider the zonal mean and averaged over the diurnal cycle, wecan assume that the heat capacity is mainly given by the ocean. Observational evidence is that the diurnal variation of the ocean surface is in the order of 1-2 K only. The energy balance (4.17) is integrated over the longitude and over the day

$$\tilde{T}(\tilde{t}) = \frac{1}{2\pi} \int_0^{2\pi} T(t) \, d\Theta \quad \text{with} \quad \tilde{T}^4 \approx \frac{1}{2\pi} \int_0^{2\pi} T^4 \, d\Theta$$

and therefore

$$C_p \, \partial_{\tilde{t}} \tilde{T} \;=\; (1-\alpha)S \cos\varphi \cdot \underbrace{\frac{1}{2\pi} \int_{-\pi/2}^{\pi/2} \cos\Theta \, d\Theta}_{2} - \epsilon\sigma\tilde{T}^4 \tag{4.18}$$

$$=\; (1-\alpha)\frac{S}{\pi} \cos\varphi - \epsilon\sigma\tilde{T}^4 \quad . \tag{4.19}$$

In the following we will drop the tilde sign.

The linearized EBM

Since we know the approximate temperature on Earth, we may linearize (4.13) around $0°C$. It reduces to

$$(1-\alpha)S \cos\varphi \cos\Theta \quad \times 1_{[-\pi/2<\Theta<\pi/2]}(\Theta) = A + BT_C \tag{4.20}$$

where $A = \epsilon \sigma 273^4 K^4 = 193 W/m^2$, $B = \epsilon \sigma 3T^3 273^3 K^3 = 2.1 W/m^2/K$ comes from the Taylor expansion, and T_C is the temperature in °C. Then,

$$A + BT_C = (1 - \alpha)S \cos\varphi \cdot \frac{1}{2\pi} \underbrace{\int_{-\pi/2}^{\pi/2} \cos\Theta \, d\Theta}_{2} \tag{4.21}$$

$$= (1 - \alpha)\frac{S}{\pi}\cos\varphi \tag{4.22}$$

$$T_C = (1 - \alpha)\frac{S}{\pi B}\cos\varphi - \frac{A}{B} \tag{4.23}$$

The global mean is therefore

$$\overline{T_C} = (1 - \alpha)\frac{S}{\pi B}\frac{1}{2}\underbrace{\int_{-\pi/2}^{\pi/2} d\varphi \cos^2\varphi}_{\frac{\pi}{2}} - \frac{A}{B} \tag{4.24}$$

$$= (1 - \alpha)\frac{S}{4B} - \frac{A}{B} \tag{4.25}$$

seen as the green line in Fig. 4.5 with 12.4°C.

```
## here is the simple calculation for the linear model:
alpha=0.3
S=1367
sigma=5.67e-8
epsilon0=0.612
lat=pi/2/90
phi=c(-89:89)
A=epsilon0 * sigma *273^4
A=213

B=epsilon0 *sigma* 3 *  273^3
rhs= 2/(2*pi)* (1-alpha ) * S* cos(lat*phi)
Tc=(rhs- A)/B
plot(phi,Tc,type="l",col="black")

Tm=  ((1-alpha ) * S/(4*B)   -A/B)  * rep(1, 179)
lines(phi,Tm,col="green")

dev.copy(png,'ebm_linear_model.png')
dev.off()
```

In section 4.3 we will explore in detail the influence of meridional transports on temperatures,
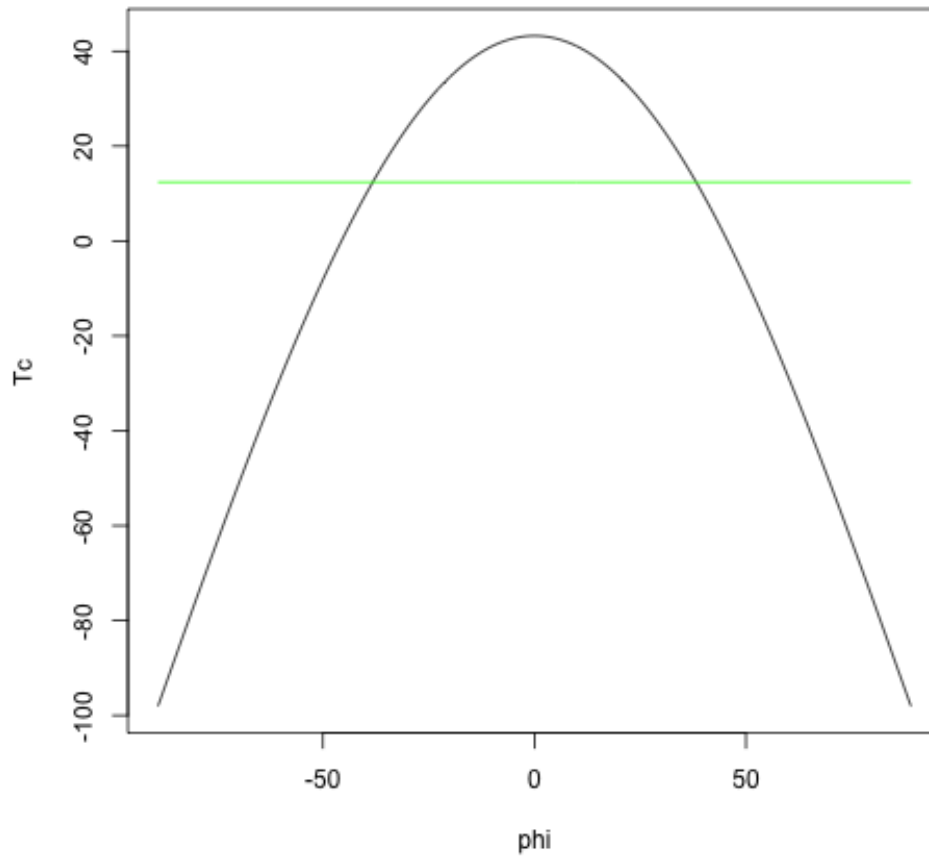
Figure 4.4: Temperatures of the linear EBM: (4.23) in red and (4.33) in green showing the mean. The model has been tuned by the parameter $A = 213W/m^2$.

where the transport is parameterized as diffusion and the radiative fluxes are as in (4.23). Here, we

start with a simplfied approach first.

Exercise 32   –   Analytical EBM

Solve the vertically integrated energy equation where we include the atmosphere and ocean in

one temperature T and describe the heat transport (sensible, latent and ocean) as diffusion:

$$C_p \, \partial_t T \; = \; k \, \partial_y^2 T \; + \; (1 - \alpha) Q_S^{top} - (A + B \; T) \qquad (4.26)$$

The albedo $\alpha = 0.3$ is chosen as a fixed parameter, $y = R\varphi$, and

$$Q_S^{top} = \frac{S}{\pi} \cdot \cos \varphi \quad . \qquad (4.27)$$

Furthermore, there is no transport across the poles. The gradient at the North and South Pole vanishes:

$$\partial_y T(\varphi = \pm \pi / 2) \; = \; 0 \quad . \qquad (4.28)$$

Solution

One can separate the dynamics into a gloal mean and a function depending on latitude.

$$\overline{T} \; = \; \frac{1}{2} \int_{-\pi/2}^{\pi/2} T d\varphi \cos \varphi \qquad (4.29)$$

$$T_1 \; = \; T - \overline{T} \qquad (4.30)$$

Therefore,
$$C_p \frac{d}{dt}\overline{T} \; = \; (1 - \alpha)\frac{S}{2\pi} \int_{-\pi/2}^{\pi/2} d\varphi \cos^2 \varphi - (A + B \; \overline{T}) \qquad (4.31)$$

$$= \; (1 - \alpha)\frac{S}{4} - (A + B \; \overline{T}) \qquad (4.32)$$

for the global mean with the solution

$$\overline{T}(t) = (1 - \alpha)S \; \frac{1}{4B} \; - \; \frac{A}{B} \; + \; \overline{T}(t = 0) \cdot \exp\left(-\frac{B}{C_p}t\right) \qquad (4.33)$$

Typical values for C_p are $2 \cdot 10^8 \, J/m^2/K$.

For T_1 we have

$$C_p \partial_t T_1 \;=\; \frac{k}{R^2} \partial_\varphi^2 T_1 + (1 - \alpha) S \left(\frac{\cos \varphi}{\pi} - \frac{1}{4} \right) - B T_1 \tag{4.34}$$

$$\;=\; \left[\frac{k}{R^2} \partial_\varphi^2 - B \right] T_1 + (1 - \alpha) S \left(\frac{\cos \varphi}{\pi} - \frac{1}{4} \right) \tag{4.35}$$

Because of the boundary condition (4.28), the solution for T_1 must have the form $a_l \cos(l\varphi)$

$$T_1 = \sum_{l=1}^{\infty} a_l \cos(l\varphi) + C \tag{4.36}$$

For the homogenous part of (4.35), we have

$$\frac{d}{dt} a_l \;=\; - \left[\frac{\frac{kl^2}{R^2} + B}{C_p} \right] a_l \tag{4.37}$$

$$a_l \;=\; \exp \left(- \left[\frac{\frac{kl^2}{R^2} + B}{C_p} \right] t \right) \tag{4.38}$$

For the inhomogenous part, we are seeking for a particular solution for (4.35):

$$T_1^p = a_1 \cos \varphi + C \tag{4.39}$$

and therefore

$$0 = \left[\frac{k}{R^2} \partial_\varphi^2 - B \right] (a_1 \cos \varphi + C) + (1 - \alpha) \frac{S}{\pi} \cdot \cos \varphi - (1 - \alpha) \frac{S}{4} \tag{4.40}$$

giving two conditions
$$0 \;=\; \left[-\frac{k}{R^2} - B \right] a_1 + (1 - \alpha) \frac{S}{\pi} \tag{4.41}$$

$$0 \;=\; -BC - (1 - \alpha) \frac{S}{4} \tag{4.42}$$

and can calulate the constants

$$a_1 \;\; = \;\; (1 - \alpha)\frac{S}{\pi}\left[\frac{k}{R^2} + B\right]^{-1} \tag{4.43}$$

$$C \;\; = \;\; -(1 - \alpha)\frac{S}{4B} \tag{4.44}$$

to get finally

$$T_1 = (1 - \alpha)\frac{S}{\pi}\left[\frac{k}{R^2} + B\right]^{-1}\cos\varphi - (1 - \alpha)\frac{S}{4B} + \sum_{l=2}^{\infty} a_l\cos(l\varphi) \tag{4.45}$$

The equilibrium solution is therefore

$$T_{eq} = \lim_{t\to\infty} T = -\frac{A}{B} \;\; + (1 - \alpha)\frac{S}{\pi}\left[\frac{k}{R^2} + B\right]^{-1}\cos\varphi \tag{4.46}$$

```
## here is the calculation for the 1 dim energy balance model:
alpha=0.3
S=1367
sigma=5.67e-8
epsilon0=0.612
lat=pi/2/90
phi=c(-89:89)

A=epsilon0 * sigma *273^4
A=213
r=40.0e6/(2*pi)
k=1*r^2
B=epsilon0 *sigma* 3 *  273^3
km= k/r^2 +B
Amod=A - (1-alpha ) * S/4  *(k/r^2)/km

rhs2= 1/(pi)* (1-alpha ) * S* cos(lat*phi) /B
Tc2=  - A/B + rhs2
plot(phi,Tc2,type="l",col="red")

rhs= 1/(pi)* (1-alpha ) * S* cos(lat*phi)  *(k/r^2 +B)^(-1)
Tc=  - Amod/B + rhs
lines(phi,Tc,type="l",col="blue")
Tm=  ((1-alpha ) * S/(4*B)  -A/B)  * rep(1, 179)
lines(phi,Tm,col="green")

dev.copy(png,'ebm_linear_1d_model.png')
dev.off()
```
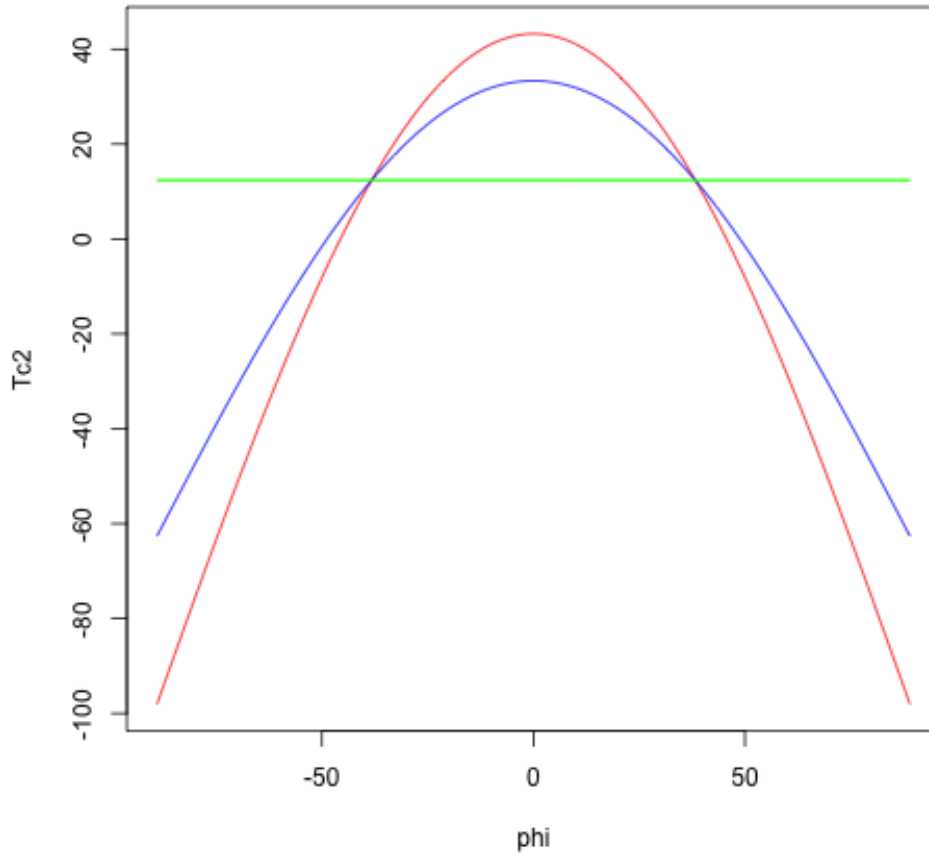
Figure 4.5: Temperatures of the linear EBM: (4.23) in red and (4.33) in green showing the mean with no diffusion. The new one-dimensional model (4.46) is in blue. The model has been tuned by the parameter A to give the same mean temperature (see code). Maximum and minimum temperatures for red are at 43°C and -98°C, whereas for blue are for 33°C and -63°C, respectively.

As a logical next step, we now integrate the non-linear energy balance numerically.

$$C_p \, \partial_t T \; = \; k \, \partial_y^2 T \; + \; (1 - \alpha) \frac{S}{\pi} \cos \varphi \; - \; \epsilon \sigma T^4 \quad . \tag{4.47}$$

Exercise 33   –   Numerical solution of 1D EBM

- Calculate the one-dimensional EBM using differnt time steps

- Identify / extract the finite difference scheme which is used approximate the 2nd derivative

- Run the program and play with the parameters (heat capacity, diffusion coefficient).

```r
# EBM_EulerForward.R
# 1D diffusion EBM equation, explicit scheme

alpha=0.3
S=1367
sigma=5.67e-8
epsilon0=0.612
lat=pi/2/90
phi=c(-90:90)
cp=4.2e6 *1 # cp_water = 4.6e3; rho_water=1e3; h=1m
r=40.0e6/(2*pi)
tabs=272
ddx=40.0e6/360
coslat=cos(phi *lat)
k=(1.5e6 + 2.5e6 * coslat)  # in m^2/s
knorm=1.5e6* rep(1, 181)


plot(phi,k,type="l",col="red", main = "Diffusion",xlim = c(-90, 90),  ylim = c(0, 4.1
lines(phi,k/2,type="l",col="blue")
lines(phi,knorm,type="l",col="green")
dev.copy(png,'Diffusion_ebm_1d.png')
dev.off()

#Constants
L.X<-179 #width of lattice
L.T<-5000000  #length of time
dx <- ddx    #space step in m
dt <- 1000 #time step in s
D<-  k          #Diffusion coefficent
globini=270  # initial condition
N.x<-L.X + 2   #number of space boxes + 2 boundary boxes
N.t<-L.T/dt      #number of time boxes

dtc=dt/cp
dtcdx=dtc/(dx^2)
dtdx=dt/(dx^2)
cfl=dtdx*max(D)  # CFL criterium, this number shall be smaller than 0.5

T<-matrix(globini,N.t,N.x)   #grid
Transport <-matrix(0,N.t,N.x)

#temporary vector which stores the state of of one timestep:
T.temp<-rep(globini,N.x)
Transport.temp<-rep(0,N.x)
```

```
#Set the starting and boundary condition, here one value in the middle:
T[1,N.x/2]<- globini

for (n in 1:(N.t-1))
{
  for (j in 2:(N.x-1))
  {
    sw=(1-alpha)*S/pi *coslat[j]
    lw=epsilon0*sigma * T.temp[j]^4
    T.temp[j]<-T[n,j]+D[j]*dtdx*(T[n,j+1]-2*T[n,j]+T[n,j-1])+dtc*(sw -lw)
    Transport.temp[j]=cp*D[j]*(T[n,j+1]-T[n,j])/ddx * 40.e6*coslat[j]
  }
  T.temp[1] <- T.temp[2]
  T.temp[N.x] <- T.temp[N.x-1]
  Transport.temp[1]=0
  Transport.temp[N.x]=0
  T[n+1,]<-T.temp
  Transport[n+1,]=Transport.temp
}

filled.contour((1:N.t)*dt/1e6,phi,T-tabs,
        color.palette=rainbow,xlab="time",ylab="latitude")

dev.copy(png,'ebm_nonlinear_1d_num.png')
dev.off()

filled.contour((1:N.t)*dt/1e6,phi,Transport*1e-15,
        color.palette=rainbow,xlab="time",ylab="latitude")

dev.copy(png,'Transport_ebm_nonlinear_1d_num.png')
dev.off()
#---
# plot equilibrium
A=epsilon0 * sigma *273^4
A=213
r=40.0e6/(2*pi)
k=1*r^2
B=epsilon0 *sigma* 3 *  273^3
km= k/r^2 +B
Amod=A - (1-alpha ) * S/4  *(k/r^2)/km
rhs2= 1/(pi)* (1-alpha ) * S* cos(lat*phi) /B
Tc2=  - A/B + rhs2
plot(phi,Tc2,type="l",col="black")

lines(phi,T[N.t,]-tabs,type="l",col="red")
max(T[N.t,]-tabs)

dev.copy(png,'End_ebm_nonlinear_1d_num.png')
dev.off()
```
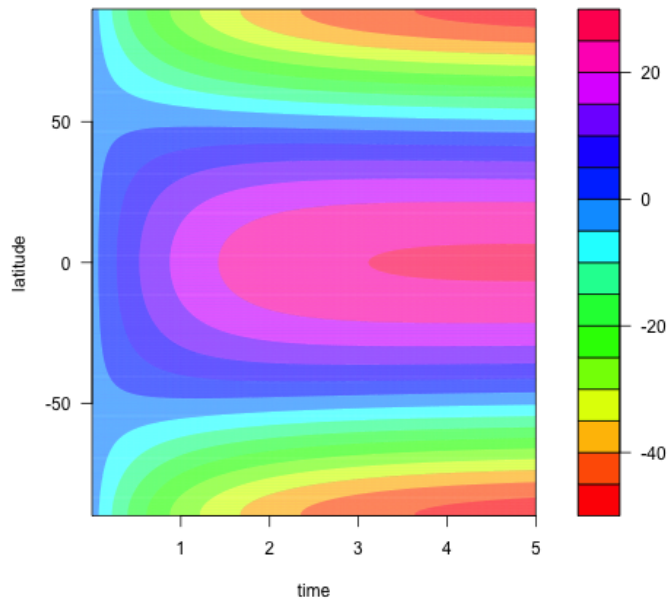
Figure 4.6: Temperature evolution of the one dimensional EBM: Units are °C.
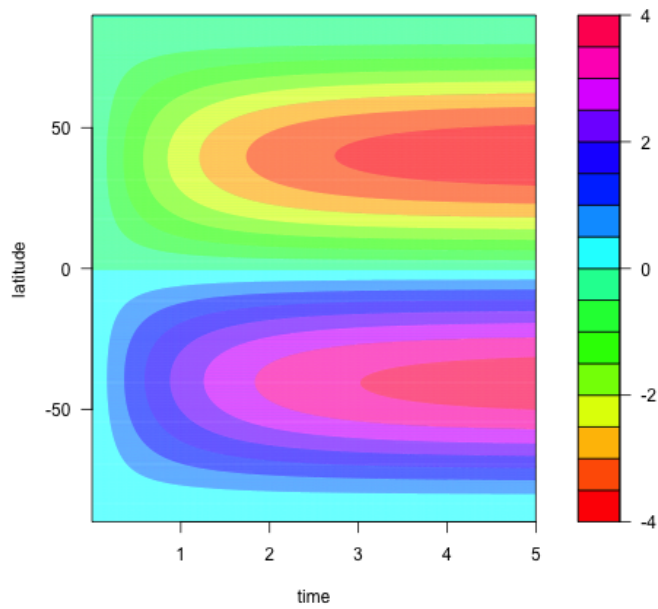
Figure 4.7: Time evolution of the northward meridional heat transport in PW $= 10^{15}$ W.
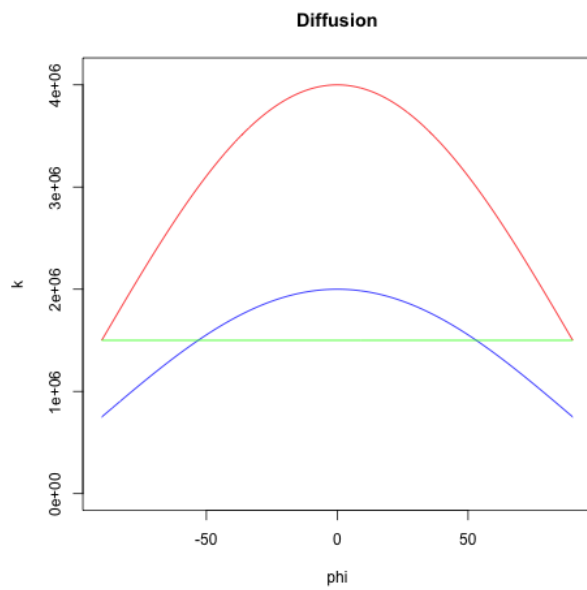
Figure 4.8: Diffusion coefficients for different versions of the model (m^2/s). Exercise 33.
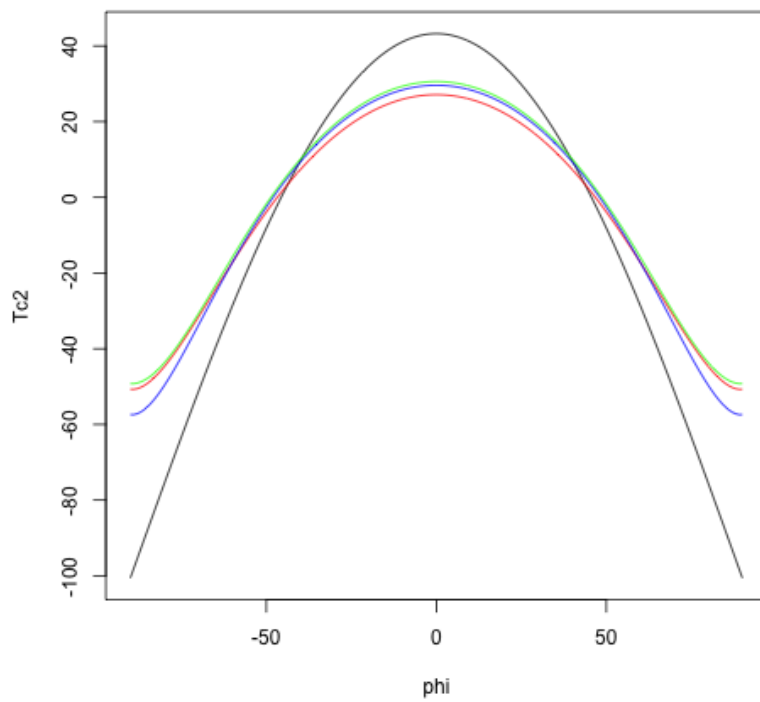
Figure 4.9: Equilibrium temperature in °C. The solutions are related to the diffusion coefficients as displayed in Fig. 4.8. Black: Analytical solution for the linearized model (4.46).

Exercise 34 – **Analytical EBM: Ice-albedo feedback**

Based in exercise 32, one can introduce a climate-dependent formulation of the planetary albedo α on the global temperature:

$$\alpha(T) = \alpha_0 - \alpha_1 \cdot \overline{T} \tag{4.48}$$

a) Solve the Energy balance model (4.26) for the case $\alpha(\overline{T})$ as in (4.48).

b) Show that the stability of the solution depends on certain parameters (like α_1).

c) Explain the ice-albedo effect through this solution!

Exercise 35 – **Analytical EBM: Budyko**

In exercise 32, the transport is parameterized as diffusion. Here, we simplfy the approach:

$$C_p \, \partial_t T = -k \, (T - \overline{T}) + (1 - \alpha)Q_S^{top} - (A + B \, T) \tag{4.49}$$

Task: Solve the Energy balance model.

Solution

One can separate the dynamics into a gloal mean $\overline{T}(t)$ and a function T_1 depending on latitude.

$$\overline{T}(t) = (1 - \alpha)S \, \frac{1}{4B} - \frac{A}{B} + \overline{T}(t = 0) \cdot \exp\left(-\frac{B}{C_p}t\right) \tag{4.50}$$

For T_1 we have

$$T_1 = (1 - \alpha)\frac{S}{\pi}\frac{1}{k + B} \cos\varphi - (1 - \alpha)\frac{S}{4B} + \sum_{l=2}^{\infty} a_l \cos(l\varphi) \tag{4.51}$$

The equilibrium solution is therefore

$$T_{eq} = \lim_{t \to \infty} T = -\frac{A}{B} + (1 - \alpha)\frac{S}{\pi}\frac{1}{k + B} \cos\varphi \tag{4.52}$$

Ice-albedo feedback

For Q_S, one needs a climate-dependent formulation of the planetary albedo α, which can be parameterized in terms of the temperature:

$$\alpha(T) = 0.42 - 0.20 \cdot \tanh\left[0.052\left(T - 276.15K\right)\right] \qquad . \qquad (4.53)$$

This parameterization incorporates high albedos of snow and ice in terms of the surface temperature (T in Kelvin).

```r
# EBM_EulerForward.R
# 1D diffusion EBM equation, explicit scheme
S=1367
sigma=5.67e-8
epsilon0=0.612
lat=pi/2/90
phi=c(-90:90)
cp=4.2e6 *1 # cp_water = 4.6e3; rho_water=1e3; h=1m
r=40.0e6/(2*pi)
tabs=272
ddx=40.0e6/360
coslat=cos(phi *lat)
k=(1.5e6 + 2.5e6 * coslat)  # in m^2/s

#Constants
L.X<-179 #width of lattice
L.T<-50000000  #length of time
dx <- ddx    #space step in m
dt <- 1000 #time step in s
D<-  k          #Diffusion coefficent

globini=270
N.x<-L.X + 2   #number of space boxes + 2 boundary boxes
N.t<-L.T/dt      #number of time boxes

dtc=dt/cp
dtcdx=dtc/(dx^2)
dtdx=dt/(dx^2)
cfl=dtdx*max(D)  # CFL criterium, this number shall be smaller than 0.5

T<-matrix(globini,N.t,N.x)   #grid
Transport <-matrix(0,N.t,N.x)

#temporary vector which stores the state of of one timestep:
T.temp<-rep(globini,N.x)
Transport.temp<-rep(0,N.x)
```

```
#Set the starting and boundary condition, here one value in the middle:
T[1,N.x/2]<- globini

for (n in 1:(N.t-1))
{
  for (j in 2:(N.x-1))
  {
    alpha=0.42 -  0.20 * tanh(0.052* ( T[n,j] - 276.15 ))
    sw=(1-alpha)*S/pi *coslat[j]
    lw=epsilon0*sigma * T.temp[j]^4
    T.temp[j]<-T[n,j]+D[j]*dtdx*(T[n,j+1]-2*T[n,j]+T[n,j-1])+dtc*(sw -lw)
    Transport.temp[j]=cp*D[j]*(T[n,j+1]-T[n,j])/ddx * 40.e6*coslat[j]
  }
  T.temp[1] <- T.temp[2]
  T.temp[N.x] <- T.temp[N.x-1]
  Transport.temp[1]=0
  Transport.temp[N.x]=0
  T[n+1,]<-T.temp
  Transport[n+1,]=Transport.temp
}

filled.contour((1:N.t)*dt/1e6,phi,T-tabs,
        color.palette=rainbow,xlab="time",ylab="latitude")

dev.copy(png,'ebm_nonlinear_1d_alb.png')
dev.off()

filled.contour((1:N.t)*dt/1e6,phi,Transport*1e-15,
        color.palette=rainbow,xlab="time",ylab="latitude")

#dev.copy(png,'Transport_ebm_nonlinear_1d_alb.png')
#dev.off()
#---
# plot equilibrium
A=epsilon0 * sigma *273^4
alpha=0.3
A=213
r=40.0e6/(2*pi)
k=1*r^2
B=epsilon0 *sigma* 3 *  273^3
km= k/r^2 +B
Amod=A - (1-alpha ) * S/4  *(k/r^2)/km
rhs2= 1/(pi)* (1-alpha ) * S* cos(lat*phi) /B
Tc2=  - A/B + rhs2
plot(phi,Tc2,type="l",col="black")

lines(phi,T[N.t,]-tabs,type="l",col="red")
max(T[N.t,]-tabs)

dev.copy(png,'End_ebm_nonlinear_1d_alb.png')
dev.off()
```
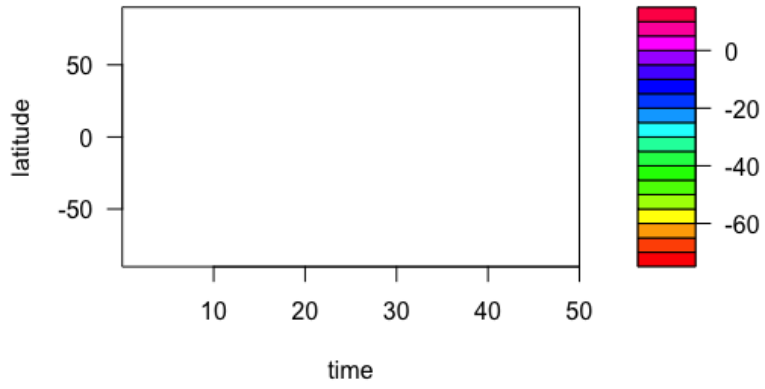
Figure 4.10: As Fig. 4.6, but including the ice-albedo feedback and a low initial condition.
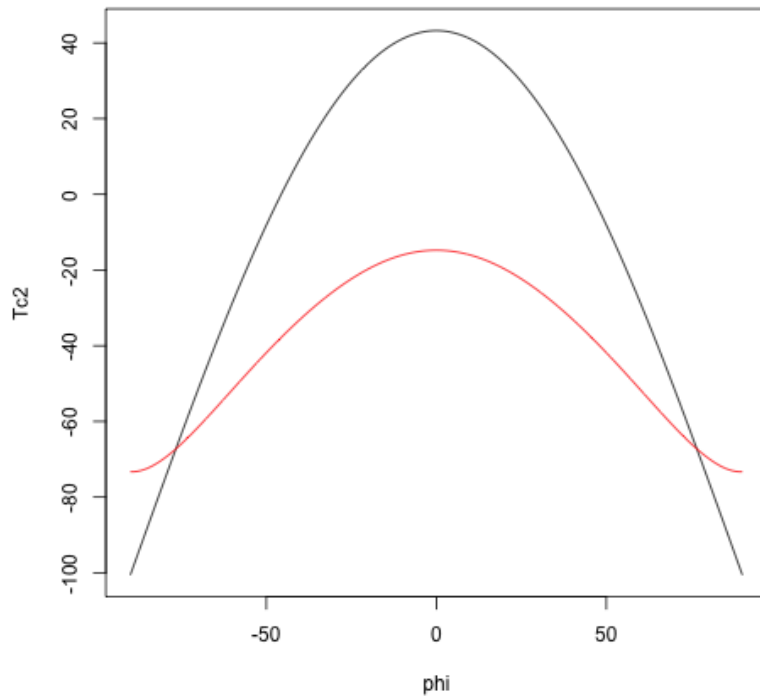
Figure 4.11: As Fig. 4.9, but including the ice-albedo feedback and a low initial condition.

4.3 Moist atmospheric energy balance model*

The model considers a zonally and annually averaged circulation of the atmosphere and calculates surface fresh water fluxes and surface heat fluxes along with sea surface temperatures. The EBM treats the transport processes as diffusion. The balances of energy will be used to derive equations for the atmospheric temperature and fresh water flux. The thermodynamic equation (internal plus potential energy) in the atmosphere in isobaric coordinates reads

$$C_p \left[\partial_t T_a + \nabla \cdot (v\, T_a) + \partial_p(\omega T_a) \right] = \partial_p Q_R + Q_L + \partial_p Q_S + \frac{RT_a}{p}\omega \qquad (4.54)$$

where v and ∇ are the horizontal vector of wind and the gradient operator, T_a atmospheric temperature, p pressure, $\omega = \frac{d}{dt}p$ vertical wind, and C_p specific heat at constant pressure $(1004\, J\, kg^{-1}\, K^{-1})$. Q_R and Q_S are the radiative and sensible heat fluxes, respectively. Q_L denotes the latent heat release due to phase transitions in the air. This term includes condensation of water vapour $(c > 0)$, evaporation of cloud water $(c < 0)$, and evaporation in unsaturated air $(e > 0)$:

$$Q_L = L_v\,(c - e) \qquad (4.55)$$

where L_v is the latent heat of condensation $(L_v = 2.5 \cdot 10^6\, J\, kg^{-1})$.

The last term on the right hand side of equation (4.54) is related to the fact that because pressure decreases with height and air is a compressible fluid, air that rises expands (and air that sinks contracts). Air that expands does work against its surroundings and because of the first law of thermodynamics (conservation of energy) this work needs to be paid for (reduction in temperature). So internal energy is consumed in expanding the parcel of air outwards against the atmosphere (expanding air cools).[1]

---

[1]Furthermore, we can assume an adiabatic process is one where no heat is exchanged with the surroundings. This is a reasonable approximation for typical rising air because other processes like conduction or radiative heat transfer are quite slow. In this context, the potential temperature is introduced. The potential temperature of a parcel of fluid at pressure P is the temperature that the parcel would acquire if adiabatically brought to a standard reference pressure

Additionally to (4.54), the budget equations for the mass mixing ratio of water vapour q_v and cloud water q_w are used:

$$\partial_t q_v \; + \; \boldsymbol{\nabla} \cdot (\, \boldsymbol{v} \, q_v) \; + \; \partial_p(\omega \, q_v) \;\; = \;\; e \; - \; c \; + \; E \tag{4.57}$$

$$\partial_t q_w \; + \; \boldsymbol{\nabla} \cdot (\, \boldsymbol{v} \, q_w) \; + \; \partial_p(\omega \, q_w) \;\; = \;\; c \; - \; \wp \tag{4.58}$$

where $\wp$ denotes the formation of precipitation and E denotes the evaporation from the ground (ocean and land).

The budget equations (4.54, 4.57) and (4.58) are now vertically integrated and zonally averaged. It is assumed that in the vertically integrated left hand side of (4.58) the first two terms vanish (stationarity, small horizontal transports). Furthermore, the vertically integrated last term on the right hand side of (4.54) is neglected. With $\omega = 0$ at the top and bottom, (4.58) reduces to

$$\int \frac{dp}{g} \, c = \int \frac{dp}{g} \, \wp \qquad , \tag{4.59}$$

where g is the gravitational acceleration ($9.81 \, m \, s^{-2}$). The net precipitation P on the ground

---

P_0, usually 1000 millibars. The potential temperature is denoted θ and, for air, is often given by

$$\theta = T \left(\frac{P_0}{P} \right)^{R/c_p} , \tag{4.56}$$

where T is the current absolute temperature (in K) of the parcel, R is the gas constant of air, and c_p is the specific heat capacity at a constant pressure. $R/c_p = 0.286$ for air (meteorology). Potential temperature is a more dynamically important quantity than the actual temperature. This is because it is not affected by the physical lifting or sinking associated with flow over obstacles or large-scale atmospheric turbulence. A parcel of air moving over a small mountain will expand and cool as it ascends the slope, then compress and warm as it descends on the other side- but the potential temperature will not change in the absence of heating, cooling, evaporation, or condensation (processes that exclude these effects are referred to as dry adiabatic). Since parcels with the same potential temperature can be exchanged without work or heating being required, lines of constant potential temperature are natural flow pathways. The equation comes from the enthalpy form of the first law of thermodynamics can be written as: $dh = T \, ds + v \, dp$, where dh denotes the enthalpy change, T the temperature, ds the change in entropy, v the specific volume, and p the pressure. For adiabatic processes, the change in entropy is zero: $dh = v \, dp$. For approximately ideal gases, such as the dry air in the Earth's atmosphere, the equation of state, $pv = RT$ can be substituted by $dpv = R/vdT \, \frac{dp}{p} = \frac{c_p}{R} \frac{dT}{T}$, where the $dh = c_p dT$ was used and both terms were divided by the product pv. Integrating yields 4.56.

$(p = p_0 = 10^5 N m^{-2} = 1000\, mb)$ is defined as

$$P = \int \frac{dp}{g} (\wp - e) \quad .$$ (4.60)

This yields the vertically integrated balances for the mixing ratio of water vapour and atmospheric temperature:

$$\int \frac{dp}{g} \partial_t (C_p T_a) + \int \frac{dp}{g} \nabla \cdot (C_p v T_a) = Q_R^{top} - Q_R^{bottom} + L_v\, P + Q_S^{bottom}$$
$$\int \frac{dp}{g} \partial_t (L_v q_v) + \int \frac{dp}{g} \nabla \cdot (L_v v q_v) = L_v\, (E - P) \quad .$$ (4.61)

The one dimensional atmosphere EBM prognoses the vertically integrated mixing ratio of water vapour and atmospheric temperature along with (4.61).[2] This yields one vertically integrated energy equation:

$$C\, \partial_t T_A + \int \frac{dp}{g} \nabla \cdot (C_p v T_a) + \int \frac{dp}{g} \nabla \cdot (L_v v q) = Q_R^{top} - F_{oa}$$ (4.62)

where $F_{oa} = Q_R^{bottom} - L_v E - Q_S^{bottom}$ denotes the ocean-atmosphere heat flux calculated by bulk formulas. The net radiation on top of the atmosphere Q_R^{top} is the difference between net solar radiation and net outgoing longwave radiation Q_{LW}^{top}. In a further approximation, the longwave radiation Q_{LW}^{top} canbe described by a linear law $A + BT$ (4.20). A climate-dependent formulation of the planetary albedo α, in terms of the surface air temperature was given in (4.53). With equation (4.62) the surface temperature T_A is calculated prognostically, while the fresh water flux for the ocean surface is given by the right hand side of equation (4.61) by evaluating the left hand side of the water vapour budget.

Meridional Transports

The transport parameterizations are based on diffusion. The mechanism of heat and moisture trans-

---

[2]To evaluate the effective change of the vertically integrated humidity and temperature in equations (4.61), the height distribution of humidity and temperature must be taken into account using an empirical relation between the lapse rate and surface temperature β_1, β_2: $C\, \partial_t T_A = (C_p \beta_1 + L_v \beta_2)\, \partial_t T_A$

port in middle and high latitudes by baroclinic instability is the most important mechanism in the atmospheric energy balance model. Consider an atmospheric condition with isotherms coincident with latitude circles. A cold anomaly, which could be thought of as a cold air outbreak from the North American continent, results in a changed surface heat flux from the ocean. In the region of strong temperature gradient, cyclones (low pressure) and anticyclones (high pressure on the northern hemisphere) are formed. These traveling weather systems move north-eastward defining the major storm track. The scale over which this process is important is about 1000 km.

This process is the main source of meridional heat transport in middle and high latitudes. The balances of heat and moisture (4.61) are averaged over a length scale of synoptic scale disturbances of O(1000) km and a time scale longer than the life time of such disturbances (e.g. two weeks). The variables can be splitted into a large-scale, long-term quantities ($\overline{T_a}, \overline{q_v}, \overline{v}$) and the deviations ($T_a', q_v', v'$). The moments $\overline{v'T_a'}$ and $\overline{v'q_v'}$ are connected mainly with transient processes in the atmosphere. The transients act as diffusion in a statistical sense bringing warm and moist air poleward due to individual high and low pressure contributions.

The eddy fluxes, in a statistically steady state of the atmosphere, scale as:

$$\overline{v'T_a'} \sim \left(\frac{\partial \overline{T_a}}{\partial y} \right) \tag{4.63}$$

where T', v' are the perturbation of potential temperature and meridional velocity. The vertical integrated sensible eddy heat transport can be calculated in terms of the surface temperature gradient T_A

$$\int \frac{dp}{g} \ \overline{v'T_a'} \ = \ - \ K_s \ \left(\frac{\partial T_A}{\partial y} \right) \ . \tag{4.64}$$

where K_s is tuned to reproduce the current climate.

The latent eddy heat transport is parameterized as

$$\overline{v'q_v'} \ = \ rh(p) \ \frac{\partial q_s}{\partial \overline{\overline{T_a}}} (\overline{T_a}, p) \ \overline{v'T_a'} \ , \tag{4.65}$$

where rh is the relative humidity and q_s the saturation water vapour. The relative humidity is prescribed. For the latent heat transport (4.65), the relative humidity and $\frac{\partial q_s}{\partial T}$ strongly decrease with height. Therefore, the surface values for the latent heat transport is a good choice in the vertical integrated model:

$$\int \frac{dp}{g} \; \overline{v'q_v'} \;\; = \;\; -K_l \;\; rh(p_0) \;\; \frac{\partial q_s}{\partial T_A}(T_A, p_0) \;\; \left(\frac{\partial T_A}{\partial y}\right) \qquad . \qquad (4.66)$$

As for the sensible heat transport, the coefficient K_l can be tuned that (4.66) reproduces the latent eddy heat transports of current climate. The eddy activity is greatly enhanced over the ocean surfaces as opposed to over land surfaces. In the Northern Hemisphere, two major storm tracks exists extending northeast across the Atlantic and Pacific oceans from the east coast of the major continents. It is along these tracks that the majority of eddy heat and vorticity transport takes place. In the Southern Hemisphere the transport is relatively homogeneous in the zonal direction.[3] In the boxmodel in section 6, we assume that the atmospheric heat transport across the box boundaries are completely by transient eddies.

---

[3]The heat transport by stationary baroclinic waves is larger in winter on the northern hemisphere when the land-sea contrast is most pronounced. Green **?** argued that stationary eddies are more transient phenomena which repeatedly occur at the same location. This happens due to fixed topographic effects providing perturbations upon which baroclinic waves can grow. These phenomena relating to stationary eddies are ultimately driven by the large scale baroclinicity of the atmosphere. Therefore, standing eddies could be parameterized as transient eddies.

Chapter 5

Ocean Circulation

5.1 Wind-driven ocean circulation

What drives the ocean currents? At first, we might answer, the winds drive the circulation. But if we think more carefully about the question, we might not be so sure. We might notice, for example, that strong currents, such as the North Equatorial Countercurrents in the Atlantic and Pacific Ocean go upwind. Spanish navigators in the 16th century noticed strong northward currents along the Florida coast that seemed to be unrelated to the wind. How can this happen? And, why are strong currents found offshore of east coasts but not offshore of west coasts?[1]

Friction is essential for the transfer of momentum in a fluid. Friction transfers momentum from the atmosphere to the ocean through the thin, frictional, Ekman layer at the sea surface. Friction transfers momentum from the ocean to the solid earth through the Ekman layer at the sea floor. Friction along the sides of subsea mountains leads to pressure differences on either side of the mountain which causes another kind of drag called *form drag*. This is the same drag that causes

---

[1]Answers to the questions can be found in a series of three remarkable papers published from 1947 to 1951. In the first, Harald Sverdrup (1947) showed that the circulation in the upper kilometer or so of the ocean is directly related to the curl of the wind stress. Henry Stommel (1948) showed that the circulation in oceanic gyres is asymmetric because the Coriolis force varies with latitude. Finally, Walter Munk (1950) added eddy viscosity and calculated the circulation of the upper layers of the Pacific. Together the three oceanographers laid the foundations for a modern theory of ocean circulation.

wind force on cars moving at high speed. In the vast interior of the ocean, however, the flow is frictionless, and vorticity is conserved. Such a flow is said to be *conservative*. Here, we apply the vorticity dynamics for the ocean and include the wind stress term in (3.39, 3.40):

$$D_t u - f v = -\frac{1}{\rho}\frac{\partial p}{\partial x} + \frac{1}{\rho}\partial_z \tau_{xz} \tag{5.1}$$

$$D_t v + f u = -\frac{1}{\rho}\frac{\partial p}{\partial y} + \frac{1}{\rho}\partial_z \tau_{yz} \tag{5.2}$$

in order to get the modified vorticity balance (3.61):

$$\frac{D}{Dt}(\zeta + f) - \frac{(\zeta + f)}{h}\frac{D}{Dt}h = \frac{1}{\rho}\operatorname{curl}_z \partial_z \tau = \frac{1}{\rho}\left(\frac{\partial}{\partial x}\partial_z \tau_{yz} - \frac{\partial}{\partial y}\partial_z \tau_{xz}\right) \tag{5.3}$$

The formulation 'wind stress curl' stands for the z-component of

$$\nabla \times \begin{pmatrix} \tau_x \\ \tau_y \\ 0 \end{pmatrix} = curl \begin{pmatrix} \tau_x \\ \tau_y \\ 0 \end{pmatrix} \qquad .$$

Exercise 36 – **Non-dimensional vorticity dynamics including wind stress**

a) Derive the the non-dimensional version of the vorticity equation (5.3) assuming that h is not varying and include friction! We can vertically integrate (5.3) over depth $\int_{-D}^{0} dz$:

$$\frac{D}{Dt}(\zeta + f) = A_H \nabla^2 \zeta + \frac{1}{\rho D}\left(\frac{\partial}{\partial x}\tau_y - \frac{\partial}{\partial y}\tau_x\right) \qquad . \tag{5.4}$$

Include the Reynolds number $Re = UL/A_H$, Rossby number $Ro = U/(f_0 L)$, and the wind stress strength number $\alpha = \tau_0 L/(\rho_0 D U^2)$. *Compare to exercises 4, 26.*

b) Estimate the order of magnitude of the characteristic numbers for the ocean ! You can use Table 5.1.

	Quantity	Ocean
horizontal velocity	U	$1.6 \cdot 10^{-2}\, ms^{-1}$
horizontal length	L	$10^6\, m$
vertical length	D	$10^3\, m$
wind stress	τ_0	$1.5 \cdot 10^{-1}\, Pa$
Coriolis parameter at 45°N	$f_0 = 2\Omega \sin \varphi_0$	$10^{-4}\, s^{-1}$
density	ρ_0	$10^3\, kgm^{-3}$
viscosity (turbulent)	A_H	$10^2 - 10^4\, m^2 s^{-1}$
Reynolds number	Re	$1.6 - 160$
wind stress strength number	α	$1 \cdot 10^3$

Table 5.1: Table shows the typical scales in the ocean system for exercise 36.

Solution of Non-dimensional vorticity dynamics including wind stress

Starting from (5.4),

$$\frac{1}{T}\frac{D}{Dt_d}\left(\frac{1}{T}\zeta_d + f_0 f_d\right) = A_H \frac{1}{L^2 T}\nabla_d^2\zeta_d + \frac{\tau_0}{\rho_0 DL}\left(\frac{\partial}{\partial x_d}\tau_{y,d} - \frac{\partial}{\partial y_d}\tau_{x,d}\right) \quad (5.5)$$

$$\frac{D}{Dt_d}\left(\frac{1}{T}\zeta_d + f_0 f_d\right) = A_H \frac{1}{L^2}\nabla_d^2\zeta_d + \frac{\tau_0 T}{\rho_0 DL}\left(\frac{\partial}{\partial x_d}\tau_{y,d} - \frac{\partial}{\partial y_d}\tau_{x,d}\right) \quad .(5.6)$$

Multiplying with T and using $T = L/U$, we obtain

$$\frac{D}{Dt_d}\left(\zeta_d + \frac{f_0 L}{U} f_d\right) = \frac{A_H}{UL}\nabla_d^2\zeta_d + \frac{\tau_0 L}{\rho_0 DU^2}\left(\frac{\partial}{\partial x_d}\tau_{y,d} - \frac{\partial}{\partial y_d}\tau_{x,d}\right) \quad (5.7)$$

and finally

$$\frac{D}{Dt_d}\left(\zeta_d + \frac{1}{Ro} f_d\right) = \frac{1}{Re}\nabla_d^2\zeta_d + \alpha\left(\frac{\partial}{\partial x_d}\tau_{y,d} - \frac{\partial}{\partial y_d}\tau_{x,d}\right) \quad (5.8)$$

5.1.1   Sverdrup relation

Suppose for simplicity that h is constant, so the only 'topography' is that of the spherical shape of the ocean. This produces a simple version of the vorticity balance in the ocean circulation, the

Sverdrup relation. For most regions, the right hand side in (5.3) or the left hand side in (5.8) is dominated by the term $v\partial_y f = v\beta$.

$$v\beta = \frac{1}{\rho}\left(\frac{\partial}{\partial x}\partial_z\tau_{yz} - \frac{\partial}{\partial y}\partial_z\tau_{xz}\right) \quad . \tag{5.9}$$

Integrating over z, we receive

$$\beta\int_h^0 dz\, v = \beta V = \frac{1}{\rho}\mathrm{curl}_z\,\boldsymbol{\tau}(z=0) = \frac{1}{\rho}\left(\frac{\partial\tau_{yz}}{\partial x} - \frac{\partial\tau_{xz}}{\partial y}\right) \quad . \tag{5.10}$$

Mass transport and Stream Lines of Sverdrup's Theory*

While Sverdrup was analyzing observations of equatorial currents, he derived the relation by the the wind stress to mass transport within the upper ocean. It is assumed that the flow is stationary, that lateral friction and molecular viscosity are small, that non-linear terms such as $u\partial u/\partial x$ are small. With these assumptions, the horizontal components of the momentum equation are:

$$\frac{\partial p}{\partial x} = f\,\rho\,v + \frac{\partial\tau_{xz}}{\partial z} \tag{5.11}$$

$$\frac{\partial p}{\partial y} = -f\,\rho\,u + \frac{\partial\tau_{yz}}{\partial z} \tag{5.12}$$

Sverdrup integrated these equations from the surface to a depth $-D$ equal to or greater than the depth at which the horizontal pressure gradient becomes zero. We can define

$$\frac{\partial P}{\partial x} = \int_{-D}^0 \frac{\partial p}{\partial x}\,dz, \qquad \frac{\partial P}{\partial y} = \int_{-D}^0 \frac{\partial p}{\partial y}\,dz, \tag{5.13}$$

M_x, M_y are the mass transports in the wind-driven layer extending down to an assumed depth of no motion:

$$M_x \equiv \int_{-D}^0 \rho\,u\,(z)\,dz, \qquad M_y \equiv \int_{-D}^0 \rho\,v\,(z)\,dz \quad . \tag{5.14}$$

The horizontal boundary condition at the sea surface is the wind stress, and the boundary at depth $-D$ is zero stress because the currents go to zero:

$$\tau_{xz}(0) = \tau_x \qquad \tau_{xz}(-D) = 0 \tag{5.15}$$

$$\tau_{yz}(0) = \tau_y \qquad \tau_{yz}(-D) = 0 \quad . \tag{5.16}$$

Using these definitions and boundary conditions, (5.11, 5.12) becomes:

$$\frac{\partial P}{\partial x} = f\, M_y + \tau_x \tag{5.17}$$

$$\frac{\partial P}{\partial y} = -f\, M_x + \tau_y \quad . \tag{5.18}$$

In a similar way, Sverdrup integrated the continuity equation over the same vertical depth, assuming the vertical velocity at the surface and at depth $-D$ are zero, to obtain:

$$\frac{\partial M_x}{\partial x} + \frac{\partial M_y}{\partial y} = 0 \tag{5.19}$$

Differentiating (5.17) with respect to y and (5.18) with respect to x, subtracting, and using (5.19) gives:

$$\beta\, M_y = \frac{\partial \tau_y}{\partial x} - \frac{\partial \tau_x}{\partial y} = \mathrm{curl}_z(\tau) \tag{5.20}$$

$$\text{where} \quad \beta \equiv \frac{\partial f}{\partial y} = \frac{2\Omega \cos\varphi}{R} \tag{5.21}$$

with R as earth's radius and φ as latitude. Over much of the open ocean, the wind is zonal and $\partial\tau_y/\partial x$ is sufficiently small that

$$M_y \approx -\frac{1}{\beta}\frac{\partial \tau_x}{\partial y} \tag{5.22}$$

Substituting (5.22) into (5.19), and (5.21) we obtain

$$\frac{\partial M_x}{\partial x} = -\frac{1}{2\,\Omega\,\cos\varphi}\left(\frac{\partial \tau_x}{\partial y}\tan\varphi + \frac{\partial^2 \tau_x}{\partial y^2}R\right) \tag{5.23}$$
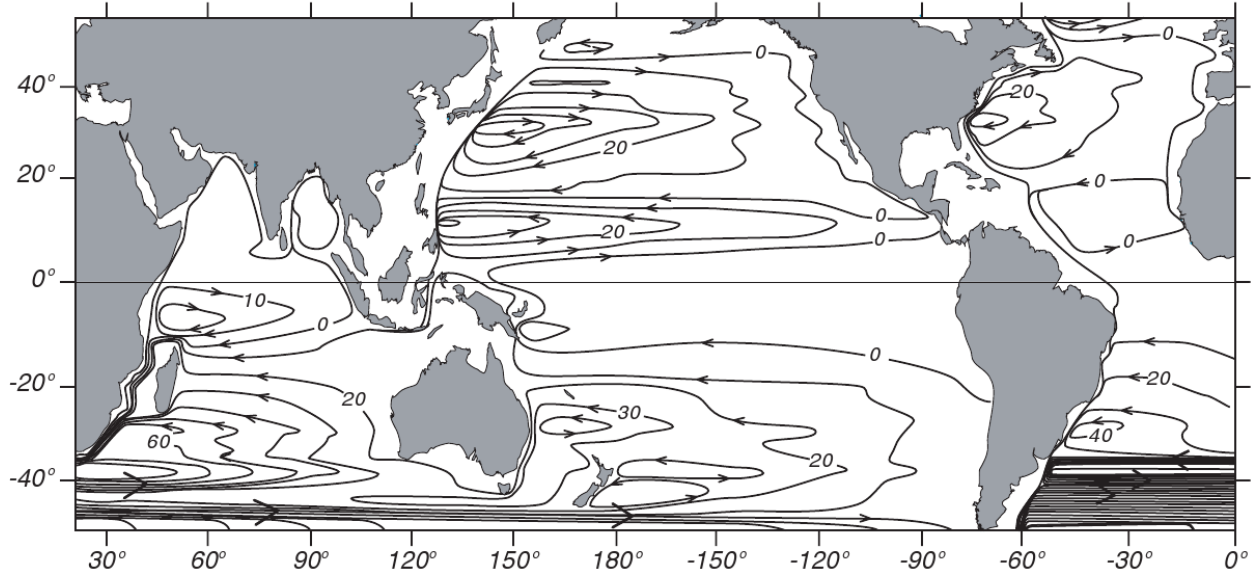
Figure 5.1: Depth-integrated Sverdrup transport applied globally using the wind stress from Hellerman and Rosenstein (1983). Contour interval is **10** Sverdrups (Tomczak and Godfrey, 1994).

Sverdrup integrated this equation from a north-south eastern boundary at $x = 0$, assuming no flow into the boundary. This requires $M_x = 0$ at $x = 0$. Then

$$M_x \;=\; -\frac{1}{2\,\Omega\,\cos\varphi}\left(\left[\int_0^x \frac{\partial \tau_x}{\partial y}dx'\right]\tan\varphi + \left[\int_0^x \frac{\partial^2 \tau_x}{\partial y^2}dx'\right]R\right) \tag{5.24}$$

$$=\; -\frac{1}{2\,\Omega\,\cos\varphi}\left(\tan\varphi\,\frac{\partial}{\partial y}\left[\int_0^x \tau_x dx'\right] + R\,\frac{\partial^2}{\partial y^2}\left[\int_0^x \tau_x dx'\right]\right) \; . \tag{5.25}$$

If τ_x can be approximated by its zonal mean, then

$$M_x = -\frac{\Delta x}{2\,\Omega\,\cos\varphi}\left[\tan\varphi\,\frac{\partial\langle\tau_x\rangle}{\partial y} + R\,\frac{\partial^2\langle\tau_x\rangle}{\partial y^2}\right] \tag{5.26}$$

where Δx is the distance from the eastern boundary of the ocean basin, and brackets indicate zonal averages of the wind stress.

5.1.2 Ekman Pumping

Ekman Pumping in a thin Ekman layer

Let us come now to the wind-driven forcing at the surface, the Ekman Pumping. The pressure terms are small because the Ekamn layer is thin. The Ekman layer near the surface of the ocean extends only about 10-20 meters deep[2]. The Ekman transports V_E, U_E describe the dynamics in the upper mixed layer:

$$fV_E = -\tau_x/\rho \tag{5.27}$$

$$fU_E = \tau_y/\rho \tag{5.28}$$

where $U_E = \int_{-E}^{0} u\, dz$ and $V_E = \int_{-E}^{0} v\, dz$ are the depth-integrated velocities in the thin friction-dominated Ekman layer at the sea surface. The vertical velocity at the surface is zero and denote w_E as the Ekman vertical velocity the bottom of the Ekman layer.

$$-\int_{-E}^{0} \frac{\partial w}{\partial z} dz = w_E = \frac{\partial}{\partial x} U_E + \frac{\partial}{\partial y} V_E \tag{5.29}$$

The curl of the wind stress τ produces a divergence of the Ekman transports leading to a vertical velocity w_E at the bottom of the Ekman layer.

$$w_E = \text{curl}\left(\frac{\tau}{\rho\, f}\right) = \frac{\partial}{\partial x}\left(\frac{\tau_y}{\rho\, f}\right) - \frac{\partial}{\partial y}\left(\frac{\tau_x}{\rho\, f}\right) \quad . \tag{5.30}$$

The order of magnitude of the Ekman vertical velocity w_E can be estimated as from a typical wind stress variation of $0.2 Nm^{-2}$ per 2000 km in y-direction:

$$w_E \simeq -\frac{\Delta \tau_x}{\rho\, f_0 \Delta y} \simeq \frac{1}{10^3 kgm^{-3}} \frac{0.2 Nm^{-2}}{10^{-4}s^{-1}\, 2 \cdot 10^6 m} \simeq 32\, \frac{m}{yr} \tag{5.31}$$

---

[2]The instrumentation sensitive enough to observe a velocity profile in such a shallow depth has only been available since around 1980. Also, wind waves modify the flow near the surface, and make observations close to the surface rather difficult.

See for a scetch see Fig. 5.2. The center of a subtropical gyre is a high pressure zone. Circulation around the high pressure is clockwise in the northern hemisphere and counterclockwise in the southern hemisphere, due to the Coriolis effect. The high pressure in the center is due to the westerly winds on the northern side of the gyre and easterly trade winds on the southern side. These cause frictional surface currents towards the latitude at the center of the gyre. This build-up of water in the center creates flow towards the equator in the upper 2 km of the ocean. This flow is returned towards the pole in an intensified western boundary current. The boundary current of the North Atlantic Gyre is the Gulf Stream, of the North Pacific Gyre the Kuroshio Current, etc..

Ekman vertical velocity and vertical geostrophic velocity

The Ekman vertical velocity must be balanced by a vertical geostrophic velocity $w_g\,(z = -E)$.

$$w_E = w_g \tag{5.32}$$

Ekman pumping drives a vertical geostrophic current in the ocean's interior. Figure 5.2 is a sketch of the cross section of the region between $10°$N and $60°$N, and it shows the pool of warm water in the upper kilometer centered on $30°$N. Conversely, divergent transports lead to low sea level. The mean north-south pressure gradients associated with the highs and lows are balanced by the Coriolis force of east-west geostrophic currents in the upper ocean. Westerlies in the north drive a southward transport, the trades in the south drive a northward transport. The converging Ekman transports must be balanced by downward geostrophic velocity (5.32).

Figure 5.3 shows the mean zonal winds in the Pacific, together with the north-south Ekman transports driven by the zonal winds. Notice that convergence of transport leads to downwelling, which produces a thick layer of warm water in the upper kilometer of the water column, and high sea level.
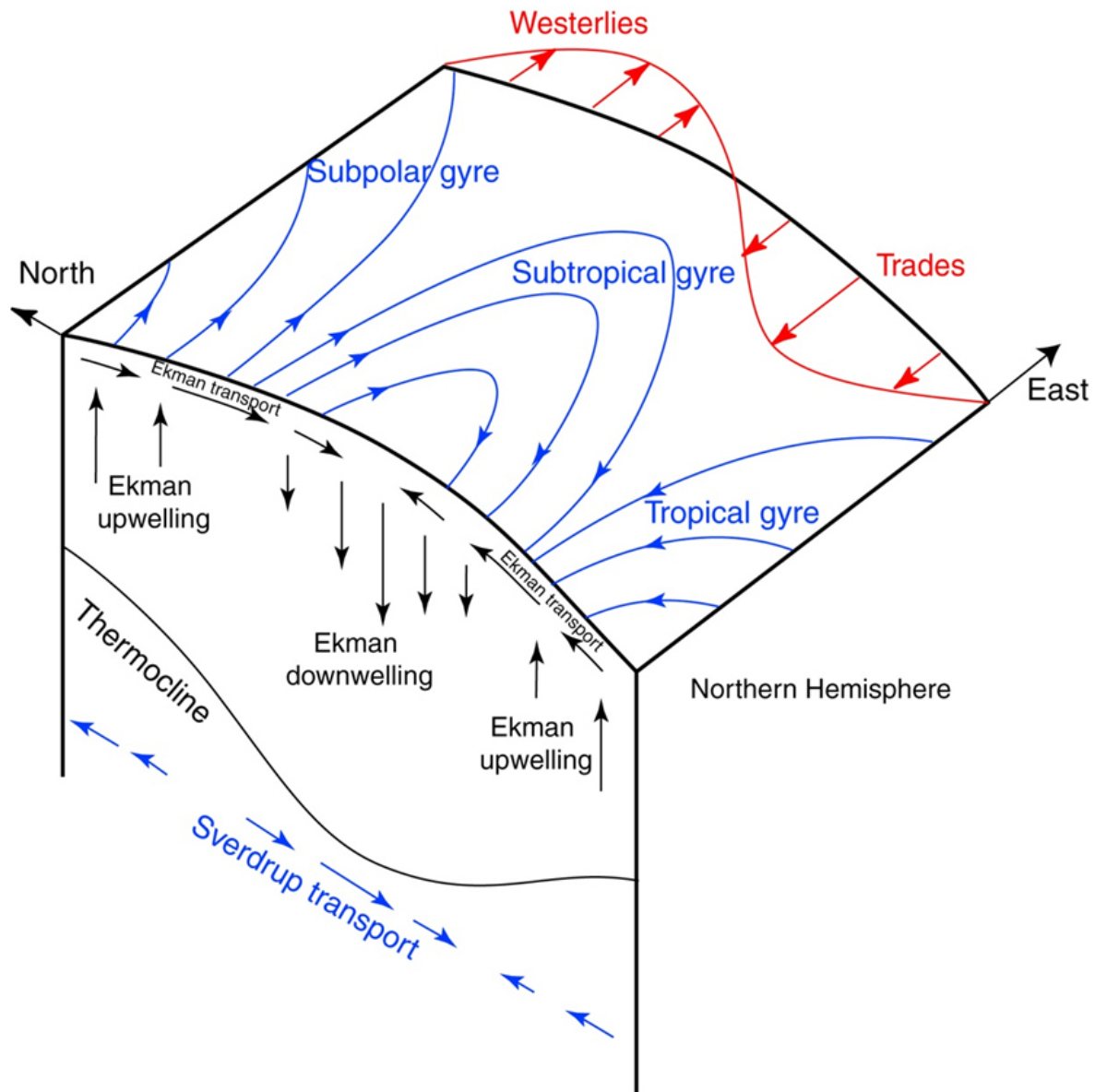
Figure 5.2: Ekman pumping that produces a downward velocity at the base of the Ekman layer forces the fluid in the interior of the ocean to move southward. Winds at the sea surface drive Ekman transports to the right of the wind in this northern hemisphere example. The converging Ekman transports driven by the trades and westerlies drive a downward geostrophic flow just below the Ekman layer.
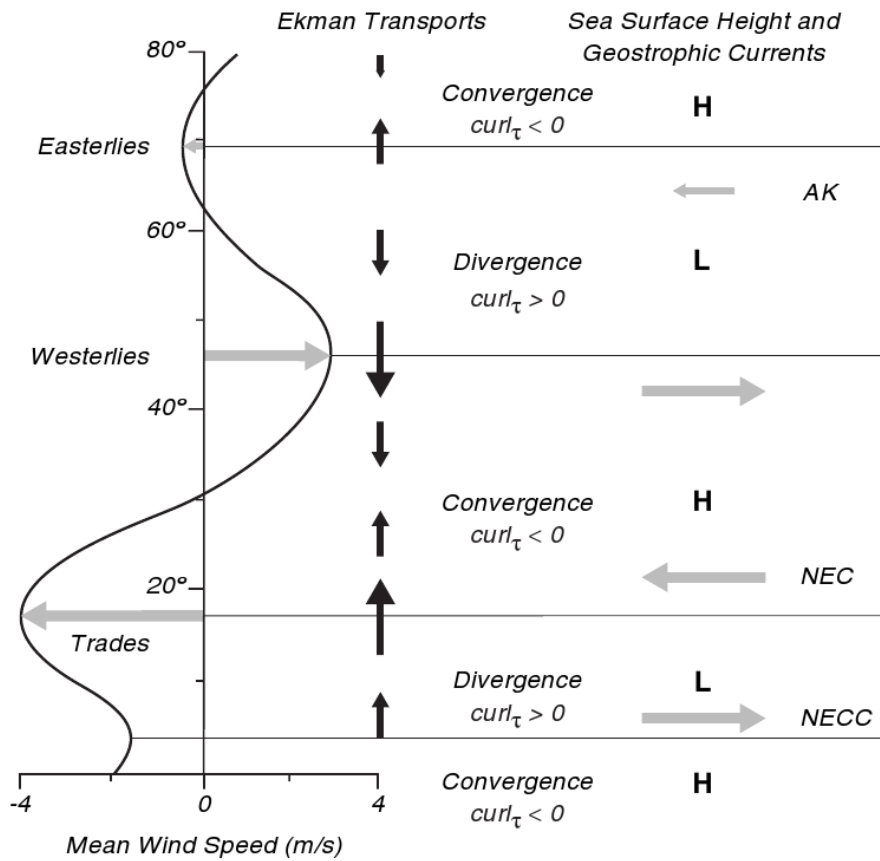
Figure 5.3: Ekman transports due to winds in the north Pacific (left) lead to Ekman pumping (center), which sets up north-south pressure gradients in the upper ocean. The pressure gradients are balanced by the Coriolis force due to east-west geostrophic currents (right). Horizontal lines indicate regions where the curl of the zonal wind stress changes sign. AK: Alaskan Current, NEC: North Equatorial Current, NECC: North Equatorial Counter Current.

Exercise 37   –   **Ekman transports and pumping**

The Ekman transports V_E, U_E describe the dynamics in the upper mixed layer:

$$fV_E = -\tau_x/\rho_0 \tag{5.33}$$

$$fU_E = \tau_y/\rho_0 \tag{5.34}$$

Derive the Ekman pumping w_E velocity at the bottom of the mixed layer

$$w_E = \mathrm{curl}\left(\frac{\tau}{f\rho_0}\right) = \frac{\partial}{\partial x}\left(\frac{\tau_y}{\rho_0 f}\right) - \frac{\partial}{\partial y}\left(\frac{\tau_x}{\rho_0 f}\right) \quad . \tag{5.35}$$

Exercise 38   –   **Sverdrup relation, Ekman transports and pumping**

The windstress vector τ is taken zonal. Assume $\tau_x = -\tau_0 \cos \pi y/B$ for an ocean basin $0 < x < L, 0 < y < B$. The wind driven meridional ocean velocity is given by the Sverdrup relation

$$\beta V = \mathrm{curl}(\tau/\rho_0) = -\frac{\partial}{\partial y}\tau_x/\rho_0 \quad . \tag{5.36}$$

1. at what latitudes y are $|V|$ and $|V_E|$ maximum? Calculate their magnitudes. Take constant $f = 10^{-4}$ s^{-1} and $\beta = 1.8 \cdot 10^{-11}$ m^{-1}s^{-1} and $B = 5000$ km, $\tau_0/\rho_0 = 10^{-4}$ m^{2}s^{-2}.

2. Calculate the maximum of w_E for constant f (value see above). Is this measurable?
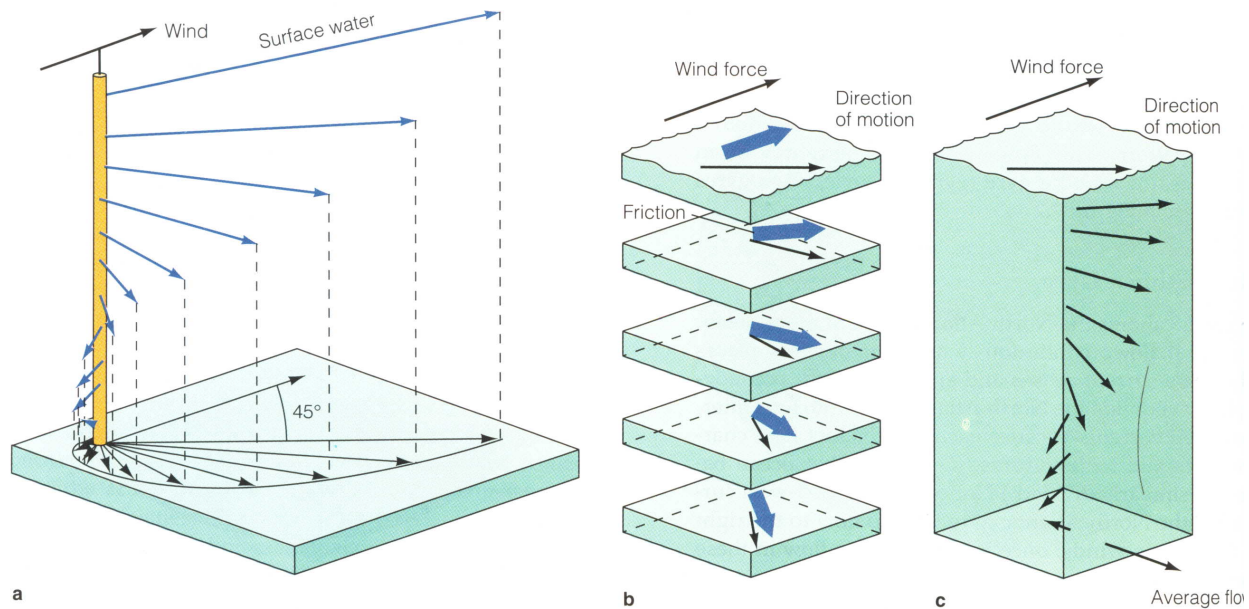
Figure 5.4: The Ekman spiral and the mechanism by which it operates. a) The Ekman spiral model. b) A body of water can be thought as a set of layers. The top layer is driven forward by the wind, and each layer below is moved by friction. Each succeeding layer moves at a slower speed, and at an angle to the layer immediately above it (to the right in the Northern Hemisphere, to the left in the Southern Hemisphere) until friction becomes negligible. (c) Though the direction of movement is different for each layer in the stack, the theoretical average direction of flow of water in the Northern Hemisphere is $90°$ to the right of the prevailing surface wind (Garrison, 1993).

5.1.3 Ekman spiral*

The Ekman spiral is a consequence of the Coriolis effect. When surface water molecules move by the force of the wind, they, in turn, drag deeper layers of water molecules below them. Each layer of water molecules is moved by friction from the shallower layer, and each deeper layer moves more slowly than the layer above it, until the movement ceases at a depth of about 100 meters. Like the surface water, however, the deeper water is deflected by the Coriolis effect-to the right in the Northern Hemisphere and to the left in the Southern Hemisphere. As a result, each successively deeper layer of water moves more slowly to the right or left, creating a spiral effect (Fig. 5.4). Because the deeper layers of water move more slowly than the shallower layers, they tend to "twist around" and flow not in the direction of the surface current.

Ekman developed the theory of the Ekman layer after Fridtjof Nansen observed that ice drifts at an angle of $20 - 40°$ to the right of the prevailing wind direction while on an Arctic expedition aboard the Fram. Nansen asked his colleague, Vilhelm Bjerknes to set one of his students upon study of the problem. Bjerknes tapped Ekman, who presented his results in 1902 as his doctoral thesis.

The mathematical formulation of the Ekman layer can be found by assuming a neutrally stratified fluid, with horizontal momentum in balance between the forces of pressure gradient, Coriolis and turbulent drag.

$$-fv \;=\; -\frac{1}{\rho_o}\frac{\partial}{\partial x}p + \nu\frac{\partial^2 u}{\partial z^2}, \tag{5.37}$$

$$fu \;=\; -\frac{1}{\rho_o}\frac{\partial}{\partial y}p + \nu\frac{\partial^2 v}{\partial z^2}, \tag{5.38}$$

where ν is the diffusive eddy viscosity, which can be derived using mixing length theory. There are many regions where an Ekman layer is theoretically plausible; they include the bottom of the atmosphere, near the surface of the earth and ocean, the bottom of the ocean, near the sea floor and at the top of the ocean, near the air-water interface. Different boundary conditions are appropriate for each of these different situations. We will consider boundary conditions of the Ekman layer in the upper ocean:

$$\text{at}\quad z = 0: \quad \nu\frac{\partial u}{\partial z} = \tau^x \quad \text{and} \quad \nu\frac{\partial v}{\partial z} = \tau^y, \tag{5.39}$$

where τ^x and τ^y are the components of the surface stress, τ, of the wind field or ice layer at the top of the ocean and u_g and v_g are the geostrophic flows as $z \to \infty : u \to u_g, v \to v_g$. In the other situations, other boundary conditions, such as the no-slip condition, may be appropriate instead.

The dynamics (5.37, 5.38) can be reformulated as

$$-fv \;=\; -fv_g + \nu\frac{\partial^2 u}{\partial z^2}, \tag{5.40}$$

$$fu \;=\; fu_g + \nu\frac{\partial^2 v}{\partial z^2}, \tag{5.41}$$

Now multiply (5.40) with i and subtract it from (5.41):

$$ifv - ifv_g + i\nu\frac{\partial^2 u}{\partial z^2} + fu - fu_g - \nu\frac{\partial^2 v}{\partial z^2} = 0 \tag{5.42}$$

Denoting $\xi = u + iv$, we get

$$f\xi - f\xi_g + i\nu\frac{\partial^2 \xi}{\partial z^2} = 0 \tag{5.43}$$

We rewite this as

$$\frac{\partial^2 \xi}{\partial z^2} - \left(\frac{if}{\nu}\right)\xi = -\left(\frac{if}{\nu}\right)\xi_g \tag{5.44}$$

We solve the inhomogenous equation (5.44) in two steps:

1. find a particular solution of the inhomogenous equation:

assume that ξ is independent on z

$$-\left(\frac{if}{\nu}\right)\xi = -\left(\frac{if}{\nu}\right)\xi_g \tag{5.45}$$

with the solution $\xi = \xi_g$

2. find a complementary function, a general solution of the homogenous part of (5.44):

$$\frac{\partial^2 \xi_h}{\partial z^2} - \left(\frac{if}{\nu}\right)\xi_h = 0 \tag{5.46}$$

$$\xi_h = C\exp(\lambda z) \quad \text{with} \quad \lambda^2 = \frac{if}{\nu} \tag{5.47}$$

Thus
$$\lambda_\pm = \pm\frac{1+i}{\sqrt{2}}\sqrt{\frac{f}{\nu}} = \pm(1+i)\sqrt{\frac{f}{2\nu}} = \pm(1+i)\,\gamma \tag{5.48}$$

Therefore

$$\xi_h = C_1 \exp(\lambda_+ z) + C_2 \exp(\lambda_- z) = C_1 \exp(\gamma z)\exp(i\gamma z) + C_2 \exp(-\gamma z)\exp(-i\gamma z)$$

As boundary condition ξ_h has to go to zero for $z \to \infty$, therefore $C_1 = 0$.

3. The complete solution is

$$\xi = \xi_g + C_2 \exp(-\gamma z)\exp(-i\gamma z) \tag{5.49}$$

As boundary condition
$$\xi(z = 0) = 0 = \xi_g + C_2 \tag{5.50}$$

Therefore
$$\xi = \xi_g \cdot (1 - \exp(-\gamma z)\exp(-i\gamma z)) \tag{5.51}$$

For simplicity, we can assume that the geostrophic flow is zonal, so that $v_g = 0$. Then,

$$u = u_g \cdot (1 - \exp(-\gamma z)\cos(\gamma z)) \tag{5.52}$$

$$v = u_g \cdot (\exp(-\gamma z)\sin(\gamma z)) \tag{5.53}$$

This variation of horizontal velocity with depth (-z) is referred to as the Ekman spiral, diagrammed above (Fig. 5.4). If we make a Taylor expansion for small z, we see that

$$u = u_g \cdot \gamma z \tag{5.54}$$

$$v = u_g \cdot \gamma z \tag{5.55}$$

Thus the low is $45°$ to the left of the limiting zonal gestrophic flow.

By applying the continuity equation we can have the vertical velocity as following

$$w = \frac{1}{f\rho_o} \left[\left(\frac{\partial \tau^y}{\partial x} - \frac{\partial \tau^x}{\partial y} \right) \left(1 - e^{-\gamma z} \cos{(\gamma z)} \right) - \left(\frac{\partial \tau^x}{\partial x} + \frac{\partial \tau^y}{\partial y} \right) e^{-\gamma z} \sin{(\gamma z)} \right]$$

Note that when vertically integrated the volume transport associated with the Ekman spiral is to the right of the wind direction in the Northern Hemisphere.

There is much difficulty associated with observing the Ekman layer for two main reasons: the theory is too simplistic as it assumes a constant eddy viscosity, which Ekman himself anticipated, recognizing that is obvious that ν cannot generally be regarded as a constant when the density of water is not uniform within the region considered and because it is difficult to design instruments with great enough sensitivity to observe the velocity profile in the ocean.

Because the real ocean does not match the idealized conditions of the Ekman spiral, wind-induced water movements often differ appreciably from theoretical predictions. In shallow water, for example, the water depth is insufficient for the full spiral to develop so that the angle between the horizontal wind direction and surface-water movements can be as little as 15 degrees. As waters deepen, the angle increases and approaches 45 degrees. The stable pycnocline inhibits the transfer of kinetic energy to deeper waters, helping to contain wind-driven currents to the mixed layer; that is, the pycnocline acts as a permeable boundary for Ekman transport and surface currents.

Exercise 39   –   Ekman layer in the atmosphere

Consider a geostrophic flow (u_g, v_g)

$$-fv_g \ = \ -\frac{1}{\rho_0}\frac{\partial p}{\partial x} \tag{5.56}$$

$$fu_g \ = \ -\frac{1}{\rho_0}\frac{\partial p}{\partial y} \quad . \tag{5.57}$$

The boundary-layer equations are then

$$-f(v - v_g) \ = \ \nu\,\frac{\partial^2 u}{\partial z^2} \tag{5.58}$$

$$f(u - u_g) \ = \ \nu\,\frac{\partial^2 v}{\partial z^2} \quad . \tag{5.59}$$

The boundary conditions are specified to be at the surface

$$\rho_0\nu\,\frac{\partial u}{\partial z} \ = \ \tau^x \tag{5.60}$$

$$\rho_0\nu\,\frac{\partial v}{\partial z} \ = \ \tau^y \tag{5.61}$$

and for $z \to -\infty : u = u_g, \quad v = v_g$.

1. Calculate the flow (u,v) as the departure from the interior flow (u_g, v_g)!

2. Calculate the net wind-driven horizontal transport through integration

$$V = \int_{-\infty}^{0} dz(v - v_g) \quad \text{and} \quad U = \int_{-\infty}^{0} dz(u - u_g) \quad . \tag{5.62}$$

What is the direction of U and V in terms of the surface wind stress τ?

3. For the case $f = f_0$ of constant Coriolis parameter, determine the divergence of the flow

$$\int_{-\infty}^{0} dz\left(\frac{\partial u}{\partial x} + \frac{\partial v}{\partial y}\right) \tag{5.63}$$

which is identical to the vertical velocity across the Ekman layer (since w(0)=0).

Exercise 40   –   Ekamn spiral in the ocean

Consider the solution (5.52,5.53) for the wind-driven Ekman layer at the surface of the ocean in the Northern Hemisphere. The geostrophic velocity is zero in this example. Show that (5.52,5.53) is a solution of (5.37, 5.38) !

5.1.4   Tea leaf paradox*

The tea leaf paradox describes a phenomenon where tea leaves in a cup of tea migrate to the center and bottom of the cup after being stirred rather than being forced to the edges of the cup, as would be expected in a spiral centrifuge.[3] Stirring the liquid makes it spin around the cup. Because of inertia, the pressure is higher along the rim than in the middle. However, near the bottom and outer edges the liquid is slowed by the friction against the cup. There the outward force cannot overcome the pressure gradient, so these pressure differences become more important for the water flow. This is called a boundary layer or more specifically an Ekman layer.

In a teacup, where the rotation is slower at the bottom, the pressure gradient takes over and creates an inward flow along the bottom. Higher up, the liquid flows outward instead. This secondary flow travels inward along the bottom bringing the leaves to the center, then up, out and down near the rim. The leaves are too heavy to lift upwards, so they stay in the middle. Combined with the primary rotational flow, the leaves will spiral inward along the bottom.

Besides tea leaves stirred in a cup, other classroom demonstrations can show the secondary circulation that arises due to the presence of friction. We discuss a simple laboratory experiment below, which demonstrates these ideas in a more controlled setting and can be readily applied to both atmospheric low and high pressure systems. All one needs is a rotating turntable, a cylindrical container (a large transparent beaker or a cylindrical insert inside a square container works fine), and some potassium permanganate crystals. When rotated at a constant rate, all the water comes

---

[3]The formation of secondary flows in an annular channel was theoretically treated by Boussinesq in 1868. The migration of near-bottom particles in river-bend flows was experimentally investigated by A.Ya.Milovich in 1913. The solution first came from Albert Einstein in a 1926 paper where he used it to explain the erosion of river banks (Baer's law) [Einstein, 1926].
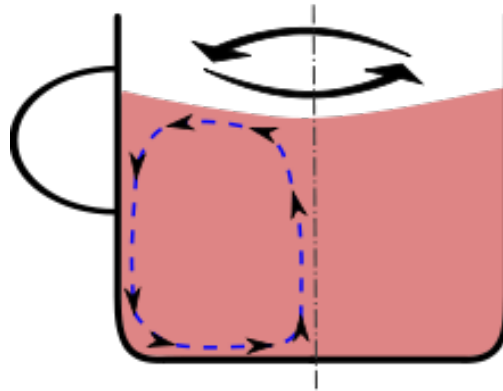
Figure 5.5:   The blue line is the secondary flow that pushes the tea leaves to the middle of the bottom.

into solid body rotation, and so there is no Coriolis or centrifugal accelerations acting. The key experimental requirement is to be able to speed up or slow down (by 10% or so) the rate of rotation of the turntable so as to induce relative motion between the water and the tank, thus creating a frictional boundary layer. The rotating platform can be used in a whole series of experiments to demonstrate atmospheric and oceanic phenomena, as presented in Marshall and Plumb (2007) and their "Weather in a Tank" website.

A tank of water is placed on the rotating platform long enough for water to reach solid body rotation, say, about 10 minutes for 10-15 rpm. Then we drop a very few potassium permanganate crystals in an equilateral triangle about the center. This shows up as three small clouds when viewed by a rotating camera. We also drop a few colored paper dots on the surface to see the flow outside the boundary layer. As the table is slowed down by a few rpm (about 10%), the permanganate on the bottom traces the near bottom circulation, which is cyclonic and inward, just like a low pressure system. The paper dots floating on the surface do not go inward. Why does this happen?

The water outside the boundary layer is still rotating with the original fast rotation rate, while the water at the bottom is rotating slower, at the new slower rotation rate. This speed differential, just like the low pressure system leads to an inward flow which is seen in the permanganate streaks

Figure 5.6: To carry out the experiment we first very slightly reduce (by 10% max) the rate of rotation of the turntable. Because of the inertia of the turning fluid, it continues to spin at its original speed and so moves relative to the tank: permanganate streaks are pulled around not in circles as one might initially expect, but rather inward turning, anticlockwise spirals, as can be seen in the top panel. A beautiful symmetric pattern is remarkably easy to achieve. This is analogous to the near-surface flow in a low pressure system, as can be seen by comparing with Fig. 1.2 (see low pressure system). To visualize the flow at the upper surface, we can float a few paper dots on the surface (black dots are the most visible in this application). We observe circular, rather than spiraling, motion. To create an analogy of a high pressure system we now simply increase the speed of the turntable by 10% or so (back up to, roughly, its original speed). We observe the dye streaks on the bottom reversing and, over time, spiraling clockwise and outwards, as can be seen in the lower panel in this figure. This should be compared to the pattern of surface winds that can be seen in the high pressure system in Fig. 1.2. From Marshall and Plumb (2007).

at the bottom (Fig. 5.6). Similarly, the pressure gradient can be reversed by increasing the speed by a few rpm to the original speed, and it leads to permanganate streaks that show an outward anti-cyclonic flow, analogous to the surface boundary layer of a High pressure system. This secondary flow in the boundary layer has important implications for movement in the vertical direction. The inward flow associated with a low pressure system leads to rising air near the center of the Low. As this air rises, it expands (pressure always decreases going upward in the atmosphere) and cools. Since the saturation of the air is very strongly dependent on the temperature, as the air cools, it may get saturated, and the water vapor may condense out to form clouds! This is why the Low pressure systems are the ones associated with stormy weather and precipitation. Conversely, high pressure systems are associated with outward motion in the boundary layer, and hence subsidence. As the air descends, it gets compressed due to the pressure increase, warms, and becomes less and less saturated. Thus the High pressure systems are fair weather systems.
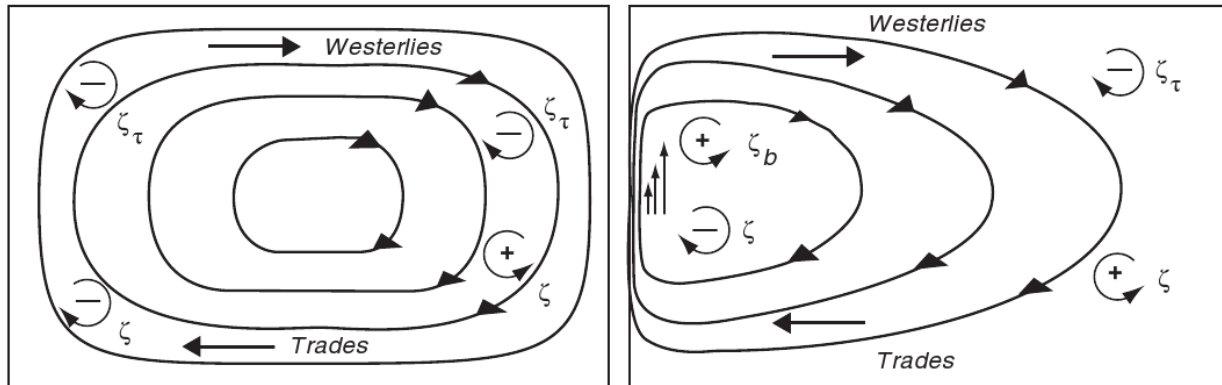
Figure 5.7: The balance of potential vorticity can clarify why western boundary currents are necessary. **Left**: Vorticity input by the wind ζ_τ balances the change in relative vorticity ζ in the east as the flow moves southward and f decreases. The two do not balance in the west where ζ must decrease as the flow moves northward and f increases. **Right**: Vorticity in the west is balanced by relative vorticity ζ_b generated by shear in the western boundary current.

5.1.5 Western Boundary Currents

The balance of vorticity provides an alternative explanation for the existence of western boundary currents. Consider the gyrescale flow in an ocean basin (Fig. 5.7), say in the North Atlantic from 10°N to 50°N. The wind blowing over the Atlantic adds negative vorticity ζ_τ. As the water flows around the gyre, the vorticity of the gyre must remain nearly constant, else the flow would spin faster or slower. Overall, the negative vorticity input by the wind must be balanced by a source of positive vorticity.

Throughout most of the basin the negative vorticity input by the wind is balanced by an increase in relative vorticity. As the flow moves southward throughout the basin, f decreases and ζ must increase according to (3.64) because the depth of the wind-driven circulation does not change much.

The balance breaks down, however, in the west where the flow returns northward. In the west, f increases, ζ decreases, and a source of positive vorticity is needed. The positive vorticity ζ_b is produced by the western boundary boundary current.

Stommel's Theory of Western Boundary Currents

At the same time Sverdrup was beginning to understand circulation in the eastern Pacific, Stommel was beginning to understand why western boundary currents occur in ocean basins. To study the circulation in the north Atlantic, Stommel (1948) used essentially the same equations used by Sverdrup (5.11, 5.12, 5.13, 5.14, 5.15 and 5.16) but he added a bottom stress proportional to velocity to (5.15) and (5.16):

$$\left(A_z\frac{\partial u}{\partial z}\right)_0 = -\tau_x = -F\cos\left(\pi\,y/b\right) \qquad \left(A_z\frac{\partial u}{\partial z}\right)_D = -R\,u \qquad (5.64)$$

$$\left(A_z\frac{\partial v}{\partial z}\right)_0 = -\tau_y = 0 \qquad \left(A_z\frac{\partial v}{\partial z}\right)_D = -R\,v \qquad (5.65)$$

where F and R are constants.

Stommel calculated steady-state solutions for flow in a rectangular basin $0 \leq y \leq b$, $0 \leq x \leq \lambda$ of constant depth D filled with water of constant density. His first solution was for a non-rotating Earth. This solution had a symmetric flow pattern with no western boundary current (Fig. 5.8, left). Next, Stommel assumed a constant rotation, which again led to a symmetric solution with no western boundary current. Finally, he assumed that the Coriolis force varies with latitude. This led to a solution with western intensification (Fig. 5.8, right).

Exercise 41   –   The Stommel model of the wind-driven circulation

The wind-driven circulation in a homogeneous ocean of constant depth h is described by

$$R\nabla^2\psi + \beta\partial_x\psi = \text{curl}(\tau/\rho_0) \qquad (5.66)$$

$$= (\partial_x\tau^y - \partial_y\tau^x)/\rho_0 \qquad (5.67)$$

where R is a coefficient of bottom friction, β the derivative of the Coriolis frequency at a central latitude, and the τ the windstress vector. Finally, ψ is the streamfunction of the depth integrated
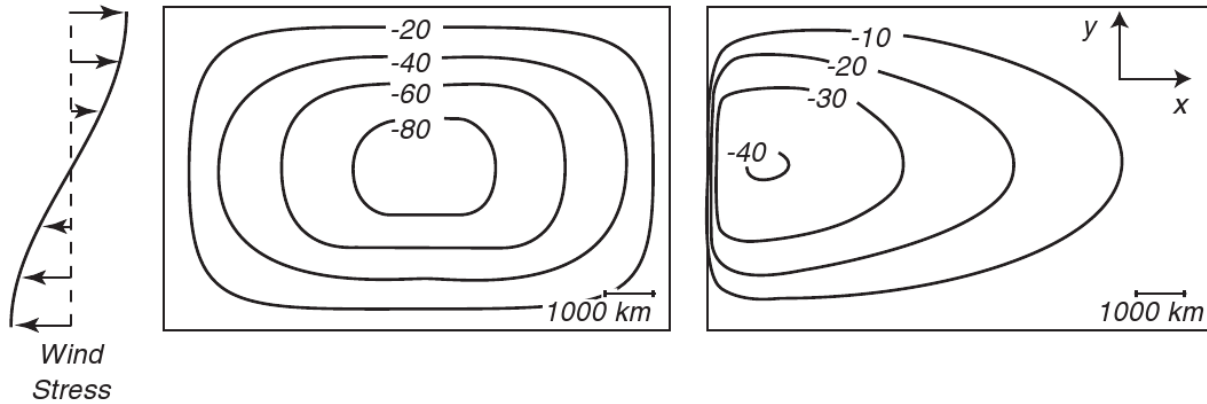
Figure 5.8: Stream function for flow in a basin as calculated by Stommel (1948). Left: Flow for non-rotating basin or flow for a basin with constant rotation. Right: Flow when rotation varies linearly with y.

velocity

$$U = (U, V) = \int_{-h}^{0} u\, dz$$

i.e.

$$U = -\partial_y \psi, \quad V = \partial_x \psi$$

1. Derive this equation from the conservation of momentum (linearized) and mass (volume!) assuming $w = 0$ at the mean surface $z = 0$ and at the bottom $z = -h$. For simplicity take Cartesian coordinates for the horizontal, $\beta = df/dy$. Boundary condition for the flux of momentum are $\tau(z = 0) = \tau$ and $\tau(z = -h) = R(-V, U)$. Hint: integrate both equations vertically and take the curl of the integrated momentum balance.

2. in the boundary layer the terms on the left hand side of (5.66) get large. Show by scaling that the width of the layer is $W = R/\beta$.

3. how large must R be to get a width $W = 100$ km? ($\beta = 2 \times 10^{-11} \ \mathrm{m^{-1}s^{-1}}$).

Munk's Solution

Sverdrup's and Stommel's work suggested the dominant processes producing a basin-wide, wind-driven circulation. Munk (1950) built upon this foundation, adding information from Rossby (1936) on lateral eddy viscosity, to obtain a solution for the circulation within an ocean basin. Munk used Sverdrup's idea of a vertically integrated mass transport flowing over a motionless deeper layer. This simplified the mathematical problem, and it is more realistic. The ocean currents are concentrated in the upper kilometer of the ocean, they are not barotropic and independent of depth. To include friction, Munk used lateral eddy friction with constant $A_H = A_x = A_y$. Equations (5.11) (5.12) become:

$$\frac{1}{\rho}\frac{\partial p}{\partial x} = \quad f\,v + \frac{\partial}{\partial z}\left(A_z\frac{\partial u}{\partial z}\right) + A_H\frac{\partial^2 u}{\partial x^2} + A_H\frac{\partial^2 u}{\partial y^2} \tag{5.68}$$

$$\frac{1}{\rho}\frac{\partial p}{\partial y} = \; - \; f\,u + \frac{\partial}{\partial z}\left(A_z\frac{\partial v}{\partial z}\right) + A_H\frac{\partial^2 v}{\partial x^2} + A_H\frac{\partial^2 v}{\partial y^2} \tag{5.69}$$

Munk integrated the equations from a depth $-D$ to the surface at $z = z_0$ which is similar to Sverdrup's integration except that the surface is not at $z = 0$. Munk assumed that currents at the depth $-D$ vanish, that (5.15) and (5.16) apply at the horizontal boundaries at the top and bottom of the layer, and that A_H is constant. To simplify the equations, Munk used the mass-transport stream function (3.47), and eliminated the pressure term by taking the y derivative of (5.68) and the x derivative of (5.69):

$$\underbrace{A_H\nabla^4\Psi}_{\text{Friction}} - \underbrace{\beta\frac{\partial\Psi}{\partial x} = -\operatorname{curl}_z\tau}_{\text{Sverdrup Balance}} \tag{5.70}$$

where

$$\nabla^4 = \frac{\partial^4}{\partial x^4} + 2\frac{\partial^4}{\partial x^2\,\partial y^2} + \frac{\partial^4}{\partial y^4} \tag{5.71}$$

is the biharmonic operator. Equation (5.70) is the same as (5.20) with the addition of the lateral friction term A_H. The friction term is large close to a lateral boundary where the horizontal derivatives of the velocity field are large, and it is small in the interior of the ocean basin. Thus in

the interior, the balance of forces is the same as that in Sverdrup's solution.

Equation (5.70) is a fourth-order partial differential equation, and four boundary conditions are needed. Munk assumed the flow at a boundary is parallel to a boundary and that there is no slip at the boundary:

$$\Psi_{\text{boundary}} = 0, \qquad \left(\frac{\partial \Psi}{\partial n}\right)_{\text{boundary}} = 0 \tag{5.72}$$

where n is normal to the boundary. Munk then solved (5.70) with (5.72) assuming the flow was in a rectangular basin extending from $x = 0$ to $x = r$, and from $y = -s$ to $y = +s$. He further assumed that the wind stress was zonal and in the form:

$$\tau = a \cos ny + b \sin ny + c \tag{5.73}$$

$$n = j\,\pi/s, \qquad j = 1, 2, ... \tag{5.74}$$

Munk's solution (figure 5.9) shows the dominant features of the gyre-scale circulation in an ocean basin. It has a circulation similar to Sverdrup's in the eastern parts of the ocean basin and a strong western boundary current in the west. Using $A_H = 5 \cdot 10^3 \frac{m^2}{s}$ gives a boundary current roughly $225 km$ wide with a shape similar to the flow observed in the Gulf Stream and the Kuroshio.

The transport in western boundary currents is independent of A_H, and it depends only on (5.20) integrated across the width of the ocean basin. Hence, it depends on the width of the ocean, the curl of the wind stress, and β. Using the best available estimates of the wind stress, Munk calculated that the Gulf Stream should have a transport of $36 Sv$ and that the Kuroshio should have a transport of $39 Sv$. The values are about one half of the measured values of the flow available to Munk. This is very good agreement considering the wind stress was not well known.[4]

---

[4]Recent recalculations show good agreement except for the region offshore of Cape Hatteras where there is a strong recirculation. Munk's solution was based on wind stress averaged over $5°$ squares. This underestimated the curl of the stress. Leetmaa and Bunker (1978) used modern drag coefficient and $2° \times 5°$ averages of stress to obtain $32 Sv$ transport in the Gulf Stream, a value very close to that calculated by Munk.
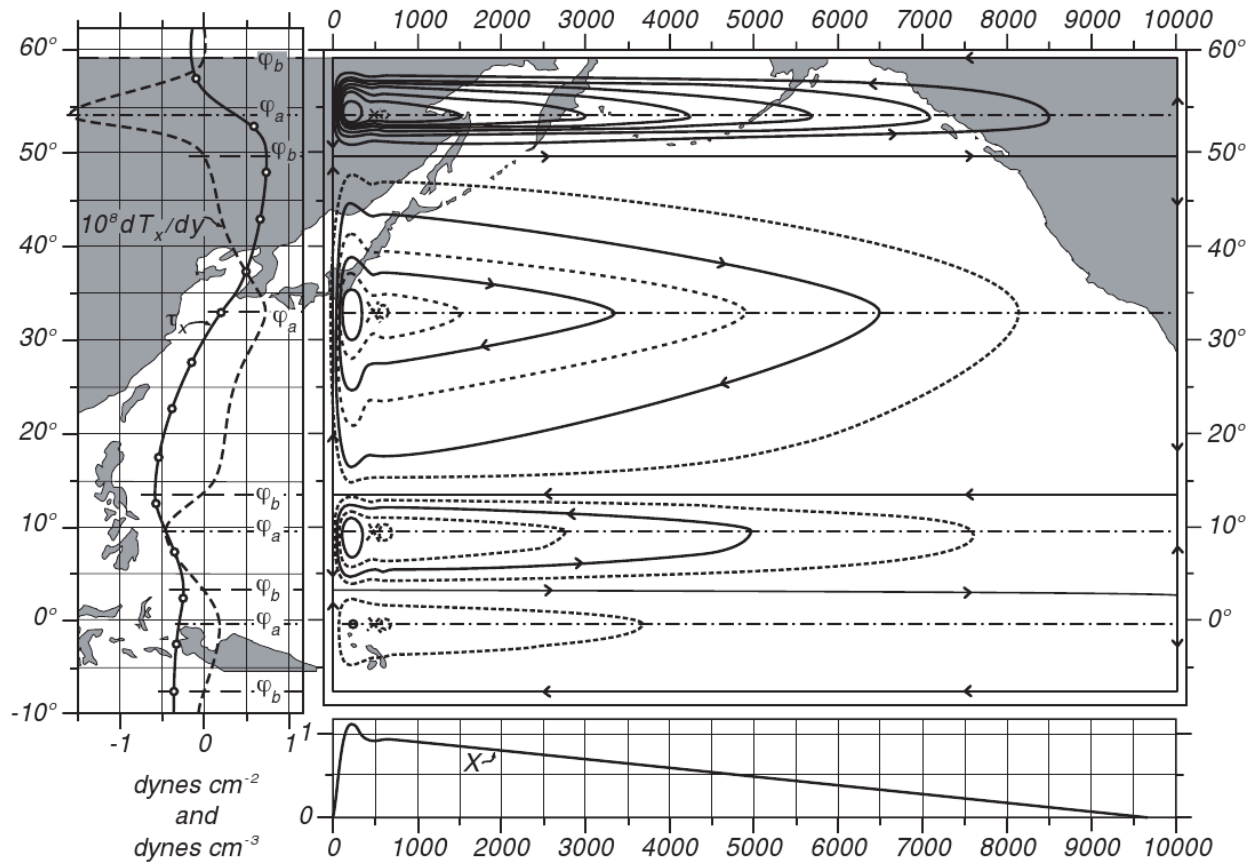
Figure 5.9: **Left**: Mean annual wind stress $\tau_x\,(y)$ over the Pacific and the curl of the wind stress. ϕ_b are the northern and southern boundaries of the gyres, where $M_y = 0$ and $\mathbf{curl}\,\tau = 0$. ϕ_0 is the center of the gyre. **Upper Right**: The mass transport stream function for a rectangular basin calculated by Munk (1950) using observed wind stress for the Pacific. Contour interval is **10** Sverdrups. The total transport between the coast and any point x, y is $\psi\,(x, y)$. The transport in the relatively narrow northern section is greatly exaggerated. **Lower Right**: North-South component of the mass transport. After Munk (1950).

Summarizing important concepts of vorticity

- Vorticity strongly constrains ocean dynamics

- Vorticity due to earth's rotation is much greater than other sources of vorticity

- Taylor and Proudman showed that vertical velocity is impossible in a uniformly rotating flow. Hence Ekman pumping requires that planetary vorticity varies with latitude.

- The curl of the wind stress adds relative vorticity to central gyres of each ocean basin. For steady state circulation in the gyre, the ocean must lose vorticity in western boundary currents.

- Positive wind stress curl leads to divergent flow in the Ekman layer. The ocean's interior geostrophic circulation adjusts through a northward mass transport.

Exercise 42   –   Cyclostrophic wind

When the flow is sufficiently near the equator so that f is small or when the Corolis force is negligible compared to the centripedal acceleration, the gradient wind equation becomes

$$\frac{v\boldsymbol{k} \times \mathbf{v}}{\boldsymbol{R}} = -\frac{1}{\rho}\boldsymbol{\nabla}_z p \tag{5.75}$$

where $\boldsymbol{k}$ is the unit vector in z direction, $\mathbf{v}$ is the velocity vector, v ist the meridional velocity, $\boldsymbol{R}$ Earth radius, $\boldsymbol{\nabla}_z$ horizontal nabla operator.

1. Derive this equation!
2. What is the associated gradient wind equation including the Coriolis force?
3. What is the Rossby number?

5.2 Thermohaline ocean circulation

Water, that is dense enough to sink from the surface to the bottom, is formed when cold air blows across the ocean at high latitudes in winter in the northern North Atlantic (e.g. in the Labrador Sea and between Norway and Greenland) and near Antarctica. The wind cools and evaporates water. If the wind is cold enough, sea ice forms, further increasing the salinity of the water because sea ice is fresher than sea water and salty water remains in the water when ice is formed. Bottom water is produced only in these regions, and the deep ocean is affected by these deep water formation processes. In other regions, cold, dense water is formed, but it is not quite salty enough to sink to the bottom. At mid and low latitudes, the density, even in winter, is sufficiently low that the water cannot sink more than a few hundred meters into the ocean. The only exception are some seas, such as the Mediterranean Sea, where evaporation is so great that the salinity of the water is sufficiently great for the water to sink to intermediate depths in the seas. If these seas are can exchange water with the open ocean, the waters formed in winter in the seas spreads out to intermediate depths in the ocean. Detailed measurements of the Atlantic current structure were made by an expedition of the research vessel Meteor from 1925-1927. On the basis of these data, Wüst [1935] characterized water masses necessary to describe the Atlantic currents and tracer distribution (Fig. 5.13). Broecker proposed a circulation model based on findings of the Meteor and other expeditions. In his model, large-scale oceanic circulation is represented by the transport system of a conveyor belt (Fig. 5.11) [Broecker and Peng, 1982].

The oceans carry about one third to one half the heat out of the tropics needed to maintain earth's temperature. Heat carried by the Gulf Stream and the North Atlantic drift warms the North Atlantic, keeping it ice free in winter, and it helps warm Europe. Norway, at 60°N is far warmer than southern Greenland or northern Labrador at the same latitude. Palm trees grow on the west coast of Ireland, but not in Newfoundland which is further south. The oceanic component of the heat-transport system is also called the Global Conveyor Belt. The basic idea is that the Gulf Stream carries heat to the North Atlantic realm. There the surface water releases heat and water to the atmosphere. Some of the ocean water becomes sufficiently cold, salty, and dense that it sinks
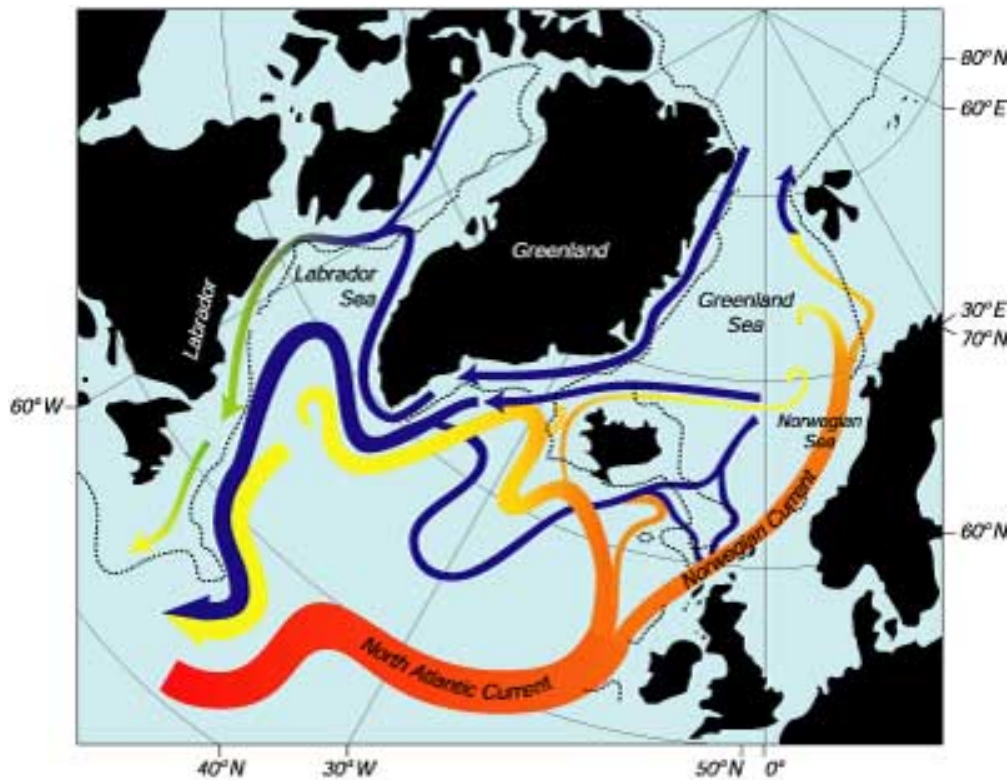
Figure 5.10: The surface (red, orange, yellow) and deep (violet, blue, green) currents in the North Atlantic. The North Atlantic Current brings warm water northward where it cools. Some sinks and returns southward as a cold, deep, western-boundary current. Some returns southward at the surface. From Woods Hole Oceanographic Institution.

to the bottom in the Norwegian and Greenland Seas. It then flows southward in very cold, bottom currents along western boundaries as a western boundary current. Some of the water remains at the surface and returns to the south in cool surface currents such as the Labrador Current and the Portugal Current (see Fig. 5.10).

The deep bottom water from the North Atlantic is mixed upward in other regions and ocean, and eventually it makes its way back to the Gulf Stream and the North Atlantic. Thus most of the water that sinks in the North Atlantic must be replaced by water from the far South Atlantic. As this surface water moves northward across the equator and eventually into the Gulf Stream, it carries heat out of the south Atlantic. So much heat is pulled northward by the formation of north-Atlantic bottom water in winter that heat transport in the Atlantic is entirely northward, even in the

southern hemisphere. Much of the solar heat absorbed by the tropical Atlantic is shipped north to warm Europe and the Northern Hemisphere. Imagine then what might happen if the supply of heat is shut off. We will get back to that topic in the next section, applying the box model.

We can make a crude estimate of the importance of the conveyor-belt circulation from a simple calculation. The Gulf Stream carries 40 Sv of $18°$C water northward. Of this, 15 Sv return southward in the deep western boundary current at a temperature of 2°C. The flow carried by the conveyor belt must therefore lose 1 Petawatts (1 Petawatt = 10^{15} Watt = 1 PW) in the North Atlantic north of 24°N. Although the calculation is very crude, it is remarkably close to the value of 1.2 ± 0.2 PW estimated by Rintoul and Wunsch (1991). Calculation: Exercise 46.

The production of bottom water is influenced by the salinity of surface waters in the North Atlantic. It is also influenced by the rate of upwelling due to mixing in other oceanic areas. First, let's look at the influence of salinity. Saltier surface waters form denser water in winter than less salty water. At first you may think that temperature is also important, but at high latitudes water in all ocean basins gets cold enough to freeze, so all ocean produce -2°C water at the surface. Of this, only the most salty will sink, and the saltiest water is in the Atlantic and under the ice on the continental shelves around Antarctica.

The the conveyor is driven by deepwater formation in the northern North Atlantic, making it the engine of conveyor belt circulation. The conveyor belt metaphor necessarily simplifies the ocean system, it is of course not a full description of the deep ocean circulation, it contains different aspects of it [Brüning and Lohmann, 1999]. Broecker's [Broecker, 1987; Broecker et al., 1991] concept provides a successful approach for global ocean circulation, although several features can be wrong like the missing Antarctic bottom water, the upwelling areas etc.. However, the global conveyor belt metaphor inspired new ideas of halting or reversing the ocean circulation and put it into a global climate context [Bryan, 1986]. This was helpful for the interpretation of Greenland ice core records (Fig. **??**) indicating different climate states with different ocean modes of operation (like on and off states of a mechanical maschine). From the analogy, it was possible to a) identify the relevance of North Atlantic deep water production and b) realize the possibility of multiple
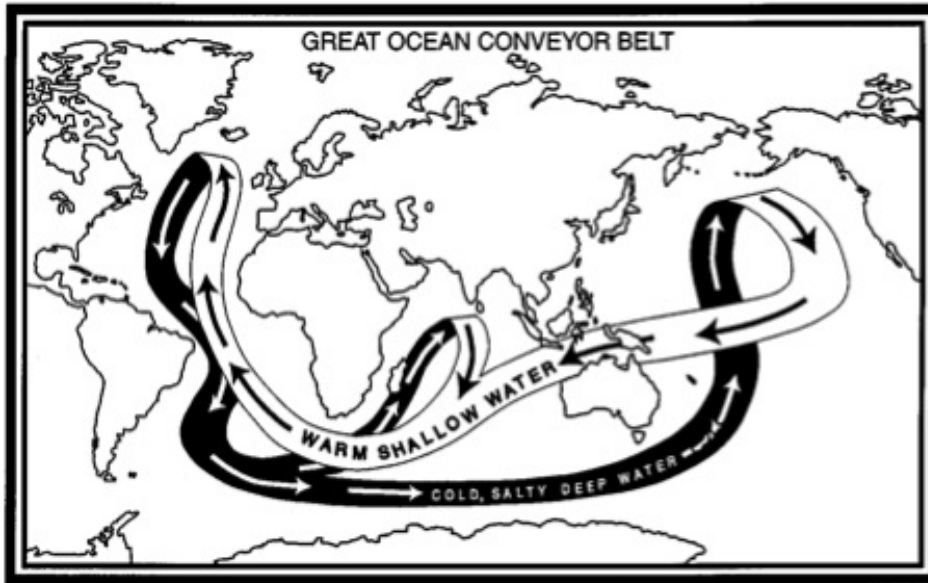
Figure 5.11: The great ocean conveyor [Broecker et al., 1991]. Warm and salty water entering the North Atlantic region is cooled. The dense water formed at the surface is convected to the deep ocean and is part of the southward return flow.

equilibria of ocean circulation states and their association with two different climatic states.

Many terms have been used to describe the deep circulation[5] and is called meridional overturning circulation. It is the zonal integral of the flow of mass plotted as a function of depth and latitude:

$$\tilde{v} = -\frac{\partial \psi}{\partial z} \tag{5.76}$$

$$\tilde{w} = \frac{\partial \psi}{\partial y} \tag{5.77}$$

with the zonally integrated velocities $\tilde{v}, \tilde{w}$, and a streamfunction $\psi(y, z)$ for the overturning circulation.

Figure 5.12 shows the meridional overturning circulation streamfunction $\psi(y, z)$ in the At-

---

[5]Abyssal circulation; Thermohaline circulation; Meridional overturning circulation; and Global conveyor. The term thermohaline circulation was once widely used, but it has disappeared almost entirely from the oceanographic literature. It is no longer used because it is clear that the flow is not only density driven.
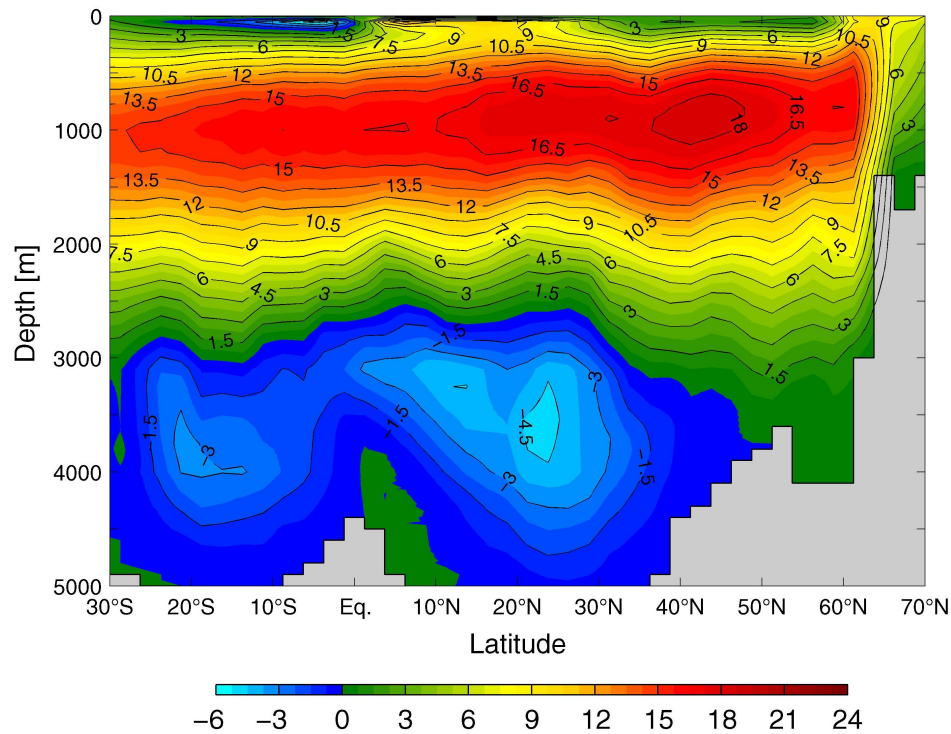
Figure 5.12: Modelled meridional overturning streamfunction in Sv (1 Sv $\equiv 10^6$ m^{3}s^{-1}) in the Atlantic Ocean. Grey areas represent zonally integrated smoothed bathymetry.

lantic. The streamfunction is calculated as a cumulative sum of zonally integrated mass transports of the ocean at each latitude from surface to the particular depth. The zonally intregrated mass transport at a certain latitude derives from the zonally averaged meridional velocity component times the height of the ocean layer and the width of the ocean. Water flows along the stream lines. For instance, increasing positive values of MOC from surface to about 1,000m depth at mid latitudes of the Northern Hemisphere denote northward flowing water. With increasing depth the values of the MOC streamfunction decrease until a minimum at about 4,000m depth is reached. These waters move southward instead. In the Atlantic two major, a shallower and a deeper over-turning cell exist according to figure 5.12. One cell shows positive values, thus, clockwise volume transport and stretches from almost the surface to about 2,500 - 3,000m depth. The other expands from about 3,000m depth to the bottom of the ocean at latitudes south of 40°N. The shallower cell denotes the modelled equivalent of North Atlantic Deep Water (NADW) while Antarctic Bottom

Water (AABW), transporting Southern Ocean water into the Atlantic, is simulated by the deeper cell. An overturning maximum of 18.7 Sv (1 Sv $\equiv 10^6$ m^{3}s^{-1}) is found at 40°- 50°N and 1,000m depth and an export into the Southern Ocean across 30°S of 14.9 Sv. This results in an overturning ratio of 0.79, so only little recirculation occurs. A closer look at Figure 5.12 reveals that NADW is predominantly formed north of 60°N with about 10 Sv. The inflow of AABW into the Atlantic is much weaker than the outflow of NADW. At 30°S a value of less than 1 Sv is calculated by the model while the maximum counter-clockwise overturning of the bottom water cell reaches 4.7 Sv at 25°N.
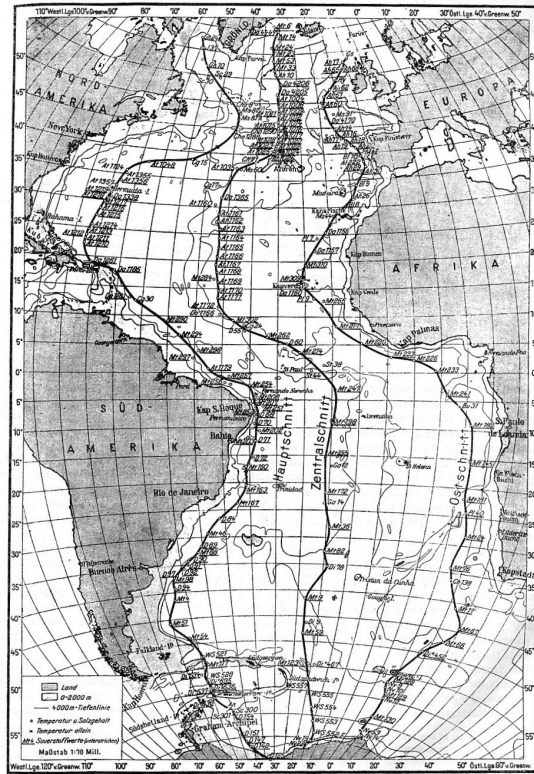
Fig. 46. Position of the stations in the three longitudinal sections.
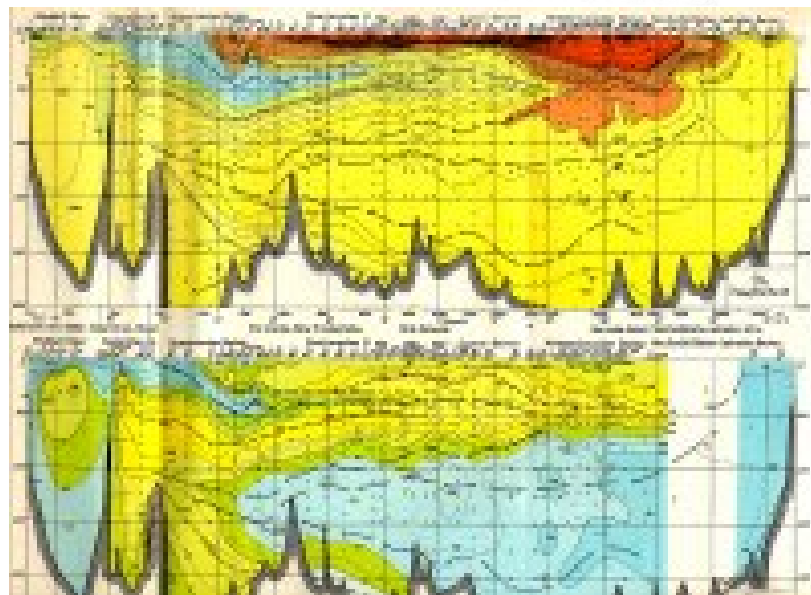
Figure 5.13: 1927-1929 Meteor Expedition, the first accurate hydrographic survey of the Atlantic from Wüst [1935]. Lower panel: Salinity and dissolved oxygen on the Hauptschnitt along the western side of the Atlantic.

Exercise 43   –   Ocean thermohaline circulation

Consider a geostrophic flow (u, v)

$$-fv = -\frac{1}{\rho_0}\frac{\partial p}{\partial x} \tag{5.78}$$

$$fu = -\frac{1}{\rho_0}\frac{\partial p}{\partial y} \quad . \tag{5.79}$$

Use the hydrostatic approximation

$$\frac{\partial p}{\partial z} = -g\rho \tag{5.80}$$

and equation (5.78) in order to derive the meridional overturning stream function $\Phi(y, z)$ as a fuction of density ρ at the basin boundaries! Φ is defined via

$$\Phi(y, z) = \int_0^z \frac{\partial \Phi}{\partial \tilde{z}}\,d\tilde{z} \tag{5.81}$$

$$\frac{\partial \Phi}{\partial \tilde{z}} = \int_{x_e}^{x_w} v(x, y, \tilde{z})\,dx \quad \text{(zonally integrated transport),} \tag{5.82}$$

where x_e and x_w are the eastward and westward boundaries in the ocean basin (think e.g. of the Atlantic Ocean). Units of Φ are $m^3 s^{-1}$. At the surface $\Phi(y, 0) = 0$.

Solution of Exercise 43: Ocean thermohaline circulation

$$\frac{\partial \Phi}{\partial z} = \int_{x_e}^{x_w} v(x, y, z)\,dx \tag{5.83}$$

$$= \frac{1}{\rho_0 f}\int_{x_e}^{x_w} \frac{\partial p}{\partial x}\,dx = \frac{1}{\rho_0 f}(p(x_w, y, z) - p(x_e, y, z)) \tag{5.84}$$

$$= -\frac{g}{\rho_0 f}\int_0^z (\rho(x_w, y, z') - \rho(x_e, y, z'))dz' \tag{5.85}$$

Exercise 44   –   Estimates of overturning

It is observed that water sinks in to the deep ocean in polar regions of the Atlantic basin at a rate of 15 Sv. (Atlantic basin: $80,000,000\,km^2 area \times 4\,km$ depth.)

1. How long would it take to 'fill up' the Atlantic basin?

2. Supposing that the local sinking is balanced by large-scale upwelling, estimate the strength of this upwelling. Hint: Upwelling $= area \times w$. Express your answer in $m\ y^{-1}$.

3. Compare this number with that of the Ekman pumping in (5.31)!

Solution of Exercise 44: Estimates of overturning

1. Timescale T to 'fill up' the Atlantic basin:

$$T = \frac{80 \cdot 10^{12}\, m^2 \cdot 4000\, m}{15 \cdot 10^6\, m^3 s^{-1}} = 2.13 \cdot 10^{10} s = 676\ years$$

2. Overturning is balanced by large-scale upwelling:

$$area \cdot w = 15 \cdot 10^6\, m^3 s^{-1}$$

$$w = 0.1875 \cdot 10^{-6} m\ s^{-1} = 5.9 \cdot 10^{-15} m\ y^{-1}.$$

3. Ekman pumping

$$w_E \simeq 32\ m\ y^{-1}.$$

Simple model of meridional overturning

It is instructive to derive a simple concept of the meridional overturning based on vorticity dynamics in the (y,z)-plane. The dynamical model in two dimensions reads

$$\frac{\partial}{\partial t} v \quad = \quad -\frac{1}{\rho_0}\frac{\partial p}{\partial y} \quad - \quad f u \quad - \quad \kappa v \tag{5.86}$$

$$\frac{\partial}{\partial t} w \quad = \quad -\frac{1}{\rho_0}\frac{\partial p}{\partial z} \quad - \quad \frac{g}{\rho_0}(\rho - \rho_0) \quad - \quad \kappa w \tag{5.87}$$

with κ as parameter for Rayleigh friction. Using the continuity equation

$$0 \quad = \quad \frac{\partial v}{\partial y} \quad + \quad \frac{\partial w}{\partial z} \tag{5.88}$$

one can introduce a streamfunction $\Phi(y, z)$ with $v = \partial_z \Phi$ and $w = -\partial_y \Phi$. The associated vorticity equation in the (y,z)-plane is therefore

$$\frac{\partial}{\partial t}\nabla^2\Phi \quad = \quad -f\frac{\partial u}{\partial z} \quad + \quad \frac{g}{\rho_0}\frac{\partial \rho}{\partial y} \quad - \quad \kappa\nabla^2\Phi \tag{5.89}$$

We can choose the ansatz[6] satisfying that the normal velocity at the boundary vanishes, $\Phi = 0$:

$$\Phi(y, z, t) \quad = \quad \Phi_{max}(t) \ \sin\left(\frac{\pi y}{L}\right) \times \sin\left(\frac{\pi z}{H}\right) \tag{5.91}$$

The parameters L and H dentote the meridional and depth extend (y goes from 0 to L, z from 0 to H). With the assumption that the term $-f\frac{\partial u}{\partial z}$ is absorbed into the viscous terms, and the integration

---

[6]In principle, a complete Galerkin approximation shall be applied

$$\Phi(y, z, t) \quad = \quad \Sigma_{k=1}^{\infty}\Sigma_{l=1}^{\infty}\Phi_{max}^{k,l}(t) \ \sin(\pi k y/L) \times \sin(\pi l z/H) \tag{5.90}$$

yielding a first order differential equation in time for $\Phi_{max}^{k,l}(t)$. For a different approach: [Maas, 1994], for an overview of simple climate models: [Olbers, 2001].

$\int_0^L dy \int_0^H dz$, we derive for the three remaining terms in (5.89):

$$\frac{d}{dt}\Phi_{max}\left(\frac{\pi^2}{L^2}+\frac{\pi^2}{H^2}\right)\int_0^L dy \sin\left(\frac{\pi y}{L}\right)\int_0^H dz \sin\left(\frac{\pi z}{H}\right) = 4LH\left(\frac{1}{L^2}+\frac{1}{H^2}\right)\frac{d}{dt}\Phi_{max}$$

$$\int_0^L dy \int_0^H dz \frac{g}{\rho_0}\frac{\partial \rho}{\partial y} = \frac{g}{\rho_0}\ H\ (\rho_{north}-\rho_{south})$$

$$\kappa\Phi_{max}\left(\frac{\pi^2}{L^2}+\frac{\pi^2}{H^2}\right)\int_0^L dy \sin\left(\frac{\pi y}{L}\right)\int_0^H dz \sin\left(\frac{\pi z}{H}\right) = \kappa\ 4LH\left(\frac{1}{L^2}+\frac{1}{H^2}\right)\Phi_{max}$$

with $\rho_{north} = \rho(y = L)$, and $\rho_{south} = \rho(y = 0)$, and the equation

$$\frac{d}{dt}\Phi_{max} = \frac{a}{\rho_0}(\rho_{north}-\rho_{south}) - \kappa\Phi_{max} \tag{5.92}$$

with $a = gLH^2/4(L^2+H^2)$.

This shows that the overturning circulation depends on the density differences on the right and left boxes. In the literature, (5.92) is simplified to a diagnostic relation

$$\Phi_{max} = \frac{a}{\rho_0\,\kappa}\ (\rho_{north}-\rho_{south}) \tag{5.93}$$

because the adjustment of Φ_{max} is quasi-instantaneous due to adjustment processes, e.g. Kelvin waves.

Here, we introduce a hemispheric (Stommel-type) or interhemispheric (Rooth-type) box model of the thermohaline circulation. The common assumption of these box models is that the oceanic overturning rate Φ can be expressed by the meridional density difference:

$$\Phi = -c\,(\alpha\Delta T - \beta\Delta S) \quad , \tag{5.94}$$

where α and β are the thermal and haline expansion coefficients, $c = a(\rho_0\kappa)^{-1}$, and Δ denotes the meridional difference operator applied to temperature T and salinity S, respectively. The
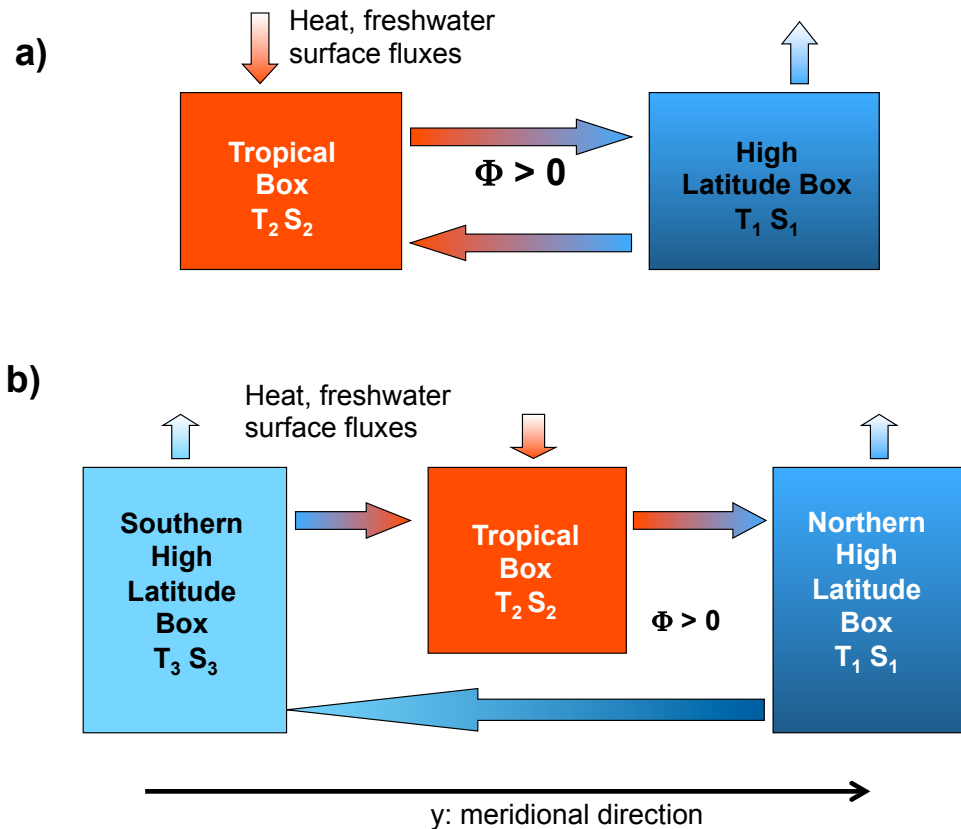
Figure 5.14: Schematic picture of the hemispheric two box model (a) and of the interhemispheric box model (b).

meriodional density differences are clearly dominated by temperature differences (Fig. 5.15a). In a single hemispheric view, the salinity difference breakes the temperature difference.

In the model of (Rooth, 1982) the Atlantic ocean is described over both hemispheres and the densities have to be taken in the North Atlantic and South Atlantic Ocean, respectively. In the interhemispheric model the densities at high northern and southern latitudes are close, the pole-to-pole differences are caused by salinity differences (Fig. 5.15b).

5.2.1 Conceptual model of the ocean circulation: Stommel's box model

The foundational paper on the analysis of the ocean circulation is by Stommel [1961] who proposes and analyzes simple "box models". This paper culminates in the analysis of the equilibrium
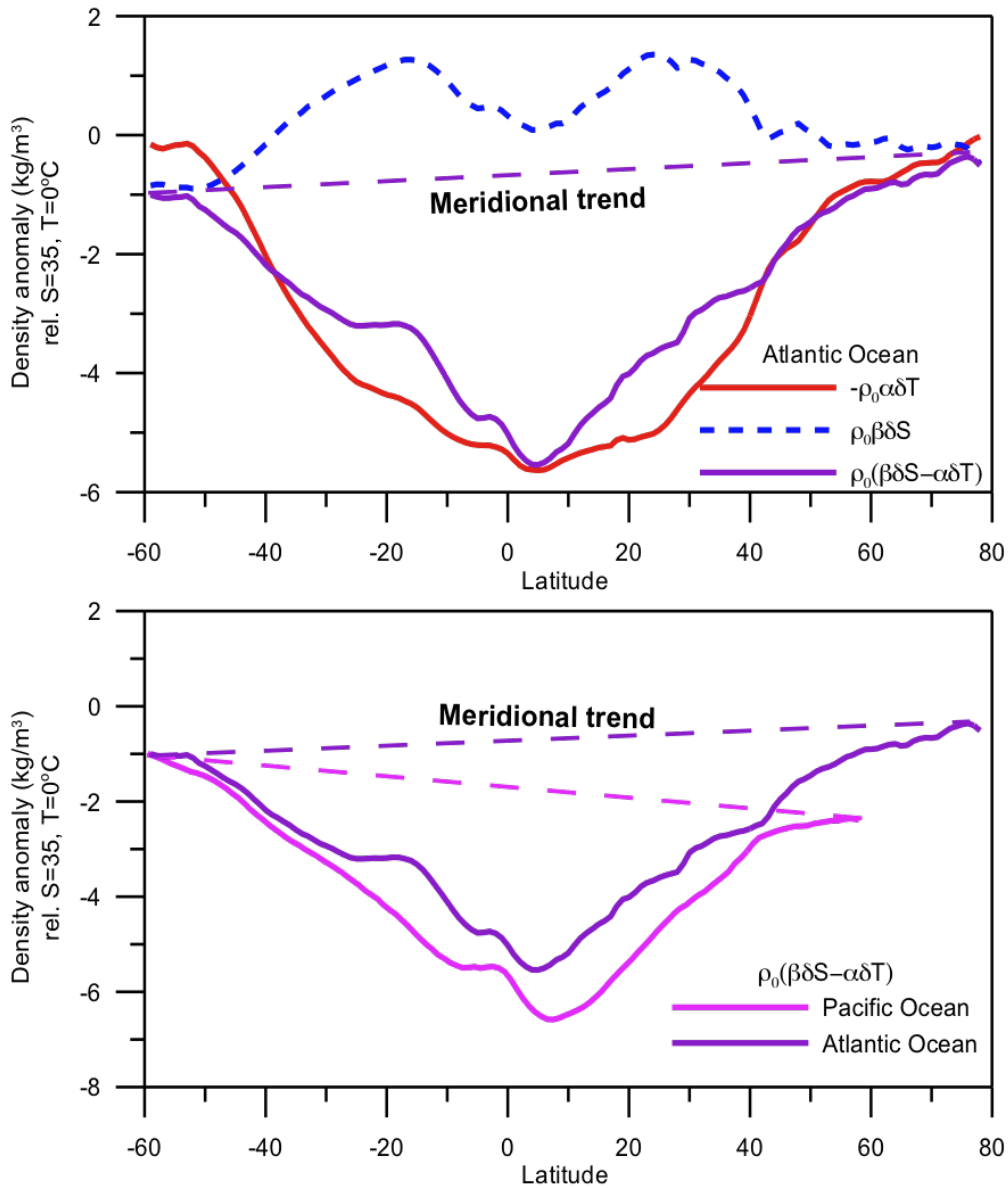
Figure 5.15: a) The Atlantic surface density is mainly related to temperature differences. b) But the pole-to-pole differences are caused by salinity differences.

solutions of a system in which two vessels connected to reservoirs are joined by a capillary that exchanges heat and salt (Fig. 5.16).

One reservoir is warm and salty, the other cold and fresh. The flow through the capillary is proportional to the difference in density of the two water masses, which is taken to be a linear

function of temperature and salinity. Upon substituting the equation of state into the equations governing the evolution of the water masses, Stommel finds two coupled nonlinear equations. In some parameter regimes there are three steady state solutions, two of which are stable. These two stable modes have opposite directions of flow, which he interprets as a competition between temperature and salinity effects on density.
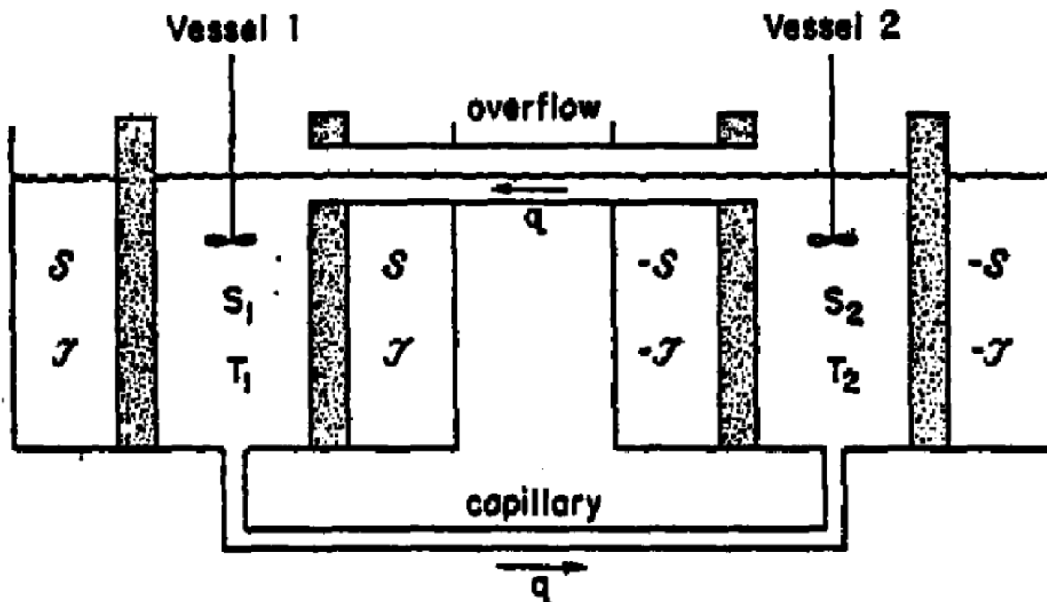
Figure 5.16: Schematic picture of the box model described by Stommel [1961].

As stated above Stommel Stommel [1961] considered a two-box ocean model where the boxes are connected by an overflow at the top and a capillary tube at the bottom (Fig. 5.16), such that the capillary flow is directed from the high density vessel to the low density vessel following with a rate Φ. The common assumption of these box models is that the oceanic overturning rate Φ can be expressed by the meridional density difference:

$$\Phi = -c\left(\alpha\Delta T - \beta\Delta S\right) \quad , \tag{5.95}$$

where α and β are the thermal and haline expansion coefficients, c is a tunable parameter, and Δ denotes the meridional difference operator applied to the variables temperature T and salinity S,

respectively. $\Delta T = T_1 - T_2$ with T_1, T_2 are the high-latitude and the tropical boxes in Fig. 5.16. The equations for temperature T and salinity S are the heat and salt budgets using an upstream scheme for the advective transport and fluxes with the atmosphere:

$$\frac{d}{dt}T_1 = \frac{\Phi}{V}T_2 - \frac{F_1^{oa}}{\rho_0 c_p h} \tag{5.96}$$

$$\frac{d}{dt}S_1 = \frac{\Phi}{V}S_2 - \frac{S_0}{h}(P-E)_1 \quad , \tag{5.97}$$

$$\frac{d}{dt}T_2 = \frac{\Phi}{V}T_1 - \frac{F_2^{oa}}{\rho_0 c_p h} \tag{5.98}$$

$$\frac{d}{dt}S_2 = \frac{\Phi}{V}S_1 - \frac{S_0}{h}(P-E)_2 \quad , \tag{5.99}$$

where V is the volume of the box with depth h, and $(P-E)$ denotes the freshwater flux (precipitation minus evaporation plus runoff). Foa is the heat flux at the ocean-atmosphere interface, S_0 is a reference salinity, and $\rho_0 c_p$ denotes the heat capacity of the ocean. Subtraction leads to

$$\frac{d}{dt}\Delta T = -\frac{\Phi}{V}\Delta T - \Delta\frac{F^{oa}}{\rho_0 c_p h} \tag{5.100}$$

$$\frac{d}{dt}\Delta S = -\frac{\Phi}{V}\Delta S - \frac{S_0}{h}\Delta(P-E) \quad . \tag{5.101}$$

The heat flux F^{oa} at the ocean-atmosphere interface can be replaced by a restoring term to the respective atmospheric temperatures, and to a first order approximation the temperatures are fixed. We now make an approximation of (5.100, 5.101) and assume that $\Delta T, c,$ and $\Delta(P-E)$ are fixed parameters. The dynamics is then given by

$$\frac{d}{dt}\Delta S = \frac{c}{V}(\alpha\Delta T - \beta\Delta S)\,\Delta S - \frac{S_0}{h}\Delta(P-E) \quad . \tag{5.102}$$

The steady state solution of (5.102) for ΔS can be obtained as

$$0 = \frac{c}{V}(\alpha\Delta T - \beta\Delta S_{eq})\,\Delta S_{eq} - \frac{S_0}{h}\Delta(P-E) \quad , \tag{5.103}$$

which leads to a quadratic equation for

$$\Delta S_{eq} = \frac{\alpha \, \Delta T}{\beta} \left(\frac{1}{2} \pm \sqrt{\frac{1}{4} - \frac{\beta S_0 V \Delta(P - E)}{ch(\alpha \Delta T)^2}} \right) \quad . \tag{5.104}$$

It can be shown (exercise 45) that the negative root leads to an unstable solution. Furthermore

$$ch(\alpha \Delta T)^2 > 4 \, \beta S_0 V \Delta(P - E) \tag{5.105}$$

which means there exists a critical $\Delta(P - E)_{crit}$ above which the flow has no solution:

$$\Delta(P - E)_{crit} = ch \frac{(\alpha \Delta T)^2}{4 \, \beta S_0 V} \quad . \tag{5.106}$$

What will hapen if $\Delta(P - E) > \Delta(P - E)_{crit}$?

Stommel [1961] modified equation (5.95) to

$$\Phi = -c \, |\alpha \Delta T - \beta \Delta S| \tag{5.107}$$

Then the steady-state solutions are classified according to the sign of $q = \alpha \Delta T - \beta \Delta S$. When $q > 0$, the circulation is driven by the thermal contrast. When $q < 0$, the haline contrast is dominant in driving the current.

Exercise 45   –   Bifurcation of Stommel's model

Consider Fig. 5.16 where the ocean surface water is heated at the equatorial region and flows toward high latitudes. At the pole the water is cooled and sinks, upwelling is at the equator.

1. Starting from (5.102), calculate the linear stability of the equilibrium solution (5.104).

2. Investigate the sensitivity of the stability with respect to $(P - E)_{crit}$ and the other parameters in the model.

Solution for Bifurcation of Stommel's model

We rewrite (5.102) into

$$\frac{V}{c}\frac{d}{dt}\beta\Delta S \quad = \quad (\alpha\Delta T - \beta\Delta S)\,\beta\Delta S \quad - \quad \frac{\beta S_0 V}{ch}\Delta(P - E) \quad . \quad (5.108)$$

Denoting $x = \beta\Delta S, \quad a = \alpha\Delta T, \quad b = \dfrac{\beta S_0 V}{ch}\Delta(P - E),$ and a non-dimentional time $t_d = t\dfrac{c}{V},$ we have

$$\frac{d}{dt_d}x = (a - x) \cdot x - b \qquad (5.109)$$

The equilibrium solutions are

$$x_{1,2} = \frac{a}{2} \pm \sqrt{\frac{a^2}{4} - b} \qquad (5.110)$$

Therefore, (5.109) can be rewritten as

$$\frac{d}{dt_d}x = f(x) = -(x - x_1) \cdot (x - x_2) \qquad (5.111)$$

The derivative is

$$f'(x) = -(x - x_1) - (x - x_2) \qquad (5.112)$$

and

$$f'(x_1) \;=\; -(x_1 - x_2) = -2\sqrt{\frac{a^2}{4} - b} < 0 \qquad \textbf{stable} \tag{5.113}$$

$$f'(x_2) \;=\; -(x_2 - x_1) = +2\sqrt{\frac{a^2}{4} - b} > 0 \qquad \textbf{unstable} \tag{5.114}$$

Furthermore,

$$b \;<\; \frac{a^2}{4} \qquad \text{which means that} \tag{5.115}$$

$$\Delta(P - E) \;<\; \Delta(P - E)_{crit} = ch\frac{(\alpha\Delta T)^2}{4\,\beta S_0 V} \quad . \tag{5.116}$$

Reversed mode of the model: What happens if $\Delta(P - E) > \Delta(P - E)_{crit}$?

Then the direction of the circulation is anti-clockwise and the current is driven predominantly by haline contrast with higher density at low latitudes. The equation has to modified according to (5.107) and the equilibrium solutions are

$$x_{3,4} = \frac{a}{2} \pm \sqrt{\frac{a^2}{4} + b} \tag{5.117}$$

This solution has the requirement that $\frac{a^2}{4} + b > 0.$ Let us now look on the linear stability of $x_{3,4}$

$$\frac{d}{dt_d}x = f(x) = (x - x_3) \cdot (x - x_4) \tag{5.118}$$

The derivative is

$$f'(x) = (x - x_3) + (x - x_4) \tag{5.119}$$

and

$$f'(x_3) = (x_3 - x_4) = +2\sqrt{\frac{a^2}{4} + b} > 0 \qquad \textbf{unstable} \qquad (5.120)$$

$$f'(x_4) = (x_4 - x_3) = -2\sqrt{\frac{a^2}{4} + b} < 0 \qquad \textbf{stable} \qquad (5.121)$$

This means tha tthere exists two stable equilibria (Fig. 5.17) for

$$-\frac{a^2}{4} < b = 2\frac{\beta S_0 V}{ch}(P - E) < \frac{a^2}{4} = \frac{(\alpha \Delta T)^2}{4} \qquad . \qquad (5.122)$$
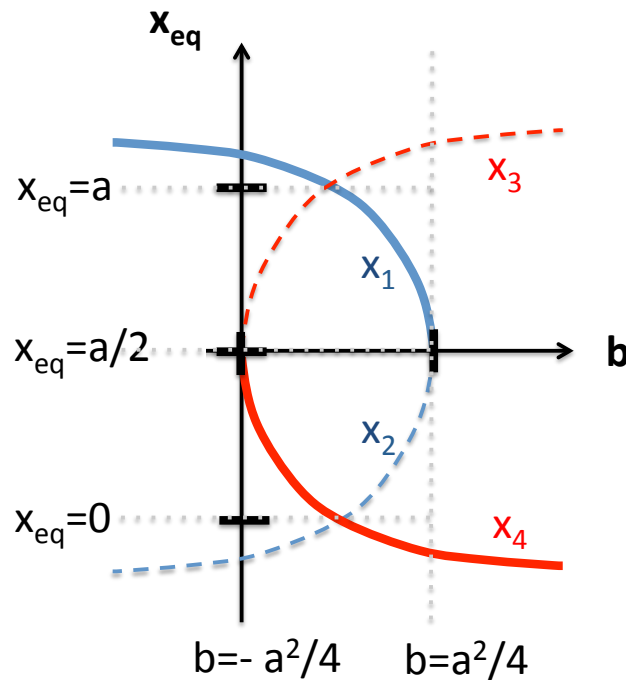
Figure 5.17: Schematic bifurcation of the Stommel box model. Dashed solutions are unstable, the solid red and blue lines represent the stable solutions, x_1 and x_4, respectively.

5.2.2 Non-normal dynamics of the ocean box model*

In this section, a category of the non-linear models following the simple thermohaline model of Stommel Stommel [1961] is analyzed. We start with (5.100, 5.101). Denoting furthermore $x \in \mathbf{R}^2$ for the anomalies of $(\Delta T, \Delta S)$, Lohmann and Schneider **?** have shown that the evolution equation is of the following structure:

$$\frac{d}{dt}x = Ax + \langle b|x \rangle \; x.$$

(5.123)

The brackets $\langle \; | \; \rangle$ denote the Euclidean scalar product. This evolution equation (5.123) can be transferred to a

$$x(t) = \frac{1}{\gamma(t)} \; \exp(At)\, x_0 \;,$$

(5.124)

with a scaling function $\gamma(t, x_0)$. The models of Stommel **?**, and many others are of this type, and their dynamics are therefore exactly known. [7]

It is useful to analyze the dynamics in the phase space spanned by temperature and salinity anomalies and investigate the model sensitivity under anomalous high latitude forcing, induced as an initial perturbation. The lines in Fig. 5.18 are phase space trajectories after perturbations of different magnitude have been injected into the North Atlantic. We notice that for most trajectories, the distances from zero $(0, 0)$ increase temporarily, where the maximal distance from zero is after a decade. After about 10 years the trajectories in Fig. 5.18 point into a "mixed temperature/salinity direction", denoted further as e_1.

Fig. 5.18 implies that the adjustment of the THC involves two phases: A fast thermal response and a slower response on the e_1-direction. The vector e_1 is identical with the most unstable mode in the system. Because the scaling function $\gamma(t)$ acts upon both temperature and salinity (5.124), the evolution of the non-linear model can be well characterized by the eigenvectors of the matrix

---

[7]It is worth knowing that (5.100, 5.101) is equivalent to the multi-dimensional Malthus-Verhulst model (also known as logistic equation), which was originally proposed to describe the evolution of a biological population.
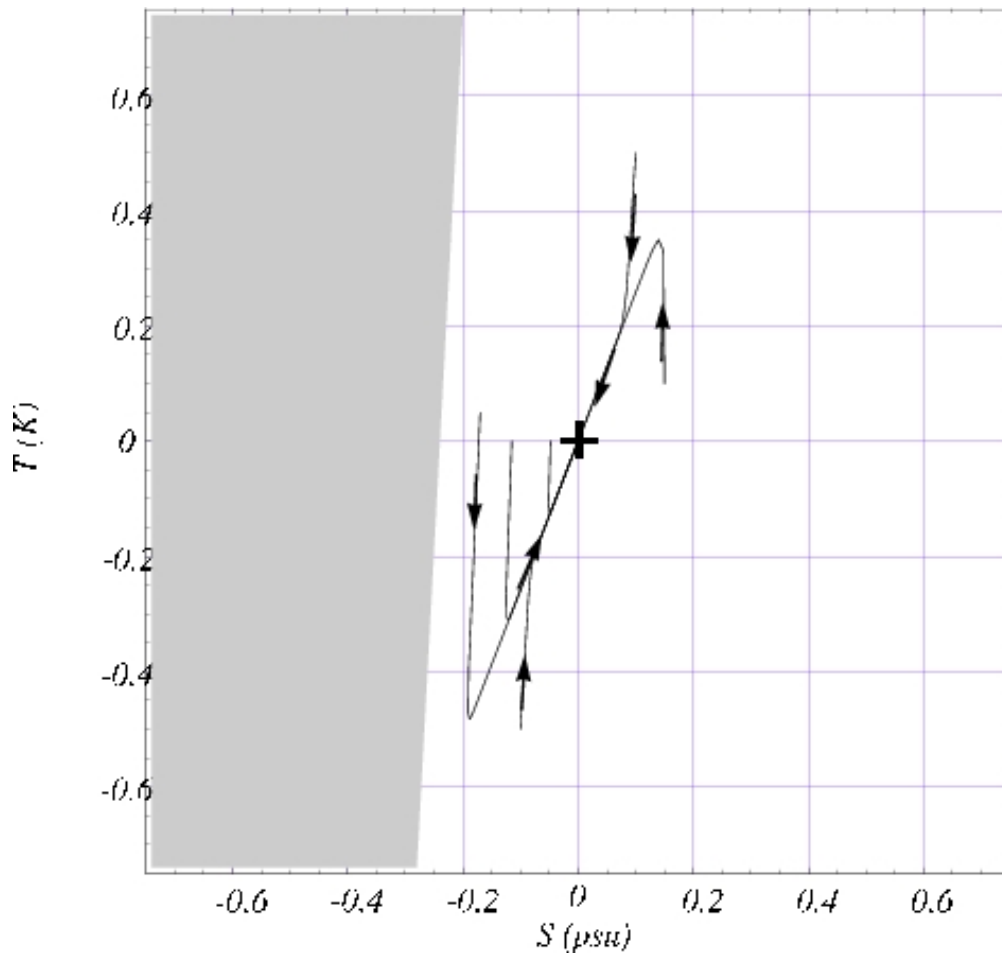
Figure 5.18: The basin of attraction (white area) and the dynamics in the thermohaline phase space. With initial conditions outside the gray area, the trajectories converge asymptotically to the origin corresponding to the thermally driven solution of the THC. Due to the fast thermal response during the first decade of relaxation, the distance of the trajectories from zero can increase temporarily.
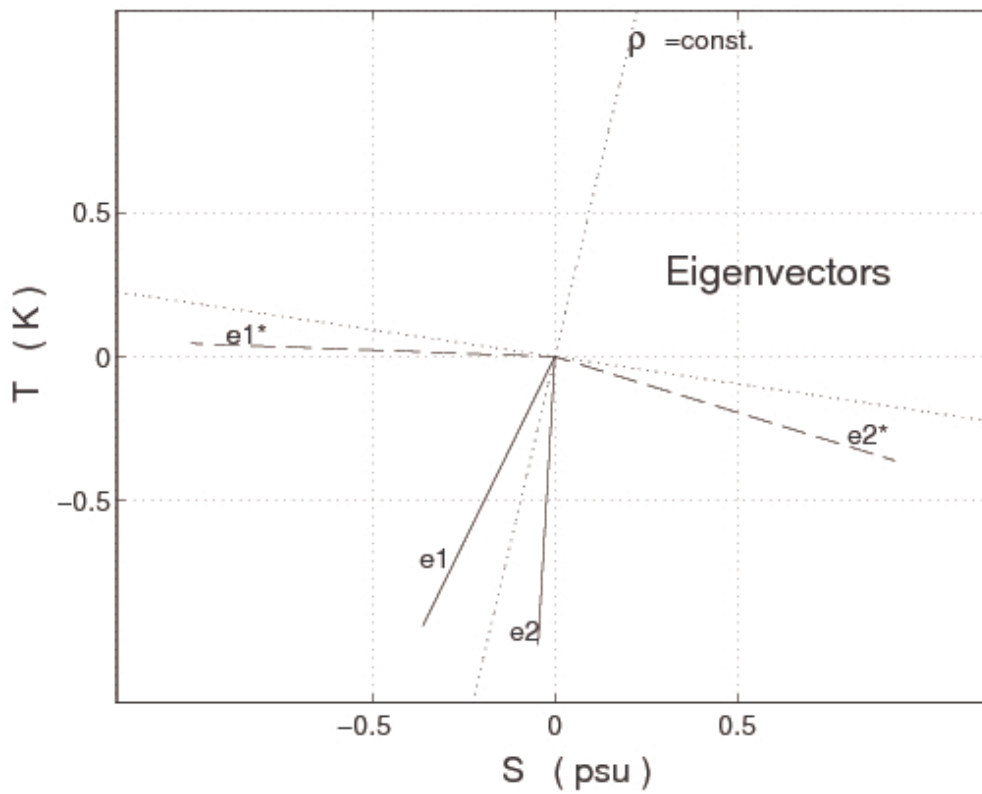
Figure 5.19: Eigenvectors e_1, e_2, and adjoint eigenvectors e_1^*, e_2^* of the tangent linear operator A^+. The dotted lines show the line of constant density and the perpendicular.

A , which is discussed in the following.

In our system, the operator A of the box model is found to be non-normal, and the eigenvectors are not orthogonal. One eigenvalue (e_2) is closely related to temperature anomalies, whereas the other (e_1) is a "mixed temperature/salinity eigenvector" (Fig. 5.19). The eigenvectors of the adjoint matrix A^+ are denoted by e_1^* and e_2^*, respectively. For the non-normal matrix A , the eigenvectors of A and A^+ do not coincide, but fulfill the "biorthogonality condition":

$$e_1^* \perp e_2 \text{ and } e_2^* \perp e_1 \,. \tag{5.125}$$

Both eigenvalues $\lambda_{1,2}$ are real and negative. Because of $\lambda_2 < \lambda_1$, the first term dominates for long time scales and the second for short time scales. Using the biorthogonality condition, we get furthermore the coefficients

$$c_i \;=\; \frac{\langle e_i^* | x_0 \rangle}{\langle e_i^* | e_i \rangle} \qquad \text{for} \quad i = 1, 2 \tag{5.126}$$

A perturbation is called "optimal", if the initial error vector has minimal projection onto the subspace with the fastest decaying perturbations, or equivalently if the coefficient c_1 is maximal. This is according to (5.126) equivalent to x_0 pointing into the direction of e_1^*. This unit vector e_1^* is called the "biorthogonal" ? to the most unstable eigenvector e_1 which we want to excite. In order to make a geometrical picture for the mathematical considerations, assume that the tail of the vector x_0 is placed on the e_1—line and its tip on the e_2—line. This vector is stretched maximally because the tail decays to zero quickly, whereas the tip is hardly unchanged due to the larger eigenvalue λ_1 . The most unstable mode e_1 and its biorthogonal e_1^* differ greatly from each other, and the perturbation that optimally excites the mode bears little resemblance to the mode itself.

It is remarkable that the optimal initial perturbation vector e_1^* does not coincide with a perturbation in sea surface density at high latitudes, which would reside on the dotted line perpendicular to $\rho = const.$ in Fig. 5.19. Even when using a space spanned by $(\alpha T, \beta S)$ instead of (T, S) ,

to take into account the different values for the thermal and haline expansion coefficients, vector e_1^* is much more dominated by the scaled salinity anomalies than the temperature anomalies of the high latitudinal box.

Numerical simulations by Manabe and Stouffer Manabe and Stouffer [1993] showed, for the North Atlantic, that between two and four times the preindustrial CO_2 concentration, a threshold value is passed and the thermohaline circulation ceases completely. One other example of early Holocene rapid climate change is the '8200 yr BP' cooling event recorded in the North Atlantic region possibly induced by freshwater. One possible explanation for this dramatic regional cooling is a shutdown in the formation of deep water in the northern North Atlantic due to freshwater input caused by catastrophic drainage of Laurentide lakes Barber et al. [1999]; Lohmann [2003]. The theoretic considerations and these numerical experiments suggest that the formation of deep water in the North Atlantic is highly sensitive to the freshwater forcing.

Chapter 6

Application: Climate-Box-Model

6.1 Model description

Here we introduce an interhemispheric box model of the deep ocean circulation to study the feedbacks in the climate system. Like in the model of Rooth [1982] the Atlantic Ocean is described over both hemispheres. The box model consists of four oceanic and three atmospheric boxes, as indicated in Fig. 6.1. The ocean boxes represent the Atlantic Ocean from $80°N$ to $60°S$. The indices of the temperatures T, the salinities S, the surface heat fluxes H, the atmospheric heat fluxes F, the radiation terms R as well as later on the volumes bear on the different boxes (N for the northern, M for the tropical, D for the deep and S for the southern box).

The discrete boxes are utterly homogeneous, which implies that the temperatures and the salinities everywhere within one box are alike. The climate model is based on mass and energy considerations. Emphasis is placed on the overturning flow Φ of the ocean circulation.

216
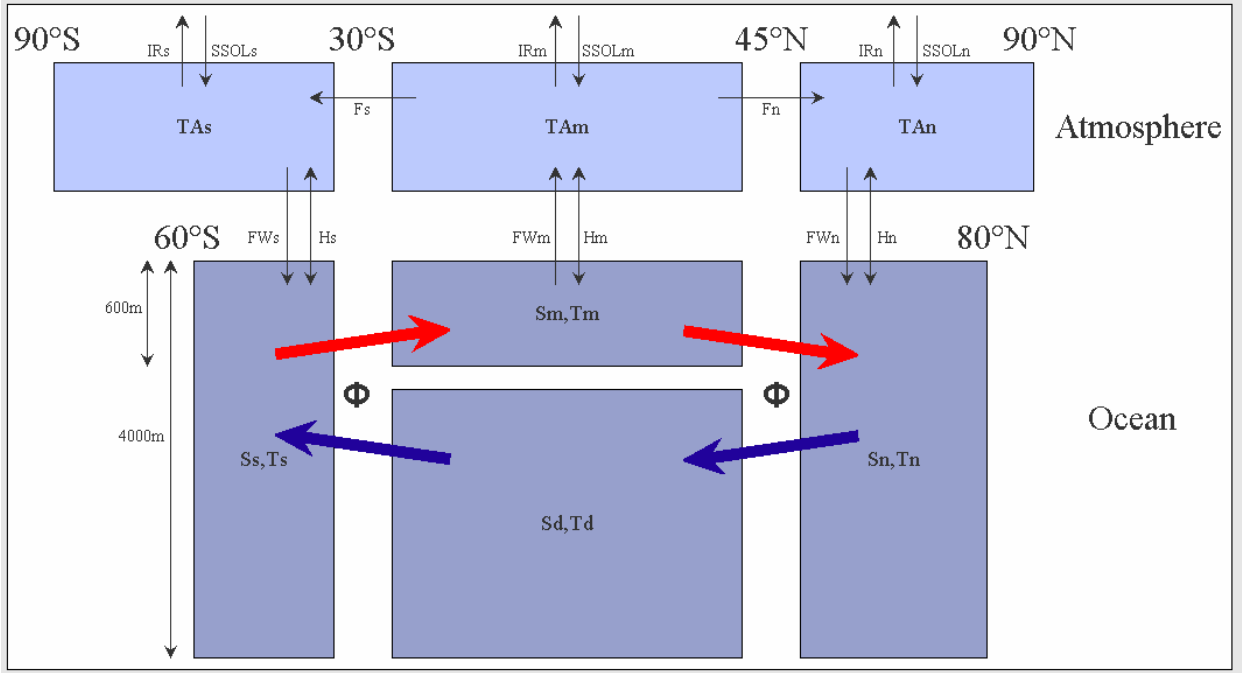
Figure 6.1: Schematic illustration of the Climate-Box-Model

The prognostic equations for the temperatures of the ocean boxes read

$$\frac{d}{dt}T_N = -\left(T_N - T_M\right)\frac{\Phi}{V_N} + \frac{H_N}{\rho_0 c_p dz_2}, \tag{6.1}$$

$$\frac{d}{dt}T_M = -\left(T_M - T_S\right)\frac{\Phi}{V_M} + \frac{H_M}{\rho_0 c_p dz_1}, \tag{6.2}$$

$$\frac{d}{dt}T_S = -\left(T_S - T_D\right)\frac{\Phi}{V_S} + \frac{H_S}{\rho_0 c_p dz_2} \quad \text{and} \tag{6.3}$$

$$\frac{d}{dt}T_D = -\left(T_D - T_N\right)\frac{\Phi}{V_D} \tag{6.4}$$

where ρ_0 denotes a reference density for saltwater and c_p the specific heat capacity of water. The factors dz_i and V_i indicate the depths and volumes of the discrete ocean boxes, respectively. The first terms in the equations are proportional to the overturning flow Φ and represent the advective

transport between the boxes. The second terms (except for the deep box) represent the surface heat fluxes coupling the ocean and atmosphere. The overturning flow is assumed to be proportional to the density gradients of the oceans boxes after Stommel [1961]. Like in Rahmstorf [1996] the northern and the southern box will be taken into account for this, which leads to the equation for the calculation of the overturning flow

$$\Phi = c \left[-\alpha \left(T_N - T_S \right) + \beta \left(S_N - S_S \right) \right] \tag{6.5}$$

The constants α and β represent the thermal and the haline expansion coefficients in the equation of state. c is an adjustable parameter which is set to produce present-day overturning rates. This form of the overturning is also explained in section 5.2.[1]

The surface heat fluxes can be simplified according to Haney [1971]:

$$H_i = Q_{1_i} - Q_2 \left(T_i - T_{A_i} \right) \tag{6.6}$$

Analogue to (6.1) to (6.4) the prognostic differential equations for the salinities consist out of two components. One of those is again the advective part, caused by the interconnection between the boxes and the other one is the influence of the freshwater fluxes between the ocean and the atmosphere. The latter is again only for the boxes near the surface, thus the equations are

$$\frac{d}{dt} S_N = - \left(S_N - S_M \right) \frac{\Phi}{V_N} - S_{ref} \frac{(P - E)_N}{dz_N}, \tag{6.7}$$

$$\frac{d}{dt} S_M = - \left(S_M - S_S \right) \frac{\Phi}{V_M} + S_{ref} \frac{(P - E)_M}{dz_M}, \tag{6.8}$$

$$\frac{d}{dt} S_S = - \left(S_S - S_D \right) \frac{\Phi}{V_S} - S_{ref} \frac{(P - E)_S}{dz_S}, \tag{6.9}$$

$$\frac{d}{dt} S_D = - \left(S_D - S_N \right) \frac{\Phi}{V_D}. \tag{6.10}$$

---

[1]For other scaling laws: [Maas, 1994]. In his model, the dynamics bears similarities with the Lorenz system.

The reference salinity S_{ref} is a characteristic average value for the entire Atlantic Ocean, and the freshwater fluxes are denoted as precipitation minus evaporation (P-E). These freshwater fluxes are calculated by the divergence of the latent heat transport in the atmosphere and are assumed to be proportional to the meridional moisture gradient explained below.

The atmospheric energy-balance-model (EBM) calculates the heat fluxes between the ocean and atmosphere, as well as horizontal latent and sensible heat transports as diffusion following Chen et al. [1995]. The EBM contains sensible and latent heat transports, radiation R_i, as well as the surface heat fluxes H_i between the atmosphere and the ocean. The atmospheric temperatures T_{A_i} follow the prognostic equations

$$c_2 \frac{d}{dt} T_{A_N} = \frac{\partial \left(F_{s_N} + F_{l_N} \right)}{\partial y} + R_N - H_N, \tag{6.11}$$

$$c_2 \frac{d}{dt} T_{A_M} = \frac{\partial \left(F_{s_S} + F_{l_S} \right)}{\partial y} + R_M - H_M, \tag{6.12}$$

$$c_2 \frac{d}{dt} T_{A_S} = \frac{\partial \left(F_{s_S} + F_{l_S} \right)}{\partial y} + R_S - H_S. \tag{6.13}$$

c_2 is related to the specific heat of air. The sensible F_{s_i} and latent F_{l_i} heat transport are described in dependence of the meridional gradient of the surface temperature T_A and moisture q

$$F_s = K_s \frac{\partial T_A}{\partial y} \tag{6.14}$$

$$F_l = K_l \left(\frac{\partial q}{\partial y} \right). \tag{6.15}$$

K_s and K_l are empirical parameters, which must be adjusted to generate realistic values for sensible and latent heat transports. The radiation terms R_i in (6.11) to (6.13) consist of an incoming solar shortwave S_i and an outgoing infrared longwave I_i part. The extraterrestrial solar radiation is not absorbed entirely, and a latitude-dependent average albedo α_i is introduced to account for the reflectance. The outgoing infrared radiation I_i is calculated through a linear formula of Budyko

[1969]. Thus, the equation for the net radiation balance is

$$R_i = S_i - I_i = S_{sol,i}(1 - \alpha_i) - (A + BT_{A_i}).$$ (6.16)

In this model, one can even include thw effect for changes in the the greenhouse gases (by multi-plying $A + BT_{A_i}$ with a factor γ) and changes in the solar constant (by changing $S_{sol,i}$) which is left to the reader (see also the exercises).

The model calculates the freshwater fluxes from the divergence of the latent heat transport ($P - E \sim \partial F_l / \partial y$). The integration of the system is implemented with an Euler-forward scheme. The time step is $1/100$ of a year to ensure the stability of the system according to the Courant-Friedrichs-Levy-Criterion (CFL-Criterion, Courant et al. [1928][2]).

6.2   Run the model

Here, we will use this box model using R. iFurthermore, it is recomended to use R studio, which provides a user interface for R. Perturbation experiments are done for the four ocean boxes. First the function sevenbox.r has to be defined, then the script must be run selecting the perturbations in the different boxes:

```
source('sevenbox.r')

sevenbox("N")  # for the northern box
y=sevenbox("N",perturbation=-0.1)
plot(y$t,y$phi)
```

One particular package is R Shiny which provides a Gui web application easy to use. Download

sevenbox.r , ui.R , server.R , run_ui.R , ageStructureFunctions.R , sevenbox_plot_func.R .

```
# go to the directory  (setwd)
source('run_ui.R')  # load Script
run_ui()   # run Script

# for multicore: provide the numbers of processors, e.g.
run_ui(8)
```

---

[2]For an English translation, refer to Courant et al. [1967].

```
#   or do the following:
library(shiny)
runApp('Boxmodel_GUI')
# if you put everything into the directory Boxmodel_GUI
```

The code creates png files of model output. The coding follows the names in Fig. 6.1, and the temperature (6.1, 6.2, 6.3 , 6.4) and salinity (6.7, 6.8, 6.9 , 6.10) budgets, respectively.

Furthermore, the interhemispheric Box model on the web is available through

https://paleosrv2.awi.de/. The username is *student* and the Password is *EbJir5ow* !

Fig. 6.2 illustrates how the model works.

Sevenbox

Simulation length [years]

1000

Start Simulation
This may take some time!

☐ Change Perturbations
☐ Change heat cap. and heat fluxes
☐ Change solar CO_2 effect
☐ Change add. fresh water fluxes

Temperature   Salinity   Ocean Flux

Sevenbox

Simulation length [years]

1000

Start Simulation
This may take some time!

Save results

☑ Change Perturbations
Choose which box should be perturbed:

north ▾

Perturbations

-0.1; -0.2

Devide multiple pertubations by semicolon!

☐ Change heat cap. and heat fluxes
☐ Change solar CO_2 effect
☐ Change add. fresh water fluxes

Temperature   Salinity   Ocean Flux

Sevenbox

Simulation length [years]

| 1000 |

Start Simulation
This may take some time!

Save results

☑ Change Perturbations
Choose which box should be perturbed:

| north ▾ |

Perturbations

| -0.1; -0.2 |

Devide multiple pertubations by semicolon!

☐ Change heat cap. and heat fluxes
☐ Change solar CO₂ effect
☐ Change add. fresh water fluxes
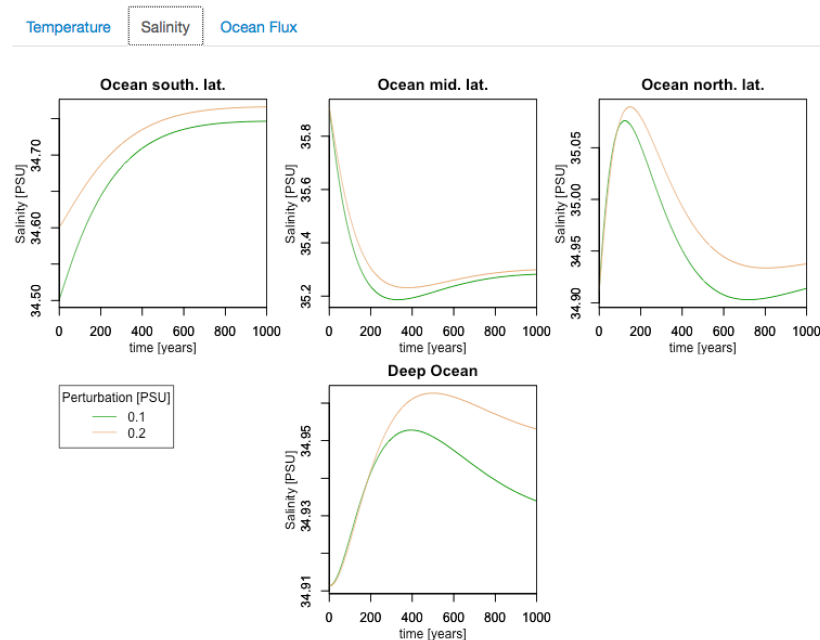
Sevenbox

Simulation length [years]

| 1000 |

Start Simulation
This may take some time!

Save results

☑ Change Perturbations
Choose which box should be perturbed:

| north ▾ |

Perturbations

| -0.1; -0.2 |

Devide multiple pertubations by semicolon!

☐ Change heat cap. and heat fluxes
☐ Change solar CO₂ effect
☐ Change add. fresh water fluxes
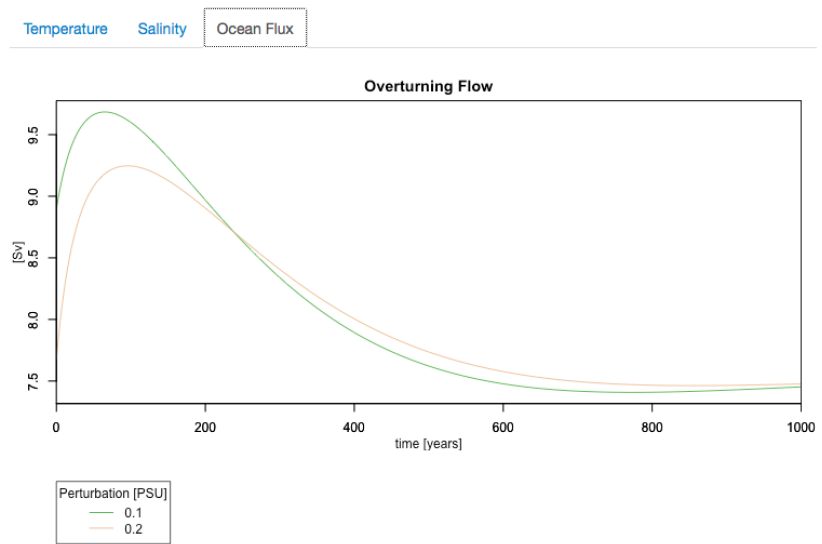
Figure 6.2: Output of the climate box model illustrating the procedure.

6.3 Model scenarios

Paleoclimatic evidence suggests (e.g. Dansgaard et al. [1993]) that some past climate shifts were associated with changes in North Atlantic Deep Water (NADW) formation. Deep water formation in the Greenland-Iceland-Norwegian Sea and in Labrador Sea drive the large-scale ocean circulation imposing strong northward heat transport. This makes the northern North Atlantic about 4 K warmer than corresponding latitudes in the Pacific and is responsible for the mild climate of Western Europe. Variations in NADW circulation therefore have the potential to cause significant climate change in the North Atlantic region.

Numerical simulations by Manabe and Stouffer [1993] showed, for the North Atlantic, that between two and four times the preindustrial CO_2 concentration, a threshold value is passed and the thermohaline circulation ceases completely. One other example of early Holocene rapid climate change is the '8200 yr BP' cooling event recorded in the North Atlantic region possibly induced by freshwater. One possible explanation for this dramatic regional cooling is a shutdown in the formation of deep water in the northern North Atlantic due to freshwater input caused by catastrophic drainage of Laurentide lakes (e.g., Barber et al. [1999]; Lohmann [2003]). After the end of the last glacial, freshwater entered into the Atlantic Ocean (Fig. **??**) and may have affected the ocean circulation.

Exercise 46 – Investigations with the box-model

1. In the regions of deep water formation in the North Atlantic, relatively small amounts of fresh water added to the surface can stabilize the water column to the extent that convection can be prevented from occurring. Such interruption decreases the poleward oceanic mass transport Φ. Furthermore, this perturbation of the meridional transport can be amplified by positive feedbacks: a weaker northward salt transport brings less dense water to high latitudes, which further reduces the high-latitude density. Discuss the case where the initial conditions in salinity at different latitudes is changed. Show this scenario in the box model!

2. Comment on the scenario of climate change as shown in the cinema movie The Day After Tomorrow: link to the website or go to the trailer.

3. Which feedbacks are acting for global warming? You can change the long wave radiation. A doubling of pCO_2 is equivalent to an additional forcing of 4 Wm^{-2}. For this you have to modify the net radiation balance (6.16) through reduction in the outgoing longwave radiation (parameter γ). Additional radiative forcing may come from increased tracer gas concentrations in the atmosphere. Please evaluate the hydrological cycle and atmospheric heat transports! What is the change in the overturning rate?

4. Change the ocean heat capacity by a factor of 10 and describe the change in the response to warming induced by 90

5. The initial values of the model represent averages for present-day climate conditions. Determine the effect of the parameter c in the numerical example (representing a different long wave radiation) Can you derive a glacial climate? The glacial climate was 3 K colder in the tropics.

6. Calculate the ocean heat transport in the model and compare it with the following estimate!

$$H = \int_{bottom}^{top} \rho_0 v T dz \qquad (6.17)$$

$$= -c_p \int_{bottom}^{top} \frac{\partial \Phi}{\partial z} T dz \qquad (6.18)$$

$$= c_p \int_{bottom}^{top} \Phi \frac{\partial T}{\partial z} dz \qquad (6.19)$$

$$= c_p \int_{T(bottom)}^{T(top)} \Phi dT \qquad (6.20)$$

where $\Phi = \rho_0 \Phi_{MOC}$ with Φ_{MOC} being the volume transport. Therefore, the heat transport can be estimated in terms of the mass transport in temperature layers:

$$H = c_p \underbrace{(T(top) - T(bottom))}_{15K} \underbrace{\Phi_{max}}_{20 \cdot 10^9 kg/s} \qquad (6.21)$$

which is about $1.2 \, PW \, (PW = 10^{15} W)$.

7. Question for specialists: The coupled model shall be used to investigate the sensitivity of the system with respect to stochastic weather perturbations reflecting unresolved effects of the atmospheric transports modeled as white noise. How will the atmospheric noise influence the stability of the system?

Chapter 7

Waves in the climate system

7.1 Shallow water dynamics

One of the most understood dynamics are the tidal equation or shallow water dynamics (e.g. Gill [1982]). The equations are derived from depth-integrating the Navier-Stokes equations, in the case where the horizontal length scale is much greater than the vertical length scale.Under this condition, conservation of mass implies that the vertical velocity of the fluid is small. The variables u and v denote zonal and meridional perturbation flow velocity, and η the height perturbation. The pressure in the vertically homogenous ocean is $p = g\rho(H + \eta)$. The dynamics is as follows:

$$\frac{\partial u}{\partial t} + u\frac{\partial u}{\partial x} + v\frac{\partial u}{\partial y} - fv = -g\frac{\partial \eta}{\partial x} \tag{7.1}$$

$$\frac{\partial v}{\partial t} + u\frac{\partial v}{\partial x} + v\frac{\partial v}{\partial y} + fu = -g\frac{\partial \eta}{\partial y} \tag{7.2}$$

where $x = R\lambda, y = R\cos\varphi$ denote eastward distance and distance from the equator, respectively. The equation for the conservation of mass

$$\frac{\partial}{\partial t}\Big(\rho\,(H+\eta)\Big) + \frac{\partial}{\partial x}\Big(u\rho\,(H+\eta)\Big) + \frac{\partial}{\partial y}\Big(v\rho\,(H+\eta)\Big) = 0$$

and since the density is constant it reads

$$\frac{\partial}{\partial t}\eta + u\frac{\partial}{\partial x}\eta + v\frac{\partial}{\partial y}\eta + \frac{\partial}{\partial x}(Hu) + \frac{\partial}{\partial y}(Hv) = 0 \qquad . \qquad (7.3)$$

Lagrangian invariant of the shallow water dynamics

The dynamical system (7.1,7.2,7.3) has the Lagrangian invariant

$$D_t\Big(\frac{\nabla^2\psi + f}{H+\eta}\Big) = D_t q = 0 \tag{7.4}$$

where $\nabla^2\psi = \partial_x v - \partial_y u$ is the relative vorticity and ψ the streamfunction. The dynamical system (7.1,7.2,7.3) has integral invariants in domains ξ where the fluxes are zero or cancel, e.g. in periodic domains. One such invariant is the energy

$$E = \frac{1}{2}\int\Big((H+\eta)(u^2+v^2)+g\eta^2\Big)d\xi \tag{7.5}$$

and for any scalar functions f(q) of potential vorticity q, another class of integral invariants has the form

$$S = \frac{1}{2}\int(H+\eta)f(q)d\xi \tag{7.6}$$

When function f is the square function $\sim q^2$, this invariant is called potential enstrophy.

Shallow water dynamics: linear model

We now simplify the system to a linear model. Ignoring bulk advection (u and v are small) in (7.1,7.2,7.3), and assuming the wave height is a small proportion of the mean height $(\eta << H)$, we have:

$$\partial_t u \quad = \quad f\,v \quad - \quad g\,\partial_x \eta \tag{7.7}$$

$$\partial_t v \quad = \quad -f\,u \quad - \quad g\,\partial_y \eta \tag{7.8}$$

$$\partial_t \eta \quad = \quad -\partial_x (Hu) \quad - \quad \partial_y (Hv) \quad . \tag{7.9}$$

Skew-Hermetian propertiy of the linear shallow water dynamics

The dynamical system (7.7,7.8,7.9) can be rewritten in a more compact form (using the non-dimensional values).

$$\partial_t W + \mathbf{L} W = 0 \tag{7.10}$$

With $W = (u, v, \eta)$ and the operaor

$$\mathbf{L} = \begin{pmatrix} 0 & -f & \partial_x \\ f & 0 & \partial_y \\ \partial_x & \partial_y & 0 \end{pmatrix} \quad . \tag{7.11}$$

The x and t dependences can be separated in form of zonally propagating waves $\exp(ikx - i\omega t)$. W can therfore be writen as

$$W(x, y, t) = \begin{pmatrix} \hat{u}(y) \\ \hat{v}(y) \\ \hat{\eta}(y) \end{pmatrix} \exp(ikx - i\omega t) = \hat{W} \exp(ikx - i\omega t) \tag{7.12}$$

This leads to an eigenvalue problem

$$-i\omega\hat{W}(k,y) + \hat{L}\hat{W}(k,y) = 0 \tag{7.13}$$

where

$$\hat{L} = \begin{pmatrix} 0 & -f & ik \\ f & 0 & \partial_y \\ ik & \partial_y & 0 \end{pmatrix} \quad . \tag{7.14}$$

The adjoint of $\hat{L}$ with respect to the inner product is the operator $\hat{L}^+$ (transpose and conjugate):

$$\hat{L}^+ = \begin{pmatrix} 0 & f & -ik \\ -f & 0 & \partial_y \\ -ik & \partial_y & 0 \end{pmatrix} \quad . \tag{7.15}$$

The operator $\hat{L}$ is skew-Hermetian, as the adjoint of $\hat{L}$ is $\hat{L}^+ = -\hat{L}$ (7.15). For two arbitrary vector functions W_1, W_2 one can define a scalar product:

$$(\hat{L}W_1, W_2) = \int_{-\infty}^{\infty} \hat{L}W_1 \cdot W_2^* dy = (W_1, -\hat{L}W_2) = (W_1, \hat{L}^+ W_2) \tag{7.16}$$

with the symbol * being the conjugate.

The skew-Hermetian property dictates that the eigenvalues of $\hat{L}$ are purely imaginary, so that we have a mathematical basis for looking for wave-like solutions. In addition, the eigenfunctions form a complete orthogonal set for the functions W satisfying $(W, W) < \infty$. This is because $\hat{L}$ is normal:

$$\hat{L}\hat{L}^+ = \hat{L}^+\hat{L} \quad . \tag{7.17}$$

Furthermore, $\hat{\mathbf{L}}$ in (7.14) belongs to the unitary group $U(3)$, forming a compact connected Lie group and has the special property $\det(\mathbf{L}) = 0$.

These considerations provide the mathematical framework for wave studies. Analytical work is presented in section 7.5 in the case of equatorial wave dynamics. The dynamical system (7.7,7.8,7.9) contains already the zoo of waves. Here, we give a short description. In the exercises, these waves are numerically solved.

Exercise 47   –   Energy conservation

Show that the dynamical system (7.1,7.2,7.3) has integral invariants in domains $\boldsymbol{\xi}$ where the fluxes are zero or cancel, e.g. in periodic domains. One such invariant is the energy

$$E = \frac{1}{2} \int \Big((H + \eta)(u^2 + v^2) + g\eta^2 \Big) d\xi \tag{7.18}$$

and for any scalar functions f(q) of potential vorticity q, another class of integral invariants has the form

$$S = \frac{1}{2} \int (H + \eta) f(q) d\xi \tag{7.19}$$

7.2 Planetary waves on the computer

Rossby (or planetary) waves are giant meanders in high-altitude winds that are a major influence on weather. They are easy to observe as (usually 4-6) large-scale meanders of the jet stream. When these loops become very pronounced, they detach the masses of cold, or warm, air that become cyclones and anticyclones and are responsible for day-to-day weather patterns at mid-latitudes.

Each large meander, or wave, within the jet stream is known as a Rossby wave (planetary wave). Rossby waves are caused by changes in the Coriolis effect with latitude. Shortwave troughs, are smaller scale waves superimposed on the Rossby waves, with a scale of 1,000 to 4,000 kilometres long, that move along through the flow pattern around large scale, or longwave, ridges and troughs within Rossby waves (Fig. 7.1).

In planetary atmospheres, they are due to the variation in the Coriolis effect with latitude. The waves were first identified in the Earth's atmosphere by Rossby [1939]. The terms "barotropic" and "baroclinic" Rossby waves are used to distinguish their vertical structure. Barotropic Rossby waves do not vary in the vertical, and have the fastest propagation speeds. The baroclinic wave modes are slower, with speeds of only a few centimetres per second or less (atmosphere).

Oceanic Rossby waves are thought to communicate climatic changes due to variability in forcing, due to both the wind and buoyancy. Both barotropic and baroclinic waves cause variations of the sea surface height, although the length of the waves made them difficult to detect until the
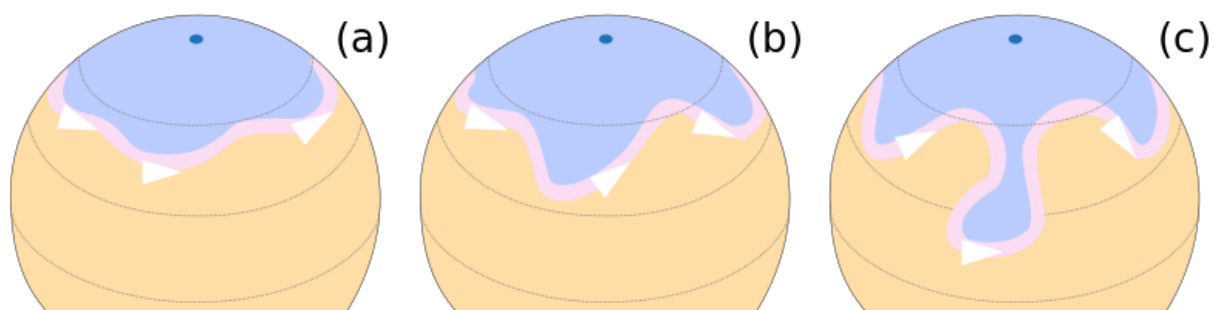
Figure 7.1: Meanders (Rossby Waves) of the Northern Hemisphere's polar jet stream developing (a), (b); then finally detaching a "drop" of cold air (c). Orange: warmer masses of air; pink: jet stream.

advent of satellite altimetry [Chelton and Schlax, 1996]. Baroclinic waves also generate signifi-
cant displacements of the oceanic thermocline, often of tens of meters. Satellite observations have
revealed the stately progression of Rossby waves across all the ocean basins, particularly at low-
and mid-latitudes. These waves can take months or even years to cross a basin like the Pacific.

The first order equations of motion into an appropriate wave equation is cumbersome, namely
because the two-dimensional geometry of the spherical surface is non-Euclidean (the Coriolis ef-
fect depends on the latitude). It can be shown [Müller et al., 1994; Müller and O'Brien, 1995;
Müller and Maier-Reimer, 2000; Gerkema et al., 2008] that tidal theory differs from the plain
waves because it accounts consistently for the globe's sphericity. If Cartesian coordinates are cho-
sen with $f = \beta y$ then the dynamics reduces to the Matsuno equation as discussed in section
7.

Their emergence is due to shear in rotating fluids, so that the Coriolis force changes along the
sheared coordinate.[1]

Exercise 48   –   Numerical solution of shallow-water gravity waves

- open shallow1D.R
- Identify the lines of the code in which the momentum equation and in which the continuum
  equation are solved.
- Run the program. Which type of waves do you see?
- Change the constants of water depth H, gravity g, describe your observations!
- Can you roughly estimate the phase speed of the waves?

```
#shallow1D.R
ni<-200 #number of grid cells
```

---

[1]The dynamics in an inertial reference frame, e.g. with a coordinate system fixed at the Sun, would not have
a Coriolis force, but would certainly observe Rossby wave propagation. In the inertial system, the near-equatorial
motion is seen to be faster than off the equator. Zero vorticity in the rotating Earth's coordinate system corresponds
to a basic flow with non-zero vorticity flow (zonal velocity $U = R\Omega \cos \varphi$) (φ: latitude) in the inertial reference
frame [Müller and Maier-Reimer, 2000]. Linearizing the dynamics in the non-rotating system around the basic state
U yields exactly Matsuno's wave equations taking the partial substantial derivative with advection U. Therefore, the
effect of Earth's rotation is formally equivalent to a shear flow system. The mean flow energy is supplied by the Earth's
rotation.

```r
nt<-20000 #number of time steps

ia.0<-1:ni
ia.m1<-c(ni,1:(ni-1))
ia.p1<-c(2:ni,1)

g<-0.1 #9.81 m/s^2
dx<-1e5 #gridcell 10km
dt<-100 #timstep 1 second
H<-1e3 #1km depth

u<-rep(0,ni) #speed at each point
h<-rep(0,ni) #pertubation at each point
u.new<-vector()
h.new<-vector()

#h[31:50,1]<--0.5  #one pertubation in the middle
#h[51:70,1]<-0.5   #one pertubation in the middle
h[50:90]<-sin(0:40/2*pi/20)

#1st step euler forward
#momentum equation:
u.new[ia.0]<-u[ia.0]-g*dt/2/dx*(h[ia.p1]-h[ia.m1])
#Continuity eq. horizontal divergence:
h.new[ia.0]<-h[ia.0]-H*dt/2*((u[ia.p1]-u[ia.m1])/dx)

#from step 3 on use Leapfrog
for (n in 2:(nt-1))
{
  u.old<-u
  h.old<-h
  h<-h.new
  u<-u.new

  u.new[ia.0]<-u.old[ia.0]-g*dt/dx*(h[ia.p1]-h[ia.m1])
  h.new[ia.0]<-h.old[ia.0]-H*dt*((u[ia.p1]-u[ia.m1])/dx)

  # modulo operator, smoothing every 10 time steps
  if ((n%%10)==0)
  { u.new[ia.0]<-(u.new[ia.0]+u[ia.0])/2
         h.new[ia.0]<-(h.new[ia.0]+h[ia.0])/2
       }

  # modulo operator: plotting
  if ((n%%101)==0)
  {par(ask = TRUE)  # to make a break
  plot(h,type="l",lwd=2,ylim=c(-1,1))
  }
}

############
```
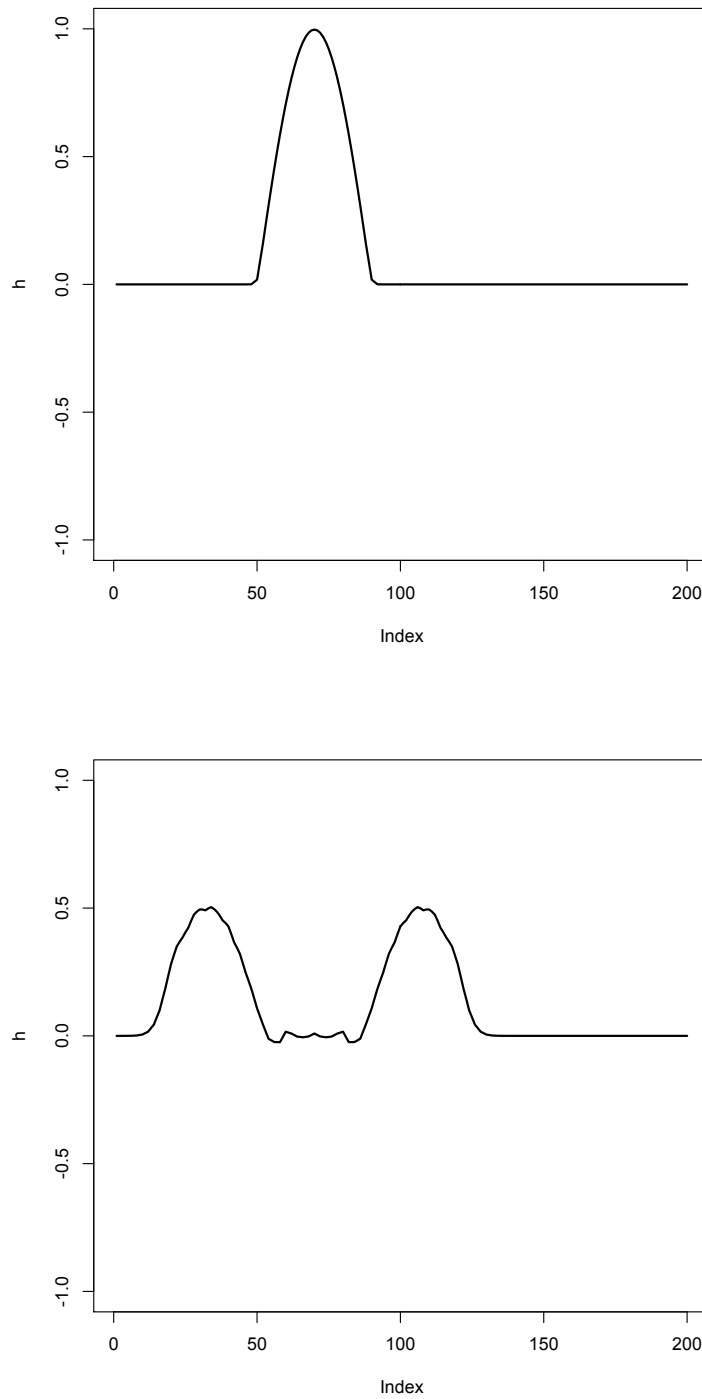
Figure 7.2: Numerical solution of 1D shallow water equation in exercise 48. Upper panel: initial condition. Lower panel: time snap shot.

Exercise 49   –   Numerical solution of the shallow water equation

Study the wave dynamics on a water Earth, for simplicity the metric terms are neglected.

- open shallow2D_rossby.R

- Identify the lines of the code in which the momentum equation and in which the continuum equation are solved.

- Run the program: Which type of waves do you see?

- Change the constants of water depth H, gravity g, describe your observations!

- Can you roughly estimate the phase speed of the waves?

```
#
# shallow2D_rossby.R
#
#This is just a definition of a function to plot vectorplots
par.uin<-function()
 {  u <- par("usr")
    p <- par("pin")
    c(p[1]/(u[2] - u[1]), p[2]/(u[4] - u[3]))
 }

quiver<-function(lon,lat,u,v,scale=1,length=0.05,maxspeed=200, ...)
  {  ypos <- lat[col(u)]
     xpos <- lon[row(u)]
     speed <- sqrt(u*u+v*v)
     u <- u*scale/maxspeed
     v <- v*scale/maxspeed
     matplot(xpos,ypos,type="p",cex=0,xlab="lon",ylab="lat", ...)
     arrows(xpos,ypos,xpos+u,ypos+v,length=length*min(par.uin()))
  }

#Program starts here
#Shallow water 2D,cyclic boundary conditions + Coriolis term

nn<- 50
ni<- 2*nn+1   #number of gridcells in one direction
nt<-10000 #number of timesteps

#The physical constants
g<-0.1 #low gravity, 0.1 m/s^2
dx<-1e5 #gridcell 10km
#dx=400e3 # 400 km
dy<-dx/2  # double resolution in meridional direction
dt<-1000 #timstep 1000 second
H<-1e3 #1km depth
Omega<-1e-4

#define three index vectors.. the middle one,
```

```r
#one shifted one cell to the left, and one to the right
#(including the periodic boundary conditions)
ia.0<-1:ni
ia.m1<-c(ni,1:(ni-1))
ia.p1<-c(2:ni,1)
u<-matrix(0,ni,ni) #speed at each point
v<-matrix(0,ni,ni) #speed at each point
h<-matrix(0,ni,ni) #pertubation at each point
f<-matrix(0,ni,ni) #pertubation at each point

lat<-c(-nn:nn)*90/nn
weight<-sin(lat*pi/180)
lon<-c(-nn:nn)*180/nn

f<-rep(weight*2*Omega,each=ni)  # Coriolis parameter
dim(f)<-c(ni,ni)
filled.contour(f)

u.new<-u
h.new<-h
v.new<-v

#Inital condition: One smooth blobs at each side of the "equator"(sin)
idit=nn/5*2
inix=ni-idit-1
iniy=ni-2*idit-1
endx=ni-1
endy=ni-1
endy2=2*idit+1
h[inix:endx,iniy:endy]<-sin(0:20/2*pi/10)*t(sin(0:40/2*pi/20))
h[inix:endx,1:endy2]<-sin(0:20/2*pi/10)*t(sin(0:40/2*pi/20))

#equator to study the Kelvin wave:
ii=idit+1
iy=nn-10
iy2=nn+10
h[1:ii,iy:iy2]<- -sin(0:20/2*pi/10)*t(sin(0:20/2*pi/10))

#Inital condition: One smooth blobs at each side of the "equator"(sin)
#h[60:80,60:80]<-sin(0:20/2*pi/10)*t(sin(0:20/2*pi/10))
#h[30:50,80:100]<-sin(0:20/2*pi/10)*t(sin(0:20/2*pi/10))

#1st step euler forward
u.new[ia.0,ia.0]<-u[ia.0,ia.0]-g*dt/2/dx*(h[ia.p1,ia.0]-h[ia.m1,ia.0])
v.new[ia.0,ia.0]<-v[ia.0,ia.0]-g*dt/2/dy*(h[ia.0,ia.p1]-h[ia.0,ia.m1])
h.new[ia.0,ia.0]<-h[ia.0,ia.0]
        -H*dt/2*((u[ia.p1,ia.0]-u[ia.m1,ia.0])/dx
        + (v[ia.0,ia.p1]-v[ia.0,ia.m1])/dy)

#Divide the screen in two parts
# par(mfcol=c(1,2))
#par(mfcol=c(2,1))
```

```
#Leapfrog from the third step on
for (n in 3:(nt-1))
{
  u.old<-u
  v.old<-v
  h.old<-h
  h<-h.new
  u<-u.new
  v<-v.new
  u.new[ia.0,ia.0]<-u.old[ia.0,ia.0]
     -g*dt/dx*(h[ia.p1,ia.0]-h[ia.m1,ia.0])+dt*f*v
  v.new[ia.0,ia.0]<-v.old[ia.0,ia.0]
     -g*dt/dy*(h[ia.0,ia.p1]-h[ia.0,ia.m1])-dt*f*u
  h.new[ia.0,ia.0]<-h.old[ia.0,ia.0]
     -H*dt*((u[ia.p1,ia.0]-u[ia.m1,ia.0])/dx
     + (v[ia.0,ia.p1]-v[ia.0,ia.m1])/dy)

#plot every 50th image
  if ((n %% 50) == 0) {
       #quiver(lon,lat,u,v,scale=200,maxspeed=1.5,length=3)
       #image(lon,lat,h,zlim=c(-1,1),col=rainbow(200)) # color coated
       persp(h/3, theta = 0, phi = 40, scale = FALSE, ltheta = -120,
     shade = 0.6, border = NA, box = FALSE,zlim=c(-0.3,0.3))
     }
  }
```
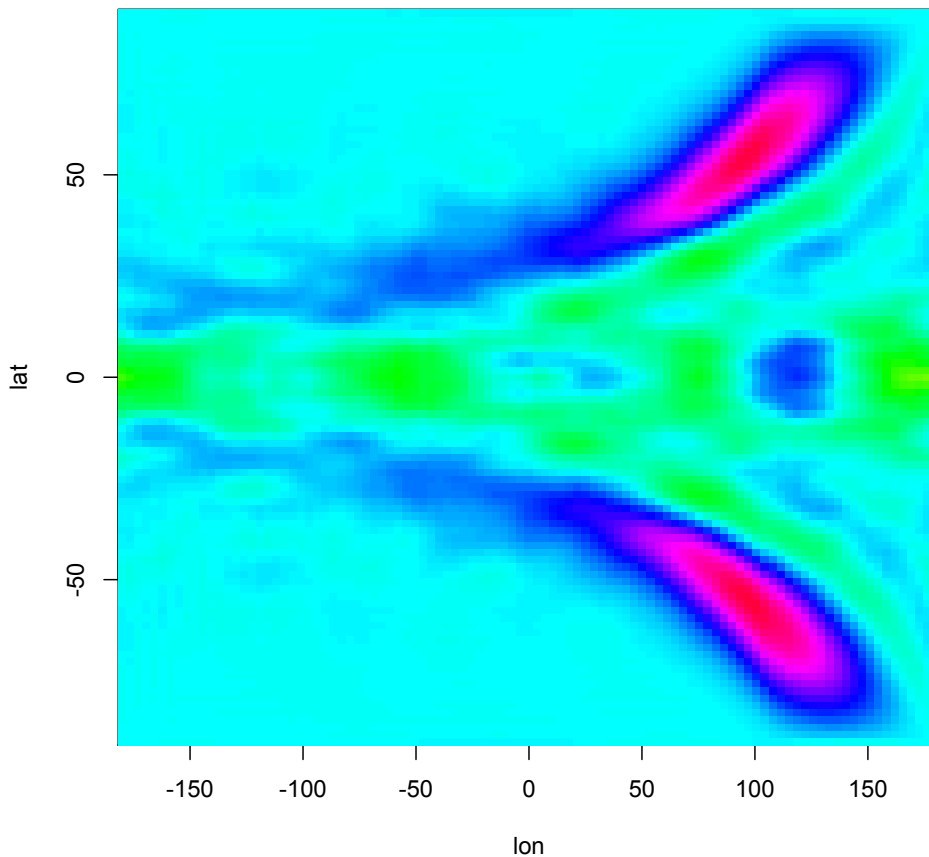
Figure 7.3: Global Rossby and Kelvin wave signatures in the exercise 49.

7.3   Plain waves

The analysis of the spherical version of the tidal problem is complicated because the Coriolis effect depends on the latitude and in general we do not have plain waves with sinus and cosinus base functions.[2] However, because of its simplicity, we will study the plain wave theory here. In this approach, the Coriolis parameters f and β are taken as **fixed parameters** in the equations. Then, the wave equations can be reduced to plain waves with eigenfunctions $\sim \exp(ikx + ily - i\omega t)$.

---

[2]This approximation may be questioned because the trapped character of the Rossby waves is no included, which is however, observed and simulated (Fig. 7.3). This shows a general problem in perturbation theory: The concept of manipulations in the differential equations (e.g., by neglecting terms) is not entirely free from ambiguities, and may lead to a undesirable transition in the solutions of the system. The type of solutions shall be of the form of the observed (macroscopic) functions and a proper framework of approximations is required (section 8.4).

7.3.1 Inertial Waves

From the equations (7.7,7.8,7.9), we drop the term $\partial_x \eta$, $\partial_y \eta$, and $f = f_0 = const.$ (no pressure gradients and constant f). Then, air or water mass moving with speed v subject only to the Coriolis force travels in a circular trajectory called an 'inertial circle'. Since the force is directed at right angles to the motion of the particle, it will move with a constant speed, and perform a complete circle with frequency f. The magnitude of the Coriolis force also determines the radius of this circle:

$$R = v/f .\tag{7.20}$$

On the Earth, a typical mid-latitude value for f is $10^{-4}s^{-1}$; hence for a typical atmospheric speed of 10 m/s the radius is 100 km, with a period of about 14 hours. In the ocean, where a typical speed is closer to 10 cm/s, the radius of an inertial circle is 1 km. These inertial circles are clockwise in the Northern Hemisphere (where trajectories are bent to the right) and anti-clockwise in the Southern Hemisphere. If the rotating system is a parabolic turntable, then f is constant and the trajectories are exact circles. On a rotating planet, f varies with latitude and the paths of particles do not form exact circles. Since the parameter f varies as the sine of the latitude, the radius of the oscillations associated with a given speed are smallest at the poles and increase toward the equator (Fig. 7.4).

$$\frac{\partial u}{\partial t} - f_0 v = 0 \tag{7.21}$$

$$\frac{\partial v}{\partial t} + f_0 u = 0 \tag{7.22}$$

yields

$$\frac{\partial^2 u}{\partial t^2} = -f_0^2 u \quad . \tag{7.23}$$
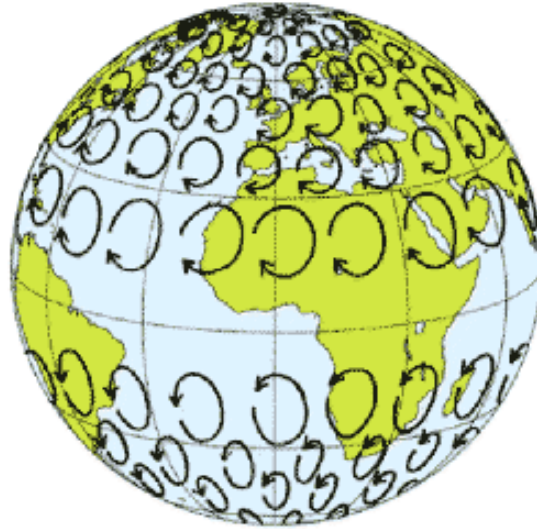
Figure 7.4: Schematic representation of inertial circles of air masses in the absence of other forces, calculated for a wind speed of approximately 50 to 70 m/s. Note that the rotation is exactly opposite of that normally experienced with air masses in weather systems around depressions.

The solution is

$$u(t) \quad = \quad u(0)\sin(f_0 t) \tag{7.24}$$

$$v(t) \quad = \quad u(0)\cos(f_0 t) \tag{7.25}$$

which is known as intertial movement and can be observed in drifting buoys (upper panel Fig. 7.5). The water parcels move around a circle of radius of $u(0)/f_0$ in a clockwise direction (anticyclonically) with a period $2\pi/f_0$.

Exercise 50   –   Inertial waves

- Derive the solution of (7.21, 7.22). Since the force is directed at right angles to the motion of the particle, it will move with a constant speed, and perform a complete circle with frequency f. Show that the magnitude of the Coriolis force determines a radius R of this circle. Hint: A typical mid-latitude value for f is $10^{-4}s^{-1}$; a typical atmospheric speed of $10m/s$, in the ocean a typical speed is closer to $10cm/s$.
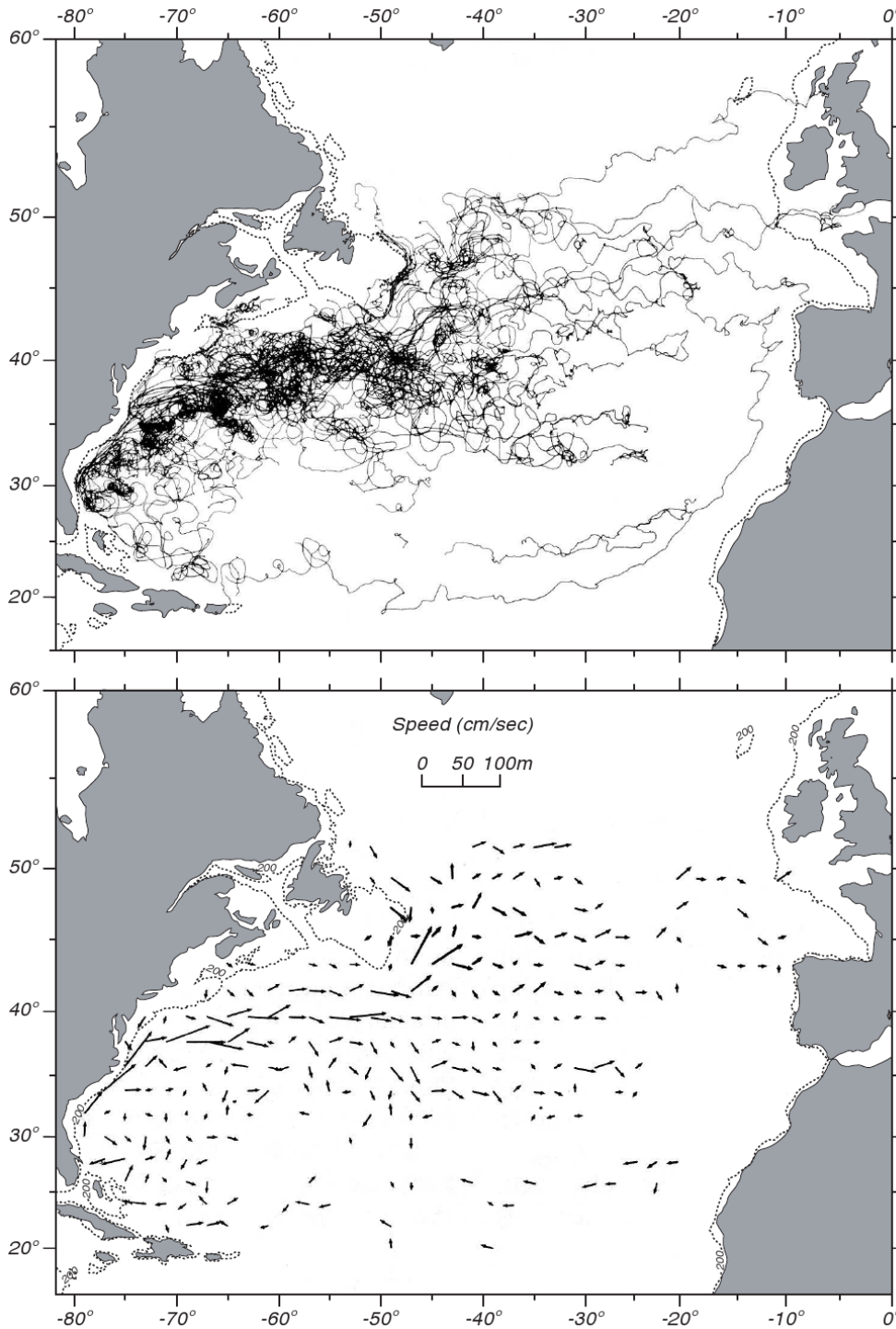
Figure 7.5: **Top:** Tracks of **110** drifting buoys deployed in the western north Atlantic. **Bottom:** Mean velocity of currents in $2° \times 2°$ boxes calculated from tracks above. Boxes with fewer than **40** observations were omitted. Length of arrow is proportional to speed. Maximum values are near **$0.6ms$** in the Gulf Stream near **37°**N **71°**W. After Richardson (1981).

- Provide the solution for the coordinates $x(t), y(t)$.

- Show that the dynamics in the inertial coordinate system reduces to

$$u_{in}(t) \quad = \quad 0 \tag{7.26}$$

$$v_{in}(t) \quad = \quad u(0) \cos \Omega t \tag{7.27}$$

The trajectory in the inertial frame is a straight line. The length of the line is twice the diameter of the inertial circle and the frequency of the oscillation is one-half that observed in the rotating frame.

7.3.2 Gravity Waves

Shallow-water gravity waves are defined through their dynamics without the effect of the Earth's rotation, i.e. $f = 0$:

$$\frac{\partial^2 \eta}{\partial t^2} = gH \left(\frac{\partial^2}{\partial x^2} + \frac{\partial^2}{\partial y^2} \right) \eta \tag{7.28}$$

With the ansatz

$$\eta = \exp(ikx + ily - i\omega t) \tag{7.29}$$

ω is given by

$$\omega(k,l) = \pm\sqrt{gH\,(k^2 + l^2)}, \tag{7.30}$$

where k and l are the zonal and meridional wavenumbers. Since there is no preferred direction in the (x,y) coordinate, we simply drop the y-dependence and introduce the phase speed

$$c = \omega/k = \pm\sqrt{gH} \quad . \tag{7.31}$$

In the limit $\beta \to 0$ i.e. $f = f_0 = const.$, the dynamics consists of gravity waves with

$$\omega^2 = f_0^2 + (ck)^2 \tag{7.32}$$

Output from a shallow water equation model of water in a bathtub. The water experiences five splashes which generate surface gravity waves that propagate away from the splash locations and reflect off the bathtub walls. (https://en.wikipedia.org/wiki/Shallow_water_equations#/media/File:Shallow_water_waves.gif)

Exercise 51   –   Baroclinic shallow-water gravity waves

In case we have a layed ocean, we consider the so-called baroclinic dynamics with the modified gravity $g' = \frac{\rho_1 - \rho_2}{\rho_1}$ using the densities $\rho_{1,2}$. Task: Derive the baroclinic dynamics using the shallow water equations for 2 different layers and subtract the equations from each other!

Exercise 52   –   Shallow-water waves

We consider tidal equation on the β−plane. This fluid dynamical system is described as

$$\partial_t u \quad = \quad f\,v \quad - \quad g\,\partial_x \eta \tag{7.33}$$

$$\partial_t v \quad = \quad -f\,u \quad - \quad g\,\partial_y \eta \tag{7.34}$$

$$\partial_t \eta \quad = \quad -\partial_x(Hu) \quad - \quad \partial_y(Hv) \quad . \tag{7.35}$$

The variables u and v denote zonal and meridional perturbation flow velocity, and η the height perturbation.

- Derive the dispersion relationships $\omega(k)$ for the cases:

  a) In the limit $\beta \to 0$, i.e. $f \to f_0$

  b) $c \to \infty$.

  c) For infinite Rossby radius $a = \sqrt{c/(2\beta)}$.

  d) When filtering out gravity waves by eliminating the time derivative in (7.35), (u, v) in (7.33, 7.34) can be taken as plane waves proportional to $\exp(ikx + ily)$, where l denotes the meridional wave number. Derive the dispersion relationships $\omega(k)$ for the so-called non-divergent Rossby waves.

- Provide typical values of $\omega(k)$ for M,N=1,2,3 and the atmosphere and ocean.

7.3.3 Extratropical Rossby Waves

From the equations (7.7,7.8,7.9), we drop the term $\partial_t \eta$ and introduce the stream function ψ through

$$u = \frac{\partial \psi}{\partial y} \quad ; \quad v = -\frac{\partial \psi}{\partial x} \tag{7.36}$$

such that (7.9) is fulfilled. Taking $\frac{\partial}{\partial y}$ of (7.7) and subtract $\frac{\partial}{\partial x}$ of (7.8) elimintates the η term as in section 1.3:

$$\frac{\partial}{\partial t} \left(\frac{\partial^2}{\partial x^2} + \frac{\partial^2}{\partial y^2} \right) \psi = -\beta \frac{\partial \psi}{\partial x} \tag{7.37}$$

With the ansatz

$$\psi = \exp(ikx + ily - i\omega t) \tag{7.38}$$

and assumption that β is just a parameter, ω is given by

$$\omega(k, l) = -\frac{\beta k}{k^2 + l^2}, \tag{7.39}$$

where k and l are the zonal and meridional wavenumbers. Again, β is used as a parameter (also called Rossby parameter) and is not expressed in terms of y:

$$\beta = \frac{df}{dy} = \frac{1}{R} \frac{d}{d\varphi} (2\Omega \sin \varphi) = \frac{2\Omega \cos \varphi}{R} \tag{7.40}$$

where φ is the latitude, Ω is the angular speed of the Earth's rotation, and R is the mean radius of the Earth. The wave speed $c = \omega/k = -\beta \left(k^2 + l^2 \right)^{-1}$. The feature that the phase speed is faster at low latitudes can be also seen in Fig. 7.3 using the full dynamics.

More information about Rossby waves: https://youtu.be/6UCiRIc0nK0

Rossby waves and extreme weather: https://youtu.be/MzW5Isbv2A0

Exercise 53   –   Rossby waves

Consider the vorticity equation

$$\frac{D}{Dt}[(\zeta + f)/h] = 0 \tag{7.41}$$

with h =const., u and v are the velocity components.

1. Assume a mean flow with constant zonal velocity U

$$u = U = const > 0 \tag{7.42}$$

and a varying north-south component

$$v = v(x, t) \tag{7.43}$$

which gives the total motion a wave-like form around a reference latitude where the wave is trapped. Derive the associated vorticity equation and linearize the vorticity equation by dropping all non-linear terms!

2. With the ansatz

$$v(x, t) = A \cos[(kx - \omega t)] \tag{7.44}$$

determine the disperion relation $\omega(k)$, group velocity $\frac{\partial \omega}{\partial k}$, and the phase velocity $c = \omega/k$.

3. Derive the wavelength $L = 2\pi/k$ of the stationary wave given by $c = 0$.

4. A typical wavelength is 6000 km, a typical U is 15 m/s. Does the wave propagate from east to west or opposite?

7.4 Kelvin waves

7.4.1 Coastal Kelvin waves

A Kelvin wave is a wave in the ocean or atmosphere that balances the Coriolis force against a topographic boundary such as a coastline. If one assumes that the Coriolis coefficient f is constant along the right boundary conditions, $u = 0$, and the zonal wind speed is set equal to zero, then the equations become the following:

$$\frac{\partial \eta}{\partial t} = -H \frac{\partial v}{\partial y} \tag{7.45}$$

$$\frac{\partial v}{\partial t} = -g \frac{\partial \eta}{\partial y} \tag{7.46}$$

and therefore

$$\frac{\partial^2 \eta}{\partial t^2} = gH \frac{\partial^2}{\partial y^2} \eta \tag{7.47}$$

The solution to these equations yields the following phase speed: $c^2 = gH$ and $\omega = \pm cl$, which is the same speed as for shallow-water gravity waves without the effect of Earth's rotation. We see that η and v have also an x-dependence

$$\eta(x, y, t) = \tilde{\eta}(x) \exp(ily - i\omega t) \tag{7.48}$$

$$v(x, y, t) = \tilde{v}(x) \exp(ily - i\omega t) \ . \tag{7.49}$$

Using (7.46), we obtain

$$-i\omega\, \tilde{v}(x) = -gil\, \tilde{\eta}(x) \quad \text{and therefore } \tilde{v}(x) = \frac{g}{\omega} l\, \tilde{\eta}(x) = \pm \frac{g}{c}\, \tilde{\eta}(x) \tag{7.50}$$

$$\text{From the u-momentum equation} \quad \frac{\partial \eta}{\partial x} = \frac{f}{g} v \tag{7.51}$$

$$\text{we obtain therefore} \quad \frac{\partial \tilde{\eta}}{\partial x} = \pm \frac{f}{c} \tilde{\eta} \tag{7.52}$$

where only the minus sign provides a useful solution (not blowing up). The solution has an exponential decay of $\tilde{\eta}(x) = \exp(-x/L_r)$ on the scale of the Rossby radius $L_r = c/f$. The wave has a trapped character along the boundary. It is important to note that for an observer traveling with the wave, the coastal boundary (maximum amplitude) is always to the right in the Northern Hemisphere and to the left in the Southern Hemisphere, i.e. these waves move equatorward/southward on a western boundary and poleward/northward on an eastern boundary. Thus, the waves move cyclonically around an ocean basin.

On the black board: A Coastal Kelvin Wave moving northward along the coast is deflected to the right, but the coast prevents the wave from turning right and instead causes water to pile up on the coast. The pile of water creates a pressure gradient directed offshore and a geostrophic current directed northward.

On the northern hemisphere: The Kelvin wave always travels with the wall on its right side (anti-clockwise). The wave amplitude decreases exponentially away from the wall. The wave is trapped along the wall by rotation. Rotation does not affect the particle motion and wave propagation; only traps the wave to the coastline.

7.4.2   Equatorial Kelvin waves

Analogous we have Equatorial Kelvin waves: assume $v = 0$, then the equations become the following:

$$\frac{\partial \eta}{\partial t} = -H \frac{\partial u}{\partial y} \tag{7.53}$$

$$\frac{\partial u}{\partial t} = -g \frac{\partial \eta}{\partial y} \tag{7.54}$$

and therefore again

$$\frac{\partial^2 \eta}{\partial t^2} = gH \frac{\partial^2}{\partial y^2} \eta \qquad (7.55)$$

The solution to these equations yields the phase speed: $c^2 = gH$ and $\omega = ck$, which is the same speed as for shallow-water gravity waves without the effect of Earth's rotation. We see that η and u have also an x-dependence

$$\eta(x, y, t) = \tilde{\eta}(y) \exp(ikx - i\omega t) \qquad (7.56)$$

$$u(x, y, t) = \tilde{u}(y) \exp(ikx - i\omega t) \quad . \qquad (7.57)$$

Using (7.54), we obtain

$$-i\omega \, \tilde{u}(y) = -gik \, \tilde{\eta}(y) \quad \text{and therefore} \quad \tilde{u}(y) = \frac{g}{\omega} k \, \tilde{\eta}(y) = \frac{g}{c} \tilde{\eta}(y) \qquad (7.58)$$

From the v-momentum equation $\quad \dfrac{\partial \eta}{\partial y} = \dfrac{\beta y}{g} u \qquad (7.59)$

we obtain therefore $\quad \dfrac{\partial \tilde{\eta}}{\partial y} = -\dfrac{\beta y}{c} \tilde{\eta} \, . \qquad (7.60)$

The solution is $\tilde{\eta}(x) = \exp(-\beta y^2 / c)$ with the scale of the Rossby radius $L_r = \sqrt{c/\beta}$. The wave has a trapped character along the equator.

A feature of a Kelvin wave is that it is non-dispersive, i.e., the phase speed of the wave crests is equal to the group speed of the wave energy for all frequencies. This means that it retains its shape in the alongshore direction over time. In the ocean these waves propagate along coastal boundaries (and hence become trapped in the vicinity of the coast itself) on a scale of about 30 km.

Equatorial Kelvin waves are a special type of Kelvin wave that balances the Coriolis Force in

the northern hemisphere against its southern hemisphere counterpart. This wave always propagates eastward and only exists on the equator. Equatorial Kelvin Waves propagating in the thermocline have wave speeds slow enough to give a Rossby Radius of Deformation that is on the order of 250 km and thus they appear to be trapped close to the equator.

7.5   Equatorial waves: Theory of Matsuno

We consider the equations (7.7,7.8,7.9) on the equatorial $\beta-$plane. In the equatorial region, the fluid dynamical system is described as

$$\partial_t u \quad = \quad \beta y \; v \quad - \quad g \, \partial_x \eta \tag{7.61}$$

$$\partial_t v \quad = \quad - \beta y \; u \quad - \quad g \, \partial_y \eta \tag{7.62}$$

$$\partial_t \eta \quad = \quad -\partial_x (H u) \quad - \quad \partial_y (H v) \quad . \tag{7.63}$$

We non-dimensionalize the system through the parameters listed in Table 7.1. In the non-dimensional form (and dropping the stars in Table 7.1), the system reads then

$$\partial_t u \quad = \quad y \; v \quad - \partial_x \eta \tag{7.64}$$

$$\partial_t v \quad = \quad -y \; u \quad - \partial_y \eta \tag{7.65}$$

$$\partial_t \eta \quad = \quad -\partial_x u \quad - \partial_y v \quad . \tag{7.66}$$

Introducing the new variables

$$q \; = \; \eta \; + \; u \tag{7.67}$$

$$r \; = \; \eta \; - \; u \tag{7.68}$$

Parameter	description	formula	typical values
H	equivalent height		
g	reduced gravity		
R	Earth's radius		$6.371 \cdot 10^6 \, m$
Ω	Earth's rotation rate	$2\pi \, day^{-1}$	$7.272 \cdot 10^{-5} \, s^{-1}$
M	zonal wave number		$0, \pm 1, \pm 2, \ldots$
N	mode number		$0, 1, 2, \ldots$
φ	latitude		
f	Coriolis parameter	$2\Omega \sin\varphi$	
β	β-term	$2\Omega/R$	$2.0 \cdot 10^{-11} \, m^{-1}s^{-1}$
c	barotropic phase speed of pure gravity wave	$\sqrt{g\overline{H}}$	atmosphere: $2000 \, ms^{-1}$ ocean: $200 \, ms^{-1}$
c	baroclinic phase speed of pure gravity wave	$\sqrt{g\overline{H}}$	atmosphere: $20 - 80 \, ms^{-1}$ ocean: $2 \, ms^{-1}$
a	meridional wave guide (Rossby radius)	$\sqrt{\frac{c}{2\beta}}$	atmosphere: $6.6 \cdot 10^5 \, m$ ocean: $6.6 \cdot 10^4 \, m$
t^*	time	$t\sqrt{2\beta c}$	
x^*	eastward distance	x/a	
y^*	meridional distance	y/a	
ω^*	frequency	$\omega/\sqrt{2\beta c}$	
k^*	zonal wave vector	Ma/R	

Table 7.1: List of parameters for the Matsuno equations.

yields

$$\partial_t q \quad = \quad -\partial_x q \quad - \quad \left[\partial_y - \frac{y}{2}\right] v \tag{7.69}$$

$$\partial_t v \quad = \quad \qquad -\frac{1}{2}\left[\partial_y + \frac{y}{2}\right] q \quad - \quad \frac{1}{2}\left[\partial_y - \frac{y}{2}\right] r \tag{7.70}$$

$$\partial_t r \quad = \quad +\partial_x r \quad - \quad \left[\partial_y + \frac{y}{2}\right] v \qquad . \tag{7.71}$$

The dynamics (7.69,7.70,7.71) describe wave propagation in an inhomogenous and anisotropic medium. Zonal wave dynamics differ significantly from those in meridional direction. The primary source of inhomogenity is due to the Coriolis force. The x and t dependences can be separated in form of zonally propagating waves $\exp(ikx - i\omega t)$. The eigenfunctions in $y-$direction are related to parabolic cylinder functions $\left(\text{or Hermite polynomials with weight } \exp(-y^2)\right)$. The Hermite polynomials are defined as

$$He_n(y) = (-1)^n e^{y^2/2} \frac{d^n}{dy^n} e^{-y^2/2} \tag{7.72}$$

The first Hermite polynomials are

$$He_0(y) \quad = \quad 1 \tag{7.73}$$

$$He_1(y) \quad = \quad x \tag{7.74}$$

$$He_2(y) \quad = \quad y^2 - 1 \tag{7.75}$$

$$He_3(y) \quad = \quad y^3 - 3y \tag{7.76}$$

$$He_4(y) \quad = \quad y^4 - 6y^2 + 3 \tag{7.77}$$

To display the Hermite polynomials:

```
# for a read.me: http://cran.r-project.org/doc/manuals/R-intro.pdf
# gemerate a list of normalized Hermite polynomials of orders 0 to 10
install.packages("orthopolynom")
normalized.p.list <- hermite.he.polynomials(5, normalized=TRUE ) # a list
print(normalized.p.list)  # display the polynomials
```
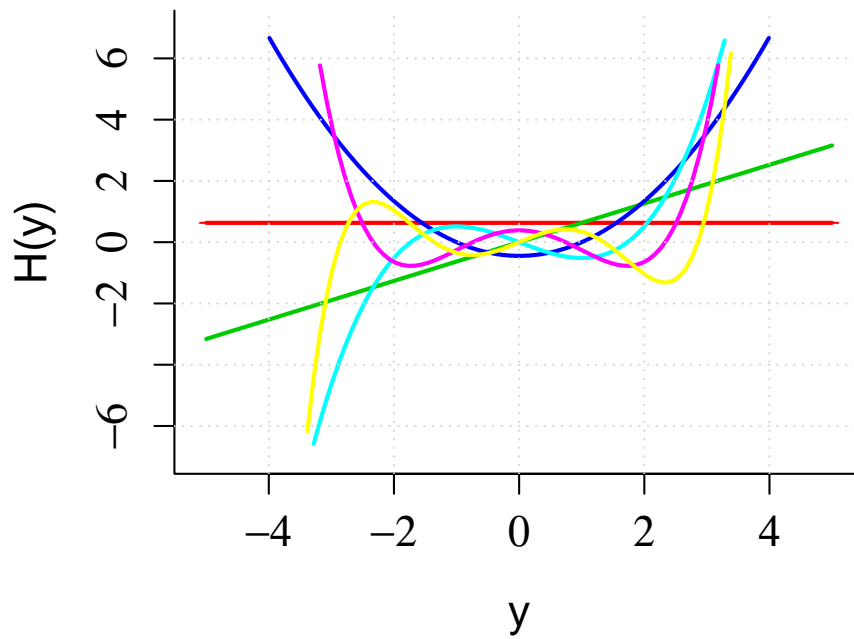
Figure 7.6: Hermite polynomials to degree 5.

```
H=normalized.p.list
ticks=seq(from=-5, to=5, by=10)
plot(H[[1]], xlim=c(-5,5),ylim=c(-7,7),col="red",ylab="H(y)",xlab="y")
for (i in 1:6) {lines(H[[i]],xlim=c(-5,5),ylim=c(-7,7),col =i+1, lwd = 2)}
grid(nx=NULL,col="lightgray",lty ="dotted",lwd=2,equilogs=TRUE)
dev.copy(png,'Hermite.png')
dev.off()
```

They satisfy following recursion relationship:

$$\left[\partial_y + \frac{y}{2}\right] D_N = N\, D_{N-1} \quad ; \qquad \left[\partial_y - \frac{y}{2}\right] D_N = -D_{N+1} \qquad . \quad (7.78)$$

The operators $[\partial_y \pm \frac{y}{2}]$ annihilate or excite one quantum of mode index number N and are called lowering and raising ladder operators in quantum mechanics. A basic feature of $D_N \sim \exp(-y^2)$ is that significant wave amplitudes are trapped in a wave guide centered at the latitude φ_0, similar to the equator-centered Yoshida guide [Gill, 1982].

The Fourier modes $\hat{\xi}_N(t) := (\hat{q}_{N-1}, \hat{v}_N, \hat{r}_{N+1})$ correspond to order $N > 0$ and wave vector k. The prognostic equations for the Fourier modes are first order in time

$$\frac{d}{dt}\, \hat{\xi}_N \;=\; A_N(k)\, \hat{\xi}_N \qquad . \tag{7.79}$$

and are described by 3×3 matrices $A_N(k)$

$$A_N(k) \;=\; \begin{pmatrix} -ik & 1 & 0 \\ -N/2 & 0 & 1/2 \\ 0 & -(N+1) & ik \end{pmatrix} \qquad . \tag{7.80}$$

Matrix $A_N(k)$ describes the dynamics of one Rossby and two gravity waves with eigenfrequencies ω (eigenvalue of $A = i\omega$) satisfying

$$\omega^3 - \omega \left(\frac{2N+1}{2} + k^2\right) - \frac{k}{2} \;=\; 0 \quad . \tag{7.81}$$

The sum of the eigenfrequencies in (7.81) is zero due to $trace\,(A_N) = 0$ and

$$\sum_{l=1}^{3} \omega_l \;=\; \lim_{T\to\infty} \frac{1}{T} \int_0^T dt\; trace\,(A_N) \;=\; 0 \quad . \tag{7.82}$$

For $N = 0$, the system matrix A_0 is specified to be

$$A_0(k) = \begin{pmatrix} \boxed{ik} & 0 & 0 \\ 0 & 0 & 1/2 \\ 0 & -1 & ik \end{pmatrix} \quad . \tag{7.83}$$

The different signs of the $\cdot_{11}$−elements in (7.80) and (7.83) originate from the requirement that the corresponding eigenmode $q_{N=0}$ in (7.83) is integrable [Gill, 1982]. This mode with $v = r = 0$ is called equatorial Kelvin wave which propagates eastward without dispersion:

$$\omega = k \quad . \tag{7.84}$$

The dynamics of the Kelvin wave is decoupled from the Yanai wave dynamics described by the second and third eigenvectors of matrix (7.83). The Yanai wave, also known as mixed planetary-gravity wave in the literature [Gill, 1982], has a quadratic relation

$$\omega^2 - k\omega - 1/2 = 0 \quad . \tag{7.85}$$

Dispersion curves for the Rossby/gravity (7.81), Kelvin (7.84), and Yanai (7.85) waves are shown in Fig. 7.7 as a function on zonal wave vector $k = Ma/R$ and mode number N. The figure depicts eastward propagating Kelvin and westward propagating Rossby modes. Gravity waves can propagate east- and westward. The Yanai wave behaves as a gravity wave for $k \geq 0$ and as a Rossby wave for $k < 0$. Note that (7.81) is invariant under $\omega \to -\omega, k \to -k$, which is a consequence of (7.82). Dispersion diagrams like Fig. 7.7 can be found in standard text books of geophysical fluid dynamics showing the upper [Gill, 1982] or right [Holton, 2004] part of Fig. 7.7, respectively.

The equatorial zone essentially acts as a waveguide, causing disturbances to be trapped in the vicinity of the equator. For the first baroclinic mode in the ocean, a typical phase speed would be about $2.8 m/s$, causing an equatorial Kelvin wave to take 2 months to cross the Pacific Ocean
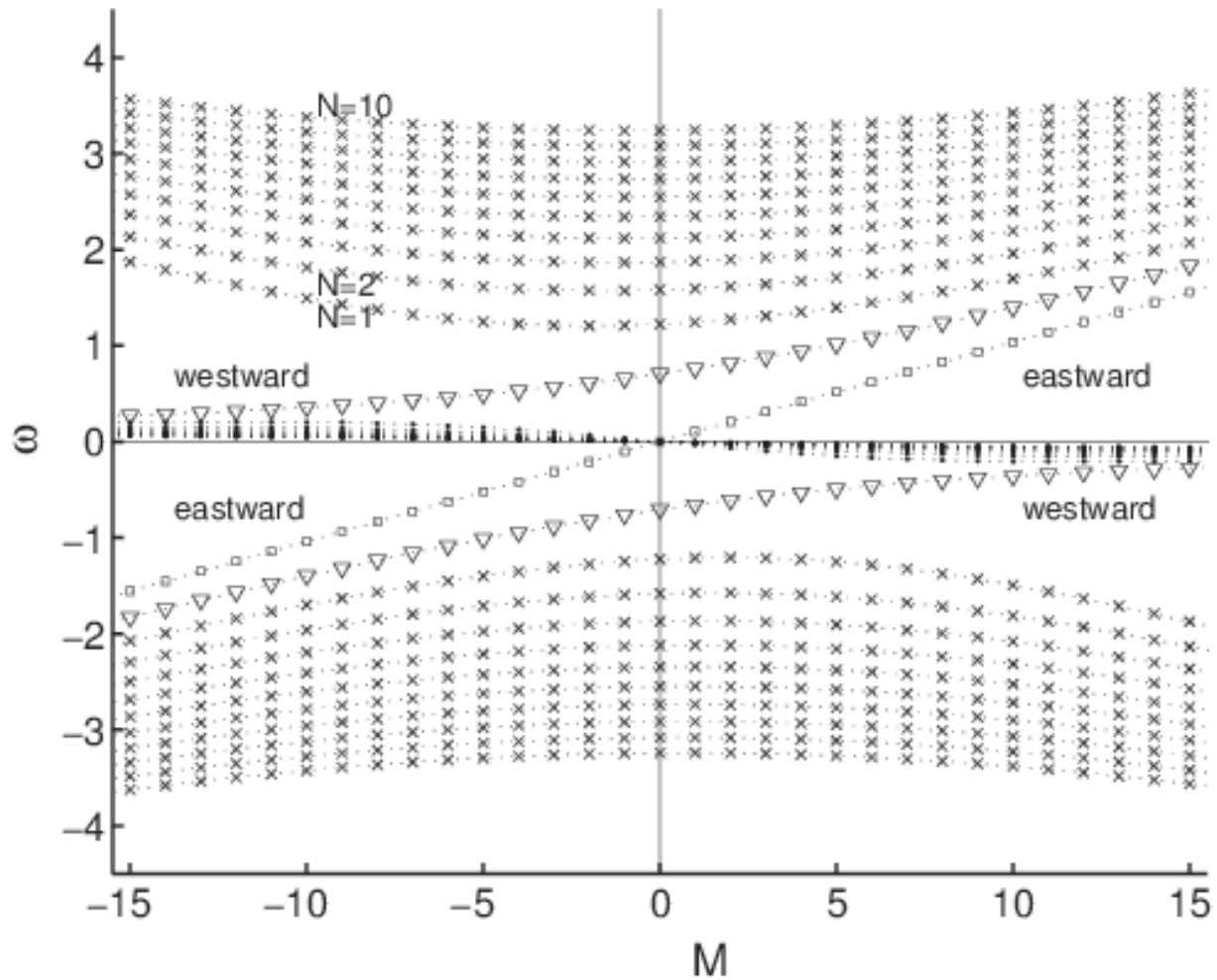
Figure 7.7: Dispersion relation for equatorial waves. Curves show dependence of frequency on zonal wave number M for mode numbers $N \leq 10$. Kelvin waves propagate eastward, Rossby waves ($\bullet$) westward, while gravity waves ($\times$) exist for both directions. Yanai waves ($\bigtriangledown$) behave Rossby-like for $M < 0$ and gravity-like for $M \geq 0$.

between New Guinea and South America; for higher ocean and atmospheric modes, the phase speeds are comparable to fluid flow speeds. Why is the Kelvin wave trapped? When the motion at the equator is to the east, any deviation toward the north is brought back toward the equator because the Coriolis force acts to the right of the direction of motion in the Northern Hemisphere, and any deviation to the south is brought back toward the equator because the Coriolis force acts to the left of the direction of motion in the Southern Hemisphere. Note that for motion toward

the west, the Coriolis force would not restore a northward or southward deviation back toward the equator; thus, equatorial Kelvin waves are only possible for eastward motion (as noted above). Both atmospheric and oceanic equatorial Kelvin waves play an important role in the dynamics of El Niño-Southern Oscillation, by transmitting changes in conditions in the Western Pacific to the Eastern Pacific [Gill, 1982]. This can be also studied in exercise 49.

It is instructive to look for approximations in tidal theory. One can simplify the solution of the Matsuno theory, or simplify the equations (7.7,7.8,7.9) which will be done in section 7.3.

When filtering out gravity waves by eliminating the time derivative in (7.63), (u, v) in (7.61, 7.62) is equivalent to $c \to \infty$. The evolution equation reduces to

$$\partial_t(\partial_y u - \partial_x v) = \beta u \qquad (7.86)$$

with plane waves proportional to $\exp(ikx + ily)$. Then, non-divergent Rossby waves with $\omega = -\beta k/(k^2 + l^2)$ are retained only. The trapped character of the waves vanishes with infinite Rossby radius $a = \sqrt{c/(2\beta)}$, a measure of the wave guide geography.

Exercise 54   –   Shallow-water dynamics: eigenfunctions

- Show that the eigenfunctions in $y-$direction, which are are related to parabolic cylinder functions $\left(\text{or Hermite polynomials with weight } \exp(-y^2)\right)$, satisfy following recursion relationship:

$$\left[\partial_y + \frac{y}{2}\right] D_N = N D_{N-1} \quad ; \qquad \left[\partial_y - \frac{y}{2}\right] D_N = -D_{N+1} \qquad .(7.87)$$

The operators $[\partial_y \pm \frac{y}{2}]$ annihilate or excite one quantum of mode index number N and are called lowering and raising ladder operators in quantum mechanics.

$$D_N(y) = \frac{1}{\pi} \int_0^\pi \sin(N\Theta - y \sin \Theta))$$

- Show that the functions are orthogonal, i.e.

$$\int_{-\infty}^{\infty} dy\, D_N(y) D_M(y) = \delta_{NM}\, N!\sqrt{2\pi}$$

- The dynamics in an inertial reference frame, e.g. with a coordinate system fixed at the Sun, would not have a Coriolis force (and thus $f = 0$), but would certainly observe Rossby wave propagation. How can this be reconciled?

  (Hint: In the inertial system, the near-equatorial motion is seen to be faster than off the equator. Zero vorticity in the rotating Earth's coordinate system corresponds to a basic flow $U = R\Omega \cos\varphi$ with non-zero vorticity flow.)

Exercise 55   –   Shallow-water dynamics: A different approach

We may seek travelling-wave solutions of the form

$$\left\{u, v, \eta\right\} = \left\{\hat{u}(y), \hat{v}(y), \hat{\eta}(y)\right\} e^{i(kx - \omega t)} \tag{7.88}$$

Please check the following arguments.

- Subsitituting this exponential form into the three equations (7.61,7.62,7.63), and eliminating u, and η leaves us with an eigenvalue equation for $\hat{v}(y)$

$$-\frac{\partial^2 \hat{v}}{\partial y^2} + \left(\frac{\beta^2}{c^2}\right) \hat{v} = \left(\frac{\omega^2}{c^2} - k^2 - \frac{\beta k}{\omega}\right) \hat{v}. \tag{7.89}$$

- Recognizing this as the Schrödinger equation of a quantum harmonic oscillator of frequency β/c, we know that we must have

$$\left(\frac{\omega^2}{c^2} - k^2 - \frac{\beta k}{\omega}\right) = \frac{\beta}{c}(2n + 1), \quad n \geq 0 \tag{7.90}$$

for the solutions to tend to zero away from the equator. For each integer n, this last equation provides a dispersion relation linking the wavenumber k to the angular frequency ω.

- In the special special case $n = 0$ the dispersion equation reduces to

$$(\omega + ck)(\omega^2 - ck\omega - c\beta) = 0, \tag{7.91}$$

but the root $\omega = -ck$ has to be discarded because we had to divide by this factor in eliminating u, η.

- The remaining pair of roots correspond to the Yanai or mixed Rossby-gravity mode whose group velocity is always to the east and interpolates between two types of $n > 0$ modes: the higher frequency Poincare gravity waves whose group velocity can be to the east or to the west, and the low-frequency equatorial Rossby waves whose dispersion relation can be approximated as

$$\omega = \frac{-\beta k}{k^2 + \beta(2n + 1)/c} \quad . \tag{7.92}$$

7.6   General form of wave equations*

The general form of the wave equation is:

$$\frac{1}{c^2}\frac{\partial^2 q}{\partial t^2} = \frac{\partial^2 q}{\partial x^2} + \frac{\partial^2 q}{\partial y^2} + \frac{\partial^2 q}{\partial z^2} \tag{7.93}$$

where q is the disturbance and c the *propagation velocity*. In general holds: $c = \nu\lambda$. By definition holds: $k\lambda = 2\pi$ and $\omega = 2\pi\nu$. Therefore,

$$c = \nu\lambda = 2\pi\nu/k = \omega/k \quad . \tag{7.94}$$

In principle, there are two types of waves:

1. Longitudinal waves: for these holds $\vec{k} \parallel \vec{c} \parallel \vec{q}$. In a longitudinal wave the particle displacement is parallel to the direction of wave propagation. The animation (http://www.acs.psu.edu/drussell/Demos/waves/wavemotion.html) shows a one-dimensional longitudinal plane wave propagating down a tube. The particles do not move down the tube with the wave; they simply oscillate back and forth about their individual equilibrium positions. Pick a single particle and watch its motion. The wave is seen as the motion of the compressed region (ie, it is a pressure wave), which moves from left to right. The second animation shows the difference between the oscillatory motion of individual particles and the propagation of the wave through the medium. The animation also identifies the regions of compression and rarefaction.

2. Transversal waves: for these holds $\vec{k} \parallel \vec{c} \perp \vec{q}$. In a transverse wave the particle displacement is perpendicular to the direction of wave propagation. The animation (http://www.acs.psu.edu/drussell/Demos/waves/wavemotion.html) below shows a one-dimensional transverse plane wave propagating from left to right. The particles do not move along with the wave; they simply oscillate up and down about their individual equilibrium positions as the wave passes by. Pick a single particle and watch its motion. The S waves

(Secondary waves) in an earthquake are examples of Transverse waves. S waves propagate with a velocity slower than P waves, arriving several seconds later.

3. Water waves: Water waves are an example of waves that involve a combination of both longitudinal and transverse motions. As a wave travels through the waver, the particles travel in clockwise circles. The radius of the circles decreases as the depth into the water increases. The animation (http://www.acs.psu.edu/drussell/Demos/waves/wavemotion.html) below shows a water wave travelling from left to right in a region where the depth of the water is greater than the wavelength of the waves. I have identified two particles in yellow to show that each particle indeed travels in a clockwise circle as the wave passes.

The *phase velocity* is given by

$$c_{\mathrm{ph}} = \omega/k \quad . \tag{7.95}$$

The *group velocity* is given by:

$$c_{\mathrm{g}} = \frac{d\omega}{dk} = c_{\mathrm{ph}} + k\frac{dc_{\mathrm{ph}}}{dk} \tag{7.96}$$

If c_{ph} does not depend on ω holds: $c_{\mathrm{ph}} = c_{\mathrm{g}}$. In a dispersive medium it is possible that $c_{\mathrm{g}} > c_{\mathrm{ph}}$ or $c_{\mathrm{g}} < c_{\mathrm{ph}}$. If one wants to transfer information with a wave, e.g. by modulation of an electromagnetic wave, the information travels with the velocity at with a change in the electromagnetic field propagates. This velocity is often almost equal to the group velocity.

For some media, the propagation velocity follows from:

- Pressure waves in a liquid or gas: $c = \sqrt{\kappa/\varrho}$, where κ is the modulus of compression.

- For pressure waves in a gas also holds: $c = \sqrt{\gamma p/\varrho} = \sqrt{\gamma RT/M}$.

Plane waves

The equation for a harmonic traveling plane wave is

$$q(\vec{x}, t) = \hat{q} \cos\left(\vec{k} \cdot \vec{x} \pm \omega t + \varphi\right) \quad .$$

When the situation is spherical or cylindrical symmetric, the the homogeneous wave equation can be solved. When the situation is spherical symmetric, the homogeneous wave equation is given by:

$$\frac{1}{c^2} \frac{\partial^2 (rq)}{\partial t^2} - \frac{\partial^2 (rq)}{\partial r^2} = 0$$

with general solution:

$$q(r, t) = C_1 \frac{f(r - ct)}{r} + C_2 \frac{g(r + ct)}{r}$$

When the situation has a cylindrical symmetry, the homogeneous wave equation becomes:

$$\frac{1}{c^2} \frac{\partial^2 q}{\partial t^2} - \frac{1}{r} \frac{\partial}{\partial r} \left(r \frac{\partial q}{\partial r}\right) = 0$$

This is a Bessel equation, with solutions which can be written as Hankel functions. For sufficient large values of r these are approximated by:

$$q(r, t) = \frac{\hat{q}}{\sqrt{r}} \cos(k(r \pm vt))$$

If an observer is moving w.r.t. the wave with a velocity c_{obs}, she/he will observe a change in frequency: the *Doppler effect*. This is given by: $\dfrac{\nu}{\nu_0} = \dfrac{c_f - c_{\text{obs}}}{c_f}$.

The general solution in one dimension

Starting point is the equation:

$$\frac{\partial^2 q(x,t)}{\partial t^2} = \sum_{m=0}^{N} \left(b_m \frac{\partial^m}{\partial x^m} \right) q(x,t)$$

where $b_m \in I\!\!R$. Substituting $q(x,t) = A\mathrm{e}^{i(kx-\omega t)}$ gives two solutions $\omega_j = \omega_j(k)$ as dispersion relations. The general solution is given by:

$$q(x,t) = \int\limits_{-\infty}^{\infty} \left(a(k)\mathrm{e}^{i(kx-\omega_1(k)t)} + b(k)\mathrm{e}^{i(kx-\omega_2(k)t)} \right) dk$$

Because in general the frequencies ω_j are non-linear in k there is dispersion and the solution cannot be written any more as a sum of functions depending only on $x \pm ct$: the wave front transforms.

7.7 Spheroidal Eigenfunctions of the Tidal Equation*

Laplace's tidal equations, governing the small amplitude dynamics of a shallow fluid on a rotating sphere, are the fundamental linear problems of large-scale geophysical fluid dynamics. Originally formulated by Laplace, its general solution and, in particular, its full dispersion relation are still not known. The current understanding of the problem rests essentially on the equatorial β-plane approximation [Matsuno, 1966] and extensive numerical studies [Longuet-Higgins, 1968]. In this framework the system has been found to exhibit Rossby waves, Yanai waves, and gravity waves, including the Kelvin wave. In spite of its elegance and fundamental significance for the terrestrial climate problem, the β-plane concept is not entirely free from ambiguities. Although the Matsuno wave equation appears to be a well-posed problem, its dispersion relation admits an unphysical, westward propagating "Kelvin" mode. This has to be ruled out a posteriori [Matsuno, 1966]. Furthermore, the β-plane concept does not yield a physically meaningful nonrotating limit. And

finally, the Matsuno equation is invariant under meridional translations. Yanai waves should thus be observed at all latitudes and every latitude defines the center of a waveguide. Such properties are not physically realizable. On the other hand, the analysis of the spherical version of the tidal problem is complicated. First, the manipulation of the first order equations of motion into an appropriate wave equation is cumbersome, namely because the two-dimensional (2D) geometry of the spherical surface is non-Euclidean. Second, as shown below, the basic wave operator in the various forms of the tidal problem is the spheroidal wave equation. For this equation, infinity is an irregular singular point precluding the establishment of recurrence relations similar to those for functions of the hypergeometric type [Flammer, 1957]. The transformation of differential operations in physical space into some simpler algebra in wave number space is thus impossible. Geometrical difficulties are largely simplified by a systematic application of tensor analysis in 2D Riemann space. Here, index notation will be used with indices m, n,... running from 1 to 2 and a semicolon denoting covariant differentiation. For details of the notation and the form of the geometrical tensors in spherical, geophysical coordinates see [Townsend et al., 1992]. The linearized equations of motion of a shallow fluid on a rotating sphere are shown in [Townsend et al., 1992] to assume the form

$$\partial_t r + j^n{}_{;n} = 0,$$

$$\partial_t j_n + \epsilon_{mn} f j^m + c^2 \partial_n r = 0,$$

where $j_n = R v_n$ is the effective momentum density, R the constant equilibrium mass per unit area, and $f = 2\Omega \sin \varphi$ using the latitude dependent Coriolis parameter. For the potential vorticity z, defined by

$$R z = \epsilon^{mn} v_{n;m} - f r / R,$$

the linearized equations of motion imply the relation

$$R \partial_t z + f^n v_n = 0,$$

where f^n is the contravariant gradient of the Coriolis parameter. Furthermore, the gradient of the divergence of a vector on the spherical surface is given by

$$j^a{}_{;an} = g^{ab}(j_{n;ab} - \epsilon_{na}\epsilon^{rs}j_{r;sb} - G_{ambn}j^m),$$

where g^{ab} is the metric and G_{ambn} the Riemannian [Townsend et al., 1992]. Using this identity and the potential vorticity equation it is fairly straightforward to derive the system

$$R^2 \left[(\partial_t^2 + f^2 - c^2\Delta)\partial_t + c^2\epsilon^{ab}f_a\partial_b\right]\partial_t z = -c^2(\Delta f)\partial_t^2 r, \tag{7.97a}$$

$$\left[(\partial_t^2 + f^2 - c^2\Delta)\partial_t + c^2\epsilon^{ab}f_b\partial_a\right]r = -2R^2 f\partial_t z, \tag{7.97b}$$

from the equations of motion, where Δ denotes the 2D Laplacian in spherical coordinates. If Cartesian coordinates (x, y) are chosen with $f = \beta y$, i.e., in particular $\Delta f = 0$, the first of these equations reduces to the Matsuno equation. To obtain (7.97a) in the spherical case, eliminate r from the equations of motion

$$(\partial_t^2 + f^2 - c^2\underline{\Delta})\partial_t j_n + c^2\epsilon_{na}\left[\partial^a(f_b j^b) + f^a j^b{}_{;b}\right] = 0, \tag{7.98}$$

with

$$\underline{\Delta} j_n = g^{ab}j_{n;ab} - a^{-2}j_n,$$

where a denotes the Earth's radius. Using

$$f^n\underline{\Delta}j_n = \Delta(f^n j_n) - (\Delta f)j^n{}_{;n}$$

.

scalar multiplication of (7.98) with the contravariant gradient of the Coriolis parameter yields (7.97a). Equation (7.98) as well as the coupled nature of the system (7.97) demonstrate that the

tidal equation is inherently a 20 vector wave equation. In order to evaluate the eigenfunctions of this system, the dependent variables are assumed to be proportional to

$$e^{-i(\omega t - M\lambda)}F(y),$$

where λ is longitude, $y = \sin\varphi$, and M the zonal wave number. Substituting this into (7.97), the system becomes

$$(P - m)V = -2\alpha y D, \tag{7.99a}$$

$$(P + m)D = 2\alpha y V, \tag{7.99b}$$

Here $D = r/R = iv^n;_n/\omega$ and $V = aRz/c = -i\alpha v_\varphi \times \cos\varphi/cv$, while

$$P = a^2\Delta - \alpha^2 y^2 + \nu^2$$

is the prolate spheroidal wave operator with Lamb parameter $u = 2a\Omega/c$, $\nu = a\omega/c$, and $m = \alpha M/\nu$. In the form (7.99) the tidal problem emerges as a system of coupled spheroidal wave equations. In special cases, exact analytical solutions can be readily obtained without considering the complete fourth order system. Elimination of j_1 between the continuity equation and the one-component of the momentum budget yields

$$\alpha D = -(\mu + y^2)^{-1}\left[(1 - y^2)\partial_y - my\right]V,$$

with $\mu = (M^2 - \nu^2)/\nu^2$, while elimination of ji between the one-component and the two-component of the momentum budget leads to

$$\alpha V = -(n^2 - y^2)^{-1}\left[(1 - y^2)\partial_y + my\right]D,$$

with $n = \nu/\alpha$. Inserting these expressions into the right hand side (rhs) of (7.99) results in

$$(P + m)V = 2(\mu + y^2)^{-1} \left[y(1 - y^2)\partial_y + m\mu\right] V, \tag{7.100a}$$

$$(P - m)D = -2(n^2 - y^2)^{-1} \left[y(1 - y^2)\partial_y + mn^2\right] D. \tag{7.100b}$$

Equation (7.100a) is the spherical generalization of the Matsuno equation, while (7.100b) is the form of the tidal equation studied by Longuet-Higgins. In view of the general solution, (7.100) may not be the most convenient form as it exhibits far less symmetry than the coupled system (7.99) suggests. It nevertheless lends itself readily to the evaluation of two special cases. For standing waves (M = 0) the spherical Matsuno equation (7.100a) is exactly solved by

$$V = (1 - y^2)^{1/2}(AS_L^1 + BS_L^{-1}),$$

with constants A and B and prolate spheroidal wave functions $S_L^{\pm 1}(y; \alpha^2)$ of order ± 1 and degree $L \geq 1$. The corwhere responding divergence becomes

$$D \sim \partial_y (1 - y^2)^{1/2}(AS_L^1 + BS_L^{-1}). \tag{7.101}$$

A closed expression for the eigenvalues of the spheroidal wave equation does not exist and approximations depend strongly on the value of the Lamb parameter. On Earth, the value of the Lamb parameter ranges from $\alpha \approx 1$ for the atmospheric Lamb wave, over $\alpha \approx 5$ for barotropic gravity waves in the ocean to $\alpha \approx 300$ for the first baroclinic mode in the ocean. For $\alpha^2 \ll 1$, spheroidal wave functions are approximated by expansions in terms of associated Legendre polynominals, and the dispersion relation for standing waves becomes to $O(\alpha^0)$ [Flammer, 1957] [Abramowitz and Stegun, 1965].

$$\nu^2 = \Lambda^2 + \alpha^2(2\Lambda^2 - 3)/(4\Lambda^2 - 3) \tag{7.102a}$$

with $\Lambda^2 = L(L+1)$. In the nonrotating limit, this reduces to the familiar $\nu^2 = L(L+1)$. For $\alpha^2 \gg 1$, the prolate spheroidal wave function S_L^K is appropriately approximated by parabolic cylinder functions of nonnegative, integer order, and the corresponding eigenvalue to $O(\alpha^0)$ becomes [Flammer, 1957] [Abramowitz and Stegun, 1965]

$$\epsilon(L, K, \alpha) = \alpha q + K^2 - 1 + p,$$

with $q = 2N + 1$, $p = (3 - q^2)/8$, and $N = L - |K|$. In the present case of standing waves ($\epsilon = \nu^2$, $K^2 = 1$) this yields the dispersion relation to $O(\alpha^0)$

$$\nu^2 = \alpha(2N_2 + 1) + p, \tag{7.102b}$$

where the mode number $N_2 = L - 1$ measures the number of zeros of j_2 in the open interval $y \in (-1, 1)$. With the inclusion of higher orders in α and $1/\alpha$, respectively, the dispersion relation (7.102) and the corresponding expansion of the spheroidal wave function permit the construction of Fig. 1 and Fig. 7 of [Longuet-Higgins, 1968] to an arbitrary degree of accuracy from [Abramowitz and Stegun, 1965] . The asymptotic expansion of (7.100a) provides an estimate of the domain of validity of the β-plane approximation in physical and wave number space. For low frequencies $\nu^2 \ll M^2$, the first order Taylor expansion of the denominator on the rhs of (7.100a) is justified and yields

$$(\alpha^2\Delta - \delta y^2 + \nu^2 - m)V = 0,$$

with $\delta = \alpha^2 - 2m/\mu$, . For large a in the low-frequency domain under consideration $\alpha^2 \gg 2m/\mu$, so that $\delta \approx \alpha^2$. Assuming $V = (1 - y^2)^{|M|/2}F$, where the absolute value of M ensures

the regularity of V at the poles for negative M, and transforming to $x = y\sqrt{\alpha}$

$$\left[(\alpha - x^2)\partial_x^2 - 2(|M| + 1)x\partial_x - \alpha x^2 + \alpha(2N_2 + 1)\right] F \approx 0$$

yields for $\alpha \gg x^2$, i.e., in the vicinity of the equator $y^2 \ll 1$

$$(\partial_x^2 - x^2 + 2N_2 + 1 - x + 2N2 + 1)F \approx O$$

the familiar β-plane version of the Matsuno equation with dispersion relation

$$\nu^3 - \left[\alpha(2N_2 + 1) + M^2\right]\nu - \alpha M = 0,$$

with $N_2 = L - |M|$. The β-plane approximation thus emerges asymptotically from the full tidal equation as an equatorial ($y^2 \ll 1$), baroclinic ($\alpha^2 \gg 1$) low-frequency approximation. While the original frequency restriction $\nu^2 \ll M^2$ admits Rossby waves only, the additional restriction to low latitudes also allows for low-frequency gravity waves in this approximation. The equatorial nature of these asymptotics is obviously not compatible with a "midlatitude β-plane," while the large u condition rules out a nonrotating limit. The β-plane approximation essentially neglects the coupling of Eqs. (7.99a) and (7.99b). In the full tidal vector equation it is this coupling that excludes the "wrong Kelvin wave" a priori. A second special, but exact solution can be obtained for inertial waves. At the inertial frequency $\nu = \alpha$, (7.100b) has the exact solution

$$D = (1 - y^2)^{1/2}(AS_L^{M-1} + BS_L^{1-M}), \tag{7.103}$$

with $L \geq 0$ and $1 - L \leq M \leq L + 1$. The dispertion relation in this case

$$\left[\epsilon = \alpha^2 - M, \ K^2 = (M - 1)^2\right]$$

can again be read from [Abramowitz and Stegun, 1965] . For small α one finds to $O(\alpha^2)$

$$\alpha^2 = \Lambda^2 + M + \alpha^2 \left[2\Lambda^2 - 2M(M-2) - 3\right]/(4\Lambda^2 - 3) \qquad (7.104\text{a})$$

admitting only $L = 0$ and $M = 0$ in the nonrotationg case, while the dispersion relation for large α becomes $O(\alpha^2)$

$$\alpha^2 = \alpha(2N_0 + 1) + M^2 - M + p \qquad (7.104\text{b})$$

where $N_0 = L - |M - 1|$ measures the number of seros of the mass perturbation r in the open interval $y \in (-1, 1)$. At $M = 0$, the relation (7.104) coincides obviously with (7.102) at $\nu = \alpha$, where $N_0(M = 0, \nu = \alpha = N_2(M = 0, \nu = \alpha)$, while in general the number of zeros of the mass perturbation r will differ from the number of zeros of j_2. The divergence (7.103) at M=0 agrees with (7.101) at $\nu = \alpha$, since for spheroidal wave functions [Flammer, 1957] :

$$M_{E/W} = \frac{1}{2} \pm \sqrt{\alpha^2 - \alpha q + p + \frac{1}{4}},$$

with

$$|M_W| = M_E - 1 < M_E. \qquad (7.105)$$

The same inequality is found from (7.104a). In contrast to the β-plane approximation, modes in this frequency domain are labeled by Np, and the phase speed of eastward propagating gravity waves is smaller than the westward speed at the same frequency and mode number. At high frequencies $\nu^2 \gg \alpha^2$, the approximation of (7.100b) by

$$(\alpha^2 \Delta - \delta y^2 + \nu^2 + m)D \approx 0,$$

with $\delta = \alpha^2 - 2M/n^3$, is uncritical. For large α and positive M not too large $\delta \approx \alpha^2$, and the

expansion of this equation similar to the Matsuno equation yields the

approximate dispersion relation

$$\nu^3 - \left[\alpha(2N_0 + 1) + M^2\right]\nu + \alpha M = 0,$$

with $N_0 = L - |M|$. The eastward propagating "Rossby" solutions of this dispersion have to be discarded, as they do not satisfy the defining inequality. On the other hand, the gravity solutions including the Kelvin wave satisfy this inequality. As a consequence of the positive sign of the last term, westward phase speeds are larger than eastward speeds. This is in agreement with the exact solution (7.104). The wave number space of the tidal equation is thus separated at the inertial frequency $\nu = \alpha$ into a lowfrequency domain, where modes are governed by N_2 and a high-frequency domain with gravity modes controlled by N_0. This is the mode number that survives the transition to the nonrotating case. For $\Omega = 0$, D is proportional to the associated Legendre polynominal P_L^M with $N_0 = L - |M|$ zeros in the open interval $y \in (-1, 1)$, and the dispersion relation $\nu^2 = L(L + 1)$ can alternatively be written

$$\nu^2(M) = N_0(N_0 + 1) + (2N_0 + 1)|M| + M^2 = \nu^2(-M)$$

. As indicated by the inequality (7.105), rotation leads primarily to the loss of this synunetry for gravity modes. At lower frequencies, additional Rossby modes emerge in rotating systems, which can no longer be accormnodated by Np. Hence, the mode number Np governs that domain of wave number space, where rotation merely modifies modes already existing in the nonrotating case. The transition between mode numbers is only possible due to the vector character of the tidal equation. On Earth, this highfrequency domain of wave number space is occupied by Lamb waves and barotropic gravity waves, which are of minor significance on larger scales. The atmosphere of Venus, on the other hand, is characterized by much lower values of the Lamb parameter, and gravity waves with $\nu \geq \alpha$ gain greater relevance for large-scale aspects of the circulation. The concept of covariant differentiation renders the derivation of wave equations from the equations

of motion fairly straightforward. The prolate spheroidal wave operator assumes a central role in these vector wave equations. For the first time since Laplace's formulation of the problem, exact analytical solutions are presented in the special cases of standing waves and inertial waves. These solutions confirm corresponding numerical calculations, while the asymptotics of the spheroidal wave equation for equatorial, baroclinic, low-frequency waves yield indeed the β-plane approximation. Furthermore, the results demonstrate a fundamental separation of the wave number space of the tidal equation at the inertial frequency. At higher frequencies, the mode number N_0 controls the dispersion of gravity waves, which experience rotation effects merely as a loss of syrrunetry with respect to $M = 0$. For a corotating observer westward

propagating gravity waves at these frequencies are faster and longer than their eastward counterparts. At low frequencies the dispersion of additional Rossby modes is incorporated by transition to the mode number N_2. This transition is primarily possible due to the vector character of the tidal problem. It can be expected that in the framework of the complete analytical theory of the tidal equation the angular momentum of eigensolutions, measured by the degree L, will be essential for this separation of the wave number space.

Part III

Third part: Stochastic climate model and Mesoscopic Dynamics

Chapter 8

Brownian motion, weather and climate

The daily observed maximum and minimum temperatures is often compared to the "normal" temperatures based upon the 30-year average. Climate averages provide a context for something like "this winter will be wetter (or drier, or colder, or warmer, etc.) than normal. It has been said "Climate is what you expect. Weather is what you get."

What is the difference between weather and climate? This can be also answered by an example/a methaphor in the football league. Predicting the outcome of the next game is difficult (weather), but predicting who will end up as German champion is unfortunately relatively easy (climate). In this section, I will give a general approach to the mean and fluctuations in the climate system. Indeed, the Brownian motion approach is a helpful analogue for weather and climate.

Brownian motion

The Roman Lucretius's scientific poem On the Nature of Things (ca. 60 BC) has a remarkable description of Brownian motion of dust particles[1]. Jan Ingenhousz had described the irregular

---

[1]He uses this as a proof of the existence of atoms: "Observe what happens when sunbeams are admitted into a building and shed light on its shadowy places. You will see a multitude of tiny particles mingling in a multitude of ways... their dancing is an actual indication of underlying movements of matter that are hidden from our sight... It originates with the atoms which move of themselves [i.e. spontaneously]. Then those small compound bodies that are least removed from the impetus of the atoms are set in motion by the impact of their invisible blows and in turn cannon against slightly larger bodies. So the movement mounts up from the atoms and gradually emerges to the level of our

motion of coal dust particles on the surface of alcohol in 1785. Nevertheless Brownian motion is traditionally regarded as discovered by the botanist Robert Brown in 1827. It is believed that Brown was studying pollen particles floating in water under the microscope. He then observed minute particles within the vacuoles of the pollen grains executing a jittery motion. By repeating the experiment with particles of dust, he was able to rule out that the motion was due to pollen particles being 'alive', although the origin of the motion was yet to be explained.

See the film: `https://en.wikipedia.org/wiki/Brownian_motion#/media/File:Brownian_motion_large.gif`.
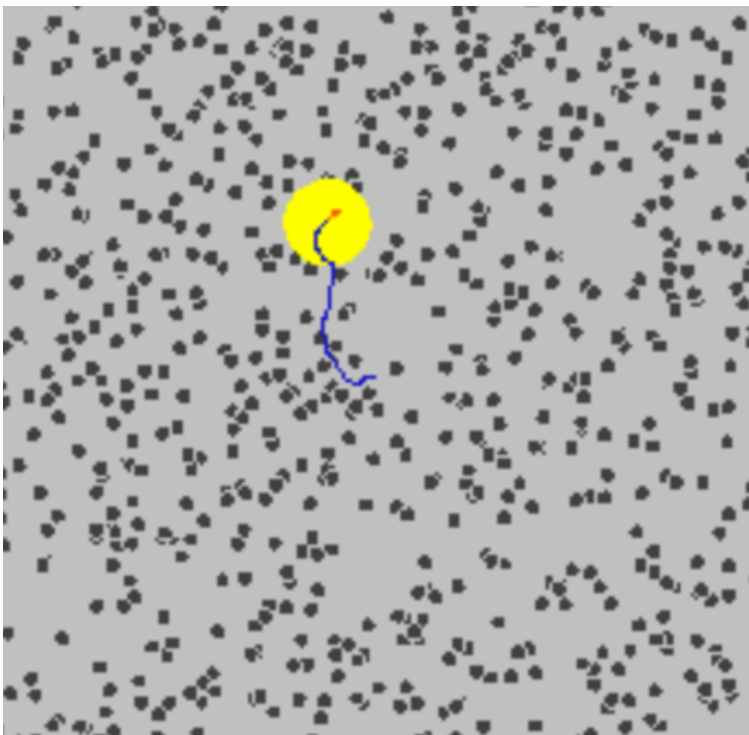
Figure 8.1: Snapshot of a movement of a Brownian particle.

The first person to describe the mathematics behind Brownian motion was Thorvald N. Thiele in 1880 in a paper on the method of least squares. This was followed independently by Louis

---

senses, so that those bodies are in motion that we see in sunbeams, moved by blows that remain invisible." Although the mingling motion of dust particles is caused largely by air currents, the glittering, tumbling motion of small dust particles is, indeed, caused chiefly by true Brownian dynamics.

Bachelier in 1900 in his PhD thesis "The theory of speculation", in which he presented a stochastic analysis of the stock and option markets. However, it was Albert Einstein's (in his 1905 paper) and Marian Smoluchowski's (1906) independent research of the problem that brought the solution to the attention of physicists, and presented it as a way to indirectly confirm the existence of atoms and molecules. The confirmation of Einstein's theory constituted empirical progress for the kinetic theory of heat. In essence, Einstein showed that the motion can be predicted directly from the kinetic model of thermal equilibrium. The importance of the theory lay in the fact that it confirmed the kinetic theory's account of the second law of thermodynamics as being an essentially statistical law.

8.1   Brownian motion: Statistical description

Einstein's argument was to determine how far a Brownian particle travels in a given time interval. Classical mechanics is unable to determine this distance because of the enormous number of bombardments a Brownian particle will undergo, roughly of the order of 1021 collisions per second. Thus Einstein was led to consider the collective motion of Brownian particles.

He regarded the increment of particle positions in unrestricted one dimensional $x-$ domain as a random variable (Δ or x, under coordinate transformation so that the origin lies at the initial position of the particle) with some probability density function $\phi(\Delta)$. Further, assuming conservation of particle number, he expanded the density (number of particles per unit volume) change
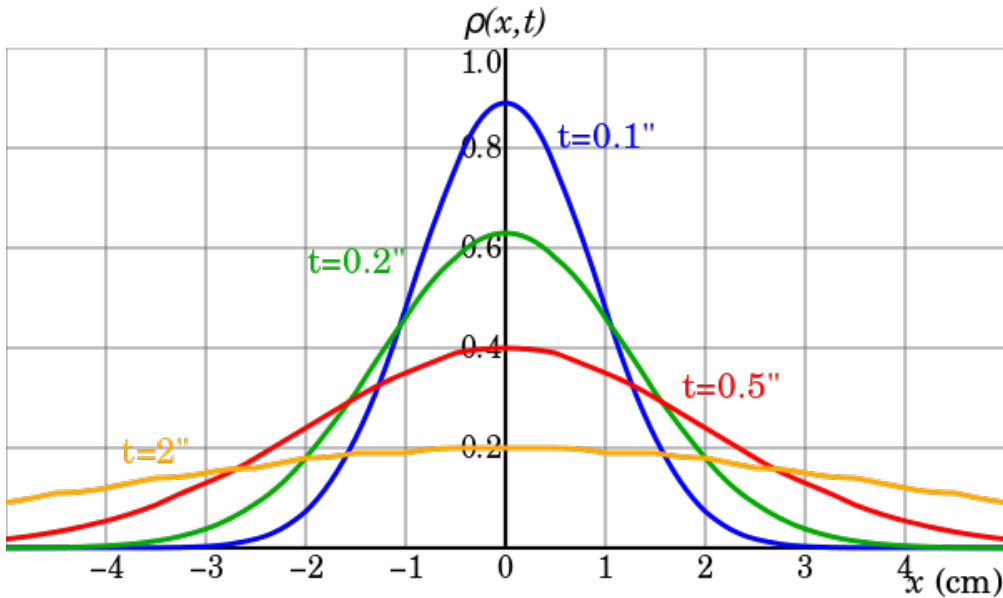
Figure 8.2: The characteristic bell-shaped curves of the diffusion of Brownian particles. The distribution begins as a Dirac delta function, indicating that all the particles are located at the origin at time t=0, and for increasing times they become flatter and flatter until the distribution becomes uniform in the asymptotic time limit.

in a Taylor series:

$$\rho(x, t + \tau) = \rho(x, t) + \tau \frac{\partial \rho(x)}{\partial t} \tag{8.1}$$

$$= \int_{-\infty}^{+\infty} \rho(x + \Delta, t) \cdot \phi(\Delta) \, \mathrm{d}\Delta \tag{8.2}$$

$$= \rho(x, t) \cdot \int_{-\infty}^{+\infty} \phi(\Delta) \, d\Delta + \frac{\partial \rho}{\partial x} \cdot \int_{-\infty}^{+\infty} \Delta \cdot \phi(\Delta) \, \mathrm{d}\Delta$$

$$+ \frac{\partial^2 \rho}{\partial x^2} \cdot \int_{-\infty}^{+\infty} \frac{\Delta^2}{2} \cdot \phi(\Delta) \, \mathrm{d}\Delta \quad + \quad \dots \tag{8.3}$$

$$= \rho(x, t) \cdot 1 + 0 + \frac{\partial^2 \rho}{\partial x^2} \cdot \int_{-\infty}^{+\infty} \frac{\Delta^2}{2} \cdot \phi(\Delta) \, \mathrm{d}\Delta \quad + \quad \dots \tag{8.4}$$

The integral in the first term is equal to one by the definition of probability, and the second and

other even terms (i.e. first and other odd moments) vanish because of space symmetry. What is left gives rise to the following relation:

$$\frac{\partial \rho}{\partial t} = \frac{\partial^2 \rho}{\partial x^2} \cdot \int_{-\infty}^{+\infty} \frac{\Delta^2}{2\,\tau} \cdot \phi(\Delta)\, \mathrm{d}\Delta + \textbf{higher order even moments}$$

Where the coefficient before the Laplacian, the second moment of probability of displacement $\boldsymbol{\Delta}$, is interpreted as mass diffusivity $\boldsymbol{D}$:

$$D = \int_{-\infty}^{+\infty} \frac{\Delta^2}{2\,\tau} \cdot \phi(\Delta)\, \mathrm{d}\Delta$$

Then the density of Brownian particles ρ at point x at time t satisfies the diffusion equation:

$$\frac{\partial \rho}{\partial t} = D \cdot \frac{\partial^2 \rho}{\partial x^2},$$

Assuming that N particles start from the origin at the initial time $t = 0$, the diffusion equation has the solution

$$\rho(x, t) = \frac{N}{\sqrt{4\pi D t}} e^{-\frac{x^2}{4Dt}}.$$

This expression allowed Einstein to calculate the moments directly. The first moment is seen to vanish, meaning that the Brownian particle is equally likely to move to the left as it is to move to the right. The second moment is, however, non-vanishing, being given by

$$\overline{x^2} = 2\,D\,t.$$

This expresses the mean squared displacement in terms of the time elapsed and the diffusivity. From this expression Einstein argued that the displacement of a Brownian particle is not proportional to the elapsed time, but rather to its square root. His argument is based on a conceptual switch from the "ensemble" of Brownian particles to the "single" Brownian particle: we can speak of the relative number of particles at a single instant just as well as of the time it takes a Brownian

particle to reach a given point.

This can be formalized as follows. The Wiener process is a continuous-time stochastic process with stationary independent increments. The Wiener process W_t is characterized by three facts:

- $W_0 = 0$

- W_t is almost surely continuous

- W_t has independent increments with normal distribution $W_t - W_{t_0} \sim N(0, t - t_0)$. $N(\mu, \sigma^2)$ denotes the normal distribution with expected value μ and variance σ^2. The condition that it has independent increments means that if then and are independent random variables.

The Wiener process can be constructed as the scaling limit of a random walk, or other discrete-time stochastic processes with stationary independent increments. It can be denoted as

$$var(W_t) = \overline{dW_t^2} = 2\sigma^2 t \qquad (8.5)$$

where $\overline{dW_t^2}$ is the mean square displacement of a Brownian particle in time t (t_0 is set to zero).[2] The so-called diffusion constant $D = \sigma^2$ is related to the mean free path λ and the average time between collisions τ:

$$2D = \frac{\lambda^2}{\tau} \quad . \qquad (8.6)$$

The time evolution of the position of the Brownian particle itself is best described using Langevin equation, an equation which involves a random force field representing the effect of the thermal fluctuations of the solvent on the particle. The displacement of a particle undergoing Brownian motion is obtained by solving the diffusion equation under appropriate boundary conditions and finding the root mean square of the solution. This shows that the displacement varies as the square

---

[2]A heuristic helpful interpretation of the stochastic differential equation is that in a small time interval of length dt, the stochastic process changes its value by an amount that is normally distributed with variance $2\sigma^2 dt$ and is independent of the past behavior of the process. This is so because the increments of a Wiener process are independent and normally distributed.

root of the time (not linearly).
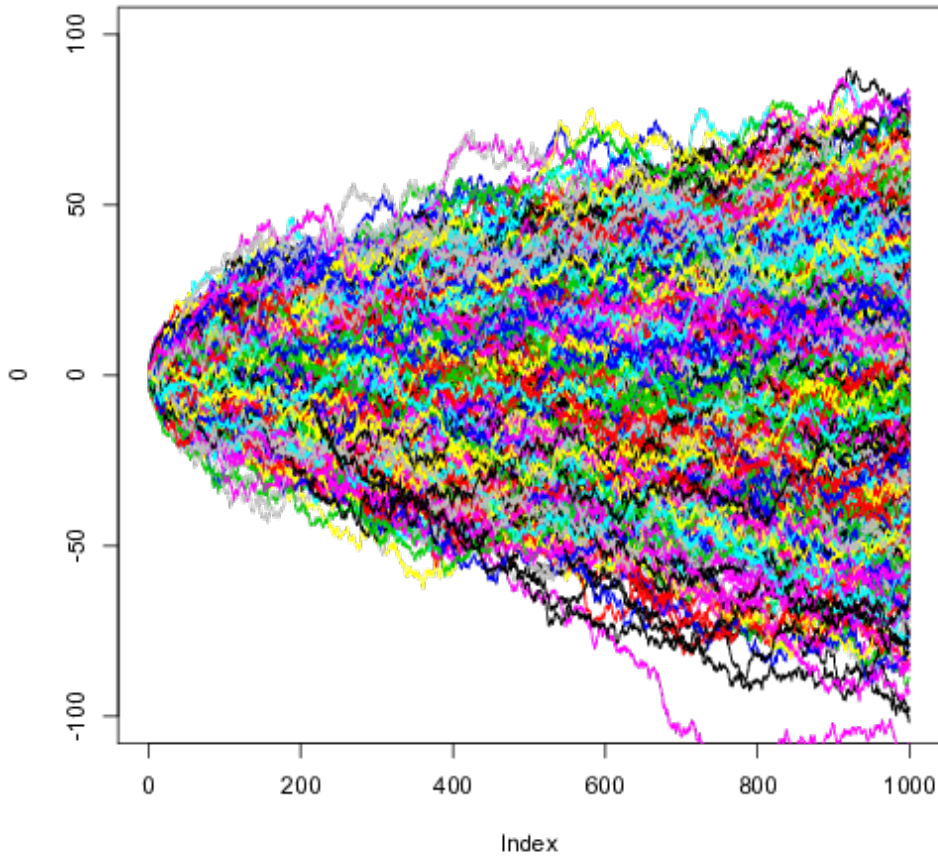
Figure 8.3: Numerical solution of the brownian motion, multiple particles. See exercise 56 for details.

Exercise 56   –   Brownian motion on a computer

Imagine a so-called red-noise process

$$\frac{dx}{dt} = -\lambda x + \xi\,.$$

(8.7)

1. Calculate the model using the following R code:

```
#brownian motion, multiple particle
#forward modelling

Nparticle<-1000 #number of particles
T<-   1000    #integration time in time units
h<-   0.5     #step size in time units

beta<-0.00001 #friction term
lambda<-1 #noise term

N<-T/h
t<-(0:(N-1))*h

x<-matrix(0,Nparticle,N) # Initial condition, all = 0


for (i in 1:(N-1))
{
  x[,i+1]<-x[,i]*(1-beta*h)+ rnorm(Nparticle)*sqrt(h)

}


plot(0,xlim=c(0,T),ylim=c(-100,100),type="n")
for (i in 1:N) lines (t,x[i,],col=i)

#analyse the densities
h<-matrix(0,N,40)

for (i in 1:(N-1)) h[i,]<-hist(x[,i],breaks=c((-20:20)*10),freq=FALSE,
              ylim=c(0,0.04))$counts

filled.contour(t,(-19:20)*10-5,h,color.palette=rainbow,xlab="time",
              ylab="space")
```

2. Show that the displacement varies as the square root of the time (not linearly).

8.2 Stochastic climate model

In a stochastic framework of climate theory one may use an appropriate stochastic differential equation (Langevin equation)

$$\frac{d}{dt}x(t) = f(x) + g(x)\xi, \tag{8.8}$$

where $\xi = \frac{d}{dt}W(t)$ is a stationary stochastic process and the functions $f, g : \mathbf{R}^n \to \mathbf{R}^n$ describe the climate dynamics. The properties of the random force are described through its distribution and its correlation properties at different times. The process ξ is assumed to have a Gaussian distribution of zero average,

$$< \xi(t) >= 0 \tag{8.9}$$

and to be δ-correlated in time,

$$< \xi(t)\xi(t+\tau) >= \delta(\tau) \tag{8.10}$$

where δ is the delta function defined by

$$\int_{\mathbf{R}} f(x)\,\delta(x - x_0)\,dx = f(x_0) \quad . \tag{8.11}$$

The brackets indicate an average over realizations of the random force.[3] For a Gaussian process only the average and second moment need to be specified since all higher moments can be expressed in terms of the first two. Note that the dependence of the correlation function on the time difference τ assumes that ξ is a stationary process. ξ is called a white-noise process (for the colors of noise: https://en.wikipedia.org/wiki/Colors_of_noise). In general, the stochastic processes can be also described by the probablity distributions (9.19) which will be considered later.

Additionally, there might be an external forcing $F(x, t)$ which is generally time-, variable-, and space-dependent. In his theoretical approach, Hasselmann [1976] formulated a linear stochas-

---

[3]Formally: $\xi(t)$ is a random variable, i.e. $\xi(t)(\alpha)$ with different realizations due to random variable α. The expectation $< \xi(t) >$ is thus the mean over all α :$< \xi(t)(\alpha) >_\alpha$. Using the ergodic hypothesis, the ensemble average $\langle \rangle$ can be expressed as the time average $\lim_{T\to\infty} \frac{1}{T} \int_{-T/2}^{T/2} dt$ of the function. Almost all points in any subset of the phase space eventually revisit the set. (https://en.wikipedia.org/wiki/Ergodic_theory

tic climate model

$$\frac{d}{dt}x(t) = Ax + \sigma\xi + F(t) \quad,$$ (8.12)

with system matrix $A \in \mathbf{R}^{n \times n}$, constant noise term σ, and stochastic process ξ. Many features of the climate system can be well described by (8.12), which is analogous to the Ornstein-Uhlenbeck process in statistical physics [Uhlenbeck and Ornstein, 1930]. Notice that $\sigma\xi$ represents a stationary random process. The relationship derived above is identical to that describing the diffusion of a fluid particle in a turbulent fluid. In a time-scale separated system, during one slow-time unit the fast uninteresting variables **y** perform many 'uncorrelated' events (provided that the fast dynamics are sufficiently chaotic). The contribution of the uncorrelated events to the dynamics of the slow interesting variables x is as a sum of independent random variables. By the weak central limit theorem this can be expressed by a normally distributed variable. Note, in the absence of any feedback effects Ax, the climate variations would continue to grow indefinitely as the Wiener process.

Numerical integration of the Langevin equation

One can numerically integrate such a nonlinear Langevin equation with flow $f(x)$ using a simple Euler-Maruyama method with a fixed time step Δt :

$$x(t + \Delta t) = x(t) + f(x)\Delta t + g(x)\sqrt{\Delta t}\Delta W_n$$ (8.13)

The variables ΔW_n are known as increments of the Wiener process; they are Gaussian numbers generated in an uncorrelated fashion, for example by using a pseudo-random number generator in combination with the Box-Müller algorithm.

```
% calculate sde in matlab\\
%
th = 1;
mu = 1.2;
sig = 0.3;
dt = 1e-2;
t= 0:dt:20;
```

```
x = zeros(1,length(t)); % Allocate output vector, set initial condition
rng(1);                  % Set random seed
for i = 1:length(t)-1
    x(i+1) = x(i)+th*(mu-x(i))*dt+sig*sqrt(dt)*randn;
end
figure;
plot(t,x);
```

and this is for the analytical solution:

```
th = 1;
mu = 1.2;
sig = 0.3;
dt = 1e-2;
t = 0:dt:20;      % Time vector
x0 = 0;           % Set initial condition
rng(1);           % Set random seed
ex = exp(-th*t);
x = x0*ex+mu*(1-ex)+sig*ex.*cumsum([0 sqrt(diff(exp(2*th*t)-1)).
        *randn(1,length(t)-1)])/sqrt(2*th);
figure;
plot(t,x);
```
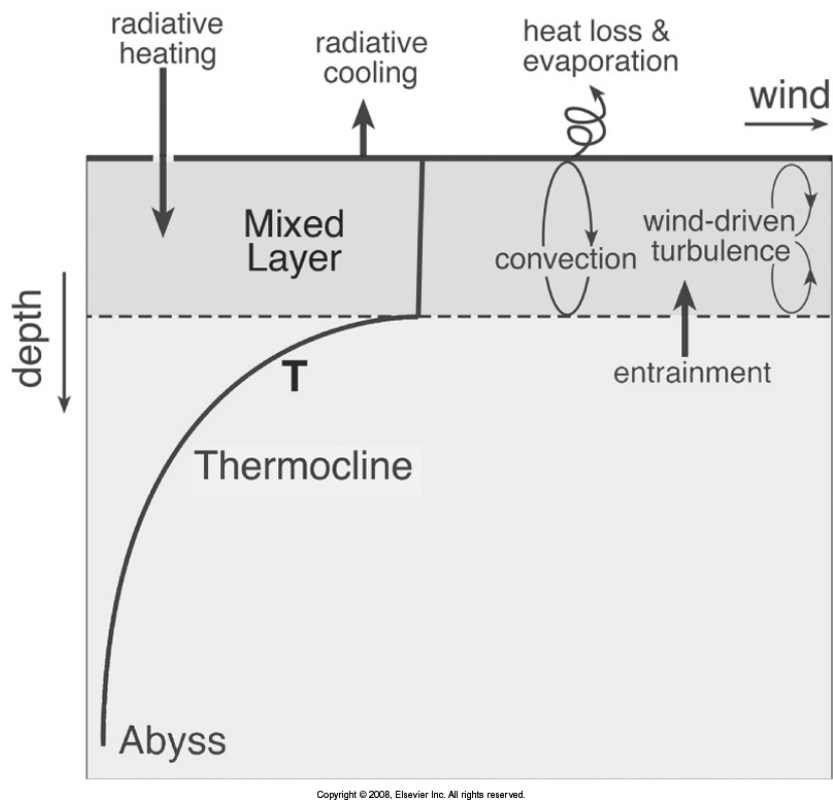
Figure 8.4: Schematic picture of mixed layer in the ocean.

Exercise 57   –   Stochastic Climate Model

Imagine that the temperature of the ocean mixed layer of depth h (Fig. 8.4) is governed by

$$\frac{dT}{dt} = -\lambda T + \frac{Q_{net}}{\gamma_O}, \tag{8.14}$$

where coefficient γ_O is given by the heat capacity time density times mixed layer depth $c_p \rho h$. ($h = 100m; c_p = 4.2 \cdot 10^3 Jkg^{-1}K^{-1}; \rho = 1023 kgm^{-3}$). λ is the typical damping rate of a temperature anomaly. Observations show that sea surface temperatures a typically damped at a rate of $15 W m^{-2} K^{-1}$.

1. Calculate the typical time scale $1/\lambda$.

2. Calculate the stochastic climate model using the R code

```
# Stochastic climate model/Ornstein-Uhlenbeck/Red Noise: Brown.R
T<-   5000    #integration time in time units
h<-   0.1    #step size in time units
X0<- 10       #inital value
beta<-0.05 #friction term
lambda<-1 #noise term
N<-T/h
t<-(0:(N-1))*h

x<-vector()
x[1]<-X0

for (i in 1:(N-1)) {
  x[i+1]<-x[i]*(1-beta*h)+ rnorm(1)*sqrt(h)
}

plot(t,x,type="l")
hist(x,freq=FALSE, col="gray")
```

From the online malterial, please see the browngui directory: BrownianMotion.zip See Figure 8.6.

3. Do the same, but for many Brownian particles in a potential (cf. Fig. 8.7).

```R
# Brownian motion, multiple particle: Brown_mult.R
# forward modelling

#the function dy/dt<-f(y,a,b,c,d)
f<-function(y,a,b,c,d)
{ return(d*y^3+c*y^2+b*y-a)     }

#constants
Ca<-10
a<-1
b<- 0.8
c<- 0
d<- -0.001

Nparticle<-1000 #number of particles
T<-  500   #integration time in time units
h<-  0.5   #step size in time units
N<-T/h
t<-(0:(N-1))*h

x<-matrix(10,Nparticle,N) # Initial condition, all = 0
# Initial condition,

for (i in 1:(N-1)) {
  x[,i+1]<- x[,i]+h*f(x[,i],a,b,c,d)   + Ca*rnorm(Nparticle)*sqrt(h)
}

ama2=max(x,2)
ami=min(x,-2)
ama=max(ama2,-ami)
plot(0,xlim=c(0,T),ylim=c(ami,ama),type="n")
for (i in 1:10) lines (t,x[i,],col=i)

#analyse the densities
h<-matrix(0,N,40)
for (i in 1:(N-1)) { h[i,]<-hist(x[,i],breaks=
      c(-20:20)*ama/10,freq=FALSE,ylim=c(0,0.04))$counts     }
hstat<-matrix(0,N)
for (i in N/2:(N-1)) hstat[]<-h[i,]+hstat[]
hstat[]<-hstat[] *2/Nparticle/N
#plot(t,hstat[],type="l")
plot(table(hstat[]), type = "h", col = "red")

# to show the time evolution, 1, 2, 4, 8, ....  time step
 op <- par(mfrow = c(3, 2))
plot(h[1,]/Nparticle,type="l")
plot(h[2,]/Nparticle,type="l")
plot(h[4,]/Nparticle,type="l")
plot(h[8,]/Nparticle,type="l")
plot(h[N/2,]/Nparticle,type="l")
```

```
plot(h[N-1,]+h[N-2,]/Nparticle/2,type="l")

filled.contour(t,(-19:20)*ama/10-ama/20,h,
      color.palette=rainbow,xlab="time",ylab="space")
```

4. Calculate the stationary density from the numerical example analytically using $\int f(y)dy$.
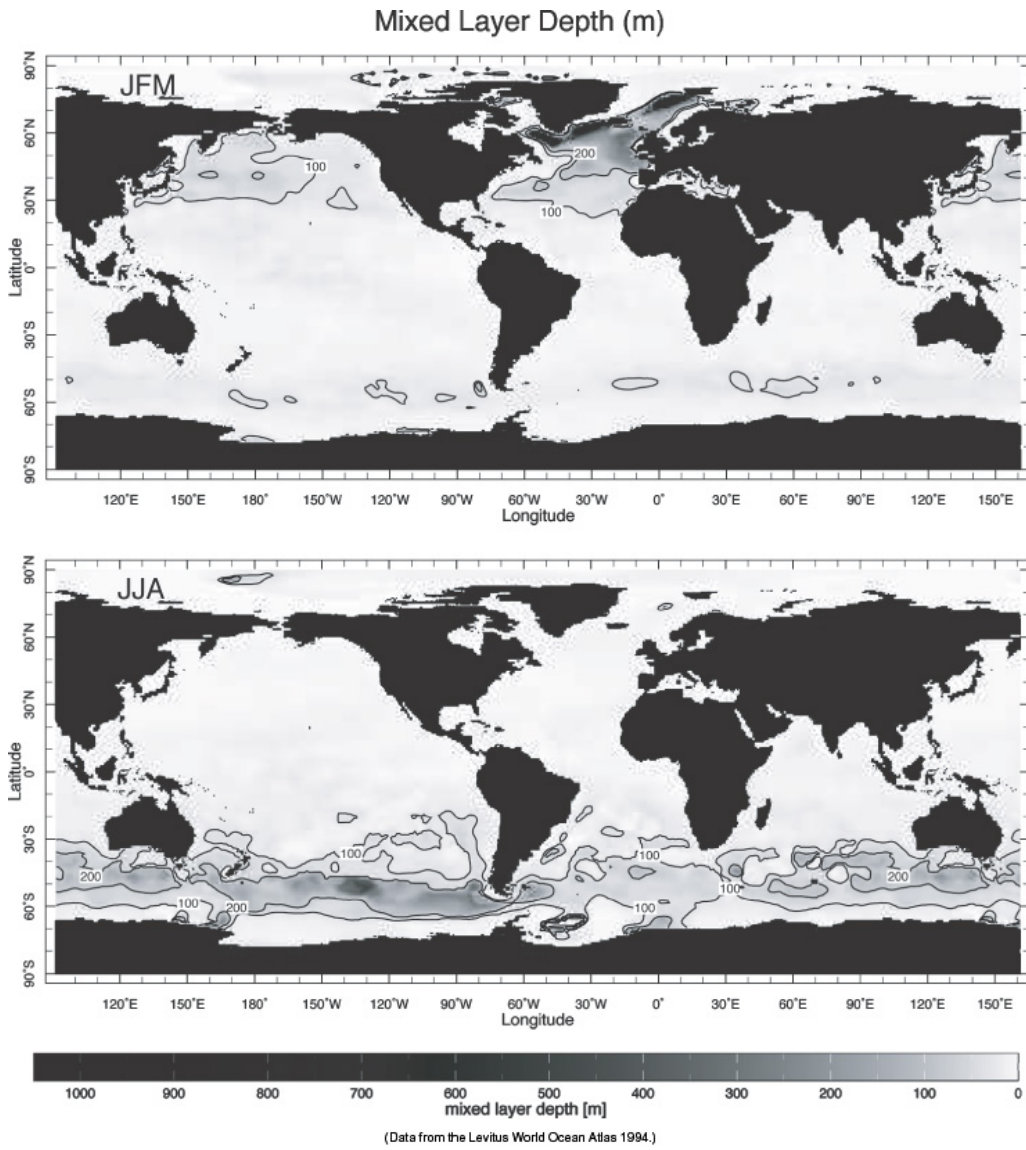
Figure 8.5: Mixed layer in the ocean distribution. Task: Describe the distribution of the seasonal mixed layer depth variations!
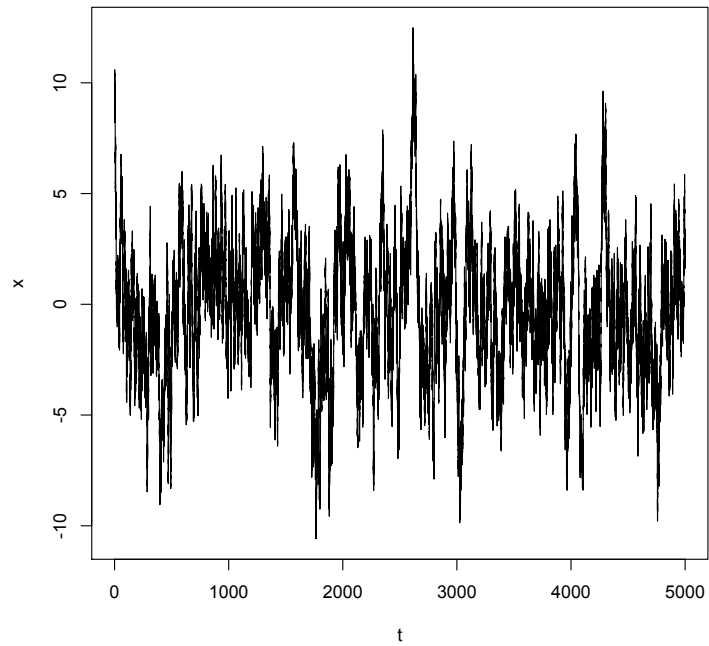
Figure 8.6: Stochastic Climate model, see (8.43).
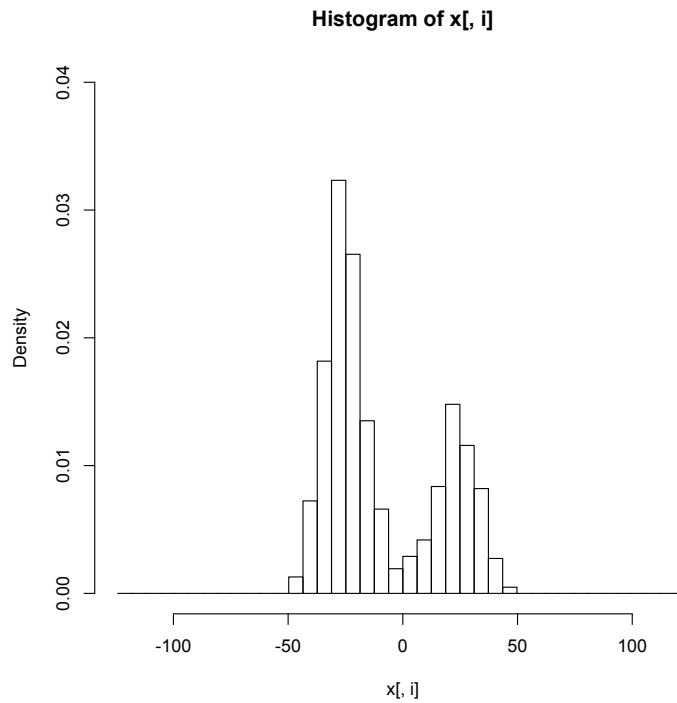
Histogram of x[, i]

Figure 8.7: Histogram: Stochastic Climate model in potential

An important example is the equation for geometric Brownian motion

$$\mathrm{d}X_t = \mu X_t \, \mathrm{d}t + \sigma X_t \, \mathrm{d}W_t. \tag{8.15}$$

which is the equation for the dynamics of the price of a stock in the Black Scholes options pricing model of financial mathematics. For an arbitrary initial value X_0 the above SDE has the analytic solution (https://en.wikipedia.org/wiki/Geometric_Brownian_motion):

$$X_t = X_0 \exp\left(\left(\mu - \frac{\sigma^2}{2}\right)t + \sigma W_t\right). \tag{8.16}$$

which is shown in Fig. 8.8.
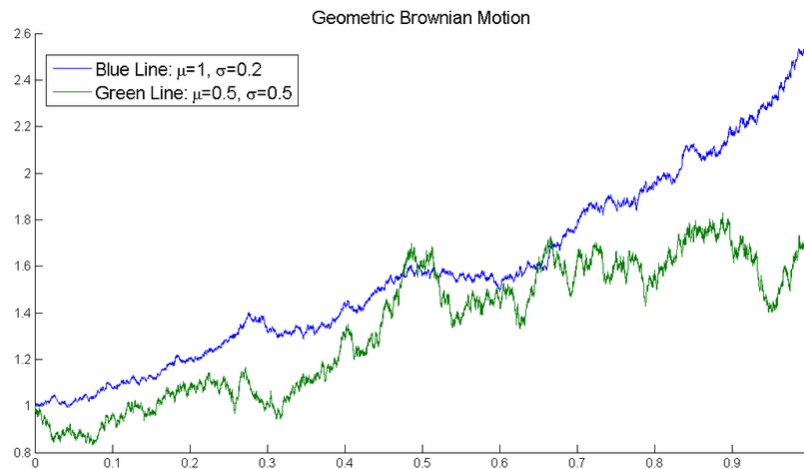
Figure 8.8: Two sample paths of Geometric Brownian motion, with different parameters. The blue line has larger drift, the green line has larger variance.

Exercise 58   –   Stochastic Stock market Model

1. Solve equation (8.16) in a similar way as exercise 57!
2. Why is X_t always positive?
3. Calculate the stationary density from the numerical example analytically using $\int f(y)dy$.

Exercise 59   –   Spectrum of Stochastic Climate Model

Imagine that the temperature of the ocean mixed layer of depth h is governed by

$$\frac{dT}{dt} = -\lambda T + \frac{Q_{net}}{\gamma_O}, \tag{8.17}$$

where coefficient γ_O is given by the heat capacity $c_p \rho h$, and λ is the typical damping rate of a temperature anomaly. The air-sea fluxes due to weather systems are represented by a white-noise process $Q_{net} = \hat{Q}_\omega e^{i\omega t}$ where $\hat{Q}_\omega$ is the amplitude of the random forcing at frequency ω and $\hat{Q}^*$ is the complex conjugate. Remember that Q_{net} can be described through its distribution and its correlation properties: a Gaussian distribution of zero average $< Q_{net} >= 0$ and δ-correlated in time $< Q_{net}(t)Q_{net}(t+\tau) >= \delta(\tau)$ The brackets indicate an average over realizations of the random force. The spectrum of a process x is defined as

$$S(\omega) := \langle \hat{x}\hat{x}^* \rangle = \widehat{Cov_x(\tau)} = \int_R \exp(i\omega\tau)Cov_x(\tau)d\tau \tag{8.18}$$

1. Calculate $S_Q(\omega)$ and describe why Q_{net} is called a white noise process.

2. Solve Eq. 8.17 for the temperature response $T = \hat{T}_\omega e^{i\omega t}$ and hence show that:

$$\hat{T}_\omega = \frac{\hat{Q}_\omega}{\gamma_O (\lambda + i\omega)} \tag{8.19}$$

3. Show that it has a spectral density $\hat{T}_\omega \hat{T}_\omega^*$ is given by:

$$\hat{T}\hat{T}^* = \frac{\hat{Q}\hat{Q}^*}{\gamma_O^2 (\lambda^2 + \omega^2)} \tag{8.20}$$

and the spectrum

$$S(\omega) =< \hat{T}\hat{T}^* >= \frac{1}{\gamma_O^2 (\lambda^2 + \omega^2)}. \tag{8.21}$$

The brackets $< \cdots >$ denote the ensemble mean. Make a sketch of the spectrum using a

log-log plot and show that fluctuations with a frequency greater than λ are damped.

4. Calculate the spectrum of a regular oszillation with noise. How does the spectrum changes when you rectify the signal?

```
a<-sin(2*pi*(1:5000)/20)+0.5*rnorm(5000)/10
plot(a,type="l",xlim = c(0,2*pi*20),xlab='time (kyrs)',ylab='forcing')
b<-pmax(-0.1,a)   # rectify the signal
plot(b,type="l",col="red",xlim=c(0,2*pi*20),
  xlab='time (kyrs)',ylab='climate')
sa<-spectrum(a,spans=10,
  main="Spectrum of forcing (spans=10)",col="blue")
sb<-spectrum(b,spans=10, col="red")
plot(sa,col="blue",main="Spectrum of the rectified signal (spans=10)")
plot(sb,add = TRUE, col = "red")
```
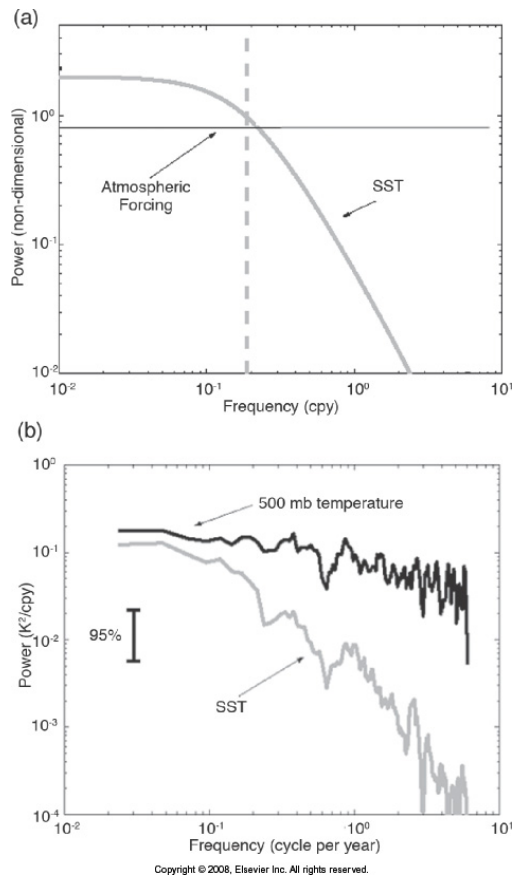
Figure 8.9: Powerspectrum of atmospheric temperature and sea surface temperature. Here $1/\lambda = 300$ days from equation (8.43).

Exercise 60   –   Climate sensitivity and variability in the Stochastic Climate Model

As in exercise 59, imagine that the temperature of the ocean mixed layer of depth h is governed by

$$\frac{dT}{dt} = -\lambda T + Q_{net} + f(t) , \tag{8.22}$$

where the air-sea fluxes due to weather systems are represented by a white-noise process with zero average $< Q_{net} >= 0$ and δ-correlated in time $< Q_{net}(t)Q_{net}(t+\tau) >= \delta(\tau)$. The function $f(t)$ is a time dependent deterministic forcing. Assume furthermore that $f(t) = c \cdot u(t)$ with $u(t)$ as unit step or the so-called Heaviside step function and solve (8.22). What is the relationship of the dissipation (through λ) and the fluctuations (through the spectrum $S(\omega)$) ?

Solution

Since $Q(t)$ is a stochastic process, it has to be solved for the moments. Because $< Q_{net} >= 0, < T(t) >$ can be solved using the Laplace transform:

$$< T(t) > = \mathcal{L}^{-1}\{F(s)\}(t) = \mathcal{L}^{-1}\left\{ \frac{< T(0) >}{s + \lambda} + \frac{c}{s} \cdot \frac{1}{s + \lambda} \right\} \tag{8.23}$$

$$= T(0) \cdot \exp(-\lambda t) + \frac{c}{\lambda} (1 - \exp(-\lambda t)) \tag{8.24}$$

because we have $< T(0) >= T(0)$. As equilibrium response, we have

$$\Delta T = \lim_{t \to \infty} < T(t) >= \frac{c}{\lambda} . \tag{8.25}$$

The fluctuation can be characterized by the spectrum (exercise 59)

$$S(\omega) =< \hat{T}\hat{T}^* >= \frac{1}{\lambda^2 + \omega^2}. \tag{8.26}$$

and therefore, the spectrum and the equilibrium response are closely coupled (fluctuation-dissipation theorem).

For some energy considerations, it is usefull to re-write equation (8.22) as

$$C \frac{dT}{dt} = -\lambda_C T + f_C \,, \tag{8.27}$$

with $C = c_p \rho dz$ as the heat capacity of the ocean. For a depth of 200 m of water distributed over the globe, $C = 4.2 \cdot 10^3 \, W s \, kg^{-1} K^{-1} \times 1000 \, kg \, m^{-3} \times 200 \, m = 8.4 \cdot 10^8 \, W s \, m^{-2} \, K^{-1}$. The temperature evolution is

$$T(t) = T(0) \cdot \exp(-\lambda_c/C \, t) + \frac{f_C}{\lambda_C} \left(1 - \exp(-\lambda_C/C \, t)\right) \tag{8.28}$$

The left hand side of (8.27) represents the heat uptake by the ocean, which plays a central role in the transient response of the system to a perturbation (8.28).

Typical changes in f_C are $4 \, W m^{-2}$ for doubling of CO_2, $\lambda_C = 1 - 2 \, W m^{-2} K^{-1}$. The typical time scale for a mixed layer ocean is $C/\lambda_C = 13 - 26$ years . Please note that the climate system is simplified by a slab ocean with homogenous temperature and heat capacity. This is an approximation as the heat capacity should vary in time as the perturbation penetrates to deeper oceanic levels.

The equilibrium temperature change ΔT is

$$\Delta T = \frac{\Delta f_C}{\lambda_C} = \frac{c}{\lambda} \tag{8.29}$$

with values of $\Delta T = 2 - 4$ K. The term $CS = \frac{1}{\lambda_C}$ is called climate sensitivity to a radiative forcing Δf_C:

$$\Delta T = CS \cdot \Delta f_C \quad . \tag{8.30}$$

In the literature, the concept of climate sensitivity is quite often used as the equilibrium temperature increase for a forcing Δf_C related to doubling of CO_2.

Exercise 61   –   Stochastic differential equation

Tasks:

1. Simulate the velocity evolution of one particle which is determined by the following stochas-
   tic $dv/dt = -b * v + k * dW(t)/dt$

2. What happens if you change the timestep?

3. Simulate the ensemble of multiple particles, plot the time evolution of the v-Distribution

4. Test the ergodic theorem: time average = ensemble average

Solution

```
#brownian motion, one particle

T<-   5000     #integration time in time units
h<-   0.1    #step size in time units
X0<- 10       #inital value

beta<-0.05 #friction term
lambda<-1 #noise term

N<-T/h
t<-(0:(N-1))*h

x<-vector()
x[1]<-X0

for (i in 1:(N-1))
{
  x[i+1]<-x[i]*(1-beta*h)+ rnorm(1)*sqrt(h)
}

plot(t,x,type="l")
# dev.print(postscript, file="random.ps")
#hist(x)
#hist(x,freq=FALSE, col="gray")
```

Solution brownian motion, multiple particle

```
#brownian motion, multiple particle
#forward modelling

#the function dy/dt<-f(y,a,b,c,d)
# double well potential
```

```r
f<-function(y,a,b,c,d)
{
  return(d*y^3+c*y^2+b*y-a)
}



#constants
Ca<-10  # noise

a<-1
b<- 0.8
c<- 0
d<- -0.001

# to do: caculate the stationary density analytically:  int 2/Ca f(y) dy

Nparticle<-1000 #number of particles
T<-  1000   #integration time in time units
h<-  0.5   #step size in time units

N<-T/h
t<-(0:(N-1))*h

x<-matrix(10,Nparticle,N) # Initial condition, all = 0
#x<-matrix(rnorm(Nparticle)*10,Nparticle,N) # Initial condition,

for (i in 1:(N-1))
{
  x[,i+1]<- x[,i]+h*f(x[,i],a,b,c,d)  + Ca*rnorm(Nparticle)*sqrt(h)
}

ama2=max(x,2)
ami=min(x,-2)
ama=max(ama2,-ami)

plot(0,xlim=c(0,T),ylim=c(ami,ama),type="n")  # frame
#plot(0,xlim=c(0,T),ylim=c(-100,100),type="n") # with fixed ylim

# plot the realizations in different colors
for (i in 1:10) lines (t,x[i,],col=i)


#analyse the densities: time evolution
h<-matrix(0,N,40)
#for (i in 1:(N-1)) h[i,]<-hist(x[,i],breaks=c((-20:20)*10),
#           plot=FALSE)$counts

for (i in 1:(N-1)) h[i,]<-hist(x[,i],breaks=c(-20:20)*ama/10,
        freq=FALSE,ylim=c(0,0.04))$counts

#hstat<-matrix(0,N)
```

```
#for (i in N/2:(N-1)) hstat[]<-h[i,]+hstat[]
#hstat[]<-hstat[] *2/Nparticle/N
#plot(t,hstat[],type="l")
 plot(table(hstat[]), type = "h", col = "red")

 op <- par(mfrow = c(3, 2))
plot(h[1,]/Nparticle,type="l")
plot(h[2,]/Nparticle,type="l")
plot(h[4,]/Nparticle,type="l")
plot(h[8,]/Nparticle,type="l")
plot(h[N/2,]/Nparticle,type="l")
plot(h[N-1,]+h[N-2,]/Nparticle/2,type="l")


#filled.contour(t,(-19:20)*10-5,h,color.palette=rainbow,xlab="time",
#              ylab="space")

filled.contour(t,(-19:20)*ama/10-ama/20,h,color.palette=rainbow,
              xlab="time",ylab="space")

#dev.print(postscript, file="/tmp/out.ps")
# system("lpr -Pps3 /tmp/out.ps")
```

8.3 Sprectral methods

8.3.1 Fourier transform

The Fourier transform decomposes a function of time (e.g., a signal) into the frequencies that make it up, similarly to how a musical chord can be expressed as the amplitude (or loudness) of its constituent notes. The Fourier transform of a function of time itself is a complex-valued function of frequency, whose absolute value represents the amount of that frequency present in the original function, and whose complex argument is the phase offset of the basic sinusoid in that frequency. The Fourier transform is called the frequency domain representation of the original signal. The term Fourier transform refers to both the frequency domain representation and the mathematical operation that associates the frequency domain representation to a function of time (see also https://en.wikipedia.org/?title=Fourier_transform).

The Fourier transformation of x is defined as

$$\hat{x}(\omega) = \int_{\mathsf{R}} x(t)e^{i\omega t}\,dt \tag{8.31}$$

and is denoted as a hat in the following.[4] And the inverse Fourier transformation of x is defined as

$$x(t) = \frac{1}{2\pi}\int_{\mathsf{R}} \hat{x}(\omega)e^{-i\omega t}\,d\omega \tag{8.32}$$

or with $\omega = 2\pi\nu$:

$$x(t) = \int_{\mathsf{R}} \hat{x}e^{-i2\pi\nu t}\,d\nu \quad . \tag{8.33}$$

---

[4]Other common notations for the Fourier transform $\hat{x}(\omega)$: $\tilde{x}(\omega)$, $\bar{x}(\omega)$, $F(\xi)$, $\mathcal{F}(x)(\omega)$, $(\mathcal{F}x)(\omega)$, $\mathcal{F}(x)$, $\mathcal{F}(\omega)$, $F(\omega)$. The sign of the exponential in the Fourier transform is something that we are concerned with for many years. Of course, there are two conventions that have been used with almost equal frequency, but I try to stick to one of them to avoid confusion. Here, we have used the convention of the positive sign in the exponential for the forward transform which represents the Fraunhofer diffraction pattern for a real-space object. This is consistent with assuming that a plane wave, going in positive direction in real space is written $\exp[i(\omega t - kx)]$ rather than a minus sign before the i, so that the phase advances with time.

Exercise 62   –   Fourier transformation

Tasks: Calculate the Fourier transformation of

1. $x(t + a)$ (time shift).

2. $x(t * a)$ (Scaling in the time domain).

3. $\frac{d}{dt}x(t)$ (time derivative).

4. $x(t) = \exp(-at^2)$ (Gaussian).

5. $x(t) = \delta(t)$ where the δ distribution is definedthrough the operator on any function y:
   $y(t_0) = \int_{\mathsf{R}} y(t)\delta(t - t_0)\ dt$

6. Show that for $x(t) = \exp(-iat)$, the Fourier transformation $\hat{x}(\omega) = 2\pi\delta(\omega - a)$. Hint: use the Fourier back transformation (8.31).

7. Calculate the Fourier transformation of a the periodic function $x(t) = \sin(\omega_0 t)$. Remember that $\sin x = \frac{1}{2i}\left(e^{ix} - e^{-ix}\right)$.

8. Prove the Uncertainty principle: the more concentrated $x(t)$ is, the more spread out its Fourier transform $\hat{x}(\omega)$ must be. In particular, the scaling property of the Fourier transform may be seen as saying: if we "squeeze" a function in t, its Fourier transform "stretches out" in ω. It is not possible to arbitrarily concentrate both a function and its Fourier transform.

9. Consider the sine and cosine transforms and show the following. Fourier's original formulation of the transform did not use complex numbers, but rather sines and cosines. Statisticians and others still use this form. An absolutely integrable function f for which Fourier inversion holds good can be expanded in terms of genuine frequencies (avoiding negative frequencies, which are sometimes considered hard to interpret physically) λ by

$$f(t) = \int_0^\infty [a(\lambda)\cos 2\pi\lambda t + b(\lambda)\sin 2\pi\lambda t]\ d\lambda. \qquad (8.34)$$

This is called an expansion as a trigonometric integral, or a Fourier integral expansion. The coefficient functions a and b can be found by using variants of the Fourier cosine transform

and the Fourier sine transform (the normalisations are, again, not standardised):

$$a(\lambda) = 2 \int_{-\infty}^{\infty} f(t) \cos(2\pi\lambda t) dt \tag{8.35}$$

$$b(\lambda) = 2 \int_{-\infty}^{\infty} f(t) \sin(2\pi\lambda t) dt. \tag{8.36}$$

Laplace transform

The Fourier transform is intimately related with the Laplace transform $F(s)$, which is also used for the solution of differential equations and the analysis of filters (https://en.wikipedia.org/wiki/Laplace_transform). We introduce the complex variable $s = -i\omega$.

$$\mathcal{L}\{x(t)\} = F(s) = \int_0^{\infty} e^{-st} x(t) dt \tag{8.37}$$

It follows (integration by parts for 8.38)

$$\mathcal{L}\left\{\frac{d}{dt}x(t)\right\} = sF(s) - x(0) \tag{8.38}$$

$$\mathcal{L}\{\exp(-at)\} = \frac{1}{s+a} \tag{8.39}$$

$$\mathcal{L}\{-\exp(-at) + \exp(-bt)\} = \frac{-1}{s+a} + \frac{1}{s+b} = \frac{a-b}{(s+a)(s+b)} \tag{8.40}$$

The Laplace transform of a sum is the sum of Laplace transforms of each term.

$$\mathcal{L}\{f(t) + g(t)\} = \mathcal{L}\{f(t)\} + \mathcal{L}\{g(t)\} \tag{8.41}$$

The Laplace transform of a multiple of a function is that multiple times the Laplace transformation

Function	Time domain $f(t) = \mathcal{L}^{-1}\{F(s)\}$	Laplace s-domain $F(s) = \mathcal{L}\{f(t)\}$
unit impulse	$\delta(t)$	1
delayed impulse	$\delta(t - \tau)$	$e^{-\tau s}$
unit step	$u(t)$	$\frac{1}{s}$
delayed unit step	$u(t - \tau)$	$\frac{1}{s}e^{-\tau s}$
exponential decay	$e^{-\alpha t} \cdot u(t)$	$\frac{1}{s+\alpha}$
sine	$\sin(\omega t) \cdot u(t)$	$\frac{\omega}{s^2+\omega^2}$
cosine	$\cos(\omega t) \cdot u(t)$	$\frac{s}{s^2+\omega^2}$
decaying sine wave	$e^{-\alpha t}\sin(\omega t) \cdot u(t)$	$\frac{\omega}{(s+\alpha)^2+\omega^2}$
decaying cosine wave	$e^{-\alpha t}\cos(\omega t) \cdot u(t)$	$\frac{s+\alpha}{(s+\alpha)^2+\omega^2}$
natural logarithm	$\ln(t) \cdot u(t)$	$-\frac{1}{s}\left[\ln(s) + \gamma\right]$
Convolution	$(f * g)(t) = \int_0^t f(\tau)g(t - \tau)\,d\tau$	$F(s) \cdot G(s)$

Table 8.1: Laplace transformation (https://en.wikipedia.org/wiki/Laplace_transform.

of that function.

$$\mathcal{L}\{af(t)\} = a\mathcal{L}\{f(t)\} \tag{8.42}$$

Using this linearity, and various trigonometric, hyperbolic, and complex number (etc.) properties and/or identities, some Laplace transforms can be obtained from others quicker than by using the definition directly.

Exercise 63   –   Laplace transformation of mixed layer model

Solve the Imagine that the temperature of the ocean mixed layer is governed by

$$\frac{dT}{dt} = -\lambda T + Q(t)\,, \tag{8.43}$$

where λ is the typical damping rate of a temperature anomaly and $Q(t)$ a forcing.

1. Use the Laplace transformation to show

$$F(s) = \frac{Q(s) + T(0)}{s + \lambda} \quad . \tag{8.44}$$

where $Q(s) = \mathcal{L}\{Q(t)\}$

2. Consider the special case $Q(t) = \exp(i\omega_0 t)$, then $Q(s) = \frac{1}{s - i\omega_0}$. The forcing and the temperature is of course a real number, by representing is as a complex number we can simultaneously keep track of both phase components. Show

$$F(s) = \frac{T(0) + Q(s)}{s + \lambda} = \frac{T(0)}{s + \lambda} + \frac{1}{(s + \lambda)} \frac{1}{(s - i\omega_0)} \tag{8.45}$$

and via the Laplace back-transformation and (8.39, 8.40) that

$$T(t) = \exp(-\lambda t)T(0) + \frac{[\exp(i\omega_0 t) - \exp(-\lambda t)]}{\lambda + i\omega_0} \quad . \tag{8.46}$$

3. Calculate the real and complex part of (8.46).

4. Show: At low frequencies, the output is equal to the input. At high frequencies it rolls off as $1/\omega$ (it is a low-pass filter) and is out of phase by $90°$.

Let $x(t)$ be the input to a general linear time-invariant system, and $y(t)$ be the output, and the Laplace transform of $x(t)$ and $y(t)$ be $X(s)$ and $Y(s)$. Then, the output is related to the input by convolution with respect to the impulse response $h(t)$ by

$$y(t) = \int_0^\infty h(t')x(t - t')dt \tag{8.47}$$

Because of the convolution, the transfer function $H(s)$ is equal to the to the ratio of the Laplace

transforms of the input and output

$$H(s) = \frac{Y(s)}{X(s)}. \tag{8.48}$$

The impulse response of a linear transformation is the image of Dirac's delta function under the transformation, analogous to the fundamental solution of a partial differential operator. The general feature of the transfer function is that is the ratio of two polynomials. Since the polynomials can be constructed from knowledge of the roots, the location of the poles and zeros completetly characterizes the response of the system. The system is globally stable if all poles lie in the left half-plane with Re(poles) < 0. For example $\mathcal{L}\left\{\exp(-at)\right\} = \frac{1}{s+a}$, i.e. the system is stable if $Re(a) < 0$. Poles off the real axes are associated with oscillations. Summarizing, the convolution that gives the output of the system can be transformed to a multiplication in the transform domain, given signals for which the transforms exist

$$y(t) = (h * x)(t) \stackrel{\text{def}}{=} \int_{-\infty}^{\infty} h(t - \tau)x(\tau) \, d\tau \stackrel{\text{def}}{=} \mathcal{L}^{-1}\{H(s)X(s)\}. \tag{8.49}$$

Transfer functions are commonly used in the analysis of systems such as single-input single-output filters, typically within the fields of signal processing, communication theory, and control theory. The term is often used exclusively to refer to linear, time-invariant systems. The descriptions below are given in terms of a complex variable, $s = \sigma - i\omega$, which bears a brief explanation. In many applications, it is sufficient to define $\sigma = 0$, which reduces the Laplace transforms with complex arguments to Fourier transforms with real argument ω. The applications where this is common are ones where there is interest only in the steady-state response.[5] The stability of linear systems will be discussed further in section **??**.

---

[5]In discrete-time systems, the relation between an input signal x(t) and output y(t) is dealt with using the z-transform, and then the transfer function is similarly written as $H(z) = \frac{Y(z)}{X(z)}$ and this is often referred to as the pulse-transfer function.

Exercise 64   –   Method of partial fraction expansion

Consider a linear time-invariant system with transfer function

$$H(s) = \frac{1}{(s+\alpha)(s+\beta)}. \tag{8.50}$$

The impulse response is simply the inverse Laplace transform of this transfer function:

$$h(t) = \mathcal{L}^{-1}\{H(s)\}. \tag{8.51}$$

To evaluate this inverse transform, we begin by expanding $H(s)$ using the method of partial fraction expansion:

$$\frac{1}{(s+\alpha)(s+\beta)} = \frac{P}{s+\alpha} + \frac{R}{s+\beta}. \tag{8.52}$$

The unknown constants P and R are the residues located at the corresponding poles of the transfer function. Each residue represents the relative contribution of that singularity to the transfer function's overall shape. By the residue theorem, the inverse Laplace transform depends only upon the poles and their residues. To find the residue P, we multiply both sides of the equation by $s + \alpha$ to get

$$\frac{1}{s+\beta} = P + \frac{R(s+\alpha)}{s+\beta}. \tag{8.53}$$

Then by letting $s = -\alpha$, the contribution from R vanishes and all that is left is

$$P = \left.\frac{1}{s+\beta}\right|_{s=-\alpha} = \frac{1}{\beta - \alpha}. \tag{8.54}$$

Similarly, the residue R is given by

$$R = \left.\frac{1}{s+\alpha}\right|_{s=-\beta} = \frac{1}{\alpha - \beta}. \tag{8.55}$$

Note that

$$R = \frac{-1}{\beta - \alpha} = -P \tag{8.56}$$

and so the substitution of R and P into the expanded expression for H(s) gives

$$H(s) = \left(\frac{1}{\beta - \alpha}\right) \cdot \left(\frac{1}{s + \alpha} - \frac{1}{s + \beta}\right). \tag{8.57}$$

Finally, using the linearity property and the known transform for exponential decay (see in the Table 8.1 of Laplace transforms, above), we can take the inverse Laplace transform of H(s) to obtain:

$$h(t) = \mathcal{L}^{-1}\{H(s)\} = \frac{1}{\beta - \alpha}\left(e^{-\alpha t} - e^{-\beta t}\right), \tag{8.58}$$

which is the impulse response of the system. (This example will be used in section **??** with more details of the Laplace transformation.)

Exercise 65   –   Convolution

The same result can be achieved using the convolution property as if the system is a series of filters with transfer functions of $1/(s + a)$ and $1/(s + b)$. That is, the inverse of

$$H(s) = \frac{1}{(s + a)(s + b)} = \frac{1}{s + a} \cdot \frac{1}{s + b} \tag{8.59}$$

is

$$\mathcal{L}^{-1}\left\{\frac{1}{s + a}\right\} * \mathcal{L}^{-1}\left\{\frac{1}{s + b}\right\} \tag{8.60}$$

$$= e^{-at} * e^{-bt} = \int_0^t e^{-ax}e^{-b(t-x)} \, dx \tag{8.61}$$

$$= \frac{e^{-at} - e^{-bt}}{b - a}. \tag{8.62}$$

An integral formula for the inverse Laplace transform, is given by the line integral:

$$x(t) = \mathcal{L}^{-1}\{F(s)\}(t) = \frac{1}{2\pi i} \lim_{T \to \infty} \int_{\gamma-iT}^{\gamma+iT} e^{st} F(s) \, ds, \tag{8.63}$$

where the integration is done along the vertical line $Re(s) = \gamma$ in the complex plane such that γ is greater than the real part of all singularities of F(s). This ensures that the contour path is in the region of convergence. If all singularities are in the left half-plane, or F(s) is a smooth function on $-\infty < Re(s) < \infty$ (i.e., no singularities), then γ can be set to zero and the above inverse integral formula above becomes identical to the inverse Fourier transform.(https://en.wikipedia.org/wiki/Residue_theorem). The function f(t)=INVLAP(F(s)) offers a simple, effective and reasonably accurate way to achieve the result.[6] The transform F(s) may be any reasonable function of complex variable s^α, where α is an integer or non-integer real exponent. Thus, the function INVLAP can solve even fractional problems and invert functions F(s) containing rational, irrational or transcendental expressions. The function does not require to compute poles nor zeroes of F(s). It is based on values of F(s) for selected complex values of the independent variable s. The resultant computational error can be held arbitrarily low at the cost of CPU time (see Examples).

Here is the matlab code for the Numerical Inversion of Laplace Transforms with some examples 0, 1, 2

8.3.2 Covariance and spectrum

A stationary process exhibits an autocovariance function of the form

$$Cov(\tau) = \langle (x(t+\tau) - \langle x \rangle)(x(t) - \langle x \rangle) \rangle \tag{8.64}$$

---

[6]It is based on the paper: J. Valsa and L. Brancik: Approximate Formulae for Numerical Inversion of Laplace Transforms, Int. Journal of Numerical Modelling: Electronic Networks, Devices and Fields, Vol. 11, (1998), pp. 153-166.

where $\langle \dots \rangle$ denotes the statistical ensemble mean.[7] Normalized to the variance (i.e. the autoco-variance function at $\tau = 0$) one gets the autocorrelation function $C(\tau)$:

$$C(\tau) = Cov(\tau)/Cov(0) \quad . \tag{8.65}$$

Many stochastic processes in nature exhibit short-range correlations, which decay exponentially:

$$C(\tau) \sim \exp(-\tau/\tau_0), \text{ for } \tau \to \infty \tag{8.66}$$

These processes exhibit a typical time scale τ_0. For a white noise process ξ (as defined in 8.10), the autocorrelation function $C(\tau)$ is given by

$$C(\tau) = \delta(\tau) \quad . \tag{8.67}$$

Spectrum of the stochastic process

The Fourier transformation of the random variable x is

$$\hat{x}(\omega) = \int_{\mathbb{R}} x(t)e^{i\omega t}\, dt \quad = \lim_{T \to \infty} \int_{-T/2}^{T/2} x(t)e^{i\omega t}\, dt \tag{8.68}$$

and is also a ramdom variable, but its power spectral density $S(\omega)$ is not:

$$S(\omega) \quad := \quad \langle \hat{x}\hat{x}^+ \rangle = \langle |\hat{x}(\omega)|^2 \rangle \quad . \tag{8.69}$$

Using the **ergodic hypothesis**, the ensemble average $S(\omega) = \langle \hat{x}\hat{x}^+ \rangle$ can be expressed as the time average

$$\lim_{T \to \infty} \frac{1}{T} \int_{-T/2}^{T/2} dt \quad \hat{x}\hat{x}^+ \tag{8.70}$$

---

[7]For the covariance, one can have two processes $Cov(\tau) = \langle (x(t+\tau) - \langle x \rangle)(y(t) - \langle y \rangle) \rangle$.

and therefore the spectrum can be expressed as

$$S(\omega) = \lim_{T \to \infty} \frac{1}{T} \int_{-T/2}^{T/2} e^{i\omega t} x(t) dt \quad \int_{-T/2}^{T/2} e^{-i\omega t'} x(t') dt' \quad . \tag{8.71}$$

The "total" integrated spectral density equals the variance of the series. Thus the spectral density within a particular interval of frequencies can be viewed as the amount of the variance explained by those frequencies. Mathematically, the spectral density is defined for both negative and positive frequencies. However, due to symmetry of the function $S(\omega)$ is quite often displayed for positive values only.

Let us calculate the inverse Fourier transformation of $S(\omega)$ and calculate the relation to the autocovariance function $Cov(\tau)$ of the stationary process $x(t)$:

$$\frac{1}{2\pi} \int_{\mathsf{R}} S(\omega) \ e^{-i\omega \tau} d\omega$$

$$= \lim_{T \to \infty} \frac{1}{T} \int_{\mathsf{R}} d\omega \frac{e^{-i\omega \tau}}{2\pi} \int_{-T/2}^{T/2} e^{i\omega t} x(t) dt \int_{-T/2}^{T/2} e^{-i\omega t'} x(t') dt'$$

$$= \lim_{T \to \infty} \frac{1}{T} \int_{-T/2}^{T/2} \int_{-T/2}^{T/2} \left(\frac{1}{2\pi} \int_{\mathsf{R}} e^{i\omega(t-t'-\tau)} d\omega \right) x(t) x(t') dt dt'$$

$$= \lim_{T \to \infty} \frac{1}{T} \int_{-T/2}^{T/2} \int_{-T/2}^{T/2} \delta(t - t' - \tau) x(t) x(t') dt dt' \tag{8.72}$$

$$= \lim_{T \to \infty} \frac{1}{T} \int_{-T/2}^{T/2} x(t) x(t - \tau) dt \tag{8.73}$$

$$= \langle x(t) x(t - \tau) \rangle = Cov(\tau) \tag{8.74}$$

The transformation (8.72) comes from the Fourier transform of the $\delta-$function:

$$\int_{\mathbf{R}} e^{-i\omega t}\delta(t)dt = 1 \quad \longrightarrow \quad \delta(t) = \frac{1}{2\pi}\int_{\mathbf{R}} e^{i\omega t}d\omega \tag{8.75}$$

As the frequency domain counterpart of the autocovariance function of a stationary process, one can calculate the spectrum as

$$S(\omega) = \widehat{Cov(\tau)} \quad , \tag{8.76}$$

where the hat denotes again the Fourier transformation. This is the Wiener-Chinchin theorem, relating the sprectrum of a random process to its autocorrelation function (Fig. **??**).

The white noise process

The white noise process is therefore a function with constant $S(\omega)$, since the autocovariance is a delta dunction (8.67). The color of a noise signal (a signal produced by a stochastic process) is generally understood to be some broad characteristic of its power spectrum. This sense of 'color' for noise signals is similar to the concept of timbre in music (which is also called "tone color"); however the latter is almost always used for sound, and may consider very detailed features of the spectrum. The practice of naming kinds of noise after colors started with white noise, a signal whose spectrum has equal power within any equal interval of frequencies. That name was given by analogy with white light, which was (incorrectly) assumed to have such a flat power spectrum over the visible range. Other color names, like pink, red, and blue were then given to noise with other spectral profiles, often (but not always) in reference to the color of light with similar spectra. Some of those names have standard definitions in certain disciplines, while others are very informal and poorly defined. Noise is somehow opposite to music where we hear distinct frequencies (see for the frequencies of music: https://en.wikipedia.org/wiki/Piano_key_frequencies).

In equal temperament, one starts from a reference such as the note A, which is usually taken to

have frequency 440 Hz. All other notes have frequencies of the form 440 Hz $*a^n$ where n is the number of semitones between the note in question and the reference note A. The ratio of an equal-tempered semitone is $a = \sqrt[12]{2} = 1.05946\ (a^{12} = 2)$. In equal temperament, enharmonic notes such as $C^{\#}$ and D^{b} are acoustically identical, they share the same frequency. Equal temperament was well-suited for the kind of music that was written from the eighteenth century onward, with its much greater range of modulations and chromatic harmonic vocabulary.

In Pythagorean tuning, intervals are derived by successions of perfect fifths, so the corresponding frequency ratios are powers of $3/2$. In conventional Western music, twelve perfect fifths in succession,

$$C - G - D - A - E - B - F^{\#} - C^{\#} - G^{\#} - D^{\#} - A^{\#} - E^{\#} - B^{\#},$$

are supposed to equal seven octaves (C = B#). However, since $(3/2)^{12}$ does not equal 2^{7}, twelve Pythagorean perfect fifths give an interval slightly larger than seven octaves. The difference is a small interval known as the Pythagorean comma, which corresponds to a ratio of $(3/2)^{12}$ to $2^{7} \approx 1.013643$. The system of equal temperament gradually became adopted because it removed the limitations on keys for modulation. The discrepancies between just and equaltempered intervals are small and easily accepted by most listeners.
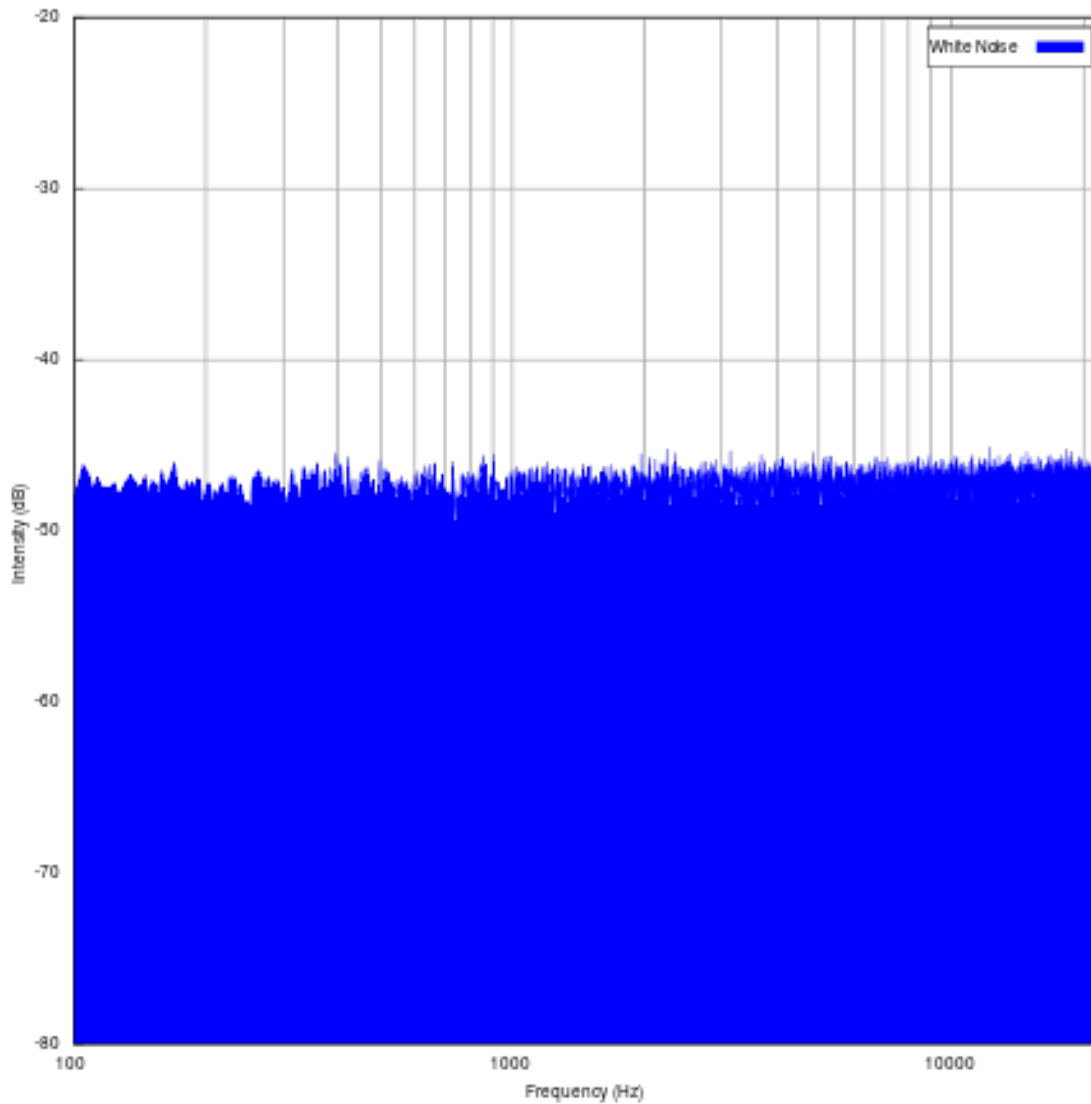
Figure 8.10: White noise spectrum. Flat power spectrum. (logarithmic frequency axis). For example, with a white noise audio signal, the range of frequencies between 40 Hz and 60 Hz contains the same amount of sound power as the range between 400 Hz and 420 Hz, since both intervals are 20 Hz wide. Note that spectra are often plotted with a logarithmic frequency axis rather than a linear one, in which case equal physical widths on the printed or displayed plot do not all have the same bandwidth, with the same physical width covering more Hz at higher frequencies than at lower frequencies. In this case a white noise spectrum that is equally sampled in the logarithm of frequency (i.e., equally sampled on the X axis) will slope upwards at higher frequencies rather than being flat.

8.4   Projection methods: coarse graining*

In order to get a first idea of coarse graining, one one may think of the transition from Rayleigh-Bénard convection to the Lorenz system (section 2.2). In our formula, the Galerkin approximation (2.40,2.40) provided a suitable projector to simply truncate the series at some specified wave number cut-off into a low-order system (such as in equations (2.41, 2.42).

The Mori-Zwanzig formalism [Mori, 1965; Zwanzig, 1960] provides a conceptual framework for the study of dimension reduction and the parametrisation of uninteresting variables by a stochastic process. It includes a generalized Langevin [1908] theory. Langevin [1908] studied Brownian motion from a different perspective to Einstein's seminal 1905 paper [Einstein, 1905], describing the motion of a single Brownian particle as a dynamic process via a stochastic differential equation, as an Ornstein-Uhlenbeck process [Uhlenbeck and Ornstein, 1930].

Ehrenfest introduced a special operation, the coarse-graining. This operation transforms a probability density in phase space into a "coarse-grained" density, that is a piecewise constant function, a result of density averaging in cells. The size of cells is assumed to be small, but finite, and does not tend to zero. The coarse-graining models uncontrollable impact of surrounding (of a thermostat, for example) onto ensemble of mechanical systems. To understand reasons for introduction of this new notion, let us take a phase drop, that is, an ensemble of mechanical systems with constant probability density localized in a small domain of phase space. Let us watch evolution of this drop in time according to the Liouville equation. After a long time, the shape of the drop may be very complicated, but the density value remains the same, and this drop remains "oil in water." The ensemble can tend to the equilibrium in the weak sense only: average value of any continuous function tends to its equilibrium value, but the entropy of the distribution remains constant. Nevertheless, if we divide the phase space into cells and supplement the mechanical motion by the periodical averaging in cells (this is the Ehrenfests' idea of coarse-graining), then the entropy increases, and the distribution density tends uniformly to the equilibrium. This periodical coarse-graining is illustrated by Fig. 8.11 in a two-dimensional phase space.
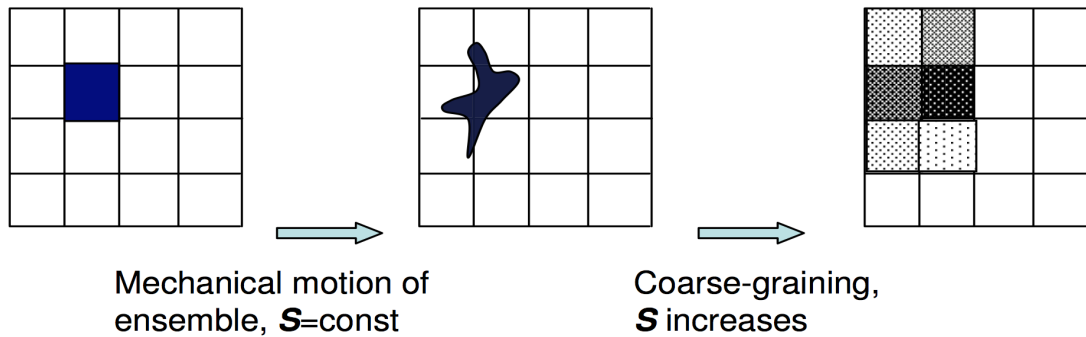
Figure 8.11: The Ehrenfests coarse-graining: two motion - coarse-graining cycles in 2D (values of probability density are presented by hatching density).

Applications of the Ehrenfests' coarse-graining[8] outside statistical physics include simple, but effective filtering. The Gaussian filtering of hydrodynamic equations that leads to the Smagorinsky equations[9] is, in its essence, again a version of the Ehrenfests' coarse-graining. The central idea of the Ehrenfests' coarse-graining remains the same in most generalizations: we combine the genuine motion with the periodic partial equlibration. The result is the Ehrenfests' chain. After that, we can find the macroscopic equation that does not depend on an initial distribution and describes the Ehrenfests' chains as results of continuous autonomous motion. Alternatively, we can just create a computational procedure without explicit equations. In the sense of entropy production, the resulting macroscopic motion is "more dissipative" than initial (microscopic) one. It is the theorem about entropy overproduction. In practice, kinetic models in the form of lattice Boltzmann models are in use (section 9.2). The coarse-graining provides theoretical basis for kinetic models. First of all, it is possible to replace projecting (partial equilibration) by involution (i.e. reflection with respect to the partial equilibrium). This entropic involution was developed for the lattice Boltzmann methods. In the original Ehrenfests' chains, "motion-partial equilibration-motion-...," dissipation is coupled with time step, but the chains "motion-involution-motion-..." are conservative. The

---

[8]P. Ehrenfest, T. Ehrenfest-Afanasyeva, The Conceptual Foundations of the Statistical Approach in Mechanics, In: Mechanics Enziklopädie der Mathematischen Wissenschaften, Vol. 4., Leipzig, 1911. Reprinted: P. Ehrenfest, T. Ehrenfest-Afanasyeva, The Conceptual Foundations of the Statistical Approach in Mechanics, Dover Phoneix, 2002.

[9]J. Smagorinsky, General Circulation Experiments with the Primitive Equations: I. The Basic Equations, Mon. Weather Rev. 91 (1963), 99–164.

family of chains between conservative (with entropic involution) and maximally dissipative (with projection) ones give us a possibility to model hydrodynamic systems with various dissipation (viscosity) coefficients that are decoupled with time steps.

Of particular interest is the work of Mori [Mori, 1965] and Zwanzig [Zwanzig, 1960] which relates the evolution of macroscopic variables to microscopic dynamics. The standard Mori-Zwanzig theory has been given a nonlinear generalization by Zwanzig [Zwanzig, 1980], and is furthermore not limited to Hamiltonian dynamics [Chorin et al., 1999; Gottwald, 2010]. This approach of modelling fast small-scale processes by a stochastic process is intuitive: provided the fast processes decorrelate rapidly enough, the slow variables experience the sum of uncorrelated events of the fast dynamics, which according to the (weak) central limit theorem corresponds to approximate Gaussian noise. A method whereby many fast degrees of freedom are replaced by a stochastic process is called stochastic model reduction.

Consider the very simple coupled linear system[10]

$$\dot{x} = L_{11}x + L_{12}y \qquad \text{the "climate" equation} \tag{8.77}$$

$$\dot{y} = L_{21}x + L_{22}y \qquad \text{the "whether" equation.} \tag{8.78}$$

Suppose we are only interested in the dynamics of x, and have only some climatic knowledge of the initial conditions of the variables y, that is the mean and variance. The whether differential equation (8.78) can be solved by the ansatz

$$y(t) = e^{L_{22}t}y(0) \cdot C(t) \tag{8.79}$$

Inserting this, we can then solve the inhomogenous problem to obtain

$$y(t) = e^{L_{22}t}y(0) + \int_0^t e^{L_{22}(t-s)}L_{21}x(s)ds,$$

---

[10]We follow the notation of [Hasselmann, 1976; Chorin et al., 1999; Gottwald, 2010].

which we may use to express the dynamics of the climate variable as

$$\dot{x} = L_{11}x + L_{12} \int_0^t e^{L_{22}(t-s)} L_{21}x(s)ds + L_{12}e^{L_{22}t}y(0). \tag{8.80}$$

This is of the form of a generalised Langevin equation, where the first term is Markovian (no dependence on the history of the process), the second is a memory term, and the last can be interpreted as a noise term, provided that the initial conditions $y(0)$ are randomly distributed. A similar reduction of the dynamics can be described by fast and slow variables applying the center manifold theory [Arnold, 1995] or slaving principle [Haken, 1996].

For the more general non-linear case, the instantaneous state of the Earth System, comprising the components 'atmosphere-ocean-cryosphere-land', can be expressed by a set of variables $\mathbf{z} = (z_1, z_2, ...)$, representing the density, velocity, temperature, etc. of the various media. The evolution of this system will be given by a series of prognostic equations of the form

$$\dot{z} = f(z), \tag{8.81}$$

with initial condition $z(0) = z_0$ and $z \in R^d$, suppose we are not interested in the full solution $z(t)$, but rather only in a few $n \leq d$ observables $\Phi(z) = (\Phi_1(z), \Phi_2(z), ..., \Phi_n(z))$. This includes the case $\Phi(z) = (z_1, ..., z_n)$, when the state space is decomposed as $z = (x, y)$ into 'interesting' variables, $x = (z_1, ..., z_n) \in \mathbb{R}^n$, and 'uninteresting' variables, $y = (z_{n+1}, ..., z_d) \in \mathbb{R}^{d-n}$. In the Earth System, a separation may be into a fast 'weather subsystem' (y) and a slow 'climate subsystem' (x) with different order of magnitude in the correlation times (or, the response/relaxation times) for the slow variable is much larger than that of the fast variable, i.e.

$$\tau_y \ll \tau_x. \tag{8.82}$$

Now let us ask the following question: what are the effective dynamics of the interesting observables for an ensemble of initial conditions $z(0)$, where $\Phi(z(0))$ is known and the uninteresting subspace is equipped with a known distribution?

Rather than investigating the dynamical system (8.81) directly, one may choose to look at how observables $V(z(t))$ evolve in time. Applying the chain rule, one can naturally define the generator

$$\mathcal{L} = f(z) \cdot \nabla,$$

and write

$$\frac{d}{dt}V(z(t)) = \mathcal{L}V(z(t)).$$

Note that $\mathcal{L}$ is the adjoint operator of the Liouville operator $\mathcal{L}^*$ with $\mathcal{L}^*\rho = -\nabla \cdot (f(z)\rho)$ controlling the evolution of densities of ensembles propagated according to (8.81). We seek for the solution $v(z, t)$ of

$$\frac{\partial v}{\partial t} = \mathcal{L}v \text{ with } v(z, 0) = \phi(z), \tag{8.83}$$

where z is an independent variable and denotes initial conditions. The solution of (8.83) can be formally written as

$$v(z, t) = e^{\mathcal{L}t}\phi(z), \tag{8.84}$$

To filter out the dynamics of the interesting variables we require a projection operator $\mathbf{P}$ that maps functions of z to functions of $\Phi(z)$. If the manifold consists for example of a product of submanifolds of relevant and irrelevant variables, one can take a conditional expectation

$$(\mathbf{P}v)(\mathbf{x}) = \frac{\int_{\mathbb{R}^{d-n}} v(z)\rho(\mathbf{x}, \mathbf{y})d\mathbf{y}}{\int_{\mathbb{R}^{d-n}} \rho(\mathbf{x}, \mathbf{y})d\mathbf{y}} \tag{8.85}$$

where $\rho(\mathbf{x}, \mathbf{y})$ denotes the joint probability function of the initial conditions for the full system (8.81). It is easy to show that this a projection ($\mathbf{P^2} = \mathbf{P}$). In the context of PDEs one may use Galerkin approximations, a perfectly valid projector would be to simply truncate the Galerkin series at some specified high wave number cut-off. We also define the orthogonal projector $\mathbf{Q}$ that projects onto y, with $\mathbf{Q} = \mathbf{1} - \mathbf{P}$. Now, the derivation of the Mori-Zwanzig equation is a two-linear: given the Cauchy problem (8.83) and its formal solution (8.84) we write, using

$P + Q = 1$,

$$\frac{\partial v}{\partial t}(z, t) = \mathcal{L}e^{\mathcal{L}t}\Phi(z) = e^{\mathcal{L}t}P\mathcal{L}\Phi(z) + e^{\mathcal{L}t}Q\mathcal{L}\Phi(z)$$

which, upon using the Duhamel-Dyson formula [Evans and Morriss, 2008] for operators A and B, yields

$$e^{t(A+B)} = e^{tA} + \int_0^t e^{(t-s)(A+B)}Be^{sA}ds.$$

By differentiation, this becomes the celebrated Mori-Zwanzig equation [Mori et al., 1974; Zwanzig, 1960]

$$\frac{\partial v}{\partial t}(z, t) = e^{\mathcal{L}t}P\mathcal{L}\Phi(z) + \int_0^t e^{(t-s)\mathcal{L}}P\mathcal{L}e^{sQ\mathcal{L}}Q\mathcal{L}\Phi(z)ds + e^{tQ\mathcal{L}}Q\mathcal{L}\Phi(z). \quad (8.86)$$

Note that the Mori-Zwanzig equation (8.86) is not an approximation but is exact and constitutes an equivalent formulation of the full problem (8.81). The Mori-Zwanzig equation (8.86) is in the form of a generalised Langevin equation. The first term on the right-hand side is Markovian, the second term is a memory term, and the last term lives in the uninteresting orthogonal subspace and can be called noise. Ideally one would like to approximate the noise term by white noise. Heuristically this should be possible in the case of time-scale separation or of weak coupling. The advantage of looking at this limit is however that the noise autocorrelation function and memory kernel can now be written as simple correlation and response functions of the unresolved dynamics. The reader is referred to [Chorin and Hald, 2006; Chorin et al., 2000; Zwanzig, 2001; Evans and Morriss, 2008; Givon et al., 2004; Lucarini et al., 2014] for more details.

The projection method includes the procedure to parameterize the turbulent energy dissipation in turbulent flows, where the larger eddies extract energy from the mean flow and ultimately transfer some of it to the smaller eddies which, in turn, pass the energy to even smaller eddies, and so on up to the smallest scales, where the eddies convert the kinetic energy into internal energy of the fluid. At this scales (also known as Kolmogorov scale), the viscous friction dominates the flow [Frisch, 1996].

The theory of scientific reduction is important for different theories: the microscopic informa-

tion in the brain with enormous amount of possible solutions is reduced to macroscopic actions and human behaviour. This implies that the actions are not deterministic, but stochastic in the sense of the standard Mori-Zwanzig theory or Brownian motion. Without being a specialist, this seems to be important for neuroscience and for the philosophy of science in general. The activity of neurons in the brain can be modelled statistically (e.g., https://en.wikipedia.org/wiki/Ising_model).

Chapter 9

Statistical Mechanics and Fluid Dynamics

The structure of fluid dynamical models is valid for systems with many degrees of freedom, many collisions, and for substances which can be described as a continuum. The transition from the highly complex dynamical equations to a reduced system is an important step since it gives more credibility to the approach and its results. The transition is also necessary since the active entangled processes are running on spatial scales from millimetres to thousands of kilometres, and temporal scales from seconds to millennia. Therefore, the unresolve processes on subgrid scales have to be described. This is the typical problem in statistical physics: How can we obtain the macroscopic dynamics from the underlying theory? Two different solutions are known, one is the so-called Mori-Zwanzig approach [Mori, 1965; Zwanzig, 1960, 1980] which relates the evolution of macroscopic variables to microscopic dynamics. The basic idea is the evolution of a system through a projection on a subset (macroscopic relevant part), where a randomness reflects the effects of the unresolved degrees of freedom. A particular example is the Brownian motion [Einstein, 1905; Langevin, 1908]. The other solution for the transition form the micro to macro-scales goes back to Boltzmann [1896]. The Boltzmann equation, also often known as the Boltzmann transport equation [Boltzmann, 1896; Bhatnagar et al., 1954; Cercignani, 1990] describes the statistical distribution of one particle in a fluid. It is one of the most important equations of non-equilibrium statistical mechanics, the area of statistical mechanics that deals with systems far from thermody-

namic equilibrium. It is applied, for instance, when there is an applied temperature gradient or electric field. Both, the Mori-Zwanzig and Boltzmann approaches play also a fundamental role in physics. The microscopic equations show no preferred time direction, whereas the macroscopic phenomena in the thermodynamics have a time direction through the enthropy. The underlying procedure is that part of the microscopic information is lost through coarse graining in space and time. Chapter 9 describes the approach from statistical mechanics towards the macroscopic theory. The Boltzmann equation and the Brownian motion are **the** approaches to understand the transition from micro to macro scales. For climate, this transition between the climate and weather scales has been formulated [Hasselmann, 1976; Leith, 1975], and later re-formulated in a mathematical context [Arnold, 2001; Chorin et al., 1999; Gottwald, 2010]. The effect of the weather on climate is seen by red-noise spectra in the climate system, showing one of the most fundamental aspects of climate, and serving also as a null hypothesis for climate variability studies. Chapter 9.4 deals with a fluid dynamical application, a 2D implementation of the Lattice Boltzmann Method (LBM) with the Bhatnagar-Gross-Krook (BGK) collision operator. The main structural parts of the program and several hints for the potential users are provided. While we do include a brief outline of the theory of LBM, detailed explanations are out of the scope of this book. Fore more details, please consult the references herein. The present code is intended to serve mainly as a showcase/practical introduction to Lattice Boltzmann Methods, hence advanced features and state-of-the-art algorithm improvements have been intentionally ommitted in favor of simplicity. One practical example, the Rayleigh-Benard convection [Rayleigh, 1916], is presented.

There are two ways of changing the descrition of the dynamics: from the micro to the macro scales. This is a common problem since we are not able to describe the systems on all temporal and spatial scales. One straitforward approach is coarse graining where the underlying dynamics is projected onto the macroscopic dynamics (section 8.4), the other is the statistical physics theory of non-equilibrium statistical mechanics (section 9.2).

A general question within the micro-macro dynamic is that of integration between the two different levels. Two distinctly different levels emerge with different rules governing each, but

they then need to be reconciled in some way to create an overall functioning system. Physical, chemical, biological, economic, social and cultural systems all exhibit this micro-macro dynamic and how the system comes to reconcile it forms a primary determinate in its identity and overall structure. This multi-dimensional nature to a system that results in the micro-macro dynamic is a product of synthesis and emergence. In many instances when we put elements together they do not simply remain discrete separate entities but they interact, co-evolve and they differentiate their states and function with respect to each other to become an interdependent whole, which comes to have properties and features that none of its parts possess. A whole new level of organization emerges that is different from the parts. This is made manifest in ecosystems; as they have co-evolved over millennia the parts are intricately interdependent forming a whole system that has features and dynamics independent from any of its parts and thus a two-tier system and a resulting emergent micro-macro dynamic. The whole ecosystem goes through processes of change - such as ecological succession - that are not associated with any of the parts but condition what creatures can viably exist within that macro regime.

We start from the point of view of kinetic theory of fluids where a gas is composed of a set of interacting particles Boltzmann [1896]. We are then interested in the probability of finding a fluid particle at a certain point in space and with a certain velocity. The moments of this probablility are related to our macroscopic fluid-dynamical quantities like density or velocity.

9.1   Mesoscopic dynamics*

Liouville equation

In the deterministic framework, the dynamics is characterized by

$$\frac{d}{dt}x(t) = f(x(t)) \quad , \tag{9.1}$$

and in the special case of classical mechanics can be descibed by a set of differential equations known as the Hamilton equations for that system. Hamiltonians can be used to describe such simple systems as a bouncing ball, a pendulum or an oscillating spring in which energy changes from kinetic to potential and back again over time. Hamiltonians can also be employed to model the energy of other more complex dynamic systems such as planetary orbits in celestial mechanics and also in quantum mechanics. The Hamilton equations are generally written as follows:

$$\dot{p} = -\frac{\partial \mathcal{H}}{\partial q} \tag{9.2}$$

$$\dot{q} = \frac{\partial \mathcal{H}}{\partial p} \tag{9.3}$$

In the above equations, the dot denotes the ordinary derivative with respect to time of the functions $p = p(t)$ (called generalized momenta) and $q = q(t)$ (called generalized coordinates), taking values in some vector space, and $\mathcal{H} = \mathcal{H}(p, q, t)$ is the so-called Hamiltonian, or (scalar valued) Hamiltonian function. The associated probability distribution for the generalized dynamics (9.1) is given in the phase space

$$p(x, t) = \delta(x - x(t)) \tag{9.4}$$

yielding the Liouville equation

$$\partial_t p = -\frac{d}{dx(t)} \left[\delta(x - x(t)) \right] \frac{d}{dt} x(t) = -\frac{\partial p}{\partial x} f(x) \quad . \tag{9.5}$$

The Liouville equation is often used in the framework of the Hamiltonian dynamics (9.3). Since the phase space velocity $(\dot{p}_i, \dot{q}_i)$ has zero divergence, and probability is conserved. Its substantial derivative can be shown to be zero and so

$$\frac{\partial}{\partial t} \rho = -\{ \rho, \mathcal{H} \}. \tag{9.6}$$

using the Poisson bracket

$$\{f, g\} = \sum_{i=1}^{N} \left[\frac{\partial f}{\partial q_i} \frac{\partial g}{\partial p_i} - \frac{\partial f}{\partial p_i} \frac{\partial g}{\partial q_i} \right]. \tag{9.7}$$

Master equation

The master equation is a phenomenological set of first-order differential equations describing the time evolution of the probability of a system to occupy each one of a discrete set of states:

$$\frac{dP_k}{dt} = \sum_{\ell} T_{k\ell} P_{\ell}, \tag{9.8}$$

where P_k is the probability for the system to be in the state k, while the matrix $T_{\ell k}$ is filled with a grid of transition-rate constants. In probability theory, this identifies the evolution as a continuous-time Markov process, with the integrated master equation obeying a Chapman-Kolmogorov equation. Note that

$$\sum_{\ell} T_{\ell k} = 0 \tag{9.9}$$

(i.e. probability is conserved), so the equation may also be written as

$$\frac{dP_k}{dt} = \sum_{\ell} (T_{k\ell} P_{\ell} - T_{\ell k} P_k). \tag{9.10}$$

allowing us to omit the term $\ell = k$ from the summation. Thus, in the latter form of the master equation there is no need to define the diagonal elements of T.

The master equation exhibits detailed balance if each of the terms of the summation disappears separately at equilibrium, i.e. if, for all states k and l having equilibrium probabilities pi_k and π_ℓ

$$T_{k\ell} \pi_{\ell} = T_{\ell k} \pi_k \tag{9.11}$$

Many physical problems in classical, quantum mechanics and problems in other sciences, can be reduced to the form of a master equation, thereby performing a great simplification of the problem. In the continous case, the Chapman-Kolmogorov equation has similarities with the Master equation. The Chapman-Kolmogorov equation is an identity relating the joint probability distributions of different sets of coordinates on a stochastic process. Suppose that $\{x_i\}$ is an indexed collection of random variables, that is, a stochastic process. Let

$$p_{i_1,\ldots,i_n}(x_1,\ldots,x_n) \tag{9.12}$$

be the joint probability density function of the values of the random variables $x1$ to x_n. Then, the Chapman-Kolmogorov equation is

$$p_{i_1,\ldots,i_{n-1}}(x_1,\ldots,x_{n-1}) = \int_{-\infty}^{\infty} p_{i_1,\ldots,i_n}(x_1,\ldots,x_n)\,dx_n \tag{9.13}$$

i.e. a straightforward marginalization over the nuisance variable.

When the stochastic process under consideration is Markovian, the Chapman-Kolmogorov equation is equivalent to an identity on transition densities. In the Markov chain setting, one assumes that $i_1 < \ldots < i_n$. Then, because of the Markov property,

$$p_{i_1,\ldots,i_n}(x_1,\ldots,x_n) = p_{i_1}(x_1)p_{i_2;i_1}(x_2 \mid x_1) \cdots p_{i_n;i_{n-1}}(x_n \mid x_{n-1}), \tag{9.14}$$

where the conditional probability $p_{i;j}(x_i \mid x_j)$ is the transition probability between the times $i > j$. So, the Chapman-Kolmogorov equation takes the form

$$p_{i_3;i_1}(x_3 \mid x_1) = \int_{-\infty}^{\infty} p_{i_3;i_2}(x_3 \mid x_2)p_{i_2;i_1}(x_2 \mid f_1)\,dx_2. \tag{9.15}$$

When the probability distribution on the state space of a Markov chain is discrete and the Markov chain is homogeneous, the Chapman-Kolmogorov equations can be expressed in terms of (possibly

infinite-dimensional) matrix multiplication, thus:

$$P(t + s) = P(t)P(s) \tag{9.16}$$

where P(t) is the transition matrix, i.e., if Xt is the state of the process at time t, then for any two points i and j in the state space, we have

$$P_{ij}(t) = P(X_t = j \mid X_0 = i). \tag{9.17}$$

Example for the Chapman-Kolmogorov and Master equations in climate dynamics are related to transitions between different states.

Fokker-Planck dynamics

In the stochastic context, we make a Taylor expansion up to order two in $dx = x(t + dt) - x(t)$ from the Master equation:

$$
\begin{aligned}
dp &= p(x, t + dt) - p(x, t) \\
&= \; < \delta(x - x(t + dt)) > - < \delta(x - x(t)) > \\
&= \; - < \frac{d}{dx(t)} \left[\delta(x - x(t)) \right] \, dx > + \frac{1}{2} < \frac{d^2}{dx^2} \left[\delta(x - x(t)) \right] \, dx^2 > \\
&= \; -\frac{\partial p}{\partial x} < dx > + \frac{1}{2} \frac{\partial^2}{\partial x^2} p < dx^2 > \\
&= \; -\frac{\partial p}{\partial x} f(x) dt + \frac{1}{2} \frac{\partial^2}{\partial x^2} p \, g^2 dt \tag{9.18}
\end{aligned}
$$

The probability density $p(x, t)$ for the variable $x(t)$ in (8.8) obeys therefore the Fokker-Planck equation

$$\partial_t p = -\frac{\partial}{\partial x} \left[f(x)p \right] + \frac{\partial}{\partial x} \left[g(x) \frac{\partial}{\partial x} \{ g(x)p \} \right] \quad . \tag{9.19}$$

Its stationary probability density of (8.8) is given by

$$p_{st}(x) \;=\; \aleph \exp\left(-2\int_{x_0}^{x}\frac{f(y)-g(y)g'(y)}{g(y)^2}\,dy\right)\quad. \tag{9.20}$$

where $\aleph$ is a normalization constant. $g'(y)$ stands for the derivative of g with respect to its argument. The extrema x_m of the steady state density obey the equation

$$f(x_m)-g(x_m)g'(x_m)=0 \tag{9.21}$$

for $g(x_m)n_e0$. Here is the crux of the noise-induced transition phenomenon: one notes that this equation is not the same as the equation $f(x_m)=0$ that determines the steady states of the system in the absence of multiplicative noise. As a result, the most probable states of the noisy system need not to coincide with the deterministic stationary states. More importantly, new solutions may appear or existing solutions may be destabilized by the noise. These are the changes in the asymptotic behavior of the system caused by the presence of the noise, e.g. **?**.

9.2   The Boltzmann Equation*

One of the most significant theoretical breakthroughs in statistical physics was due to Ludwig Boltzmann (Boltzmann [1896], Boltzmann [1995] for a recent reprint of his famous lectures on kinetic theory), who pioneered non-equilibrium statistical mechanics. Boltzmann postulated that a gas was composed of a set of interacting particles, whose dynamics could be (at least in principle) modelled by classical dynamics. Due to the very large number of particles in such a system, a statistical approach was adopted, based on simplified physics composed of particle streaming in space and billiard-like inter-particle collisions (which are assumed elastic). Instrumental to the theory is the single-particle distribution function (hereafter SPDF), $f(\vec{x},\vec{e},t)$ which represents the probability density of having a particle at the point $(\vec{x},\vec{e})$ in the phase space. Hence, the

quantity

$$f(\vec{x}, \vec{e}, t)d\vec{x}d\vec{e} \tag{9.22}$$

represents the probability of finding a particle inside an infinitesimal space cubelet centered around $\vec{x}$, and inside an infinitesimal momentum-space cubelet around $\vec{e}$ at any given time t. In the presence of a body-force $\vec{F}$, the SPDF will evolve according to

$$f(\vec{x} + d\vec{x}, \vec{e} + d\vec{e}, t + dt)d\vec{x}d\vec{e} = f(\vec{x}, \vec{e}, t)d\vec{x}d\vec{e}, \tag{9.23}$$

where $d\vec{x} = \vec{e}dt$ and $d\vec{e} = \vec{F}dt/m.$ If we also include the effect of the collisions, and denote by $\Gamma_+ d\vec{x}d\vec{e}dt$ the probability for a particle to start from outside the $d\vec{x} \times d\vec{e}$ domain and to enter this phase-space region during the infinitesimal time dt and by $\Gamma_- d\vec{x}d\vec{e}dt$ the probability for a particle to start from the $d\vec{x} \times d\vec{e}$ domain and leave this phase-space region during the infinitesimal time dt, the evolution of the SPDF becomes

$$f(\vec{x} + d\vec{x}, \vec{e} + d\vec{e}, t + dt)d\vec{x}d\vec{e} = f(\vec{x}, \vec{e}, t)d\vec{x}d\vec{e} + (\Gamma_+ - \Gamma_-)\,d\vec{x}d\vec{e}dt \tag{9.24}$$

Expanding the LHS into a Taylor series around the phase-space point $(\vec{x}, \vec{u}, t)$, we obtain:

$$f(\vec{x}+d\vec{x}, \vec{e}+d\vec{e}, t+dt)d\vec{x}d\vec{e} = f(\vec{x}, \vec{e}, t)d\vec{x}d\vec{e}+\left(\frac{\partial f}{\partial t}\right)dt+(\nabla_{\vec{x}}f)\cdot d\vec{x}+(\nabla_{\vec{e}}f)\cdot d\vec{e}+\ldots \tag{9.25}$$

Inserting Eq. (9.25) into Eq. (9.24) and cancelling terms, we easily obtain Boltzmann's Equation:

$$\frac{\partial f}{\partial t} + \vec{e} \cdot \nabla_{\vec{x}}f + \vec{F}/m \cdot \nabla_{\vec{e}}f = \Gamma_+ - \Gamma_- \tag{9.26}$$

where $\nabla_{\vec{x}}$ is the gradient operator in physical space and $\nabla_{\vec{e}}$ the same in momentum space.[1]

For the sake of clarity, we have not written the collision operator explicitly yet. The important

---

[1]The collisionless Boltzmann equation is often mistakenly called the Liouville equation (the Liouville Equation is an N-particle equation being N the number of microscopic particles). The Boltzmann equation is a mesoscopic dynamics with degrees of freedom $<< N$.

point is that the separation of the dynamics into collisions and streaming is already apparent from

Eq. (9.26). The collision operator, which is in itself a complex integro-differential expression,

reads

$$\Gamma_+ - \Gamma_- \equiv \int d\vec{e}_1 \int d\Omega \, \sigma(\Omega) \, |\vec{e} - \vec{e}_1| \, \left[f(\vec{e}\,')f(\vec{e}_1') - f(\vec{e})f(\vec{e}_1) \right] \tag{9.27}$$

where σ is the differential cross-section in the case of the 2-particle collisions (which is a func-

tion of the solid angle Ω only), unprimed velocities are incoming (before collision) and primed

velocities are outgoing (after collision).[2] In another notation

$$\Gamma_+(\vec{x}, \vec{e}, t) = \int d\vec{e}_1 \int d\vec{e}\,' \int d\vec{e}_1' \quad P_{(e', e_1') \to (e, e_1)} \quad f(\vec{e}\,')f(\vec{e}_1') \tag{9.28}$$

$$\Gamma_-(\vec{x}, \vec{e}, t) = \int d\vec{e}_1 \int d\vec{e}\,' \int d\vec{e}_1' \quad P_{(e, e_1) \to (e', e_1')} \quad f(\vec{e})f(\vec{e}_1) \tag{9.29}$$

where $P_{(e', e_1') \to (e, e_1)}$ is the probability density to go from initial state (e', e_1') to final state (e, e_1)

in time dt. It follows from symmetry considerations that $P_{(e', e_1') \to (e, e_1)} = P_{(e, e_1) \to (e', e_1')}$ and

$$d\vec{e}\,' d\vec{e}_1' P_{(e', e_1') \to (e, e_1)} = d\Omega \, \sigma(\Omega) \, |\vec{e} - \vec{e}_1| \tag{9.30}$$

A fundamental property of the collision operator [Cercignani, 1987] is that it conserves mass,

momentum and kinetic energy (hence also a linear combination thereof). Also, it can be shown

that the local Maxwell-Boltzmann distribution pertains to a certain class of positive SPDFs for

which the collision integral vanishes (variational principle, Lagrange parameters). It can be shown

---

[2]Of course, finding or modeling the collision term is the biggest challenge in the kinetic theory. In the simplest model one only takes into account binary collisions and assumes that the colliding particles are uncorrelated (i.e. molecular chaos assumption). The collisions are proportianal to the velocity difference between the particles $|\vec{u} - \vec{u}_1|$. Consider an elastic collision of two spherically symmetric (spin-less) molecules with mass m and velocities $\vec{e}$ and $\vec{e}_1$. After collision their respective velocities are $\vec{e}\,'$ and $\vec{e}_1'$. Then the following conservation laws apply:
Momentum conservation: $m(\vec{e} + \vec{e}_1) = m(\vec{e}\,' + \vec{e}_1')$.
Energy conservation: $m/2 \quad \vec{e} \cdot \vec{e} + m_1/2 \quad \vec{e}_1 \cdot \vec{e}_1 = m/2 \quad \vec{e}\,' \cdot \vec{e}\,' + m_1/2 \quad \vec{e}_1' \cdot \vec{e}_1'$.

that this equilibrium distribution is given by

$$f_0(\vec{x}, \vec{e}) = \rho(\vec{x}) \left[\frac{m}{2\pi k T(\vec{x})} \right]^{3/2} \exp\{-m \left[\vec{e} - \vec{u}(\vec{x}) \right]^2 / 2kT(\vec{x})\} \qquad (9.31)$$

where $\rho(\vec{x}), \vec{u}(\vec{x})$ and $T(\vec{x})$ are the local density, macroscopic velocity, and temperature, re-spectively.[3] If there are no external forces such as gravity or electrostatic interactions we have $\rho(\vec{x}) = \rho_0 = N/V$. In case the temperature is also independent of position, and if the gas as a whole is not moving ($\vec{u} = 0$), then $f(\vec{x}, \vec{e}) = \rho_0 f_0(\vec{e})$, with

$$f_0(\vec{e}) = \left[\frac{m}{2\pi k T} \right]^{3/2} e^{-m\vec{e}^2/2kT},$$

This implies that, if this distribution is attained, we also have a state where incoming SPDFs ex-actly balance the outgoing ones, maintaining a local dynamic equilibrium. This observation is of paramount importance for our method, which uses the (discretized) Maxwell-Boltzmann distribu-tion as the equilibrium distribution functions.

9.3   H-Theorem and approximation of the Boltzmann equation*

The other important feature of this equation is that the integral

$$H = \int \int d\vec{x} d\vec{e} \; f(\vec{x}, \vec{e}, t) \ln f(\vec{x}, \vec{e}, t) \qquad (9.34)$$

---

[3]This experssion of the SPDF can be approximated through a Taylor series of the exponential: $\exp(y) = 1 + y$. Task: Show that

$$f_a^{eq}(\vec{x}, \vec{e}) = \rho(\vec{x}) \left[1 + 3\frac{\vec{u} \cdot \vec{e}}{c_s^2} + \frac{9}{2}\frac{(\vec{u} \cdot \vec{e})^2}{c_s^4} - \frac{3}{2}\frac{\vec{e}^2}{c_s^2} \right], \qquad (9.32)$$

with the speed of sound c_s and

$$\frac{1}{c_s^2} = \frac{1}{\gamma}\frac{m}{kT} \qquad (9.33)$$

and γ the adiabatic factor.

can only decrease. This can be seen by using the following:

$$\frac{dH}{dt} = \int d\vec{e}_1 \int d\Omega \, \sigma(\Omega) \, |\vec{e} - \vec{e}_1| \, \left[f(\vec{e}') f(\vec{e}_1') - f(\vec{e}) f(\vec{e}_1) \right] \left[1 + \ln f(\vec{e}_1) \right] \quad (9.35)$$

and the same term for

$$\frac{dH}{dt} = \int d\vec{e}_1 \int d\Omega \, \sigma(\Omega) \, |\vec{e} - \vec{e}_1| \, \left[f(\vec{e}') f(\vec{e}_1') - f(\vec{e}) f(\vec{e}_1) \right] \left[1 + \ln f(\vec{e}_1') \right] \quad (9.36)$$

The term is also invariant with respect to the notation ('), i.e.

$$\frac{dH}{dt} = \int d\vec{e}_1 \int d\Omega \, \sigma(\Omega) \, |\vec{e} - \vec{e}_1| \, \left[f(\vec{e}) f(\vec{e}_1) - f(\vec{e}') f(\vec{e}_1') \right] \left[1 + \ln f(\vec{e}_1') \right] \quad (9.37)$$

and

$$\frac{dH}{dt} = \int d\vec{e}_1 \int d\Omega \, \sigma(\Omega) \, |\vec{e} - \vec{e}_1| \, \left[f(\vec{e}) f(\vec{e}_1) - f(\vec{e}') f(\vec{e}_1') \right] \left[1 + \ln f(\vec{e}_2') \right] \quad (9.38)$$

Use furthermore

$$\eta' = f(\vec{e}') f(\vec{e}_1') \quad \text{and} \quad \eta = f(\vec{e}) f(\vec{e}_1) \tag{9.39}$$

$$E = (\eta' - \eta) \left[\ln \eta - \ln \eta' \right] \tag{9.40}$$

and recognize that E is negative. $\frac{d}{dt} H$ is equal zero for

$$f(\vec{e}') f(\vec{e}_1') = f(\vec{e}) f(\vec{e}_1) \quad . \tag{9.41}$$

For a system of N statistically independent particles, H is related to the thermodynamic entropy S through:

$$S \stackrel{\text{def}}{=} -NkH \tag{9.42}$$

Therefore, according to the H-theorem, S can only increase.[4] The same function H is also used as "information function":

$$I = -\sum_i f_i \ln f_i = < -\ln f > . \tag{9.43}$$

where the f_i can be interpreted as probablity and not only as a measure of the breadth of the spread of states available to a single particle in a gas of like particles, where f_i represented the relative frequency distribution of each possible state. When all the probabilities f_i are equal, I is maximal, and we have minimal information about the system. When our information is maximal (i.e., one f_i is equal to one and the rest to zero, such that we know what state the system is in), the function is minimal. This information function is also called "reduced entropic function" in thermodynamics [Shannon, 1948]. Gibbs proposed a general formula for statistical-mechanical entropy, no longer requiring identical and non-interacting particles, but instead based on the probability distribution p_i for the complete microstate i of the total system:

$$S = -k \sum_i p_i \ln p_i \tag{9.44}$$

$$\frac{dS}{dt} = -k \sum_i \left(\frac{dp_i}{dt} \ln p_i + \frac{dp_i}{dt} \right) = -k \sum_i \frac{dp_i}{dt} \ln p_i \tag{9.45}$$

---

[4]Please see the link to the Lyapunov function for the Lorenz system in Chapter 2.2.

because $\sum_i \frac{dp_i}{dt} = \frac{d}{dt} \sum_i p_i = \frac{d}{dt}(1) = 0$. Now, formulate a master equation [van Kampen, 1981] for the average rate of jumps[5] from state α to β, and from state β to α:

$$\frac{dp_\alpha}{dt} = \sum_\beta \nu_{\alpha\beta}(p_\beta - p_\alpha) \tag{9.46}$$

$$\frac{dp_\beta}{dt} = \sum_\alpha \nu_{\alpha\beta}(p_\alpha - p_\beta) \tag{9.47}$$

where the reversibility of the dynamics ensures that the same transition constant $\nu_{\alpha\beta}$ appears in both expressions. So

$$\frac{dS}{dt} = \frac{1}{2}k \sum_{\alpha,\beta} \nu_{\alpha\beta}(\ln p_\beta - \ln p_\alpha)(p_\beta - p_\alpha). \tag{9.48}$$

But the two brackets will have the same sign (the same argument as in equation 9.40), so each contribution to dS/dt cannot be negative and therefore, $\frac{dS}{dt} \geq 0$ for an isolated system. Due to the complex expression for the collision operator, it became clear that approximations were desirable. It was also proven (see Cercignani [1990]) that such approximations were also reasonable, since the details of the two-body interaction are not likely to influence significantly experimentally-measured quantities. Hence, approximate collision operators were proposed, all of which had to $\boxed{1}$ conserve local mass, momentum and energy and $\boxed{2}$ develop a collisional contribution in Boltzmann's equation (9.26) which tends to a local Maxwellian distribution. It was soon realized that a model developed at the middle of last century Bhatnagar et al. [1954] (also known as Bhatnagar-Gross-Krook; hereafter BGK) satisfied both of these conditions. Chapman and Enskog developed a general procedure for the approximate solution of Boltzmann's equation. For certain simple model systems such as hard spheres their method produces predictions for (or its moments) which may

---

[5]The master equation is quite often written as: $\frac{d\vec{P}}{dt} = A\vec{P}$, where $\vec{P}$ is a column vector (where element i represents state i), and A is the matrix of connections. The way connections among states are made determines the dimension of the problem. When the connections are time-independent rate constants, the master equation represents a kinetic scheme and the process is Markovian (any jumping time probability density function for state i is an exponential, with a rate equal to the value of the connection). When the connections depend on the actual time (i.e. matrix A depends on the time, $A \to A(t)$), and the process is not stationary. For an application in meteorogy, e.g. Egger [2001].

be tested in computer simulations. Another more modern approach to the numerical solution of the transport equation is the "Lattice Boltzmann" method in which the continuous variables and are restricted to a set of discrete values; the time change of these values is then described by a modified transport equation which lends itself to fast computation. The moments of the distribution function represent macroscopic variables density and velocity fields:

$$\rho(\vec{x}, t) \;=\; m \int d\vec{e} f(\vec{x}, \vec{e}, t) \tag{9.49}$$

$$\rho(\vec{x}, t)\vec{u}(\vec{x}, t) \;=\; m \int d\vec{e}\,\vec{e} f(\vec{x}, \vec{e}, t) \tag{9.50}$$

Note that the molecular velocities $\vec{e}$ is different from the macroscopic veleocity field $\vec{u}(\vec{x}, t)$. The basic idea was that each collision changes the SPDF by an amount which is proportional to the departure from the local Maxwellian distribution:

$$\Gamma_+ - \Gamma_- = -\frac{f(\vec{x}, \vec{e}, t) - f_0(\vec{x}, \vec{e})}{\tau} \tag{9.51}$$

with relaxation constant τ. In dimensionless units, τ is replaced by the dimensionless Knudsen number $Kn = l/L$ with l is the mean-free-path. It is the small parameter in the kinetics - fluid dynamics transition. If the $Kn \gg 1$ then the continuum assumption of fluid mechanics is no longer a good approximation and kinetic equations must be used.

9.4 Application: Lattice Boltzmann Dynamics

9.4.1 Lattice Boltzmann Methods*

LBMs recently proved to be viable alternatives to traditional computational fluid dynamics (CFD). The latter adopts a strategy consisting of: writing the macroscopic flow equations; discretizing the macroscopic equations using finite differences, finite volumes or finite elements; solving the discretized equations on a computer. In contrast, LBM takes a different route towards the same results. The LBM approach is composed of formulating a mesoscopic model for the evolution of the PDF such that the desired macroscopic flow equations are obtained. The end result of both approaches are similar. However, the algorithms differ due to the different perspective on the physics of the flow. There are in principle an infinite set of possible mesoscopic models. However, we focus on the most common ones, which consist of a streaming and a collision process. These LBMs use a simplified collision operator Bhatnagar et al. [1954], hence they are also referred to as LBM-BGK models.

There are several possible choices for the underlying lattice. These are usually classified in the literature using the $D\alpha Q\beta$-notation, where α is an integer number denoting the space dimensionality and β is another integer indicating the number of discrete velocities (including the particle at rest) within the momentum discretization. Some restrictions have to be fulfilled (especially Galilean and rotational invariance)[6] to ensure that a particular discretization can simulate the Navier-Stokes equations. Among the lattices in common use there are the $D2Q9$ and $D3Q19$-models (see for example discussion in He and Luo [1997]). Our focus here is the $2D$ case, hence we have chosen the $D2Q9$ momentum discretization. The discrete velocity directions for the $D2Q9$ lattice are shown in Fig 9.1. The macroscopic variables are defined as functions of the

---

[6]A lattice with reduced symmetry can be (and has been) used, see d'Humieres et al. [2001], where a $D3Q13$-lattice is used. However, this approach also departs from the classical BGK-LBM dynamics.
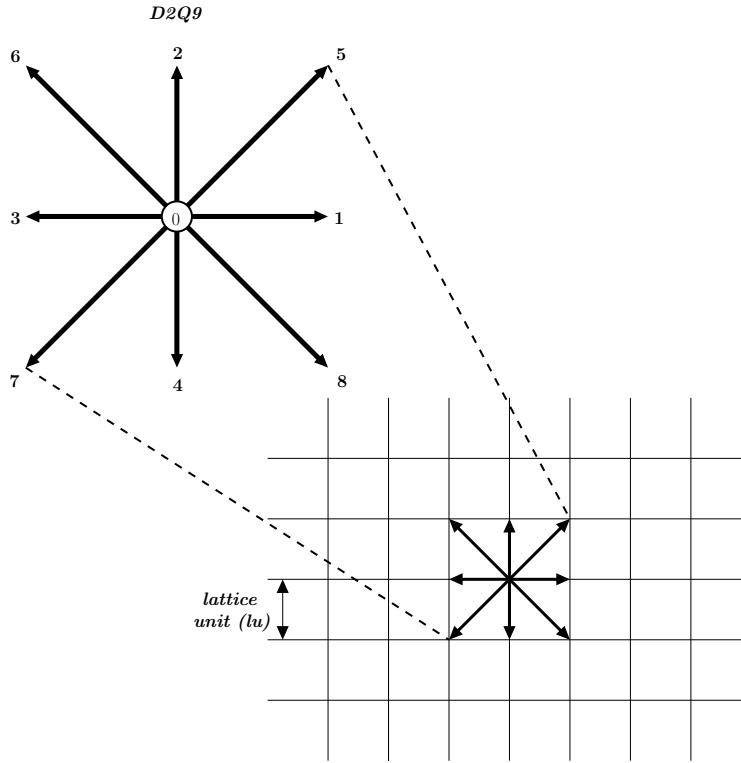
Figure 9.1: Discrete lattice velocities for the $D2Q9$ model.

particle distribution functions (hereafter DFs) according to:

$$\rho = \sum_{a=0}^{\beta-1} f_a \qquad \text{(macroscopic fluid density)} \qquad (9.52)$$

$$\text{and} \quad \vec{u} = \frac{1}{\rho} \sum_{a=0}^{\beta-1} f_a \vec{e}_a \qquad \text{(macroscopic velocity)}. \qquad (9.53)$$

The DFs at each lattice point are updated using the equation:

$$\underbrace{f_a(\vec{x} + \vec{e}_a \delta_t, t + \delta_t) = f_a(\vec{x}, t)}_{\text{Streaming}} \underbrace{- \frac{[f_a(\vec{x}, t) - f_a^{eq}(\vec{x}, t)]}{\tau}}_{\text{Collision}}, \qquad (9.54)$$

where $a \in [0, \beta - 1]$ is an index spanning the (discretized) momentum space and τ is a relaxation parameter, which is related to the fluid viscosity. The streaming step, where the DFs are translated

to the neighbouring sites according to the respective discrete velocity direction, is illustrated in Fig. 9.2, in the $D2Q9$ model. The collision step (illustrated in Fig. 9.3) consists of a re-distribution of the DFs towards the local discretized Maxwellian equilibrium DFs, in such a way that local mass and momentum are invariant. The equilibrium DFs can be obtained from the local Maxwell-

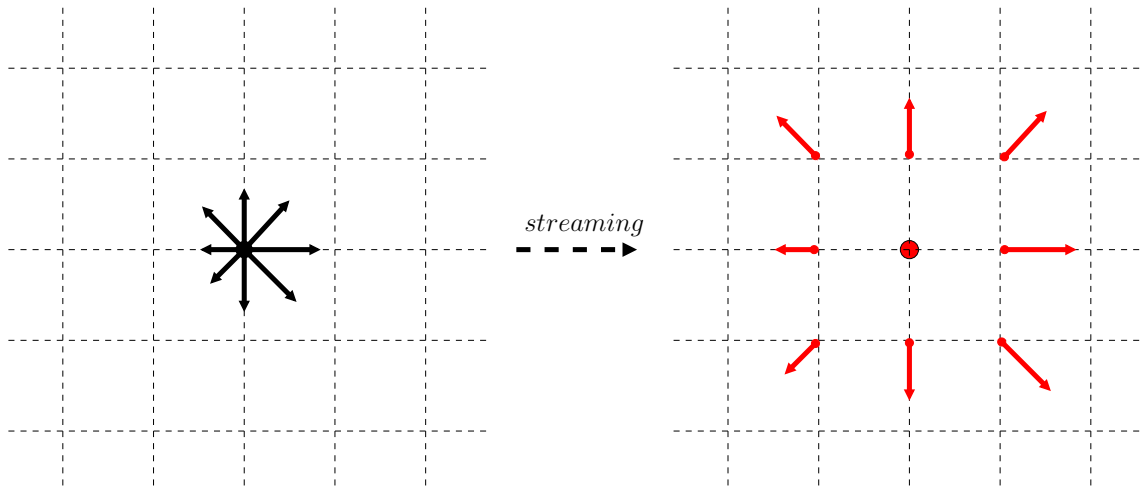Figure 9.2: Illustration of the streaming process on a $D2Q9$ lattice. Note that the magnitude of the DFs remain unchanged, but they move to a neighbouring node according to their direction.
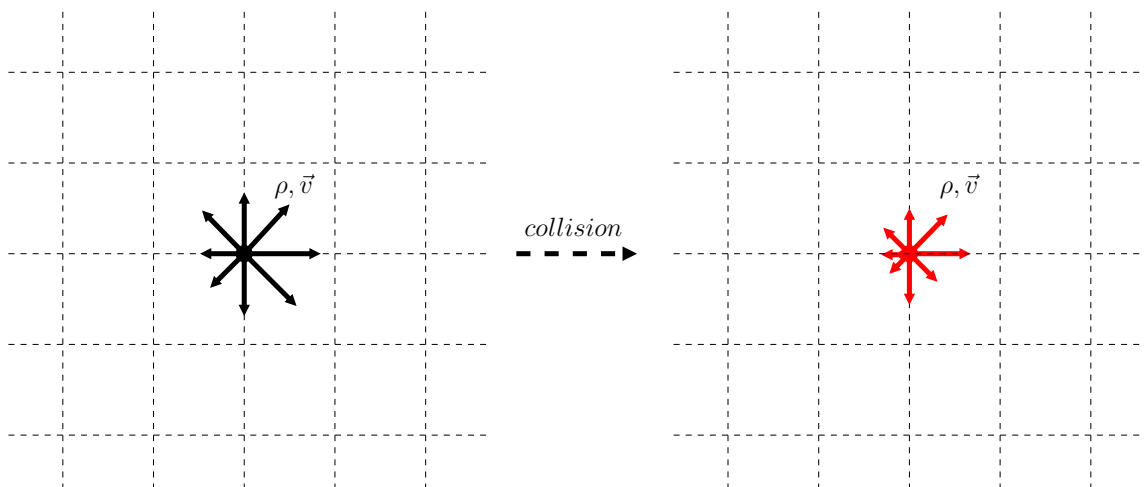

Figure 9.3: Illustration of the collision process on a $D2Q9$ lattice. Note that the local density ρ and velocity $\vec{v}$ are conserved, but the DFs change according to the relaxation-to-local-Maxwellian rule.

Boltzmann SPDF (see for example He and Luo [1997]); they are

$$f_a^{eq}(\vec{x}) = w_a \rho(\vec{x}) \left[1 + 3 \frac{\vec{e}_a \cdot \vec{u}}{c^2} + \frac{9}{2} \frac{(\vec{e}_a \cdot \vec{u})^2}{c^4} - \frac{3}{2} \frac{\vec{u}^2}{c^2} \right] , \qquad (9.55)$$

where for the $D2Q9$ model the weights are $w_{a=0} = 4/9, w_{a=\{1..4\}} = 1/9, w_{a=\{5..8\}} = 1/36$ and c is the propagation speed on the lattice, $c = \delta_x / \delta_t$. Under the afore-mentioned assumption of a low Mach number, and further taking $\{Kn^7, \delta_t, \delta_x\} \to 0$, this model recovers the incompressible Navier-Stokes equations:

$$\nabla \cdot \vec{u} = 0 , \qquad (9.56)$$

$$\rho \partial_t \vec{u} + \rho \vec{u} \cdot \nabla \vec{u} = -\nabla P + \rho \nu \nabla^2 \vec{u} \qquad (9.57)$$

with an isothermal equation of state:

$$P = c_s^2 \rho , \qquad (9.58)$$

where P is the pressure. The viscosity of the fluid is related to the relaxation parameter τ by the equation

$$\nu = c_s^2 (\tau - 1/2) \frac{\delta_x^2}{\delta_t} \Rightarrow \tau = \frac{\nu}{c_s^2} \frac{\delta_t}{\delta_x^2} + \frac{1}{2} \xrightarrow[c_s^2|_{D2Q9}=1/3]{} \tau_{D2Q9} = 3\nu \frac{\delta_t}{\delta_x^2} + \frac{1}{2} \qquad (9.59)$$

The proof of these results follows from the Chapman-Enskog analysis. Eq. (9.59) provides a straightforward method for adjusting the fluid viscosity in the model. It is obvious that $\tau \geq 0.5$ is required in order to ensure a positive viscosity. The limit $\tau \to 0.5$ corresponds to the inviscid flow, while the $\tau \to \infty$ limit represents the Stokes (creeping) flow. The model described so far is only applicable to athermal liquids. While there are many flow situations which can be attributed to this class, thermal effects are often essential to many natural phenomena. A suitable approach consists of solving the passive scalar equation for temperature on a separate lattice. The temperature field is

---

[7]The assumption of $Kn \equiv \frac{\lambda}{L} \to 0$ is a requirement for continuum models to apply, hence it is not specific to LBM.

influenced by the fluid advection, and influences the fluid through a buoyancy term. This approach is only valid in the Boussinesq approximation, which is a reasonable assumption for many flows (for example, in ocean flows). The LB evolution algorithm is the same on the temperature lattice, but with different equilibrium DFs. Also, because the macroscopic quantity is a scalar (in contrast to the LBM for the velocity field, which is a vector), a lattice with fewer velocity directions is sufficient (D2Q5). The evolution equation on the temperature lattice is described by the same type of LB equation:

$$\underbrace{g_a(\vec{x} + \vec{e}_a\delta_t, t + \delta_t) = g_a(\vec{x}, t)}_{\text{Streaming}} \underbrace{- \frac{[g_a(\vec{x}, t) - g_a^{eq}(\vec{x}, t)]}{\tau_T}}_{\text{Collision}}, \tag{9.60}$$

The macroscopic temperature is recovered by summation:

$$T = \sum_{i=0}^{4} g_i \tag{9.61}$$

The main difference however lies in modified equilibrium distributions:

$$g_i^{eq} = T w_{T,i} \left[1 + 3e_{T,i}^{\rightarrow} \cdot \vec{u}\right] \tag{9.62}$$

where the weights on the thermal lattice read $w_{i=0} = 1/3$, $w_{i=\{1..4\}} = 1/6$, and the thermal diffusivity is related to the thermal relaxation time τ_T through:

$$\tau_T = 3\kappa \frac{\delta_t}{\delta_x^2} + 1/2 \tag{9.63}$$

The back-coupling to the velocity field is accomplished through an additional force term in the RHS Eq. (9.54):

$$dF_i = -3w_i \rho \beta g (T - T_0)(\vec{e}_i \cdot \hat{j}) \tag{9.64}$$

9.4.2   Simulation set-up of the Rayleigh-Bénard convection

An important part of any numerical simulation is relating the simulation input parameters and output results to the exact flow we intend to model. The key concept during these procedures is *dynamic similarity*, which tells us that two flows with different physical parameters are effectively equivalent as long as several dimensionless numbers are the same. This idea is of special importance in experimental and numerical fluid dynamics (e.g., sections 1.4, 7.5). Similarily, in CFD, the fluid solver usually works in a different lengthscale than the original, physical system that is to be simulated. We can distinguish **3** different frames of reference in a simulation, described below. The dimensionless system may seem like an unnecessary complication in the beginning, but it reflects the fact that flows are often given in the literature in this form.

1. **Physical system:** is the actual system that we intend to simulate. Here, we measure things in the usual meters, seconds and kilograms. A problem with this system is that it is very dependent on the units, which are not important to the mathematics behind the PDEs governing the flow. However, any practical application of fluid mechanics has to start from this system and return to it when results are to be reported.

2. **Dimensionless system:** by choosing typical length- and time-scales for our flows, we can non-dimensionalize the equations, which then become more amenable to numerical simulation. Note that, sometimes, it is necessary to choose also a typical mass and/or temperature, depending on the form we take for the macroscopic equations.

3. **Discrete system:** is the coordinate system in which our numerical simulation lives. The input parameters for our simulation propagate from the physical system, through the non-dimensional system until here. Due to reasons of numerical stability, several restrictions are in place at this level, as will be discussed during the practical examples below.

The application we are looking at is the two-dimensional convection driven by a temperature gradient (Rayleigh-Bénard convection). The geometry consists of a rectangular channel, with periodic BCs at the sides and no-slip and constant temperature BCs on the top and bottom walls (section 2.2). Now we can non-dimensionalize the equations by choosing some typical values

for lengthscale L and timescale T of the system. As a reference length L, we take the distance between the two walls. We also need a value for scaling our temperature. Since we are imposing a specific temperature difference throughout our fluid domain, the temperature values will be within this range everywhere, and it makes sense to scale temperature by this value (ΔT). The presence of the gravitational constant in the equations provides us a natural timeframe. The first guess would be to take $g = L/T^2$, but we can make a better choice which also allows us to cancel-out the thermal expansion coefficient in the dimensionless system, namely:

$$g = \frac{L}{\alpha(\Delta T)T^2} \Rightarrow T = \sqrt{\frac{L}{g\alpha(\Delta T)}} \tag{9.65}$$

The physical quantities can then be written in terms of the dimensionless ones as $p = \rho_0 \frac{L^2}{T^2} p_d$ and for temperature $T = T_d(\Delta T) + T_0$. Plugging-in these expressions into the eqs. in section 2.2 we eventually obtain:

$$\boldsymbol{\nabla}_d \cdot \vec{u}_d = 0 \tag{9.66}$$

$$\partial_{t_d} \vec{u}_d + (\vec{u}_d \cdot \boldsymbol{\nabla}_d)\vec{u}_d = -\boldsymbol{\nabla}_d p_d + \sqrt{\frac{Pr}{Ra}}\boldsymbol{\nabla}_d^2 \vec{u}_d + T_d \hat{j} \tag{9.67}$$

$$\partial_{t_d} T_d + \boldsymbol{\nabla}_d \cdot (\vec{u}_d T_d) = \sqrt{\frac{1}{RaPr}}\boldsymbol{\nabla}_d^2 T_d \tag{9.68}$$

Where Ra and Pr are the characteristic Rayleigh and Prandtl numbers of the system, defined as

$$Pr \equiv \frac{\nu}{\kappa} \tag{9.69}$$

$$Ra \equiv \frac{g\alpha(\Delta T)L^3}{\nu\kappa} = Pr \cdot \frac{g\alpha(\Delta T)L^3}{\nu^2} \tag{9.70}$$

$$\xrightarrow{eq.\textbf{9.65}} \nu = \frac{T}{L^2}\nu = \sqrt{\frac{Pr}{Ra}}; \quad \kappa = \sqrt{\frac{1}{RaPr}} \tag{9.71}$$

The temperature BCs become in the dimensionless system:

$$T_{d,hot} = 1$$

$$T_{d,cold} = 0$$

Discretization of the dimensionless system   Let us denote by N the number of gridpoints we use to discretize and by N_{iter} the number of time iterations which will resolve our unit timescale T_d. We then have the following discrete space- and time-step in the dimensionless system:

$$\delta_x = \frac{1}{N-2}; \quad \delta_t = \frac{1}{N_{iter}-1} \tag{9.72}$$

Note that for computing the space-step we need to subtract 1 because p points always delimitate $p-1$ segments, and $(2 \times 0.5) = 1$ due to the interpretation of the horizontal walls half-way between 1st and 2nd (respectively half-way between $N-1^{th}$ and N^{th}) lattice rows. For time-steps, we obviously do not have the second issue, thus we only subtract 1.

In a sense, we repeat the procedure we applied to non-dimensionalize the original equations, except that we use δ_x and δ_t instead of the previous L and T. There is no need to rewrite the equations, since we are interested at this stage only on the parameters that we need to provide to our simulation to get the desired flow. We can easily write expressions for the most relevant quantities in the discrete (LB) system:

$$\vec{u_{lb}} = \frac{\delta_t}{\delta_x}\vec{u_d}; \quad g_{lb} = \frac{\delta_t^2}{\delta_x}g_d;$$

$$\nu_{lb} = \frac{\delta_t}{\delta_x^2}\nu_d = \frac{\delta_t}{\delta_x^2}\sqrt{\frac{Pr}{Ra}}; \quad \kappa_{lb} = \frac{\delta_t}{\delta_x^2}\kappa_d = \frac{\delta_t}{\delta_x^2}\sqrt{\frac{1}{RaPr}}; \tag{9.73}$$

In order to ensure that the compressibility effects do not become significant, a general rule is to keep $\delta_t \sim \delta_x^2$. Let us denote by β the proportionality factor (i.e. $\delta_t = \beta\delta_x^2$). The choice of β is not very obvious. If it is chosen too big, the timesteps get too large and the accuracy of the simulation decreases. However, if β is too small, the simulation takes a long time. This means

a compromise for β has to be found (Here, we choose $\beta = 11.18$ for $\delta_x = 0.02$). Once the number of gridpoints is given, this relation gives number of timesteps to resolve t_{0p}.

We also need to choose a representative value for the temperature, but we can simply pick a one-to-one mapping from the dimensionless system.

$$T_{lb} = T_d \tag{9.74}$$

We could write the formulae for converting the results back to the dimensionless and/or physical system.

9.4.3 System preparations and running a simulation

There are only a few parameters that define the behavior of the system: The number of gridpoints (lx, ly) defines the size of the lattice and thereby directly affects the accuracy of the results. On the one hand we get better results with a finer grid but on the other hand the computational cost increases dramatically. The parameter N_t0 descibes the maximal simulation time in units of t_{0d}. For a given physical system t_{0d} can be calculated using eq. 9.65. N_t0 should be high enough to overcome the inital conditions.

Remember that the Rayleigh (Ra) and Prandtl (Pr) numbers are dimensionless numbers that define the character of the flow. Pr is the ratio of the viscosity ν and the thermal conductivity k. Ra describes the heat transfer of a buoyancy driven flow. Some results for different sets of parameters can be seen in figure 9.4. As seen in section 9.4.2 *beta* is the factor that couples the spatial and temporal step sizes of the lattice. As for the grid resolution, a compromise between accuracy of the results and computing time has to be found!

Run simulation   After installation run R and change the working directory of R to the path where the *.r-files of the model are located:

```
setwd('Path/of/Rayleigh_Benard_model')
```

If all parameters are set properly, the model is loaded and executed by the command
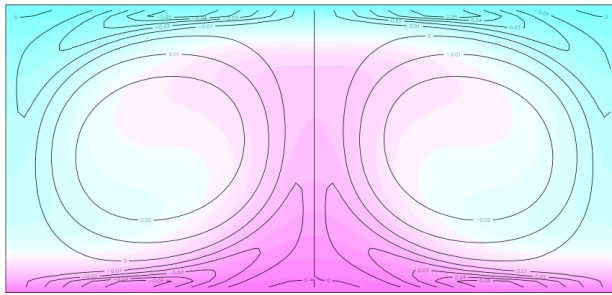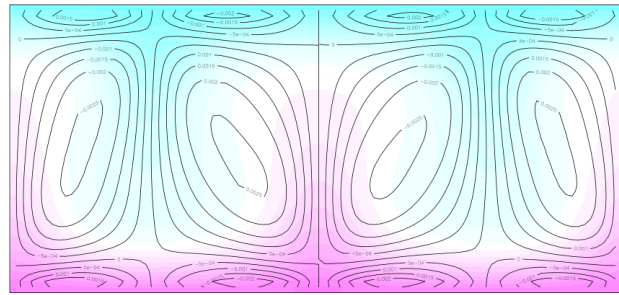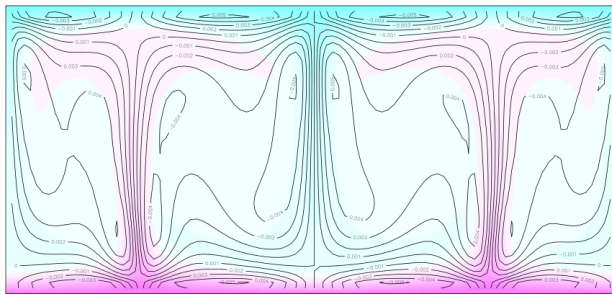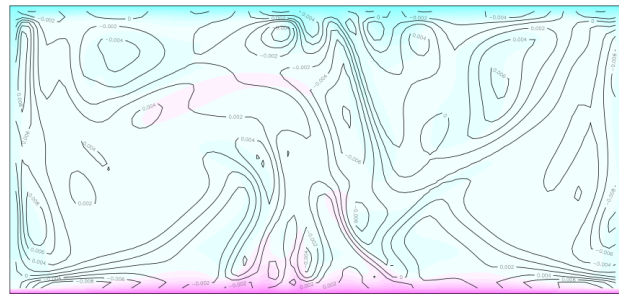
(a) $Ra = 2 \cdot 10^4$, $Pr = 0.1$

(b) $Ra = 2 \cdot 10^4$, $Pr = 10$

(c) $Ra = 5 \cdot 10^5$, $Pr = 10$

(d) $Ra = 1 \cdot 10^7$, $Pr = 10$

Figure 9.4: Four examples of the flow for different sets of Ra and Pr. The contours show lines of constant vorticity; the colors in the background display the temperatures (purple - warm, blue - cold).

```
source('rayleigh-benard.R')
```

After the simulation has completed the results can be found in the folder defined by the parameter *out_dir*. For a new run, the old directory has to be removed or renamed. All necessary files and parameters are shortly described here. Your application should come with the following files:

- rayleigh-benard.R | The R source code

- rb_functions.R | Some extra R functions needed by the model

- rb_plot_functions.R | Some R functions for plotting the results

There are two different types of parameters that can be edited: the 'model parameters' (which define the 'physical' values needed for the simulation), and the 'output parameters' (which define the frequency and kind of output).

Here is some R-code of the code calculating the macroscopic moments rho, ux, uy, T:

```
#Compute macroscopic values
  rho = colSums(flIn, dims=1);
  T = colSums(TIn, dims=1);
  ux = colSums( cx_fl*flIn, dims=1 ) / rho;
  uy = colSums( cy_fl*flIn, dims=1 ) / rho;
```

which is related to (9.52, 9.53) and (9.61), respectively. *cx_fl* and *cy_fl* denote the 9-dimensional momentum component ($\vec{e}_a$ in 9.53) and are related to the microscopic velocities $\vec{e}$ in the distribution function $f(\vec{x}, \vec{e}, t)$ of the Boltzmann dynamics (9.26). The main part of the code is the collision step for momentum and temperature:

```
#Collision Step
  #Fluid momentum
  for (i in idxRangeFluid){
    cu_fl = 3* (cx_fl[i] * ux + cy_fl[i] * uy);
    flEq= rho * w_fl[i] *
        (1 + cu_fl + 0.5 * cu_fl^2 - 1.5 * (ux^2 + uy^2));
    force = 3* w_fl[i]* rho * (T-T0)*
        (cx_fl[i] * g[1] + cy_fl[i] * g[2])/(T_bot - T_top);
    flOut[i,,] = (1.-omega_fl)*flIn[i,,] + omega_fl*flEq + force;
  }

  #Temperature
  for (i in idxRangeTemp){
    cu_T = 3* (cx_T[i] * ux + cy_T[i] * uy);
    TEq = T * w_T[i] * (1 + cu_T);
    TOut[i,,] = (1.-omega_T)*TIn[i,,] + omega_T*TEq;
  }
```

where *fl_Eq* and *T_Eq* denote the local Maxwell-Boltzmann single-particle distribution function.

Exercise 66   –   Investigations with the LB-model

1. Vary the Rayleigh and the Prandtl number by $R_a = 20000, 40000, 60000$ and $Pr = 0.5, 1, 1.5, 5, 10$ and describe the dynamics (words, figures) ! For high values of R_a the spatial resolution might be chosen higher (to the double). Here are the standart values:

```
lx  = 100;    #Number of horizontal cells
ly  = 52;    #Number of vertical cells
```

2. Vary the initial perturbation and obtain the reversed circulation! Look at the line

```
#Set small trigger to break symmetry
T[lx/2+1, 1] = 1.1 * T_bot;
```

Here, some remarks related to the boundary conditions are in order. When using a Dirichlet boundary condition, one prescribes the value of a variable at the boundary, e.g. temperature or density in our case. When using a Neumann boundary condition, one prescribes the gradient normal to the boundary of a variable at the boundary, e.g. the heat flux or density flux. When using a mixed boundary condition, different types of boundary conditions can be used for different variables (e.g. for temperature and salinity).

In viscous flows, no-slip condition enforced at walls:

-Tangential fluid velocity equal to wall velocity.

-Normal velocity component is set to be zero.

This is realized through a bounce back condition: a particle travelling in the e_1-direction is bounced back into the opposite e_5-direction. A modified version of the previous problem is an ocean box with solid walls and free slip at the surface (no friction). This is implemented by mirroring (relative to horizontal-axis) the distribution functions in the fluid-lattice:

```
#"Bounce Back" Boundary Conditions for Fluid
  for (i in idxRangeFluid){
    flOut[i,,1]  = flIn[opp_fl[i],,1];
    flOut[i,,ly] = flIn[opp_fl[i],,ly];
  }
```

Used when physical geometry of interest and expected flow pattern and the thermal solution are

of a periodically repeating nature (as in the Rayleigh-Bénard problem). This reduces computational effort in problem.

Exercise 67   –   Ocean-like circulation

1. Evaluate the effect of different external temperatures (hemispheric, double hemispheric).

   The R code is

   `ocean_rb.R`

   Here are two options:

   ```
   # Pre-compute imposed temperature-profile on top (linear)
   tempTop = array(0, c(lx));
   for (x in 2:lx-1) {
     tempTop[x] = THot - (THot-TCold)*(x-2)/(lx-3);
    }
   ```

   for a single hemisphere, and for a double hemisphere version:

   ```
   # Pre-compute imposed temperature-profile on top (linear+sinus)
   tempTop = array(0, c(lx));
   bett= 0.2 # right boundary
   alph= (0.1-bett)/lx ;
   gamma =1.-alph * lx/2 -bett;
   for (x in 2:lx-1) {
     tempTop[x] = alph *x + bett + gamma * sin( 3.1416* x/lx);
   }
   ```

   Describe the dynamics with respect to the temperature at the top layer tempTop !

2. In lattice Boltzmann models, it is relatively easy to insert obstacles. The R code is

   `ocean_rb_ridge.R`

   Discuss the influence of the ridge on the ocean circulation!

3. Manage to change the Rayleigh-Bénard convection from a no-slip to free slip bounday conditions at the top. The upper plate is just removed and we have an air-water interface. What are the differences? Make a plot!

4. Provide a model for the atmospheric cells (the atmosphere is mainly heated from below).

5. Calculate the ocean heat transport in the model and compare it with the estimate in exercise 46! Use dimensionless parameters!

(a) Two hemisphere temperature

(b) Ridge and a two hemisphere temperature

(c) Linear temperature gradient

(d) Flow including a ridge
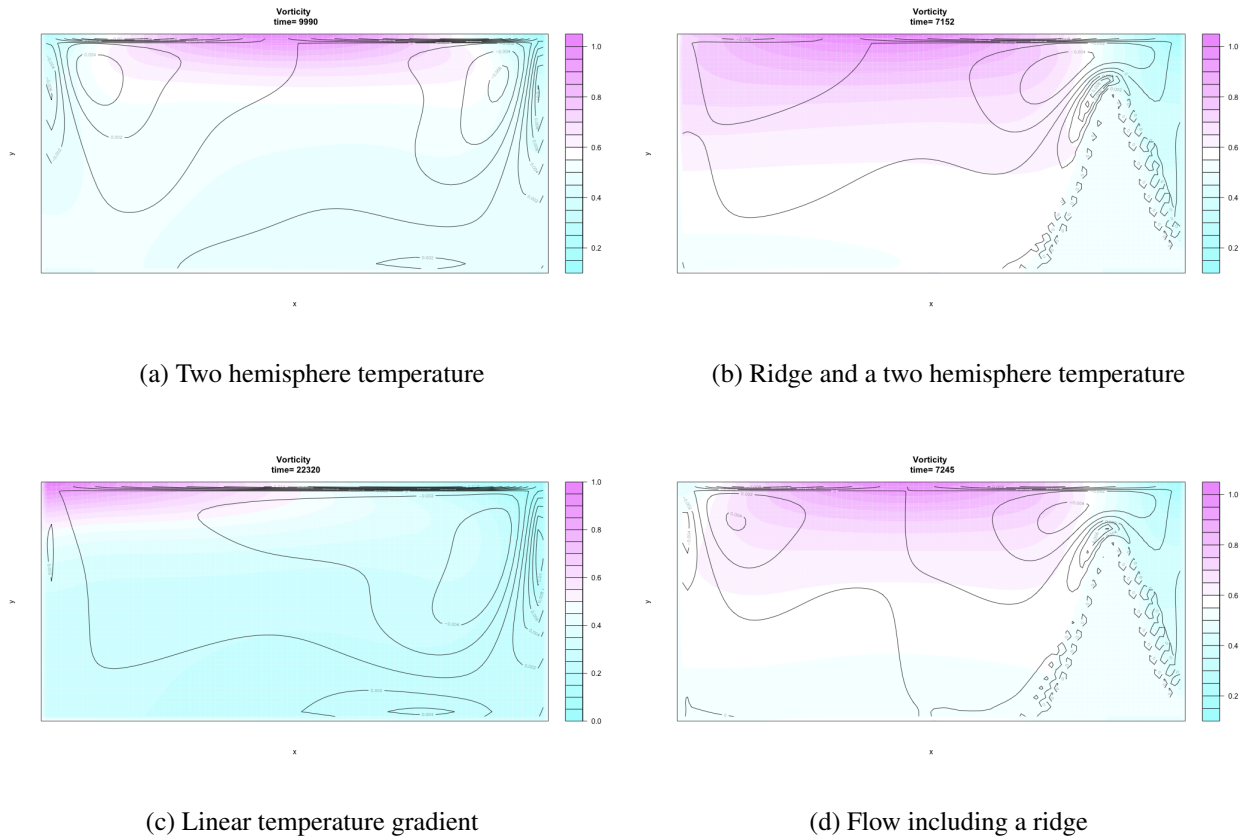
Figure 9.5: Four examples of the ocean flow for different boundary conditions, and fixed Prandtl number=1 and Rayleigh number=45000. The contours show lines of constant vorticity; the colors in the background display the temperatures (purple - warm, blue - cold). For the right scenarios, an obstacle representing an oceanic sill is implemented.

Part IV

Fourth part: Programming and tools

Chapter 10

Programming in R

10.1 Install R

The latest version of R for Linux, OS X and Windows is freely available on the CRAN webpage: http://cran.r-project.org (Fig. 10.1). Download and install the R version for your operating system (for many linux distributions R is also available in the package management system).Furthermore, look at the web page for R studio http://www.rstudio.com/, R studio is a free and open source user interface for R. One particular package is Shiny. This makes it super simple for R users like you to turn analyses into interactive web applications that anyone can use.
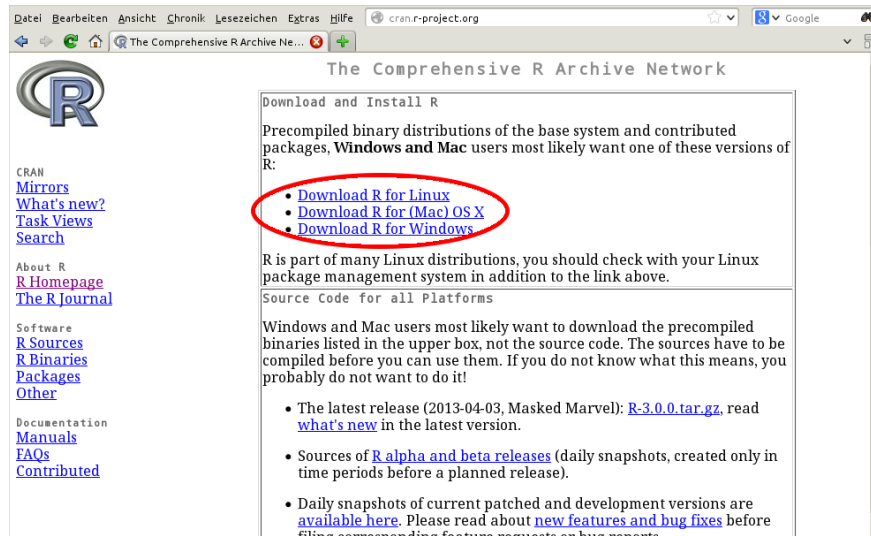
Figure 10.1: R is available for download from the CRAN webpage: http://cran.r-project.org.

10.2 Examples to start

Please see the web page for some information how to get R running: http://www.r-project.org/, https://paleodyn.uni-bremen.de/gl/r.html. Using R for Introductory Statistics. Here is some introduction to basics.

```
############# this letter is used for comments

#?function    shows the help for a function
?sin

#There is no definition needed for simple (scalar) variables
#but instead of =, <- is used
#just assign name<-value
a<-1

#Print the number on the screen:
a #prints only on the console
print(a) #prints always

#simple algebraic calculations
a<-2*3
a<-a/2
print(a) # and print again

#some vector / array functions
#vectors / arrays normally need to be defined that R can distinguish it
#from a scalar.
```

```r
y<-vector() #Produces an empty vector...

#the size of vectors in R is dynamic... I can now assign y[1]...
#Assign elements of the vector [i], Vectors index are starting with 1

y[1]<-1
y[2]<-2
print(y)
print(y[1])

#very often vectors filled with equidistant values are needed
x<-1:10    #x = vector (1,2,3,4,5,6,7,8,9,10)
print(x)
x<-(1:100)/5  # (0.2,0.4,0.6 ..........)
print(x)

#Control structures:
#for loop: for (variable in array) { }
for (i in 1:100)
{
  print(i)
}

#plotting function

#plot(y), plot y against equidistant steps
y<-1:100
plot(y)

#plot(x,y), plot y against x
x<-(1:100)*5
plot(x,y)   #note the changes in the x-axis

# more advanced functions:

#further parameters that can be used in plotting commands.
#type = "l" : as line type
#col = "color": plotting color
#ylim = c(minval,maxval):Set the limits of the y-axis
#main = "title": sets the title

plot(x,y,col="red",main="example",type="l",ylim=c(1,70))

# overplotting: line(x,y) or line(y) is the same as the plot command
# but plots a line on an already existing plot
# whereas plot is starting a new plot

z<-x^2 / 100
plot(x,y,col="red",main="example",type="l",ylim=c(1,70))
lines(x,z,col="blue")
```

```
#defining a function
multiply <- function(x,y)
{
  return(x*y)
}

print(multiply(3,4))
```

10.3   Reading and writing data

```
#Data Input from File, place file in dir. getwd()
#Store a table from a text file in an R-variable D
D<-read.table("test.txt",header=T)

# What read.table does is try to read data
# from the file named as the first argument.
# If header is specified as T (True),
# the first line will be read as the column names
# to which the values are assigned.  Header defaults to F (False).
# The function write.table() performs the opposite transformation.


#reading and writing data
x<-(1:100)*5
y<-x^2
write.table(y,file="xytdata.dat") # writing

#dev.print(pdf, MyPlot.pdf)
```

1. Load a R file into the R workspace

2. Save the file using another name

3. Keep the original version when modifying the file

4. Execute the whole file (CTRL-A to mark everything, CTRL-R to run it)

5. All functions are then in the memory

Exercise 68   –   Simple start of R

1. Download and install the R-Software. http://cran.r-project.org → Download CRAN → search a city near you Choose your system (Windows / Mac / Linux) Follow the instructions.

2. Create a vector t "t<-seq(-2*pi,2*pi,by=0.01)"

   plot several functions in one window $(\sin(t), \cos(t), \exp\left(\frac{t}{5}\right), \left(\frac{t}{5}\right)^2, \left(\frac{t}{5}\right)^3)$. Try some of the plot arguments: Set ylim, label the axes, set a different colour for each function, vary the line width. Save the plot as a figure.

   For help try "?plot" or "?plot.default"

3. Set up a vector of length 20 and create a vector b with a linear relationship to a (e.g. $a = 3b + 7$). Calculate the correlation("cor(a,b)").

4. Set up two random vectors a,b of length 20 and calculate the correlation. Repeat this procedure several times to get a feeling for the correlation coefficient. Than vary the length of vector a and b (vary the sample number) and discuss how the correlation coefficient changes (e.g. 10,50,100,1000).

5. Repeat the experiment from task 4 100 times by using a loop. Create before the loop an empty vector ("cor.val<-vector()") and save the correlation of a and b in this vector (e.g. "cor.val[i]<-cor(a,b)") for each realisation. Compute the mean value and plot the histogram of cor.val. What happens with the histogram when the length of a and b is varied (e.g. 10,50,100)? Save two different histograms as a figure and explain the difference between them.

6. Repeat the procedure of task 5. with partly linear dependent vectors: ("a<-rnorm(100); b<-r*a+rnorm(100)") Choose one value for r and shortly discuss the mean value and the histogram of cor.val compared to task 5. Save the histogram as a figure.

```
# Important R-commands
rnorm(N) # create vector with N normal distribution random numbers
cor(a,b) # calculates the correlation coefficient
```

```
hist(a)   # histogram of vector a
mean(a)   # mean value of vector a


# Helpful introductions to R can be found in e.g.
```

link to Rintro.pdf

link to http://cran.r-project.org/doc/manuals/R-intro.pdf

Exercise 69   –   Short programming questions

Write down the output for the following R-commands:

a) `0:10`

b) `a<-c(0,5,3,4); mean(a)`

c) `max(a)-min(a)`

d) `paste("The mean value of a is",mean(a),"for sure",sep="_")`

e) `a*2+c(1,1,1,0)`

f) `my.fun<-function(n){return(n*n+1)}`

   `my.fun(10)-my.fun(1)`

Exercise 70   –   Difference equations

Consider the discretised form of (2.93) with $r = r_0(1 - x)$. Using the Euler scheme

$$\frac{d}{dt}x \approx \frac{x_{n+1} - x_n}{\Delta t} \quad . \tag{10.1}$$

1. Write down the iteration x_{n+1} as a function of x_n for the case 1a!

2. What is the solution of x_{n+1} as a function of x_0? Consider the stability for the cases $r > 0$,

   $0 > \Delta t\, r > -1, \quad -1 > \Delta t\, r > -2, \quad -2 > \Delta t\, r$. Do you have a graphical

   interpretation of the oscillation/decay?

3. Write down the iteration x_{n+1} as a function of x_n for the case 1b!

```
# ODE1.R
#demonstration of Euler forward method in 1st order ODE: dy/dt=A*y

#constants
A<-  -0.5  #growth / decay rate
T<-  20    #integration time in time units
dt<-  .1    #step size in time units
Y0<- 100   #inital value


n<-T/dt          #number of time steps (time / timestep)
t<-(0:(n-1))*dt  #create a vector of discrete timesteps
y<-vector()      #define an empty vector for the state variable y(t)
y[1]<-Y0         #assign initial value
```
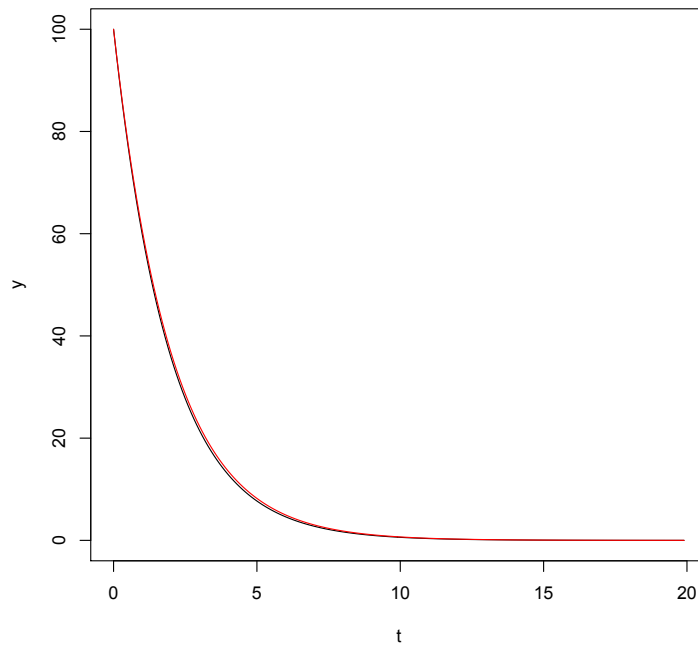
Figure 10.2: Euler forward method in exercise 71.

```
for (i in 1:(n-1))
{
  y[i+1]<-y[i]+dt*A*y[i]
}

plot(t,y,type="l") #plot the result against time

#additionaly plot the analytical solution in red
lines(t,Y0*exp(A*t),col="red")
```

Exercise 71 – Euler numerical scheme

Demonstration of the Euler forward scheme on the first order ODE: dy/dt=A*y

- Describe one physical process which can be described with this ODE

- Write the analytic solution for this ODE

- Write the ODE as finite differences

- Open the program ODE1.R and try roughly to understand the code (where is the integration?)

- Run the code and compare the numerical results with the analytic ones.

Exercise 72   –   Numerical solution of 1D Diffusion

- What is the differential equation for the 1D Diffusion

- Open DiffusionEulerForward.R

- Identify / extract the finite difference scheme which is used approximate the 2nd derivative

- Run the program and play with the parameters. Which time steps can be taken?

```r
#Diffusion_EulerForward.R
# 1D diffusion equation, explicit scheme

#Constants
L.X<-50 #width of lattice
L.T<-5  #length of time
dx <- 1    #space step
dt <- 0.1  #time step
D<-1             #Diffusion coefficent


N.x<-L.X/dx + 2    #number of space boxes + 2 boundary boxes
N.t<-L.T/dt        #number of time boxes

u<-matrix(0,N.t,N.x)   #grid
#temporary vector which stores the state of of one timestep:
u.temp<-rep(0,N.x)

#Set the starting and boundary condition, here one value in the middle:
u[1,N.x/2]<-1


for (n in 1:(N.t-1))
{
  for (j in 2:(N.x-1))
  {
    u.temp[j]<-u[n,j]+D*dt/(dx^2)*(u[n,j+1]-2*u[n,j]+u[n,j-1])
  }
  u[n+1,]<-u.temp
}


filled.contour((1:N.t)*dt,(1:N.x)*dx,u,
        color.palette=rainbow,xlab="time",ylab="space")
```
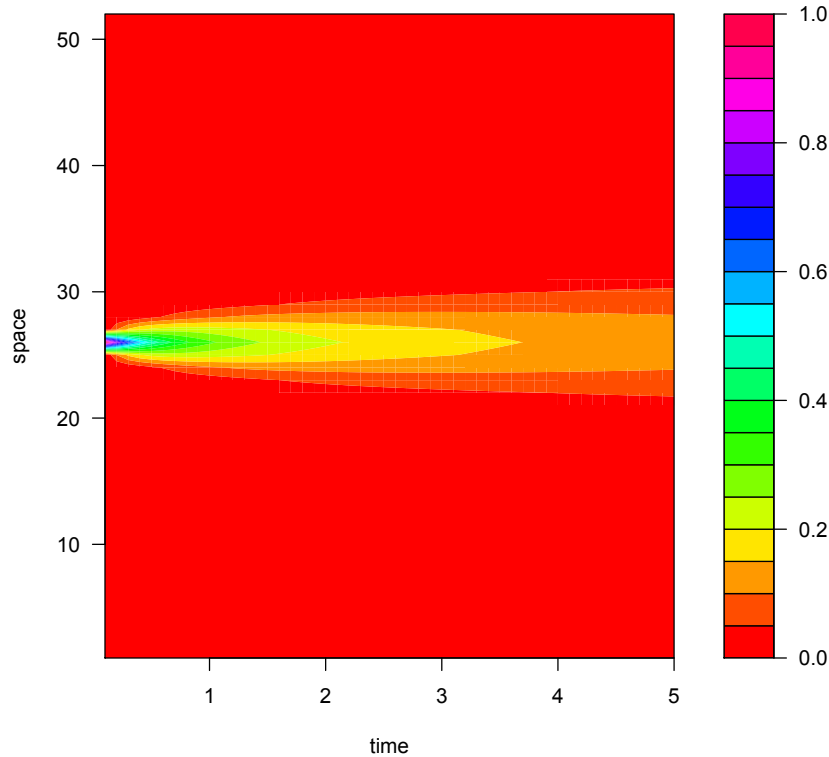
Figure 10.3: Numerical solution of 1D diffusion in exercise 72.

10.4 CFL criterium*

In mathematics, the Courant-Friedrichs-Lewy (CFL) condition is a necessary condition for convergence while solving certain partial differential equations (usually hyperbolic PDEs) numerically by the method of finite differences. It arises in the numerical analysis of explicit time integration schemes, when these are used for the numerical solution. As a consequence, the time step must be less than a certain time in many explicit time-marching computer simulations, otherwise the simulation produces incorrect results. The condition is named after Richard Courant, Kurt Friedrichs, and Hans Lewy who described it in their 1928 paper.

The principle behind the condition is that, for example, if a wave is moving across a discrete

spatial grid and we want to compute its amplitude at discrete time steps of equal duration, then this duration must be less than the time for the wave to travel to adjacent grid points. As a corollary, when the grid point separation is reduced, the upper limit for the time step also decreases. In essence, the numerical domain of dependence of any point in space and time (as determined by initial conditions and the parameters of the approximation scheme) must include the analytical domain of dependence (wherein the initial conditions have an effect on the exact value of the solution at that point) to assure that the scheme can access the information required to form the solution.

We have to turn the differential equation into algebraic equations, also often called discrete equations. The key property of the equations is that they are algebraic, which makes them easy to solve. As usual, we anticipate that uni is already computed such that u_i^{n+1} is the only unknown. Solving with respect to the diffusion equation this unknown is easy:

$$u_i^{n+1} = u_i^n + F(u_{i+1}^n - 2u_i^n + u_{i-1}^n) \tag{10.2}$$

with $F = D\,\frac{\Delta t}{\Delta x^2}$ as the mesh Fourier number which should be < 0.5.

Courant, R.; Friedrichs, K.; Lewy, H. (1928), Über die partiellen Differenzengleichungen der mathematischen Physik, Mathematische Annalen, 100 (1): 32-74, doi:10.1007/BF01448839

10.5   R Markdown

R Markdown documents are fully reproducible. Use a productive notebook interface to weave together narrative text and code to produce elegantly formatted output. Use multiple languages including R, Python, and SQL.

https://rmarkdown.rstudio.com/lesson-1.html

Allaire, JJ, Yihui Xie, Jonathan McPherson, Javier Luraschi, Kevin Ushey, Aron Atkins, Hadley Wickham, Joe Cheng, and Winston Chang. 2018. Rmarkdown: Dynamic Documents for R. https://CRAN.R-project.org/package=rmarkdown.

https://rmarkdown.rstudio.com/articles_intro.html

R Markdown works the same, only that it adds the option to insert R code blocks. An R code block could look something like this:

```
```{r}
# place R code here, e.g. to make a plot:
require(ggplot2)
x <- 1:10; y <- x^2
qplot(x, y)
```
```

When you convert the R Markdown file to HTML, the R code gets executed, the R output captured and inserted into the document, and you have got everything nicely together, with very little work.

To create an R Markdown document in RStudio, all you have to do is go to File, New File, and then select R Markdown. Accept the default settings, and R Studio will generate a new R Markdown file with a few lines of example content. To convert the file into HTML, simply click on the Ḱnit HTMLb̈utton. If you have previously stored your R Markdown file somewhere on your harddisk (with suffix .Rmd), RStudio will automatically save the generated HTML file in the same location, with the same name and suffix .html. The HTML file is self-contained, including all images, so it's easy to publish it on a web page or share it with people. RStudio also provides you with the option to publish the document online on the RPubs website. Just click on the P̈ublishb̈utton in the HTML view.

To learn more about R Markdown, go to: http://rmarkdown.rstudio.com

Chapter 11

Netcdf and climate data operators

11.1 NetCDF

NetCDF (Network Common Data Form) is a set of software libraries and self-describing, machine-independent data formats that support the creation, access, and sharing of array-oriented scientific data. The project homepage is hosted by the Unidata program at the University Corporation for Atmospheric Research (UCAR). They are also the chief source of netCDF software, standards development, updates etc. The format is an open standard.

The software libraries supplied by UCAR provide read-write access to netCDF files, encoding and decoding the necessary arrays and metadata. The core library is written in C, and provides an API for C, C++ and Fortran applications. An independent implementation, also developed and maintained by Unidata, is written in 100% Java, which extends the core data model and adds additional functionality. Interfaces to netCDF based on the C library are also available in other languages including R (ncdf and ncvar packages), Perl, Python, Ruby, Matlab, IDL, and Octave.

A wide range of application software has been written which makes use of netCDF files. These range from command line utilities to graphical visualization packages.

- A commonly used set of Unix command line utilities for netCDF files is the NetCDF Operators (NCO) suite, which provide a range of commands for manipulation and analysis of

364

netCDF files including basic record concatenating, slicing and averaging.

- NcBrowse is a generic netCDF file viewer that includes Java graphics, animations and 3D visualizations for a wide range of netCDF file conventions.

- ncview is a visual browser for netCDF format files. Typically you would use ncview to get a quick and easy, push-button look at your netCDF files. You can view simple movies of the data, view along various dimensions, take a look at the actual data values, change color maps, invert the data, etc.

- Panoply is a netCDF file viewer developed at the NASA Goddard Institute for Space Studies which focuses on presentation of geo-gridded data. It is written in Java and thus platform independent. Although its feature set overlaps with ncBrowse and ncview, Panoply is distinguished by offering a wide variety of map projections and ability to work with different scale color tables.

- The NCAR Command Language is used to analyze and visualize data in netCDF files (among other formats).

- PyNIO is a Python programming language module that allows read and/or write access to a variety of data formats, including netCDF.

- Ferret is an interactive computer visualization and analysis environment designed to meet the needs of oceanographers and meteorologists analyzing large and complex gridded data sets. Ferret offers a Mathematica-like approach to analysis; new variables may be defined interactively as mathematical expressions involving data set variables. Calculations may be applied over arbitrarily shaped regions. Fully documented graphics are produced with a single command.

- nCDF-Browser is a visual nCDF browser, written in the IDL programming language. Variables, attributes, and dimensions can be immediately downloaded to the IDL command line

for further processing. All the Coyote Library files necessary to run nCDF-Browser are available in the zip file.

- ArcGIS version 9.2 supports netCDF files. The Multidimension Tools toolbox can be used to create raster layers, feature layers, and table views from netCDF data in ArcMap, or convert feature, raster, and table data to netCDF.

- Origin 8 imports netCDF files as matrix books where each book can hold a 4D array. Users can select a subset of the imported data to make surface, controur or image plots.

- The Geospatial Data Abstraction Library provides support for read and write access to netCDF data.

Exercise netcdf

In this exercise we will learn to know various helpful tools and techniques that are used in the analysis and processing of climate data. First, we will learn to know the NetCDF file format in a few short practical demonstrations. Second, some data analysis will be performed on available gridded climate data. In a third step we will transfer our knowledge to shell-programming, in that we combine a number of common command-line tools in order to solve a simple scientific problem. To this end, a Linux-shell, in combination with common shell-programs, is necessary. Since not every attendee of this course has such a computing environment available, the shell-program will be demonstrated by the tutor.

Topics that this exercise considers are:

- **Net**work **C**ommon **D**ata **F**orm (NetCDF): general information on the topic and how to use NetCDF files

- **C**limate **D**ata **O**perators (CDO): several examples of data reduction, analysis and transformation of NetCDF files, including operator piping

- **B**ourne-**a**gain **sh**ell (Bash): definition of variables, if-then-else construct, checking for the existence of a specific file, for-counter-loops, integer-arithmetic, pipes, initializing of shell variables with program output, generation of strings via variable concatenation; these programming-methods are illustrated at the example of a simple scientific model of sea-level rise

- **S**tream **ED**itor (SED): removing spaces from a string

- **b**asic **c**alculator (bc): simple floating-point arithmetic

In the following some information regarding tools and methods of this exercise is collected in the form of a very general overview. This information collection is intended as a supplement to the lecture. Few further information sources are listed in the subsection "Further Reading". This list is obviously far from being complete, there is a vast amount of freely-accessible information available on-line.

A very precise definition on the characteristic and purpose of NetCDF is given in the NetCDF FAQ, "What is netCDF?" (for a link, see section "Further Reading"):

> "NetCDF (network Common Data Form) is a set of interfaces for array-oriented data access and a freely distributed collection of data access libraries for C, Fortran, C++, Java, and other languages. The netCDF libraries support a machine-independent format for representing scientific data. Together, the interfaces, libraries, and format support the creation, access, and sharing of scientific data."

NetCDF is a data-container that has been established as a widely used file-standard in science and engineering. It has been developed for storing array-oriented values in compact and interchangeable files. The most important characteristics of NetCDF files can as well be found in the NetCDF FAQ, "What is netCDF?". An excerpt, that highlights the advantages of NetCDF with respect to this exercise, is listed here:

- Self-Describing. A NetCDF file includes a description of the data that it contains.

- Portable. A NetCDF file can be accessed by computers that apply different formats of storing integers, characters, and floating-point numbers.

- Scalable. A small subset of a large dataset may be accessed efficiently.

- Appendable. Data may be appended to a properly structured NetCDF file without copying the dataset or redefining its structure.

These characteristics make NetCDF a perfect choice for storing any kind of array-oriented data. The data form that we will work with in this exercise is as well array-oriented - therefore, we will use NetCDF as data container for both input and output of computations.

Since NetCDF is a binary format (in contrast to ASCII-text, which can be examined and edited by means of any common text editor), reading, writing and changing of NetCDF files necessitates the use of dedicated software. Fortunately, such software is freely available and can easily be installed on any UNIX system. The following tools are of particular importance:

- ncview (lightweight but mighty explorer for NetCDF files)

- ncbrowse (a Java-based alternative to ncview for Windows)

- Panoply (a flexible Java-based generator of geographic maps of NetCDF data)

- ncdump (tool for "dumping" the contents of a NetCDF file to human-readable ASCII-text; the complete description and structure of the NetCDF file is preserved)

- ncgen (complementary to ncdump, generates a binary NetCDF file from a NetCDF ASCII-dump)

- ncks (mighty toolbox for modification of NetCDF files)

- cdo (mighty toolbox for analysis and modification of NetCDF files, strong focus on climatological data)

11.2   The Bash, a popular UNIX-Shell

Shells with their scripting ability are probably the most powerful tool of UNIX-systems, which make UNIX-computers the choice for tackling complex scientific problems that involve the analysis and processing of large amounts of data. Particularly the bash-shell is a famous tool for scientists and commonly used during the daily work routine. Yet, giving a comprehensive overview on the use and ability of the bash clearly exceeds the scope of this course. Please refer to a bash-scripting guide referenced below if you would like to gain further insights into the topic and gain abilities in shell-scripting - and note: "... the only way to really learn scripting is to write scripts" (Advanced Bash-Scripting Guide).

Further Reading

The following resources provide an introduction to tools and methods considered in this exercise:

- NetCDF: The NetCDF FAQ
  (www.unidata.ucar.edu/software/netcdf/docs/faq.html)
  The NetCDF Fact Sheet
  (http://www.unidata.ucar.edu/publications/factsheets/current/netcdf_factsheet.pdf)

- CDO: The CDO User's Guide
  (https://code.zmaw.de/projects/cdo/embedded/1.6.3/cdo.html)
  The CDO Reference Card
  (http://www.iac.ethz.ch/edu/courses/master/modules/radiation_and_climate_change/download/cdo_refcard.pdf)

- Bash: Bash Guide for Beginners
  (http://www.tldp.org/LDP/Bash-Beginners-Guide/html/)
  Advanced Bash-Scripting Guide
  (http://www.tldp.org/LDP/abs/html/)

Practical exercises for UNIX, cdo, netcdf

For those of you who consider to work in a scientific field with a strong focus on programming or the analysis of large amounts of data: Consider to gain experience with a UNIX-environment, e.g. Ubuntu. In many scientific fields, definitely in climate sciences, UNIX-like operating-systems are the computing environments of choice. Many tools that are necessary for efficiently working in such scientific fields are not natively available on Windows-systems; even if ports are available, they may still suffer from limitations or incompatibilities. It definitely makes sense for you to setup an own partition on your laptop with a Linux-system, and to learn how to use and program the available software tools. For every free UNIX-environment (e.g. Ubuntu) and the included software tools, a vast amount of detailed, yet free, documentation, addressing both novices and experts, can be found on-line.

Visualizing the content of a NetCDF file

Among the provided data files you find a gridded global distribution of sea-ice concentration (variable seaice) and surface temperature (variable tsurf) retrieved from a simulation with a comprehensive climate model (file INIOM_PD_3901-4000_tsurf_seaice.nc). NetCDF is a binary data format that cannot be directly visualized with a simple text editor, special software exists for this purpose. Windows-users please use the program **ncbrowse**, linux-users may alternatively use the native Linux-tool **ncview**.

Please open the NetCDF file and visually inspect the content of variable tsurf. Try to generate an animation of the time evolution of tsurf and answer the following questions:

- What obvious time-dependent pattern is visible?

- How can this pattern be explained, considering that you see the time evolution of a global climatological field?

Creating a PDF that visualizes a regional selection of the content of a NetCDF file

Now please visualize a global distribution of seaice also found in the provided NetCDF file INIOM_PD_3901-4000_tsurf_seaice.nc. The software to be used for this task is **panoply**. Create two plots of Arctic sea-ice distribution, from **45°N** to the North Pole, for March and September of model year 3911, 18:00:00. Apply a meaningful colorbar and export the figure to PDF. Answer the following questions:

- Where do you identify the southernmost extent of sea-ice in boreal winter?

- Where is the sea-ice retreat in summer, by visual inspection, most prominent?

Hint: You can create a map centered on the North Pole by applying a stereographic projection.

Identifying the spatial resolution and physical unit of a NetCDF data set

By use of the tool **ncdump** it is possible to generate a human-readable description of a NetCDF file, that may also include the full data record. Sometimes you are only interested in the header information, and do not want the data record to be extracted (extracting the data record to ASCII can lead to HUGE dumps). If you have ncdump available, extract only the NetCDF data header of file INIOM_PD_3901-4000_tsurf_seaice.nc. This can be done in a Linux shell-terminal via entering the following command:

```
ncdump -h INIOM_PD_3901-4000_tsurf_seaice.nc > headerdump.nc
# the parameter '-h' forces ncdump to omit the extensive data record
# the character '>' is an output-redirection command, that makes
# the output produced by ncdump is written to a file (headerdump.nc)
```

Open the resulting file, or alternatively the file INIOM_PD_39010131_tsurf_seaice.nc.dump that has been provided to you, in an arbitrary text-viewer or -editor, analyze the file content, and answer the following questions:

- What is the horizontal data resolution in units of degrees? Hint: Calculate the meridional (latitudinal) and zonal (longitudinal) resolution of the data set from the number of longi-

tudes and latitudes. Assume that grid cells are equally spaced, and the data set has a global coverage.

- What is the physical unit of variable tsurf?

- If you analyze the header dump of the file INIOM_PD_3901-4000_tsurf_seaice.nc: What is the time resolution of the data? Assume that the complete data set covers a time span of 100 calendar years.

11.3   Reducing data sets with climate data operators

While NetCDF defines a file format (and supporting programs and routines) that can store climatological data in a practical way, the CDO are a collection of operators that allow analysis and modification of gridded binary climatological data. In climate sciences, the CDO have become a very common software tool due to the vast number of available operators and their flexibility:

- more than 400 designated operators are available

- operator-piping allows the application of complex methods on climatological data in a compact way

- the CDO are command-line programs; in combination with shell-scripts they can be automated, and enhanced complexity of data processing and analysis may be achieved

CDO operator piping in combination with shell-programming can be demonstrated shortly in the following very short bash-script, where two input files are interpolated to a common resolution, the resulting fields are added, and the sum is time-averaged, the result being stored in a new file. Shell-programming allows for the diagnostic output of additional information to the screen, here the spatial-average of the field resulting from the CDO-operator-chain. You may find this code in file fldmean.sh that is among the distributed files.

```bash
#!/bin/bash

#select level 6, interpolate to 1x1 degree, convert from deg C to K
cdo timmean -addc,273.15 -remapcon,r360x180 -sellevel,6 input.nc output.nc
#note: the rightmost command ist executed first

#compute global mean
spat_avg=$(cdo output -fldmean output.nc)

#print result to screen
echo
echo
echo "average of global ocean surface temperature is ${spat_avg} K."

#clean up
rm output.nc
```

In the following tasks we will process NetCDF files using the CDO. In order to fulfill these tasks, you may refer to the documentation that is available online (https://code.zmaw.de/projects/cdo/embedded/index.html). For convenience, some useful CDO commands are summarized in the following listing. You may find this code in file cdo_examples.txt that is among the distributed files.

```
#extract a variable named "varname" from file input.nc
cdo selvar,varname input.nc output.nc

#extract the first month of all years in file input.nc
cdo selmon,1 input.nc output.nc

#calculate a time average over a time series input.nc
cdo timmean input.nc output.nc

#generate a seasonal mean from input.nc
cdo seasmean input.nc output.nc

#generate a year mean from input.nc
cdo yearmean input.nc output.nc

#calculate an average annual cycle from file input.nc
cdo ymonmean input.nc output.nc

#select a region from input.nc, longitude "a" to "b", latitude "c" to "d"
cdo sellonlatbox,a,b,c,d input.nc output.nc

#calculate a spatial average of field input.nc
cdo fldmean input.nc output.nc
```

```
#write the output of a CDO operator "a" to the screen (omits file output.nc)
cdo output -a input.nc

#calculate the difference between two NetCDF files input1.nc and input2.nc
cdo sub input1.nc input2.nc output.nc

#multiply two fields input1.nc and input2.nc
cdo mul input1.nc input2.nc output.nc

#add a constant "a" to field input.nc
cdo addc,a input.nc output.nc

#select only regions of input2.nc, for which mask input1.nc is true (i.e. 1)
#represents an if-then programming construct
cdo ifthen input1.nc input2.nc output.nc

#use input2.nc, where mask input1.nc is true - otherwise use input3.nc
#represents an if-then-else programming construct
cdo ifthenelse input1.nc input2.nc input3.nc output.nc

#reduce a data range (a,b) in input.nc to the constant value "c"
cdo setrtoc,a,b,c input.nc output.nc

#replace a data range (a,b) in input.nc by the missing value ("NaN")
cdo setrtomiss,a,b input.nc output.nc

#calculate the trend of a time series in input.nc;
#the trend is defined by offset "a" and slope "b" of the regression line;
#"a" is stored in a.nc, "b" is stored in b.nc
cdo trend input.nc a.nc b.nc

#calculate the horizontal area covered by each grid cell of input.nc
cdo gridarea input.nc output.nc
```

Reducing NetCDF data sets

The file INIOM_PD_3901-4000_tsurf_seaice.nc contains two time series of climatological fields.
Reduce the NetCDF file by performing the following tasks using the CDO:

- Task 1: Split the data set in two separate data sets, one for variable tsurf, one for variable
  seaice.

- Task 2: Calculate a time average over the full time period available in each of the separate
  data sets created in Task 1.

- Task 3: For each of the data sets created in Task 1 calculate an average annual cycle that is representative for the full time period of the time series.

  Hint: In order to create an average annual cycle (multi-year monthly mean), you have to generate a new data set that contains twelve months. The data stored in each time step (month) n of this new data set o must represent the average over all corresponding months contained in the full time series of the initial data set i, i.e. (see CDO documentation):

$$o\left(n, x\right) = \text{mean}\left(i\left(t, x\right), \text{month}(i(t)) == n\right); \quad n \in \left(1, 12\right)$$

- Task 4: Calculate a seasonal mean from the average annual cycle of both variables retrieved in Task 3.

- Task 5: Select only the Northern Hemisphere of the time average retrieved in Task 2.

- Task 6: Calculate the global average temperature from the data set retrieved in Task 2.

- Task 7: Repeat Task 4 using CDO-pipes, i.e. pipe the output of the CDO operator that calculates the average annual cycle of a data set created in Task 3 into the operator for the seasonal mean. Is there any difference between the file generated in this task with respect to the result retrieved in Task 4?

In the following we will further analyze and transform files that were generated during previous tasks.

- Task 8: Transfer the time-average temperature field, retrieved in Task 2 above, to units of °C. What is the average temperature in °C over the Northern Hemisphere?

- Task 9: Calculate global average monthly temperatures for the average annual cycle retrieved in Task 3.

- Task 10: What is the global- and time-averaged temperature over land and ocean? As input you may use the file generated in Task 2. You need to supply to CDO a mask that defines distributions of land and ocean; use variable SLM of file T31GR30_jan_surf.nc.

- Task 11: What is the global average trend in the temperature time series created in Task 1?

- Task 12: Calculate the monthly average sea-ice cover in units of km^2 in the Northern Hemisphere. Use the average annual cycle of the sea-ice field generated in Task 3.

11.3.1 A simple model of sea level rise

In this task we will learn how shell-programming can help in solving scientific problems. We will, based on simple assumptions, write a shell-script that generates a NetCDF data set of a rising sea level, attributed to a loss of land ice, and produces a data set that illustrates the resulting continental flooding. This shell-script can be considered as a very simplified model of continental flooding due to sea-level rise. The only necessary input for this model is a global data set of surface elevation.

The world's water is unevenly distributed among four major climate subsystems and three different states of matter. Respective climate subsystems are the atmosphere (water vapor and droplets, ice crystals), the ocean (liquid water and frozen, solid water), and the land surface (liquid and solid water). The subsystem of the Earth composed of frozen water is commonly referred to as the Cryosphere. It includes permafrost, lake and river ice, sea ice, snow, glaciers, ice caps and ice sheets. Within the Cryosphere, ice sheets are the largest storage of frozen water. At present, there are two major ice-sheets, the Greenland Ice-Sheet (GIS) and the Antarctic Ice-Sheet (AIS), containing water volumes of **7.3** m and **56.6** m sea level equivalent, respectively (see Table 4.1 of the contribution of Working Group 1 to the Fourth Assessment Report by the IPCC, page 342 of http://www.ipcc.ch/pdf/assessment-report/ar4/wg1/ar4-wg1-chapter4.pdf). This means that, assumed both the GIS and the AIS melted completely, the global average sea level would rise by **63.9** m, leading to a flooding of large parts of coastal regions, where **44%** of humankind live.

The relative volume distribution of water between the different physical states of matter (solid, liquid, evaporated) depends on the average surface temperature of the Earth. There have been geologic time scales that were much warmer than present, where virtually no ice sheets were available (see e.g. Fig. 2 of Zachos et al., 2001, http://science.sciencemag.org/content/292/5517/686.full). Anthropogenic emissions of, particularly, carbon dioxide, are expected to increase the average surface temperature on Earth via a modification of the global radiative energy balance, since carbon dioxide in the atmosphere contributes to the so-called greenhouse effect (see the publication by Arrhenius, 1896, available at http://www.rsc.org/images/Arrhenius1896_tcm18-173546.pdf). Due to global warming, the volume of water stored in ice sheets will become smaller, and ultimately increase the volume of the global oceans, thus causing sea level to rise.

Outline of the exercise Here, we develop a simple model of sea level rise which illustrates regions of the earth that are flooded if the GIS and AIS melt. Our work employs command line tools that are freely available and should be present on the computer of any scientist that performs numerical modelling or substantial scientific data processing. If you run a linux system, these tools should either already be available, or should be installted with a minimum amount of work.

As it is the case for any scientific model, which is per definition only an idealization of a natural system, our methodology is based on several simplifications. First of all, it is assumed that the melt process of available ice sheets is linear and occurs over a time period of **1000** y. Furthermore, we do not apply a physical flow model that simulates water inflow from the coast, since such a model can hardly be designed and formulated within the framework of this exercise. Instead, we will calculate water height over land via subtracting the rising sea level from the global elevation field. Negative values indicate the presence of water over land.

Our work depends on the availability of a gridded land elevation data set and a land-sea-mask that separates the land surface into regions that belong to land and ocean. These data sets are also the only input files that are necessary for our analysis. The files are taken from a set of boundary

conditions for numerical models of the circulation of the atmosphere. These have been derived from global elevation data sets, that are commonly generated using modern satellite-based radar interferometry, e.g. by the satellite system ICESat (`icesat.gsfc.nasa.gov/icesat/`). For use in climate modelling, this data has been interpolated to the resolution of the climate model. The orography in a climate model itself is therefore also a model - a model of the land surface elevation, whose accuracy depends on the quality of the measurement and on the grid resolution to which it is interpolated to. Higher resolution of the model grid means better agreement of the gridded orography with the original high-resolution orography data set. The data set used here originates from the boundary conditions of the Atmosphere General Circulation Model ECHAM5 at T63-resolution, which corresponds to a horizontal resolution of $1.9°$ by $1.9°$. Close to the equator, this corresponds to roughly 200 km by 200 km per grid cell.

```bash
#!/bin/bash

#some definitions that control the script
n_time_steps=1000 #number of time steps over which sea level rises
time_unit='1year' #resolution of the time axis
time_reference='2000-01-01,00:00:00' #reference time (first date)
sl_start=0 #sea level ramp starts with elevation of 0 m
sl_end=75 #sea level ramp ends with elevation of 75 m

#definition of input files
orography_file='data/orography.nc'
lsm_file='data/land_sea_mask.nc'

#definition of output files
sea_level_output_file="sea_level_time_series.nc"
flooding_file='flooding_due_to_ice_melt.nc'

#clean up from (potential) previous runs of this script
if [ -e ${sea_level_output_file} ]
then
  rm ${sea_level_output_file}
fi
if [ -e ${flooding_file} ]
then
  rm ${flooding_file}
fi

#find minimum and maximum values of orography (necessary for file processing)
min_val=$(cdo output -fldmin ${orography_file} | sed 's/ //g')
max_val=$(cdo output -fldmax ${orography_file} | sed 's/ //g')
```

```
#subtract / add small value from / to min_val and max_val
#in order to increase the data range
#(cdo setrtomiss, used below, does not include limits of the
#processed data range, but we need to include these)
min_val=$(echo "scale=3; ${min_val}-1" | bc)
max_val=$(echo "scale=3; ${max_val}-1" | bc)

#generate a NetCDF file that contains n_time_steps, all values NaN;
#this file will be used to generate a time-dependent sea level data set;
#our approach, taking an existing NetCDF file and modifying it, saves
#lots of tedious work in setting up a new NetCDF file from scratch,
#which involves definition of dimensions, variables, and the definition of
#links between these
for ((i=0; i<${n_time_steps}; i+=1))
do
  #generate n_time_steps copies of orography,
  #add a time axis, and replace all values by NaN
  echo "creating file timestep_${i}.nc ..."
  cdo setrtomiss,${min_val},${max_val} \
      -settaxis,${time_reference},${time_unit} \
      ${orography_file} timestep_${i}.nc 2>/dev/null
done

#merge the above generated files to one NetCDF file
cdo mergetime timestep_?.nc timestep_??.nc timestep_???.nc timeseries.nc

#set a proper time axis for the whole time series
cdo settaxis,${time_reference},${time_unit} timeseries.nc timeseries_timeaxis.nc

#clean up temporary files
rm timestep_*.nc timeseries.nc

#run a loop that generates a linear sea level ramp, starting a sea_level_start
#and ending at sea_level_end
c_sl=${sl_start}
for ((i=0; i<${n_time_steps}; i+=1))
do
  #redefine current_sea_level c_sl depending on the value of i
  c_sl=$(echo "scale=3; ${sl_start}+${sl_end}*${i}/(${n_time_steps}-1)" | bc)

  #generate a three digit string of i containing a leading zero (for file names)
  if [ ${i} -le 9 ]
  then
    counter_str="00${i}"
  else
    if [ ${i} -le 99 ]
    then
      counter_str="0${i}"
    else
      counter_str="${i}"
    fi
```

```
  fi

  #generate from each time step of timeseries_timeaxis.nc a NetCDF file that
  #contains a global field corresponding to the respective sea level at that time
  echo "creating file sea_level_time_series_${counter_str}.nc ..."
  cdo setmisstoc,${c_sl} \
      -setrtomiss,${min_val},${max_val} \
      -seltimestep,$((i+1)) \
      timeseries_timeaxis.nc sea_level_time_series_${counter_str}.nc 2>/dev/null
done

#merge the single time steps of the sea level time series into one file
cdo mergetime sea_level_time_series_???.nc ${sea_level_output_file}

#clean up temporary files
rm sea_level_time_series_???.nc timeseries_timeaxis.nc

#subtract sea level from elevation in order to calculate water height over land
#negative values will depict water
cdo sub ${orography_file} ${sea_level_output_file} tmp.nc

#remove the elevation and sea level from the data set so that all values in file
#flooding_file depict the water level caused by flooding
cdo mulc,-1 \
    -mul ${lsm_file} \
    -setmisstoc,0 \
    -setrtomiss,0,${max_val} \
    tmp.nc ${flooding_file}

#clean up
rm tmp.nc
```

Exercise 73   –   Shell and netcdf

Modify the above source code with the purpose of simulating the flooding that results from
1010 years of sea-level rise due to ocean warming. To this end you need to:

1. Make a literature research with the purpose of finding an estimate of rates r of current or
   near-future annual sea-level rise due to ocean warming; commonly such estimates are in the
   order of a few millimeters per year. Convert your choice of r to units of m/y

2. Modify the above given shell-script so that it creates a 1010 y linear ramp that contains
   the time-dependent global sea level SSH, starting with zero and ending with the value
   $SSH_{\text{end}} = r \cdot 1010$ y.

Run both the unmodified version of the model, simulating sea-level rise due to land-ice melt,

and the modified version of the model, simulating sea-level rise due to ocean warming.

Note: in order to execute a bash script "script.sh", open a Linux shell-session, navigate to the folder where the script is located, and execute the command "./script.sh". You might have to activate executable rights for this script by executing "chmod u+x script.sh" in advance.

Analyze and discuss your results:

1. Make a time-dependent analysis of the flooding that is predicted by this simple model of sea level rise; you could, for example, generate plots of the flooding over land for two or three interesting time steps that you select from the 1010 y time series.

2. Make a similar analysis for the sea level rise that is simulated by the unchanged original shell-script, which considers melting of land-ice.

3. Compare the results of both analyses and discuss differences. Where are regions located, where people should not live anymore in the future?

4. Make a critical analysis of the flooding simulated by this very simple model.

 For the last point, these are questions that you might consider:

1. What are weak points of the simulation? Consider in your discussion the term "volume conservation", the stationarity of the applied sea level rise, and the spatial resolution of the orographic data. How would you expect the simulated flooding to look like if the spatial resolution of orography was higher?

2. The model, in its current version, has at least one dramatic flaw. Where is the simulated flooding, that should only be attributed to water inflow from the ocean, obviously wrong? What is the reason for the erroneous result?

3. Could you imagine what additional physical processes a corrected version of the model would need to contain in order to avoid the identified problem? Give a short description of your ideas, maybe illustrate them with some sketches.

Exercise 74 – Evaluate possible zones of wine production and climatic conditions

 For wine production there exists some empirical laws:

Northern Hemisphere: degree of latitude 40 – 50

Southern Hemisphere: degree of latitude 30 – 40

The climatic demands are:

1. Vegetation period 180 – 250 days (days with daily mean > 5 °C)

2. Mean temperature 9 °C– 21 °C

3. White wines optimal annual mean temperature 9.5–11.5 °C

4. Red Wines optimal annual mean temperature 10.5–13 °C

5. Sunshine hours per year: 1500–2000 h

6. Precipitation 480 mm–700 mm

Task: Please calculate the possible zones of red wine production using 4 and 6 using temperature and precipitation constraints. The resulting figure should be similar to Fig. 11.1. Here are the links for getting the CRU surface temperature:

http://climexp.knmi.nl//CRUData/cru_ts3.23.1901.2014.tmp.dat_1.nc

and precipitation data:

http://climexp.knmi.nl//CRUData/cru_ts3.23.1901.2014.pre.dat_1.nc

Choose two different reference periods: 1901-1920 and 1991-2010

Calculate furthermore the zones for future scenarios (RCP4.5 and RCP8) for the years 2081-2100. Data are accessible here:

http://cmip-pcmdi.llnl.gov/cmip5/data_getting_started.html.

For this, choose one particular model and compare the zones with a reference period using the same model (e.g., 1960-1980). Some people could speculate that the alcohol belts (Fig. 11.2) may be shifting under global warming. Can this be substantiated by your results?

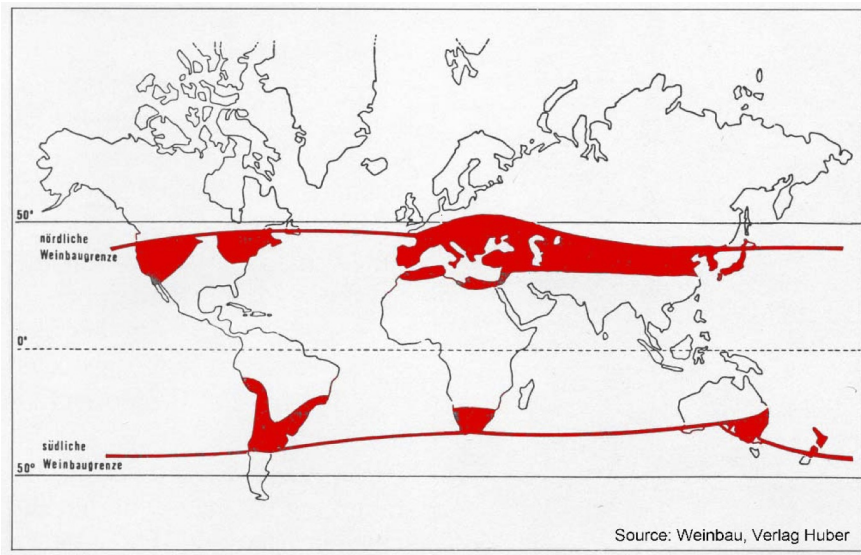Hint: use the cdo commands from the lecture!

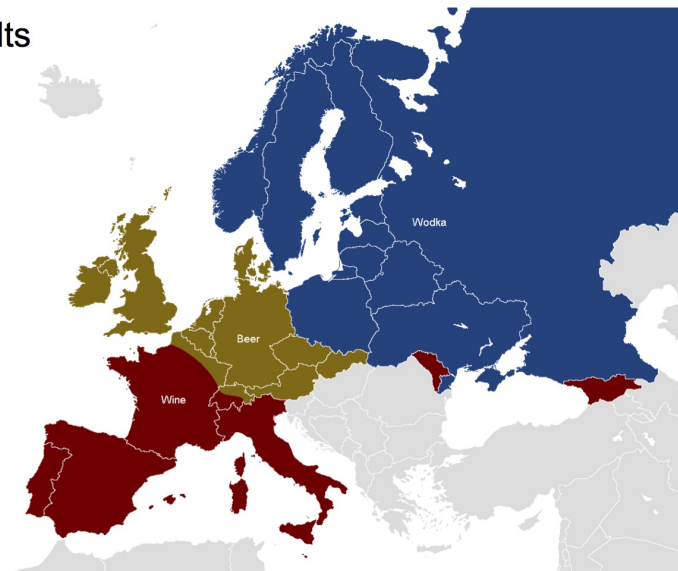Figure 11.1: Zones of todays wine production.

Figure 11.2: Alcohol belts in Europe.

Bibliography

Abramowitz, M. and Stegun, I. A. (1965). Handbook of mathematical functions with formulas, graph, and mathematical tables. *Applied Mathematics Series*, 55:1046.

Arnold, L. (1995). *Random dynamical systems*. Springer.

Arnold, L. (2001). *Hasselmann's program revisited: The analysis of stochasticity in deterministic climate models*, volume 49. Birkhäuser, Boston.

Baker, G. L. and Blackburn, J. A. (2005). *The pendulum: a case study in physics*, volume 8. Oxford University Press Oxford.

Barber, D., Dyke, A., Hillaire-Marcel, C., Jennings, J., Andrews, J., Kerwin, M., Bilodeau, G., McNeely, R., Southon, J., Morehead, M., and Gagnonk, J.-M. (1999). Forcing of the cold event of 8,200 years ago by catastrophic drainage of laurentide lakes. *Nature*, 400(6742):344–348.

Bhatnagar, P., Gross, E. P., and Krook, M. K. (1954). A model for collision process in gases. i. small amplitude processes in charged and neutral one-component system. *Phys. Rev*, 94:511.

Boltzmann, L. (1896). *Vorlesungen über Gastheorie : 2 Volumes (in German)*. Leipzig 1895/98 UB: O 5262-6.

Boltzmann, L. (1995). *Lectures on Gas Theory*. Dover Publ. New York. ISBN 978-0486684550.

Broecker, S. and Peng, T.-H. (1982). *Tracers in the Sea*. Columbia University.

Broecker, W. S. (1987). The biggest chill. *Natural History*, 97(2):74–82.

Broecker, W. S. et al. (1991). The great ocean conveyor. *Oceanography*, 4(2):79–89.

Brüning, R. and Lohmann, G. (1999). Charles s. peirce on creative metaphor: a case study on the conveyor belt metaphor in oceanography. *Foundations of science*, 4(4):389–403.

Bryan, F. (1986). High latitude salinity effects and inter-hemispheric thermohaline circulations. *Nature*, 323(3):301–304.

Buckingham, E. (1914). On physically similar systems; illustrations of the use of dimensional equations. *Physical Review*, 4(4):345–376.

Budyko, M. I. (1969). The effect of solar radiation variations on the climate of earth. *Tellus*, 21:611–619.

Busch, W. (1865). *Max und Moritz (in German); Max and Maurice, a Juvenile History in Seven Tricks* . Braun und Schneider, München.

Cercignani, C. (1987). *The Boltzmann equation and its applications*. Springer New York. ISBN 978-0387966373.

Cercignani, C. (1990). *Mathematical methods in kinetic theory*. Plenum, 2 edition. ISBN 978-0306434600.

Chelton, D. B. and Schlax, M. G. (1996). Global Observations of Oceanic Rossby Waves. *Science*, 272:234–238.

Chen, D., Gerdes, R., and Lohmann, G. (1995). A 1-d atmospheric energy balance model developed for ocean modelling. *Theoretical and Applied Climatology*, 51:25–38.

Chorin, A. J. and Hald, O. H. (2006). Stochastic tools in mathematics and science. surveys and tutorials in the applied mathematical sciences, vol. 1.

Chorin, A. J., Kast, A. P., and Kupferman, R. (1999). Unresolved computation and optimal predictions. *Communications on pure and applied mathematics*, 52(10):1231–1254.

Chorin, A. J., Kupferman, R., and Levy, D. (2000). Optimal prediction for hamiltonian partial differential equations. *Journal of Computational Physics*, 162(1):267–297.

Courant, R., Friedrichs, K., and Lewy, H. (1928). Über die partiellen Differenzengleichungen der mathematischen Physik. *Mathematische Annalen*, 100:32–74.

Courant, R., Friedrichs, K., and Lewy, H. (1967). On the partial difference equations of mathematical physics. *IBM J. Res. Dev.*, 11(2):215–234.

Dansgaard, W., Johnsen, S., Clausen, H., Dahl-Jensen, D., Gundestrup, N., Hammer, C., C.S. Hvidberg, J. S., Sveinbjoernsdottir, A., Jouzel, J., and Bond, G. (1993). Evidence for general instability of past climate from a 250-kyr ice-core record. *Nature*, 364:218–220.

d'Humieres, D., Bouzidi, M., and Lallemand, P. (2001). Thirteen-velocity three-dimensional lattice boltzmann model. *PRE*, 63(6, Part 2).

Dijkstra, H., Raa, L. T., and Weijer, W. (2004). A systematic approach to determine thresholds of the ocean's thermohaline circulation. *Tellus A*, 56 (4):362.

Doedel, E. J., Champneys, A. R., Fairgrieve, T. F., Kuznetsov, Y. A., Sandstede, B., and Wang, X. (1997). Continuation and bifurcation software for ordinary differential equations (with homcont). *Available by anonymous ftp from ftp cs concordia ca, directory pub/doedel/auto*.

Egger, J. (2001). Master equations for climatic parameter sets. *Climate Dynamics*, 18(1-2):169–177.

Einstein, A. (1905). Investigations on the theory of the brownian movement. *Ann. der Physik*, 17:549–560.

Einstein, A. (1926). Die Ursache der Mäanderbildung der Flußläufe und des sogenannten Baerschen Gesetzes. *Naturwissenschaften*, 14:223–224.

Evans, D. J. and Morriss, G. (2008). *Statistical mechanics of nonequilibrium liquids*. Cambridge University Press.

Fairbanks, R. G. (1989). A 17, 000-year glacio-eustatic sea level record: influence of glacial melting rates on the younger dryas event and deep-ocean circulation. *Nature*, 342(6250):637–642.

Feigenbaum, M. J. (1980). The transition to aperiodic behaviour in turbulent systems. *Commun. Math. Phys.*, 77.

Flammer, C. (1957). *Spheroidal wave functions*. Stanford University Press.

Frisch, U. (1996). *Turbulence: the legacy of A.N. Kolmogorov*. Cambridge University Press. ISBN 0-521-45103-5.

Gerkema, T., Zimmerman, J., Maas, L., and Van Haren, H. (2008). Geophysical and astrophysical fluid dynamics beyond the traditional approximation. *Reviews of Geophysics*, 46(2).

Gill, A. E. (1982). *Atmosphere-ocean dynamics*, volume 30. Academic Press. International Geophysics Series.

Givon, D., Kupferman, R., and Stuart, A. (2004). Extracting macroscopic dynamics: model problems and algorithms. *Nonlinearity*, 17(6):R55.

Gottwald, G. (2010). On recent trends in climate dynamics. *AMS Gazette*, 37(5).

Grassberger, P. and Procaccia, I. (1983). Measuring the strangeness of strange attractors. *Physica D: Nonlinear Phenomena*, 9(2):189–208.

Haken, H. (1996). Slaving principle revisited. *Physica D: Nonlinear Phenomena*, 97(1):95–103.

Haney, R. L. (1971). Surface thermal boundary conditions for ocean circulation models. *Journal of Physical Oceanography*, 1:241–248.

Hasselmann, K. (1976). Stochastic climate models. Part I. Theory. *Tellus*, 6:473–485.

He, X. and Luo, L. S. (1997). Theory of the lattice Boltzmann method: From the Boltzmann equation to the lattice Boltzmann equation. *Phys. Rev. E*, 56(6):6811–6817.

Holton, J. R. (2004). *An Introduction to Dynamic Meteorology*. Elsevier Academic Press, Burlington, MA.

Kambe, T. (2007). *Elementary Fluid Mechanics*. World Scientific Publishing.

Kuznetsov, Y. A. (1998). *Elements of applied bifurcation theory*, volume 112. Springer, New York.

Landau, L. D. and Lifshitz, E. M. (1959). *Fluid Mechanics*, volume 6 of *Course of Theoretical Physics*. Pergamon Press, Oxford.

Langevin, P. (1908). On the theory of brownian motion. *Comptes Rendues*, 146:530–533.

Leith, C. (1975). Climate response and fluctuation dissipation. *Journal of the Atmospheric Sciences*, 32(10):2022–2026.

Lohmann, G. (2003). Atmospheric and oceanic freshwater transport during weak atlantic overturning circulation. *Tellus A*, 55(5):438–449.

Longuet-Higgins, M. S. (1968). The eigenfunctions of laplace's tidal equations over a sphere. *Philosophical Transactions for the Royal Society of London. Series A, Mathematical and Physical Sciences*, pages 511–607.

Lorenz, E. (1982). Atmospheric predictability experiments with a large numerical model. *Tellus A*, 34:505–513.

Lorenz, E. N. (1960). Maximum simplification of the dynamic equations. *Tellus*, 12(3):243–254.

Lorenz, E. N. (1963). Deterministic nonperiodic flow. *Journal of the atmospheric sciences*, 20(2):130–141.

Lorenz, E. N. (1976). Nondeterministic theories of climatic change. *Quaternary Research*, 6(4):495–506.

Lorenz, E. N. (1984). Irregularity: a fundamental property of the atmosphere*. *Tellus A*, 36(2):98–110.

Lucarini, V., Blender, R., Herbert, C., Pascale, S., Ragone, F., and Wouters, J. (2014). Mathematical and physical ideas for climate science. *Rev. Gephys.*

Maas, L. R. (1994). A simple model for the three-dimensional, thermally and wind-driven ocean circulation. *Tellus A*, 46(5):671–680.

Manabe, S. and Stouffer, R. (1993). Century-scale effects of increased atmospheric CO_2 on the ocean atmosphere system. *Nature*, 364:215–218.

Mandelbrot, B. B. (1967). How long is the coast of britain: Statistical self-similarity and fractal dimension. *Science*, 155:636–638.

Mandelbrot, B. B. (1983). *The fractal geometry of nature*. Macmillan.

Matsuno, T. (1966). Quasi-geostrophic motions in the equatorial area. *J. Meteor. Soc. Japan*, 44(1):25–43.

Mori, H. (1965). Transport, collective motion, and brownian motion. *Progress of Theoretical Physics*, 33(3):423–455.

Mori, H., Fujisaka, H., and Shigematsu, H. (1974). A new expansion of the master equation. *Progress of Theoretical Physics*, 51(1):109–122.

Müller and Maier-Reimer (2000). Trapped rossby waves. *Phys. Rev. E*, 61:1468 – 1485.

Müller, D., Kelly, B., and O'brien, J. (1994). Spheroidal eigenfunctions of the tidal equation. *Physical review letters*, 73(11):1557.

Müller, D. and O'Brien, J. (1995). Shallow water waves on the rotating sphere. *Physical Review E*, 51(5):4418.

Olbers, D. (2001). A gallery of simple models from climate physics. *In: Stochastic Climate Models, Progress in Probability (Eds.: P. Imkeller and J. von Storch)*, 49:3–63.

Peitgen, H.-O. and Richter, P. (1986). *The Beauty of Fractals*. Heidelberg: Springer-Verlag.

Proudman, J. (1916). On the motion of solids in a liquid possessing vorticity. *Proc. R. Soc. Lond. A*, 92:408–424.

Rahmstorf, S. (1996). On the freshwater forcing and transport of the Atlantic thermohaline circulation. *Climate Dynamics*, 12:799–811.

Rayleigh, L. (1916). On convection currents in a horizontal layber of fluid, when the higher temperature is on the under side. *Phil. Mag.*, 6:529–546.

Rooth, C. (1982). Hydrology and ocean circulation. *Progress in Oceanography*, 11:131–149.

Rossby, C.-G. (1939). "relation between variations in the intensity of the zonal circulation of the atmosphere and the displacements of the semi-permanent centers of action". *Journal of Marine Research*, 2 (1):38–55.

Saltzman, B. (1962). Finite amplitude free convection as an initial value problem – i. *Journal of the Atmoshpheric Sciences*, 19:329–341.

Shannon, C. E. (1948). A Mathematical Theory of Communication. *Bell System Technical Journal*, 27 (3):379–423.

Stommel, H. (1961). Thermohaline convection with two stable regimes of flow. *Tellus*, 13:224–230.

Strogatz, S. (2000). *Non-linear Dynamics and Chaos: With applications to Physics, Biology, Chemistry and Engineering*. Perseus Books.

Taylor, G. (1917). Motion of solids in fluids when the flow is not irrotational. *Proc. R. Soc. Lond. A*, 93:92–113.

Townsend, S., Lenosky, T., Muller, D., Nichols, C., and Elser, V. (1992). Negatively curved graphitic sheet model of amorphous carbon. *Physical Review Letters*, 69(6):921–924.

Tritton, D. J. (1988). *Physical Fluid Dynamics*. Oxford University Press, Science Publication. ISBN 978-0-19-854493-7.

Uhlenbeck, G. E. and Ornstein, L. S. (1930). On the theory of the brownian motion. *Physical review*, 36(5):823.

van Kampen, N. G. (1981). *Stochastic processes in physics and chemistry*. North Holland. IISBN 978-0-444-52965-7.

Wüst, G. (1935). Schichtung und Zirkulation des Atlantischen Ozeans. Das Bodenwasser und die Stratosphäre. *Wiss. Ergebn. Dtsch. Atlant. Exped. 'Meteor' 1925-1927*, 6(1):1–288.

Zwanzig, R. (1960). Ensemble method in the theory of irreversibility. *The Journal of Chemical Physics*, 33:1338.

Zwanzig, R. (1980). Problems in nonlinear transport theory. In *Systems far from equilibrium*, pages 198–225. Springer.

Zwanzig, R. (2001). *Nonequilibrium statistical mechanics*. Oxford University Press, USA.